Modelling chemical weathering in contrasted watersheds:

new implementations and application at the global scale

Juan Luis Lechuga Crespo

Bilbao, 2020

Doctoral thesis

Université Fédérale
Toulouse Midi-Pyrénées

Universidad del País Vasco
Euskal Herriko Unibertsitatea

INP TOULOUSE

eman ta zabal zazu

Universidad del País Vasco
Euskal Herriko Unibertsitatea

Juan Luis Lechuga Crespo

Presenta la siguiente memoria de tesis para optar al grado de Doctor en Ingeniería Ambiental por la Universidad del País Vasco/Euskal Herriko Unibertsitatea (UPV/EHU).

Modelling chemical weathering in contrasted watersheds

New implementations and application at the global scale

Directora
Dra. **Estilita Ruiz Romera**
Departamento de Ingeniería Química y del Medio Ambiente
Escuela de Ingeniería de Bilbao (UPV/EHU)

Director
Dr. **José Miguel Sánchez Pérez**
Laboratoire écologie fonctionnelle et environnement
École Nationale Supérieure Agronomique de Toulouse (INP Toulouse)

Universidad del País Vasco/Euskal Herriko Unibertsitatea (UPV/EHU)
Escuela de Ingeniería de Bilbao
Departamento de Ingeniería Química y del Medio Ambiente

Agradecimientos

Han pasado cuatro años desde que me embarqué en este viaje del doctorado, y lo más importante que he aprendido es que *la Ciencia la hacen personas*. En estas líneas quiero agradecerle a toda esa gente con la que aprendí, he aprendido, y aprendo a hacer Ciencia. No puedo nombrarles a todos, pero sí hay algunos que merecen mención especial.

En primer lugar, a quienes me abrieron las puertas al mundo de la investigación. A mi directora Estilita, gracias por tener la puerta de tu despacho siempre abierta desde 2014, cuando llegué a Bilbao. Gracias por abrirme también las puertas del laboratorio, las de docencia, y las del muestreo (aunque alguna vez fuéramos hasta sin botas). Durante estos últimos cuatro años, creo que la frase que más me habrás dicho es *"Juan Luis, tranquilo, las cosas van más despacio"* (creo que eso todavía me queda por aprender). A mi director Josemi, gracias por acoger a este canario y abrirle la puerta a la investigación internacional. Gracias por darme un hueco en el laboratorio de Toulouse, por darme la experiencia de AGUAMOD, y por calmar mis constantes nervios en persona, por Skype, o por teléfono, *"tranquilo Juan Luis, que el artículo llega"* (y al final, llegó). A los dos, ¡muchas gracias!

Sin duda, lo mejor de este doctorado ha sido la gente con la que he podido compartirlo. La "sala de becarios" no es sólo una sala del departamento con mesas, sillas, y una corriente de aire brutal; son los momentos compartidos en ella, los cafés de las 11, las comidas en el office, las pastas de cumpleaños, las cañas de los viernes, las cenas, y las *sagardotegis*. Por todo ello, gracias Nere, David, Ainhoa, Naia, María, Alberto, Ana, Edu, Rafa, Paula, Clara, Iker García, Iker Obregón, Jon Solar, Kepa, Alberto, Mikel, Miryam, Bea, Iratxe, Rubia, Leire, Asier, Iñigo, Víctor, Aitziber, Sara y seguro que me olvido de

alguien (¡que me perdone!). De este grupo, dos personas se merecen mención especial: Miren, contigo puedo preparar una disolución mientras hablamos de microorganismos, puedo tomarme un café mientras hablamos de la vida, o puedo echarme una(s) caña(s) y/o sidra(s) acompañadas de buenas risas, ¡gracias por esa energía! Y Jess, contigo también he compartido risas, pero además dudas, cansancio, estrés, e incluso alguna lágrima. Todo ello en Bilbao, en Toulouse y en los caminos de ida y vuelta (eso sí, con nuestra banda sonora de fondo) ¡Gracias por acompañarme en este viaje! A todas y todos ¡gracias! eskerrik asko!

In addition, I am grateful to the ENSAT people. Especialmente, me gustaría agradecerte, Columba, el haberte enfrentado conmigo a la sobrecogedora burocracia francesa, y por haber compartido muy buenos (y no tan buenos) momentos en mis estancias en Toulouse ¡gracias! Rox, ton enthousiasme est engageant, je te remercie vraiment pour les belles bières, les bons conseils et ta énergie positive. In addition, I cannot forget about Xi (with whom I improved my Chinese!), Clément, Jérémy, Pankyes, Marilen, Jaime, Mélanie, Roberta, Liliana, Minerva, Rebeca, Himanshu, Vanessa, Zied, Sam, and the other colleagues at the lab (sorry if I miss anybody!), thank you all! Il y a trois personnes ici qui sont été aussi très importantes : Sabine Sauvage, avec toi j'appris beaucoup, ta énergie positive est toujours agréable, je suis très content d'avoir travaillé avec toi. Jean Luc Probst, qui m'a montré le monde de la géochimie, avec vous j'ai eu des très intéressantes discussions scientifiques. Et un grand merci pour Annick, qui est été la personne le plus sympa avec moi quand je suis arrivé à Toulouse et qui je remerci le plus pour son aide avec tout. Vraiment Annick, sans toi, tout ça ne sera pas possible, merci ! !

A parte de toda esta gente que me ha acompañado en Bilbao y en Toulouse, no me puedo olvidar de quienes me apoyan allá donde esté: mi gente de Canarias. Aunque cada vez nos veamos menos, os agradezco que estéis ahí cuando ha sido necesario salir de esta tesis de doctorado por un tiempo. Wendy, Yoli, Ainoa, Fran, García, Facun (¡gracias por venir a verme!), Betan, San Gil, Airam, Leyre, Dulli, Judi, Pablo, Carlos, Pacheco (mis canarios en Bilbao), Ale, Mary, Tamara, Amaranta, Lucía, y a muchos otros que se me quedarán en el tintero ¡muchas gracias!

Thank you very much to Philippe Amiotte Suchet, Jens Hartmann, Chris George, Michelle van Vliet and everyone who has helped me improve this manuscript.

También quiero mencionar los momentos con toda la gente de AGUAMOD, especialmente con Maite. Ha sido un placer trabajar contigo, he aprendido un montón de ti, mila esker! Eskerrik asko bidai honetan emandako laguntzagatik Iñaki, surekin zientzia ikasi dut (baita euskara ere!).

Mención especial se merecen mis abuelas, que siempre han estado ahí, aunque fuera en la distancia. Abuela Evelia, gracias por tus bizcochones, chicharrones y natillas, pero también por tus ganas y alegría. Abuela Pilar, te fuiste cuando estaba a mitad de camino, gracias por estar siempre allí para nosotros. Te tengo en mi mente. Y al resto de mi familia, tíos, primos, y demás familiares ¡gracias!

Por último, quiero agradecer a aquéllos que sí que han estado todos y cada uno de los días de esta tesis. Este viaje ha sido tan duro para mí como para ellos. Ainara, me has apoyado en los momentos duros, me has animado en los bajos, y te has alegrado conmigo en los altos, sé que esto sin ti no habría sido posible. Gracias por aguantar las incontables horas de guagua entre Toulouse y Bilbao, me siento muy afortunado de haber hecho este viaje contigo, no podría haber tenido mejor compañía. Nunca podré agradecértelo suficientemente, eskerrik asko maitia. Elena, eres la mejor hermana mayor que podría haber tenido, siempre te he admirado y lo sigo haciendo, gracias por estar siempre ahí. A mi padre: pa, sé que con una llamada o un mensaje al día te es suficiente para saber que estoy bien, pero sé que me tienes en tu mente constantemente y no puedo empezar a agradecerte todo lo que has hecho por mí. A mi madre: ma, tu energía y cariño han hecho que aguantara hasta en los peores momentos de este viaje, no sé como lo haces, pero muchas gracias. El apoyo y el cariño que recibo de ustedes han sido los pilares en los que se apoya todo lo que he podido hacer hasta ahora, ojalá que se sientan tan orgullosos de mí como yo lo estoy de ustedes.

A todos y todas ¡gracias! Eskerrik asko! Thank you! Merci!

Abstract

The biogeochemical cycles describe the matter and energy flux between ecosystems in the Earth System. However, climate change, human population growth and other global change hazards alter the natural balance of these cycles. Within this context, understanding which mechanisms control the mass transfer, and assessing their spatial and temporal evolution becomes necessary to balance a sustainable development with the environmental protection. In the biogeochemical cycles, the relative importance of the different factors involved changes with the spatial and temporal scales used for their evaluation, creating the need of tools capable of integrating these factors for analysis. Commonly, these tools involve modelling.

With regards to biogeochemical cycling research, focus has been pointed to the Critical Zone, a part of the environment comprising from the ground surface to the consolidated rock. Is within this zone where the geochemical cycle interacts with the biogeochemical cycles through the physical and chemical weathering processes. Weathering conditions the chemical composition of the aquatic environments through the liberation of products from the solid phase. In the continental zone, rivers act not only as reaction matrix in the Critical Zone, but also as a vector of transport for those products from the hydrographic basin to other environments, such as lakes or oceans. At the local level, this matter transfer is of interest for ecological analysis both at the river and wetland scale; while at the global scale, these processes impact on the oceanic and atmospheric composition in geological scales.

The main objective of this work is to evaluate the role of chemical weathering in the biogeochemical cycles, paying special attention to the major ions derived from rocks through the modelling of this process at different spatial and temporal scales. In

particular, a global-to-local and static-to-dynamic approach has been followed.

At the beginning of this work, there existed several modelling tools capable of assessing the chemical weathering using a mechanistic approach, however, their application to large spatial and temporal scales is conditioned to the availability of input data and computing resources. As an alternative, there were other empirical models applicable at the global scale. Taking as starting point the most recent studies, and after the evaluation of 1751 river compositions, in this work we have been able to confirm that hydrology, lithology, and soil are the most relevant factors at the global scale regarding chemical weathering. Indeed, its implication on each major ion liberation has been proved, allowing the yield of the first global scale maps of specific fluxes derived from rocks, as well as the comparison of hot spots between ions. At the global scale, $3374 \cdot 10^6$ $Mg \cdot y^{-1}$ dissolved matter is yielded from rocks, where 58 % is Ca^{2+}, 24 % is Na^{+}, 15 % is Mg^{2+}, and 3 % is K^{+} with respect to the cation flux, and a 74 % is alkalinity, 18 % is SO_4^{2-}, y 8 % is Cl^{-} with regards to the anion flux.

Besides, a more detailed analysis at a local scale case study (the Deba river basin, Gipuzkoa, Basque Country) has been accomplished, paying attention to the processes responsible of the chemical composition of the waters, as well as to the hydrological effect on the temporal evolution of the exports to the ocean. In this catchment, the effect of evaporitic springs and gypsum deposits in one of its headwaters has been shown to have a great impact on the stream water chemical composition down to the outlet. This study has also permitted to highlight the advantages of combining punctual sampling information with continuous registries to evaluate the temporal evolution of the system. Identifying the moments after the flood events as those with the greatest relative dissolved exports to the ocean within the year.

Once the main processes governing the chemical composition of water in this study were identified, the application of the global model to the basin scale has been performed through the coupling of the model to the physically-based hydrological model (SWAT). Such assessment has allowed to evaluate the possibilities and limitations of the models in local scales, both under a static and a dynamic approach. The model allows to obtain results with a mean discrepancy of 13 % with respect to reality, when the effects of point sources (such as the evaporitic springs and gypsum deposits) do not condition the ionic composition.

Acknowledging the limitations at the local scale, the model has been again applied at the global scale, aiming to evaluate not only the spatial distribution of the chemical weathering derived fluxes, but the impact of this process on the global carbon cycle under a climate change context. The results from this simulation have allowed to see that the potential impacts derived from the climate change on the hydrological balance

will increase between an 8 and 13 % the CO_2 consumption rates derived from the chemical weathering of rocks, but its growth will not been nor spatially nor temporally homogeneous.

The results from this PhD thesis have allowed to the assess the role of chemical weathering at the global scale, specially on the carbon cycle. Future research should focus on improving the model configuration and integrating the results from other studies following a local-to-global approach.

Resumen

Los ciclos biogeoquímicos describen el flujo de materia y energía entre los ecosistemas del Sistema Tierra. Sin embargo, el cambio climático, el aumento de la población y otras amenazas del cambio global alteran el equilibrio natural de estos ciclos. En este contexto se vuelve necesario tanto entender qué mecanismos controlan la transferencia de materia, como estimar su evolución espacial y temporal, para poder equilibrar un desarrollo sostenible con la protección del medioambiente. La relevancia de distintos factores involucrados en los distintos ciclos biogeoquímicos cambia con respecto a la escala temporal y espacial utilizada para su evaluación, creando la necesidad de herramientas capaces de integrar dichos factores para poder llevar a cabo su análisis. Generalmente, estas herramientas implican trabajo de modelización.

Con relación a la investigación en los ciclos biogeoquímicos, la atención se ha centrado en la Zona Crítica, un espacio del ecosistema que comprende desde la superficie del suelo hasta la roca consolidada. Es en esta zona donde los ciclos geoquímicos interaccionan con los ciclos biogeoquímicos a través de la alteración física y química. La alteración condiciona la composición química de los entornos acuáticos tras la liberación de productos de la fase rocosa. En la zona continental, los ríos actúan no únicamente como matriz de reacción en la Zona Crítica, sino también como vector de transporte de esos productos desde la cuenca hidrográfica hacia otros entornos, como lagos u océanos. A nivel local, esta transferencia de materia resulta de interés para análisis ecológicos tanto a nivel de río como a nivel de estuario, mientras que a nivel global el impacto de estos procesos afecta a la composición de los océanos e incluso de la atmósfera en escalas geológicas.

El objetivo principal de este trabajo es evaluar el papel de la erosión química en los

ciclos biogeoquímicos, prestando especial atención a los iones mayoritarios derivados de las rocas, a través del modelado de este proceso a diferentes escalas espaciales y temporales. En particular, se ha seguido un enfoque espacial de global-a-local y temporal de estático-a-dinámico.

Al inicio de este trabajo, existían varias herramientas de modelización capaces de evaluar la erosión química desde un punto de vista físico y termodinámico, sin embargo, su aplicación a grandes escalas espaciales y temporales se ve condicionada por disponibilidad de datos de entrada y de recursos de computación. Como alternativa, también constaban otros modelos de base empírica que permitían su aplicación a escala global. Tomando como referencia los estudios más actuales, y tras la evaluación de la composición de 1751 ríos en este trabajo, se ha podido confirmar que la hidrología, la litología y el suelo son los factores más relevantes a nivel global respecto a la erosión química. También se ha podido constatar que su implicación en la liberación de cada ion mayoritario de la roca es diferente, permitiendo obtener los primeros mapas a nivel global de flujos específicos derivados de la roca, así como la comparación de puntos calientes de cada ion. A nivel global, $3374 \cdot 10^6$ Mg·año^{-1} de material disuelto se libera de las rocas, siendo un 58 % Ca^{2+}, un 24 % Na^{+}, un 15 % Mg^{2+}, y un 3 % K^{+} respecto al flujo de cationes, y un 74 % alcalinidad, un 18 % SO_4^{2-}, y un 8 % Cl^{-} respecto al flujo de aniones.

Paralelamente, se ha realizado un análisis más detallado de un caso local (la cuenca del río Deba, Gipuzkoa, País Vasco) prestando atención a los procesos condicionantes de la composición química de las aguas, así como al efecto de la hidrología sobre la evolución temporal de los flujos al océano. En esta cuenca destaca el importante efecto que ejercen las fuentes de evaporitas y los depósitos de yesos en una de las partes de cabecera, que condicionan fuertemente la química de las aguas hasta la desembocadura. Este estudio también ha permitido subrayar la ventaja de combinar muestreos puntuales con registros en continuo para evaluar la evolución temporal del sistema. Identificando los momentos después de las crecidas como los de mayores exportaciones disueltas relativas al océano a lo largo del año.

Una vez identificados los procesos determinantes de la composición química del agua en este caso de estudio, se ha trasladado la aplicación del modelo global hasta la escala de cuenca mediante la integración de dicho modelo a un modelo hidrológico de base física (SWAT). Este estudio ha permitido evaluar las posibilidades y las limitaciones del modelo en escalas locales, tanto de forma estática como dinámica. El modelo permite obtener unos resultados con una discrepancia media respecto a la realidad del 13 % siempre que los efectos puntuales (como las fuentes de evaporitas y los depósitos de yesos) no condicionen la presencia de iones mayoritarios.

Conocidas las limitaciones que pueden existir a escalas locales, el modelo se ha aplicado a escala global nuevamente, tratando de evaluar no sólo la distribución espacial de los flujos derivados de la erosión química, sino el impacto que este proceso genera sobre el ciclo global del carbono bajo un contexto de cambio climático. Los resultados de la simulación nos han permitido ver que los potenciales impactos derivados del cambio climático en la hidrología aumentarán globalmente entre un 8 y un 13 % las tasas de consumo de CO_2 por la erosión de las rocas, pero su aumento no será uniforme ni espacial ni temporalmente.

Los resultados de esta tesis doctoral permiten evaluar el papel de la erosión química a la escala global, especialmente en el ciclo del carbono. Investigación futura debería centrarse en mejorar la configuración del modelo e integrar los resultados de otros estudios con enfoques local-a-global.

Résumé

Les cycles biogéochimiques décrivent le flux de matière et d'énergie entre les environnements du système Terre. Cependant, le changement climatique, l'augmentation de la population et d'autres menaces du changement global altèrent l'équilibre naturel de ces cycles. Dans ce contexte, il devient nécessaire de comprendre quels mécanismes contrôlent le transfert de matière et estimer son évolution spatiale et temporelle, pour équilibrer le développement durable avec la protection de l'environnement. L'importance relatif des différents facteurs intervenant évoluent par rapport à l'échelle temporelle et spatiale utilisée pour leur évaluation, créent la nécessité des outils capables d'intégrer ces facteurs afin de réaliser les analyses. Normalement, ces outils utilisent la modélisation.

Par rapport à la recherche des cycles biogéochimiques, attention c'était dirigé à la Zone Critique, une zone de l'environnement allant de la surface du sol à la roche consolidée. C'est dans cette zone que les cycles géochimiques interagissent avec les cycles biogéochimiques par l'altération physique et chimique. C'est l'altération qui conditionne la composition des milieux aquatiques après la libération des produits par la phase rocheuse. Dans la zone continentale, les rivières agissent non seulement comme matrice de réaction dans la zone critique, mais aussi comme vecteur de transport de ces produits du bassin hydrographique vers d'autres environnements, tels que les lacs ou les océans. Au niveau local, ce transfert de matière présente un intérêt pour les analyses écologiques à la fois au niveau des fleuves et des estuaires, tandis qu'au niveau globale ces processus affectent la composition des océans et même l'atmosphère à l'échelle géologique.

L'objectif principal de ce travail est d'évaluer le rôle de l'érosion chimique dans les

cycles biogéochimiques, en accordant une attention particulière aux ions majoritaires dérivés des roches, à travers la modélisation de ce processus à différentes échelles spatiales et temporelles. En particulier, une approche spatiale globale-locale et temporelle statique-dynamique a été suivie.

Au début de ce travail, il y avait plusieurs outils de modélisation capables d'évaluer l'érosion chimique d'un point de vue physique et thermodynamique, cependant, son application à de grandes échelles spatiales et temporelles est conditionnée par la disponibilité des données d'entrée et des ressources informatiques. Comme alternative, il y avait aussi d'autres modèles empiriques qui permettaient son application à l'échelle mondiale. En prenant comme référence les études les plus récentes et après l'évaluation de la composition chimique de 1751 rivières dans ce travail, il a été possible de confirmer que l'hydrologie, la lithologie et le sol sont les facteurs les plus pertinents à l'échelle mondiale en ce qui concerne l'altération chimique. Il a également été vérifié que leur implication dans la libération de chaque ion majeur de la roche est différente, permettant d'obtenir les premières cartes globales d'écoulements spécifiques dérivés de la roche, ainsi que la comparaison des points chauds de chaque ion. À l'échelle mondiale, $3374 \cdot 10^6$ $Mg \cdot an^{-1}$ de matière dissoute sont libérés des roches, soit un 58% de Ca^{2+}, un 24% de Na^+, un 15% de Mg^{2+} et un 3% de K^+ par rapport au flux de cations et un 74% d'alcalinité, un 18% SO_4^{2-} et un 8% Cl^- en ce qui concerne le flux d'anions.

Parallèlement, étude plus détaillé à été réalisé dans un cas d'étude local (le bassin versant de Deba, Gipuzkoa, Pays Basque), en prêtant attention aux processus de conditionnement de la composition chimique des eaux, ainsi qu'à l'effet de l'hydrologie sur l'évolution temporelle des écoulements vers l'océan. Dans ce bassin, se distingue l'effet important exercé par les sources d'évaporites et les dépôts de gypse dans l'une des parties de tête, qui conditionnent fortement la chimie jusqu'à la bouche. Cette étude a également mis en évidence l'avantage de combiner des échantillonnages ponctuels avec des enregistrements continus pour évaluer l'évolution temporelle du système. En identifient les moments après les crues comme ceux de plus grande exportation dissous relatif vers l'océan tout au long de l'année.

Une fois identifiés les processus déterminants de la composition chimique de l'eau dans cette étude de cas, l'application du modèle global a été transférée à l'échelle du bassin en intégrant ce modèle dans un modèle physique hydrologique (SWAT). Cette étude a permis d'évaluer les possibilités et les limites du modèle à l'échelle locale, à la fois statiquement et dynamiquement. Le modèle permet d'obtenir des résultats avec un écart moyen de 13% par rapport à la réalité, tant que les effets ponctuels (tels que les sources d'évaporites et les dépôts de gypse) ne conditionnent pas la présence d'ions majoritaires.

Connaissant les limitations qui peuvent exister à l'échelle locale, le modèle a été appliqué à nouveau à l'échelle mondiale, essayant d'évaluer non seulement la distribution spatiale des flux issus de l'érosion chimique, mais l'impact que ce processus génère sur le cycle global de carbone dans un contexte de changement climatique. Les résultats de la simulation nous ont permis de voir que les impacts potentiels dérivés du changement climatique sur l'hydrologie augmenteraient globalement les taux de consommation de CO_2 de 8 à 13% en raison de l'érosion des roches, mais leur augmentation ne serait pas uniforme ni spatiale ni temporairement.

Les résultats de cette thèse de doctorat nous ont permis d'évaluer le rôle de l'érosion chimique à l'échelle mondiale, notamment dans le cycle du carbone. Les recherches futures devraient se concentrer sur l'amélioration de la configuration du modèle et l'intégration des résultats d'autres études aux approches locales à mondiales.

Index

List of Figures

List of Tables

Part I

INTRODUCTION

CHAPTER 1

General introduction

1.1 ENGLISH - General introduction

Worldwide water resources are suffering an increasing pressure derived from human activities. At the same time, social concern about environmental issues is growing too. Proof of such interest is the 1992 Dublin conference on water (Koudstaal et al., 1992), the European Water Framework Directive (WFD 2000/60/CE, of the European Parliament and of the Council, 2000), or the growing number of research products generated in the last 100 years. The number of scientific articles under the topic "water" presents an increasing trend along with the Web of Science's historical record: from 104 in 1900 to 198,885 in 2019 (Web of Science, consulted on May 22nd, 2020). This growth highlights that water resources have become more present in resource management

policymaking, social concern, and research, due to the critical role they pose for life sustain, economic growth, and ecosystem services, among others.

In this growing interest context, recent studies focus on integration of all spheres of the environment in the *Earth system* approach. The hydrosphere—particularly rivers—is considered as the most important connection between atmosphere, pedosphere, biosphere, and oceans (Meybeck, 2003) within the environment. During the Anthropocene, "a new human-dominated geological epoch" according to Lewis and Maslin (2015), safeguarding aquatic resources is of most relevance. Despite of the knowledge gained in each sphere and their integration, relevant gaps of knowledge are still present. Today's research aims to fill these knowledge gaps facing numerous challenges, such as the need for worldwide data, the uniformity on its resolutions, and the large number of processes involved (Savenije et al., 2014; Strokal et al., 2019).

In the Earth system, matter flows between components of the environment following different sequences. The ensemble of large-steady *reservoirs* (e.g. the ocean), smaller-dynamic *exchange pools*, and the fluxes between them (derived from different biological, geological, or chemical *processes*) define the different *pathways* conforming the *cycles*. Within a *biogeochemical cycle*, the elements flow between the biotic and abiotic part of the biosphere, while in a *geochemical cycle* the elements move within the Earth's crust and its surface. Water has a dual role in these cycles: it acts as a matrix for many biochemical reactions, and as a vector for matter transport. Such dual role conditions the hydrological balance and the water quality, having a considerable impact on the coastal ecosystem (Caddy & Bakun, 1994; Sun et al., 2016) and inland waters (Cole et al., 2007). Great effort has been—and is—put on understanding these cycles, identifying which variables affect them and assessing their influence in terms of space and time. Indeed, accomplishing a fully Earth-system analysis to face the global change hazards requires a deep knowledge of all these biogeochemical and geochemical cycles, both independently and integrated.

Due to the complexity of the Earth system, *box models* are a common approach followed in biogeochemical and geochemical cycling studies. Cycles are a holistic method

to understand how all the boxes (reservoirs and exchange pools) are related (through processes), paying attention to one element—or a group of them—at a time. On the one hand, carbon, nitrogen, sulphur, or phosphorus are some of the most studied biogeochemical cycles due to the large impact that global change carries on these elements. For instance, fossil fuel combustion increases C and S emissions to the atmosphere (Falkowski et al., 2000; Spiro et al., 1992), while fertilization changes N and P cycling (Vitousek et al., 1997). On the other hand, geochemical cycles refer to the movement of elements in or under the Earth crust (*internal cycle*) and on the surface (*external cycle*). Inorganic elements are those commonly related to these cycles, including Ca, Mg, Na, K, and other relevant nutrients for the biosphere.

Despite the common consideration that the internal geochemical cycle is relatively "stable" in shorter periods than in geological timescales (R. A. Berner et al., 1983), the external geochemical cycle more dynamic (e.g. Bhatt et al., 2018), with shorter residence times due to the influence of external forces (such as the water cycle or human activities). Hydrology and other biogeochemical cycles affect continental mass transfer rates to oceans (Meybeck, 2003). Interest on these interactions arise in many scientific fields since they impact in the long-term climate regulation (Amiotte Suchet, 1995; Garrels & Mackenzie, 1972; Meybeck, 1979) and deliver nutrients to freshwater and oceans (Sun et al., 2016) and life act as a catalyst for this process, generating carbonic acid through organic matter decay or retrieving nutrients from the minerals (DiPietro, 2013).

In the environment, the place where the external geochemical cycle is in contact with the other biogeochemical cycles is the Critical Zone (CZ) (S. P. Anderson et al., 2007; Gaillardet et al., 2018). It spans from the top of the vegetation to the bedrock and integrates many processes belonging to different biogeochemical cycles. In the CZ, rock is transformed to soil through *weathering*, where *physical weathering* (erosion) regards the mechanical break of particles reducing their volume and *chemical weathering* relates to the chemical change commonly related to water or air contact. One can think about the CZ as a reactor where rock uplift supports material while transport retrieves matter from the reactor (S. P. Anderson et al., 2007).

Consequently, chemical weathering is a crucial process regarding the CZ evolution, responsible for the bedrock transformation into soil and an essential process in surface water composition. Its study has long been of interest for several researchers working in different fields, such as hydro-chemists studying water composition (Meybeck, 1987), oceanographers using riverine inputs (Sun et al., 2016), wetland ecologists understanding saline dynamics (Herbert et al., 2015), geo-chemists understanding bedrock chemical denudation (Gaillardet et al., 1999), or earth-scientists studying biogeochemical cycling (Hartmann, Moosdorf, et al., 2014). Given the broad interest on chemical weathering, and regarding that it is a complex process controlled by many factors (Hartmann et al., 2009, and references therein), there is a need of developing useful tools, and an efficient way to assess this process is through modelling.

Modelling chemical weathering has been the object of study in several research projects, being notorious contributions those by Meybeck (1979, 1987), J. L. Probst (1992), Amiotte Suchet and Probst (1996), Gaillardet et al. (1999), Goddéris et al. (2006), Goddéris et al. (2009), Hartmann et al. (2009), and more recently Hartmann, Moosdorf, et al. (2014). These and many other researchers have targeted chemical weathering and tried to model its spatial and temporal evolution following different modelling approaches:

- **Physical modelling** based on a physical description of the natural laws governing the chemical weathering processes.
- **Empirical modelling** where the natural laws are described by statistical regressions instead of by its physical expressions.

A common challenge is found in both approaches: changing spatial and temporal scales. When applying *physical models* at large spatial or temporal scales, the challenge of setting up the model becomes a barrier, because of the lack of input data or the computational resources needed. In contrast, when applying *empirical models* to lower cases, their performance is constraint by the spatial and temporal range to which the model was calibrated. The development of physically-based models helps in growing understanding about the process, while empirical modelling helps in assessing first

snapshots about potential responses, which may be used to establish future hypothesis and focus research effort. A usual application of empirically-based models is the identification of *hot spots* and *hot moments*, places and times with disproportionally stronger rates of a process, respectively. Such identification is relevant to evaluate their impact on the elemental cycles, and to predict how are they expected to change under future scenarios. Such information is significant for stakeholders and policymakers in the Anthropocene.

In this sense, the present PhD thesis is framed within the context of the development, validation, and application of a chemical weathering model, following an empirical approach, and paying attention to its performance on different spatial and temporal scales. In a broad context, an empirically-based model will be constructed at the global scale, using extensive field data and statistical modelling. Then, this model's performance will be tested in smaller spatial case studies, both in large and small basins. Later, the model will be coupled with a hydrological model to test the model performance on different temporal situations (daily, monthly, seasonal, and annual). Finally, its application will allow a global dynamic study of chemical weathering implication on the carbon cycle, as an illustration of the model's applicability.

This PhD manuscript is structured in 9 chapters:

- **Chapter 1** gives a broad introduction to the research topic and presents general concepts used along the main body of the study.
- **Chapter 2** contains a scientific literature review regarding chemical weathering within the context of global biogeochemical cycles, paying attention to the previous works on modelling this process. The hypothesis and objectives of the present work are stated in this chapter.
- **Chapter 3** describes the materials and methods followed in the present study, focusing on the input data, the modelling techniques at different spatial and temporal scales, as well as the field and laboratory methods.
- **Chapter 4** presents the global empirical model development through the different

databases used and the modelling techniques applied. A global spatially explicit application of the model is presented as well.

- **Chapter 5** introduces a local case study where a monitoring program was established, allowing the evaluation of the main geochemical processes, using riverine exports as a proxy for its evaluation. From this chapter, the *in situ* temporal and spatial data are retrieved to test the model's performance at the local scale and under a dynamic approach.
- **Chapter 6** shows the integration of the chemical weathering model on a hydrological model and tests its performance on the previously presented local case study, to evaluate the model's limits.
- **Chapter 7** contains an application of the model at the global scale, following a dynamic approach at the basin level, illustrating a potential application of the model for the carbon cycle evaluation.
- **Chapter 8** compiles a general discussion on the insights gained, where all the results and conclusions reached in previous chapters are articulated to illustrate the possibilities of using an empirical model on different spatial and temporal scales, as well as presenting a conceptual approach to explain chemical weathering at the global scale, and an evaluation of the limits to this model application.
- **Chapter 9** states the conclusions reached in the present study and formulates hypotheses for future lines of research.

1.2 ESPAÑOL - Introducción general

Los recursos acuáticos mundiales sufren una presión creciente derivada de las actividades humanas. Al mismo tiempo, la preocupación social sobre los asuntos medioambientales también está creciendo. Prueba de dicho interés son la conferencia sobre el agua en 1992, Dublín (Koudstaal y col., 1992), la Directiva Marco del Agua (WFD 2000/60/CE, del European Parliament and of the Council, 2000), y el creciente número de productos de investigación generados en los últimos 100 años. De hecho, la búsqueda del término "agua" en Web of Science presenta un crecimiento de los artículos científicos a lo largo de su registro histórico, de 104 en 1900 a 198,885 en 2019 (Web of Science, consultado el 22 de mayo de 2020). Este crecimiento subraya que los recursos acuáticos se han vuelto más presentes en el desarrollo de políticas de gestión de recursos, en la preocupación social, y en la investigación, debido al papel fundamental que juega en el mantenimiento de la vida, el crecimiento económico y los servicios de los ecosistemas, entre otros.

En este contexto de interés creciente, estudios recientes se centran en la integración de todas las esferas del entorno en un enfoque de Sistema Tierra. La hidrosfera – particularmente los ríos – se considera como la conexión más importante entre la atmósfera, la pedosfera, la biosfera y los océanos (Meybeck, 2003) en el entorno. Durante el Antropoceno (Lewis & Maslin, 2015), salvaguardar los recursos acuáticos es de la mayor relevancia. A pesar del conocimiento ganado en cada una de las esferas y en su integración; todavía existen lagunas de investigación. La investigación actual pretende rellenar estas lagunas mientras se enfrenta a numerosos retos, como la necesidad de datos mundiales, la uniformidad de sus resoluciones, o el gran número de procesos involucrados (Savenije y col., 2014; Strokal y col., 2019).

En términos del sistema Tierra, la materia se cicla entre los reservorios a través de vías (o procesos), todos ellos integrados entre sí. El agua tiene un papel dual en esta red: actúa como matriz para las reacciones bioquímicas, y juega un papel de vector de transporte de materia. Este papel dual condiciona el balance hidrológico y la calidad

del agua, teniendo un impacto considerable en el ecosistema costero (Caddy & Bakun, 1994; Sun y col., 2016) y en las aguas interiores (Cole y col., 2007). Grandes esfuerzos han sido – y son – puestos en entender estos procesos, identificar qué variables les afectan, y evaluar su influencia en términos de espacio y tiempo. De hecho, conseguir un análisis de un sistema Tierra completo para enfrentar las amenazas del cambio global requiere un conocimiento profundo de todos estos procesos, tanto de cada uno individualmente como de su integración.

Debido a la complejidad del sistema Tierra, los modelos de caja son un enfoque común seguido en el estudio de ciclos biogeoquímicos y ciclos geoquímicos. Por un lado, los ciclos biogeoquímicos son un método holístico para entender cómo todos estos procesos están relacionados, prestando atención a un elemento – o un grupo de ellos – cada vez. El carbono, el nitrógeno, el azufre, o el fósforo son algunos de los elementos más estudiados en los ciclos biogeoquímicos, debidos al gran impacto que el cambio global acarrea en estos elementos. Por ejemplo, las emisiones de combustibles fósiles incrementan las emisiones de C y S a la atmósfera (Falkowski y col., 2000; Spiro y col., 1992), mientras que la fertilización cambia los ciclos del N y el P (Vitousek y col., 1997). Por otro lado, los ciclos geoquímicos se refieren al movimiento de elementos en o bajo la corteza terrestre (*ciclo interno*) o en su superficie (*ciclo externo*), y estos ciclos están menos estudiados respecto al contexto de cambio global. Los elementos inorgánicos son aquéllos que están comúnmente involucrados en estos ciclos, incluyendo Ca, Mg, Na, K, y otros elementos que, aunque normalmente se encuentran en las rocas, son nutrientes relevantes para la biosfera.

A pesar de la consideración común de que el ciclo geoquímico interno es relativamente “estable” en periodos más cortos de tiempo que los geológicos (R. A. Berner y col., 1983), el ciclo externo es más dinámico (e.g. Bhatt y col., 2018). El ciclo geoquímico interno es más lento que el ciclo externo, donde los tiempos de residencia son mucho más cortos debido a la influencia de fuerzas externas (como el ciclo del agua). La hidrología y los otros ciclos biogeoquímicos afectan a la transferencia de materia continental a los océanos (Meybeck, 2003). El interés en estas interacciones surge en muchos campos científicos ya que a largo plazo afectan al clima (Amiotte Suchet, 1995;

Garrels & Mackenzie, 1972; Meybeck, 1979) y aportan nutrientes a las aguas dulces y océanos.

En el medio ambiente, el lugar donde el ciclo geoquímico externo está en contacto con los otros ciclos biogeoquímicos es la Zona Crítica (CZ) (S. P. Anderson y col., 2007; Gaillardet y col., 2018). Esta zona se extiende desde la superficie del suelo hasta la roca consolidada e integra muchos procesos pertenecientes a diferentes ciclos biogeoquímicos. En la CZ, la roca se transforma en suelo a través de la alteración, donde la *alteración física* se refiera a la rotura mecánica de las partículas, recudiendo su volumen, mientras que la *alteración química* se relaciona con el cambio químico comúnmente relacionado con el contacto con agua o aire. Uno puede pensar en la CZ como un reactor donde la roca aporta material mientras que el transporte retira material del reactor (S. P. Anderson y col., 2007) y los organismos vivos actúan como un catalizador para este proceso, generando ácido carbónico a través de la descomposición de la materia orgánica o extrayendo nutrientes de los minerales (DiPietro, 2013).

Consecuentemente, la alteración química es un proceso clave respecto a la CZ, responsable de la transformación de la roca consolidada en suelo, un proceso clave en la composición del agua superficial y un vínculo entre los ciclos geoquímicos y biogeoquímicos. Su estudio ha sido de interés para numerosos investigadores trabajando en distintos campos, desde hidro-químicos que estudian la composición del agua (Meybeck, 1987), oceanógrafos que emplean los aportes de los ríos (Sun y col., 2016), ecólogos de los humedales estudiando las dinámicas salinas (Herbert y col., 2015), geo-químicos que estudian la erosión química de la roca (Gaillardet y col., 1999), o investigadores de la Tierra que estudian los ciclos biogeoquímicos (Hartmann, Moosdorf y col., 2014). Dado el amplio interés en la erosión química y teniendo en cuenta que es un proceso complejo controlado por muchas variables (Hartmann y col., 2009), existe la necesidad de desarrollar herramientas útiles para estos científicos, siendo la modelización una alternativa efectiva.

El modelado de la alteración química ha sido objeto de estudio en muchos proyectos de investigación, siendo notorias las contribuciones de Meybeck (1979, 1987), J. L.

Probst (1992), Amiotte Suchet y Probst (1996), Gaillardet y col. (1999), Goddéris y col. (2006), Goddéris y col. (2009), Hartmann y col. (2009), y más recientemente Hartmann, Moosdorf y col. (2014). Estos y otros muchos investigadores han trabajado sobre la alteración química y han intentado modelar su evolución espacial y temporal siguiendo diferentes enfoques de modelización:

- **Modelización física**, basada en la descripción física de las leyes naturales que gobierna el proceso de alteración química.
- **Modelización empírica**, donde las leyes naturales se describen mediante regresiones estadísticas en lugar de por expresiones físicas.

Un reto común se encuentra en los dos enfoques: *los cambios de escala espaciales y temporales*. Cuando se aplican *modelos físicos* en escalas temporales o espaciales grandes, el reto de montar un modelo se vuelve una barrera, debido a la no disponibilidad de datos de entrada, o a la gran cantidad de recursos computacionales necesarios. Por el contrario, cuando se aplican *modelos empíricos* a casos menores, su desempeño está limitado al rango espacial y temporal para el que el modelo fue calibrado. El desarrollo de modelos físicos ayuda a ganar conocimiento sobre el proceso, mientras que los modelos empíricos permiten generar una primera imagen sobre las respuestas potenciales, que pueden ser utilizadas para establecer hipótesis de trabajo para centrar los esfuerzos de investigación.

En este sentido, la presente tesis doctoral se encuentra en el contexto del desarrollo, la validación, y la aplicación de modelos de alteración química, siguiendo un enfoque empírico y prestando atención a su desempeño en diferentes escalas espaciales y temporales. En un contexto más amplio, un modelo empírico se desarrollará a la escala global, usando datos de campo y modelización estadística. Seguidamente, este modelo se probará en escalas menores, tanto en cuencas grandes como pequeñas. Luego, el modelo se integrará con un modelo hidrológico para comprobar el desempeño en diferentes escalas temporales. Finalmente, su aplicación permitirá un estudio global dinámico de la implicación de la alteración química en el ciclo del carbono, como una ilustración de la aplicabilidad del modelo.

Este manuscrito se estructura en 9 capítulos:

- El **capítulo 1** da una introducción general al tema de investigación y presenta los conceptos generales usados a lo largo del cuerpo principal del estudio.
- El **capítulo 2** contiene una revisión de la literatura científica respecto a la alteración química en el contexto de los ciclos biogeoquímicos globales, prestando especial atención a los trabajos previos en la modelización de este proceso. Las hipótesis y los objetivos de este trabajo se enuncian en este capítulo.
- El **capítulo 3** describe los materiales y métodos seguidos en este estudio, centrándose en los datos de entrada, las técnicas de modelización a diferentes escalas espaciales y temporales, así como los métodos de campo y laboratorio.
- El **capítulo 4** presenta el desarrollo de un modelo global empírico a través de las diferentes bases de datos y las técnicas de modelización aplicadas. También se presenta la aplicación espacial del modelo a escala global.
- El **capítulo 5** muestra un caso de estudio donde se estableció un programa de monitoreo, que permitió evaluar los procesos geoquímicos principales, usando las cargas del río como indicador de su evaluación. De este capítulo, los datos temporales *in situ* y los datos espaciales se recogerán para evaluar el desempeño del modelo en una escala local y bajo un enfoque dinámica.
- El **capítulo 6** muestra la integración del modelo de alteración química en un modelo hidrológico para comprobar su desempeño en el caso local presentado previamente, para evaluar los límites del modelo.
- El **capítulo 7** ccontiene una aplicación del modelo a escala global, siguiendo un enfoque dinámico a escala de cuenca, ilustrando una aplicación potencial del modelo para la evaluación del ciclo del carbono.
- El **capítulo 8** recoge una discusión general de los conocimientos ganados, donde todos los resultados y conclusiones alcanzados en capítulos previos se articulan para ilustrar las posibilidades de usar un modelo empírico en diferentes contextos espaciales y temporales, así como presentar un modelo conceptual para explicar la alteración química a la escala global, y una evaluación de las limitaciones de

la aplicación de este modelo.

- El **capítulo 9** enuncia las conclusiones alcanzadas en este estudio, así como formula hipótesis para futuras líneas de investigación.

1.3 FRANÇAIS - Introduction générale

Les ressources aquatiques mondiales subissent une pression croissante des activités humaines. Dans le même temps, les préoccupations sociales concernant les questions environnementales augmentent également. La conférence sur l'eau de 1992, à Dublin (Koudstaal et al., 1992), la directive-cadre sur l'eau (WFD 2000/60/CE, du European Parliament and of the Council, 2000), et le nombre croissant de produits de recherche générés au cours des 100 dernières années témoignent d'un tel intérêt. En fait, la recherche du terme "eau" dans le Web of Science montre une croissance des articles scientifiques tout au long de son historique, de 104 en 1900 à 198 885 en 2019 (Web of Science, consulté le 22 mai 2020) . Cette croissance souligne que les ressources aquatiques sont devenues plus présentes dans l'élaboration des politiques de gestion des ressources, dans les préoccupations sociales et dans la recherche, en raison du rôle fondamental qu'elles jouent dans le maintien de la vie, la croissance économique et les services écosystémiques, parmi des autres.

Dans ce contexte d'intérêt croissant, des études récentes se concentrent sur l'intégration de toutes les sphères de l'environnement dans une approche du système Terre. L'hydrosphère - en particulier les rivières - est considérée comme le lien le plus important entre l'atmosphère, la pédosphère, la biosphère et les océans (Meybeck, 2003) dans l'environnement, où la zone critique est une partie active de l'environnement en ce qui concerne l'intégration de toutes ces domaines (Gaillardet et al., 2018). Pendant l'Anthropocène, "une nouvelle époque géologique dominé par les humains" (Lewis & Maslin, 2015), la sauvegarde des ressources aquatiques est de la plus haute importance. Malgré les connaissances acquises dans chacun des domaines et dans leur intégration, il existe encore des lacunes dans la recherche. Les recherches actuelles visent à combler ces lacunes tout en faisant face à de nombreux défis, tels que le besoin de données mondiales, l'uniformité de ses résolutions ou le grand nombre de processus impliqués (Savenije et al., 2014; Strokal et al., 2019).

Dans le système Terre, la matière circule à travers les components de l'environnement

depuis différentes séquences. L'union des grands et stables *réservoirs* (comme l'océan), plus petites et dynamiques *zones d'échange*, et des fluxes parmi eux (dérives des *processus* biologiques, géologiques, et chimiques) défini des voies (ou processus) qui conforment les *cycles*. Dans un cycle biogéochimique, les éléments circulent entre le part biotique et abiotique de la biosphère, mais dans un cycle géochimique, les éléments se mouvent dans la croûte terrestre et sa surface. L'eau a un double rôle dans ces cycles : elle est une matrice pour les réactions biochimiques et un vecteur de transport de matière. Ce double rôle conditionne l'équilibre hydrologique et la qualité de l'eau, ayant un impact considérable sur l'écosystème côtier (Caddy & Bakun, 1994; Sun et al., 2016) et sur les eaux intérieures (Cole et al., 2007). De grands efforts ont été - et sont - déployés pour comprendre ces cycles, identifier les variables qui les affectent et évaluer leur influence en termes d'espace et de temps. En fait, obtenir une analyse d'un système Terre complet pour faire face aux menaces du changement global nécessite une connaissance approfondie de tous ces processus, à la fois indépendamment et intégrés.

En raison de la complexité du système Terre, les *modèles en boîte* sont une approche courante suivie dans l'étude des cycles biogéochimiques et des cycles géochimiques. Les cycles sont une méthode holistique pour comprendre comment tous ces boîtes (réservoirs et zones d'échange) sont liées (par les processus), en prêtant attention à un élément – ou à un groupe d'entre eux – à chaque fois. Dans un côté, le carbone, l'azote, le soufre ou le phosphore sont parmi les éléments les plus étudiés des cycles biogéochimiques, en raison du grand impact que le changement global a sur ces éléments. Par exemple, les émissions de combustibles fossiles augmentent les émissions de C et de S dans l'atmosphère (Falkowski et al., 2000; Spiro et al., 1992), tandis que la fertilisation modifie les cycles de N et P (Smith et al., 1999; Vitousek et al., 1997). D'autre part, les cycles géochimiques se réfèrent au mouvement des éléments dans ou sous la croûte terrestre (cycle interne) ou à sa surface (cycle externe). Les éléments inorganiques sont ceux qui sont généralement liés à ces cycles, y compris le Ca, le Mg, le Na, le K et d'autres éléments qui sont des nutriments pertinents pour la biosphère.

Malgré la considération commune que le cycle géochimique interne est relativement "stable" dans des périodes plus courtes que les périodes géologiques (R. A. Berner

et al., 1983), le cycle externe est plus dynamique (par exemple Bhatt et al., 2018), avec les temps de séjour plus courtes depuis l'influence des forçages externes (comme le cycle de l'eau et les activités humaines). L'hydrologie et les autres cycles biogéochimiques affectent le transfert de matière continentale vers les océans (Meybeck, 2003). L'intérêt pour ces interactions se pose dans de nombreux domaines scientifiques car elles affectent le climat à long terme (Amiotte Suchet, 1995 ; Garrels & Mackenzie, 1972 ; Meybeck, 1979) et fournissent des nutriments aux eaux douces et aux océans.

Dans l'environnement, l'endroit où le cycle géochimique externe est en contact avec les autres cycles biogéochimiques est la Zone Critique (CZ) (S. P. Anderson et al., 2007). Il s'étend de la limite supérieure de la végétation à la roche consolidée et intègre de nombreux processus appartenant à différents cycles biogéochimiques. Dans la CZ, la roche est transformée en sol par *altération*, où *l'altération physique* (l'érosion) fait référence à la dégradation mécanique des particules tandis que *l'altération chimique* est liée au changement chimique communément lié au contact avec de l'eau ou de l'air. On peut considérer la CZ comme un réacteur où la roche apporte de la matière tandis que le transport retire la matière du réacteur (S. P. Anderson et al., 2007) et la vie joue une rôle catalyseur pour ce processus, en apportent l'acide carbonique par la décomposition de la matière organique ou l'extraction des nutriments des minéraux.

Par conséquent, l'altération chimique est un processus clé par rapport à l'évolution de la CZ, responsable de la transformation de la roche consolidée en sol, un processus essentiel dans la composition des eaux de surface, et un line entre les cycles géochimiques et biogéochimiques. Son étude a intéressé de nombreux chercheurs travaillant dans différents domaines, des hydro-chimistes qui étudient la composition de l'eau (Meybeck, 1987), des océanographes qui utilisent les contributions des rivières (Sun et al., 2016), des écologistes des zones humides étudient la dynamique saline (Herbert et al., 2015), les géochimistes étudient l'érosion chimique des roches (Gaillardet et al., 1999) ou les chercheurs de la Terre étudient les cycles biogéochimiques (Hartmann, Moosdorf et al., 2014). Étant donné le grand intérêt pour l'érosion chimique et considérant qu'il s'agit d'un processus complexe contrôlé par de nombreuses variables

(Hartmann et al., 2009, et references contenues), il est nécessaire de développer des outils utiles, et la modélisation étant une alternative efficace.

La modélisation de l'altération chimique a été étudiée dans de nombreux projets de recherche, je citerai parmi d'autres les contributions de Meybeck (1979, 1987), J. L. Probst (1992), Amiotte Suchet et Probst (1996), Gaillardet et al. (1999), Goddéris et al. (2006), Goddéris et al. (2009), Hartmann et al. (2009) et plus récemment Hartmann, Moosdorf et al. (2014). Ces chercheurs et de nombreux autres ont travaillé sur l'altération chimique et ont essayé de modéliser son évolution spatiale et temporelle en suivant différentes approches de modélisation :

- **Modélisation physique** basée sur la description physique des lois naturels qui régissent le processus d'altération chimique.
- **Modélisation empirique** où les lois naturels sont décrit par des régressions statistiques plutôt que par des expressions physiques.

Un défi commun se trouve dans les deux approches : les *changements d'échelle* spatiale et temporelle. Lorsque des *modèles physiques* sont appliqués à de grandes échelles spatiales ou temporelles, le défi de l'assemblage d'un modèle devient un obstacle, en raison de l'indisponibilité des données d'entrée ou de la grande quantité de ressources de calcul requises. En revanche, lorsque des *modèles empiriques* sont appliqués à des cas mineurs, leur performance est limitée à la plage spatiale et temporelle pour laquelle le modèle a été calibré. Le développement de modèles-physiques permet d'acquérir des connaissances sur le processus, tandis que les modèles empiriques nous permettent de générer une première image des réponses potentielles, qui peut être utilisée pour établir des hypothèses de travail pour concentrer les efforts de recherche. Une application commune des modèles empiriques c'est l'identification des *hot spots* et *hot moments*, lieus et moments avec unes taux énormément grands, respectivement. Tel identification est précis pour l'évaluation des impacts dans des cycles des éléments, et pour prédire comme ces processus changeraient dans des scenarios futurs. Cette information est significative pour les gestionnaires et les politiques dans l'Anthropocène.

En ce sens, la présente thèse de doctorat s'inscrit dans le cadre du développement, de la validation et de l'application d'un modèle d'altération chimique, suivant une approche empirique et prêtant attention à ses performances à différentes échelles spatiales et temporelles. Dans un contexte plus large, un modèle empirique sera développé à l'échelle mondiale, utilisant des données de terrain et une modélisation statistique. Ce modèle sera ensuite testé à des échelles plus fines, à petite comme à grande échelle. Après, le modèle sera intégré à un modèle hydrologique pour vérifier les performances à différentes échelles de temps (journalier, mensuel, saisonnier, et annuel). Enfin, son application permettra une étude globale dynamique de l'implication de l'altération chimique dans le cycle du carbone, à titre d'illustration de l'applicabilité du modèle.

Ce manuscrit c'est structuré en 9 chapitres :

- Le **chapitre 1** donne une introduction générale au sujet de recherche et présente les concepts généraux utilisés dans le corps principal de l'étude.
- Le **chapitre 2** contient une revue de la littérature scientifique concernant l'altération chimique dans le contexte des cycles biogéochimiques mondiaux, en accordant une attention particulière aux travaux antérieurs de modélisation de ce processus. Les hypothèses et objectifs de ce travail sont énoncés dans ce chapitre.
- Le **chapitre 3** décrit les matériaux et les méthodes suivis dans cette étude, en se concentrant sur les données d'entrée, les techniques de modélisation à différentes échelles spatiales et temporelles, ainsi que les méthodes de terrain et de laboratoire.
- Le **chapitre 4** présente le développement d'un modèle global empirique à travers les différentes bases de données et les techniques de modélisation appliquées. L'application spatiale du modèle à l'échelle mondiale est également présentée.
- Le **chapitre 5** présente une étude de cas où un programme d'échantillonnage a été établi, qui a permis d'évaluer les principaux processus géochimiques, en utilisant les charges fluviales comme indicateur de son évaluation. À partir de ce chapitre, des données temporelles et spatiales *in situ* seront collectées pour évaluer les performances du modèle à une échelle locale dynamique.

- Le **chapitre 6** montre l'intégration du modèle d'altération chimique dans un modèle hydrologique pour vérifier sa performance dans le cas local présenté précédemment, pour évaluer les limites du modèle.
- Le **chapitre 7** contient une application du modèle à l'échelle mondiale, en suivant une approche dynamique à l'échelle du bassin, pour montrer une application potentielle du modèle dans l'évaluation du cycle du carbone.
- Le **chapitre 8** rassemble une discussion générale sur les connaissances acquises, où tous les résultats et conclusions des chapitres précédents sont articulés pour illustrer les possibilités d'utiliser un modèle empirique dans différents contextes spatiaux et temporels, ainsi que pour présenter un modèle conceptuel à appliquer à l'étude de l'altération chimique à l'échelle mondiale ainsi que l'évaluation des limites de l'application de ce modèle.
- Le **chapitre 9** énonce les conclusions de cette étude et formule des hypothèses pour les futurs axes de recherche.

Bibliography

Amiotte Suchet, P. (1995). *Cycle du carbone, érosion chimique des continents et transferts vers les océans* (Doctoral dissertation). Université Louis-Pasteur. Strasbourg, Institut de Géologie. https://www.persee.fr/doc/sgeol_0302-2684_1995_mon_97_1

Amiotte Suchet, P., & Probst, J. L. (1996). Origines du carbone inorganique dissous dans les eaux de la Garonne. Variations saisonnières et interannuelles. / Sources of dissolved inorganic carbon in the Garonne river water. Seasonal and inter annual variations. *Sciences Géologiques. Bulletin*, *49*(1), 101–126. https://doi.org/10.3406/sgeol.1996.1938

Anderson, S. P., von Blanckenburg, F., & White, A. (2007). Physical and Chemical Controls on the Critical Zone. *Elements*, *3*(5), 315–319. https://doi.org/10.2113/gselements.3.5.315

Berner, R. A., Lasaga, A. C., & Garrels, R. M. (1983). The carbonate-silicate geochemical cycle and its effect on atmospheric carbon dioxide over the past 100 million years. *American Journal of Science*, *283*, 641–683. https://doi.org/10.2475/ajs.283.7.641

Bhatt, M. P., Hartmann, J., & Acevedo, M. F. (2018). Seasonal variations of biogeochemical matter export along the Langtang-Narayani river system in central Himalaya. *Geochimica et Cosmochimica Acta*, *238*, 208–234. https://doi.org/10.1016/j.gca.2018.06.033

Caddy, J. F., & Bakun, A. (1994). A tentative classification of coastal marine ecosystems based on dominant processes of nutrient supply. *Ocean & Coastal Management*, *23*, 201–211. https://doi.org/10.1016/0964-5691(94)90019-1

Cole, J. J., Prairie, Y. T., Caraco, N., McDowell, W. H., Tranvik, L. J., Striegl, R. G., Duarte, C. M., Kortelainen, P., Downing, J. A., Middelburg, J. J., & Melack, J. M. (2007). Plumbing the Global Carbon Cycle: Integrating Inland Waters into the Terrestrial Carbon Budget. *Ecosystems*, *10*(1), 172–185. https://doi.org/10.1007/s10021-006-9013-8

DiPietro, J. A. (2013). Component: The Rock/Sediment Type. In J. A. DiPietro (Ed.), *Landscape Evolution in the United States* (pp. 15–27). https://doi.org/10.1016/B978-0-12-397799-1.00002-6

European Parliament and of the Council. (2000). Directive 2000/60/EC of the European Parliament and of the Council of 23 October 2000 establishing a framework for Community action in the field of water policy: WFD. https://eur-lex.europa.eu/legal-content/EN/TXT/?uri=celex:32000L0060

Falkowski, P., Scholes, R. J., Boyle, E., Canadell, J. G., Canfield, D., Elser, J., Gruber, N., Hibbard, K., Högberg, P., Linder, S., Mackenzie, F. T., Moore, B., Pedersen, T., Rosenthal, Y., Seitzinger, S. P., Smetacek, V., & Steffen, W. (2000). The global carbon cycle: a test of our knowledge of Earth as a system. *Science*, *290*(5490), 291–296. https://doi.org/10.1126/science.290.5490.291

Gaillardet, J., Braud, I., Hankard, F., Anquetin, S., Bour, O., Dorfliger, N., de Dreuzy, J. R., Galle, S., Galy, C., Gogo, S., Gourcy, L., Habets, F., Laggoun, F., Longuevergne, L., Le Borgne, T., Naaim-Bouvet, F., Nord, G., Simonneaux, V., Six, D., … Zitouna, R. (2018). OZCAR: The French Network of Critical Zone Observatories. *Vadose Zone Journal*, *17*(1), 180067. https://doi.org/10.2136/vzj2018.04.0067

Gaillardet, J., Dupré, B., Louvat, P., & Allègre, C. J. (1999). Global silicate weathering and CO2 consumption rates deduced from the chemistry of large rivers. *Chemical Geology*, *159*, 3–30. https://doi.org/10.1016/S0009-2541(99)00031-5

Garrels, R. M., & Mackenzie, F. T. (1972). A quantitative model for the sedimentary rock cycle. *Marine Chemistry*, *1*, 27–41. https://doi.org/10.1016/0304-4203(72)90004-7

Goddéris, Y., François, L. M., Probst, A., Schott, J., Moncoulon, D., Labat, D., & Viville, D. (2006). Modelling weathering processes at the catchment scale: The WITCH numerical model. *Geochimica et Cosmochimica Acta*, *70*(5), 1128–1147. https://doi.org/10.1016/j.gca.2005.11.018

Goddéris, Y., Roelandt, C., Schott, J., Pierret, M.-C., & Francois, L. M. (2009). Towards an Integrated Model of Weathering, Climate, and Biospheric Processes. *Reviews in Mineralogy and Geochemistry*, *70*(1), 411–434. https://doi.org/10.2138/rmg.2009.70.9

Hartmann, J., Jansen, N., Dürr, H. H., Kempe, S., & Köhler, P. (2009). Global CO2-consumption by chemical weathering: What is the contribution of highly active weathering regions? *Global and Planetary Change*, *69*(4), 185–194. https://doi.org/10.1016/j.gloplacha.2009.07.007

Hartmann, J., Moosdorf, N., Lauerwald, R., Hinderer, M., & West, A. J. (2014). Global chemical weathering and associated P-release — The role of lithology, temperature and soil properties. *Chemical Geology*, *363*, 145–163. https://doi.org/10.1016/j.chemgeo.2013.10.025

Herbert, E. R., Boon, P., Burgin, A. J., Neubauer, S. C., Franklin, R. B., Ardón, M., Hopfensperger, K. N., Lamers, L. P. M., & Gell, P. (2015). A global perspective on wetland salinization: ecological consequences of a growing threat to freshwater wetlands. *Ecosphere*, *6*(10), art206. https://doi.org/10.1890/ES14-00534.1

Koudstaal, R., Rijsberman, F. R., & Savenije, H. (1992). Water and sustainable development. *International Conference on water and Environment: DEvelopment Issues for the 21st Century*.

Lewis, S. L., & Maslin, M. A. (2015). Defining the anthropocene. *Nature*, *519*(7542), 171–180. https://doi.org/10.1038/nature14258

Meybeck, M. (1979). Concentrations des eaux fluviales en éléments majeurs et apports. *Revue de géologie dynamique et de géographie physique*, *21*(3), 215.

Meybeck, M. (1987). Global chemical weathering of surficial rocks estimated from river dissolved loads. *American Journal of Science*, *287*, 401–428. https://doi.org/10.2475/ajs.287.5.401

Meybeck, M. (2003). Global Occurrence of Major Elements in Rivers. In H. D. Holland & K. K. Turekian (Eds.), *Treatise on Geochemistry* (pp. 207–223). https://doi.org/10.1016/B0-08-043751-6/05164-1

Probst, J. L. (1992). *Géochimie et hydrologie de l'érosion continentale. Mécanismes, bilan global actuel et fluctuations au cours des 500 derniers millions d'années.* (Doctoral dissertation). Université Louis-Pasteur. Strasbourg, Institut de Géologie. www.persee.fr/doc/sgeol_0302-2684_1992_mon_94_1

Savenije, H., Hoekstra, A. Y., & van der Zaag, P. (2014). Evolving water science in the Anthropocene. *Hydrology and Earth System Sciences*, *18*(1), 319–332. https://doi.org/10.5194/hess-18-319-2014

Smith, V. H., Tilman, G. D., & Nekola, J. C. (1999). Eutrophication: impacts of excess nutrient inputs on freshwater, marine, and terrestrial ecosystems. *Environmental pollution*, *100*, 179–196. https://doi.org/10.1016/S0269-7491(99)00091-3

Spiro, P. A., Jacob, D. J., & Logan, J. A. (1992). Global inventory of sulfur emissions with 11 resolution. *Journal of Geophysical Research*, *97*(D5), 6023–6036. https://doi.org/10.1029/91JD03139

Strokal, M., Spanier, J. E., Kroeze, C., Koelmans, A. A., Flörke, M., Franssen, W., Hofstra, N., Langan, S., Tang, T., van Vliet, M. T. H., Wada, Y., Wang, M., van Wijnen, J., & Williams, R. (2019). Global multi-pollutant modelling of water quality: scientific challenges and future directions. *Current Opinion in Environmental Sustainability*, *36*, 116–125. https://doi.org/10.1016/j.cosust.2018.11.004

Sun, X., Higgins, J., & Turchyn, A. V. (2016). Diffusive cation fluxes in deep-sea sediments and insight into the global geochemical cycles of calcium, magnesium, sodium and potassium. *Marine Geology*, *373*, 64–77. https://doi.org/10.1016/j.margeo.2015.12.011

Vitousek, P. M., Aber, J. D., Howarth, R. W., Likens, G. E., Matson, P. A., Schindler, D. W., Schlesinger, W. H., & Tilman, D. G. (1997). Human alteration of the global nitrogen cycle: sources and consequences. *Ecological Applications*, *7*(3), 737–750. https://doi.org/10.1890/1051-0761(1997)007[0737:HAOTGN]2.0.CO;2

CHAPTER 2

Scientific context

2.1 The Earth as a closed system

The study of the matter transport between the different environmental spheres–lithosphere, biosphere, hydrosphere, and atmosphere–is commonly approached using the cycle concept in natural sciences, using box models with reservoirs, exchange pools, and fluxes. Commonly, cycles at the global scale are considered within the boundaries of resilience, but recent studies concern about human activities impact these balances (Steffen et al., 2015). Understanding how matter is cycled through the environment and how human activities affect these cycles is necessary for managing resources sustainably.

Matter cycles follow several pathways of reservoirs and exchange pools, where mat-

ter remains for a relatively long time (e.g. atmosphere, vegetation, ocean, etc.), and fluxes derived from processes (e.g. transport, erosion, deposition, etc.) (Hedges, 1992). Cycles may be classified as *biogeochemical* when there are biological, geological, and chemical pathways involved, or as *geochemical* if the biological role is almost absent, usually concerning the inorganic cycling of elements in the Earth's crust and underneath. Indeed, several reservoirs of the geochemical cycles slightly interact with biogeochemical cycles, while some others are more strongly shared. Despite this classification, the geochemical processes play a relevant role in life sustainment by releasing relevant nutrients to other reservoirs, eventually involved in biogeochemical processes (Bleam, 2017).

The zone where the external geochemical and biogeochemical cycles meet each other is the critical zone. Understanding the matter movement between reservoirs in the Earth system requires a thorough comprehension of the critical zone. The processes given within this area have profound implications on the different cycles, especially on the matter release from the geochemical to the biogeochemical cycle.

2.2 The Critical Zone

The Critical Zone (CZ) is the *"(...) special interfacial region of mass and energy flux, which comprises terrestrial, lacustrine, and marine components of the uppermost continental crust (...)"*, following the definition provided by the National Research Council (National Research Council, 2001). It is an interface of atmosphere, geosphere, and hydrosphere which provides sustainment for life (S. P. Anderson et al., 2004; S. P. Anderson et al., 2007; Brantley et al., 2011; Goddéris & Brantley, 2013). From a practical point of view, it comprises all layers found between the ground surface and the bedrock horizon, where the soil and saprolite regolith sheets are found over the continuous fresh rock 2.1.

Considering a homogeneous CZ volume like the one shown in Figure 2.1, several

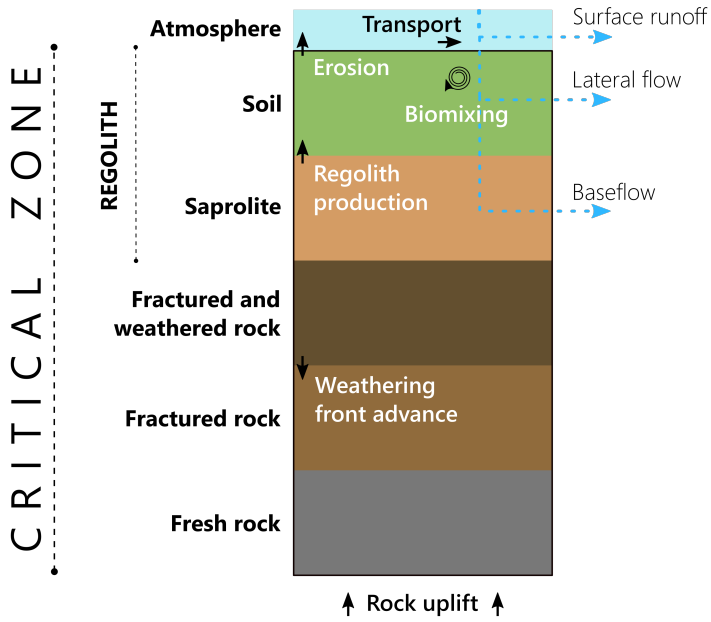

Figure 2.1: A conceptualization of the critical zone, including main layers and main processes. Modified from S. P. Anderson et al., 2007.

processes are found within the vertical range. On the lower part of the CZ, the weathering front evolves downwards, transforming rock into saprolite, increasing the regolith thickness. On the top soil, transport processes retrieve matter, decreasing the CZ thickness (S. P. Anderson et al., 2007). Depending on whether the relative rates of these processes are either balanced or biased, the situation of the CZ is steady or dynamic, respectively. In fact, a classification may be stated considering the thickness and vertical composition of the CZ: *transport-limited* areas where regolith is deep and depleted from solutes, and *weathering-limited* areas where the soil layer is thin or absent and other phases interact directly with rock (S. P. Anderson et al., 2002; S. P. Anderson et al., 2007). As a consequence of this spatial and temporal heterogeneity, the CZ shapes the landscape, determines the surface water composition at the watershed level, and it establishes hot spots for biogeochemical processes.

Understanding the processes given within the CZ and their implications on other cycles, especially in the hot spots and hot moments identification (McClain et al., 2003),

is key to gain understanding on the Earth system. Indeed, weathering is the main process in this CZ, comprising the breakdown of rocks into smaller parts (through regolith production), and the transfer of chemical compounds into water (through dissolution, ion exchange, redox, etc.) (S. P. Anderson et al., 2007). A previous study (McClain et al., 2003) has recommended stakeholders to take into consideration the spatial and temporal distribution of hot spots and hot moments, especially when assessing bioactive elements. This assessment relies on an accurate spatial and temporal assessment of the CZ processes.

Despite the great relevance that this zone poses on matter cycling, its *in situ* assessment is challenging due to the considerable heterogeneity found. Some recent studies have accomplished this using uranium-series isotopes (Guo et al., 2020). However, an alternative to win insights on these processes is using proxies instead, such as solid and dissolved exports carried by rivers (Keller, 2019). Many researchers have worked on such approaches at several scales, but their estimates vary even within the latest global reports (Milliman & Farnsworth, 2011). Even though great efforts have been put on understanding the drivers of these riverine loads and on assessing the implications of weathering in the environment, gaps of knowledge remain (S. P. Anderson et al., 2004).

2.3 The soil

Soil is the Earth's Crust uppermost layer, located over the *saprolite* layer within the *regolith* concept. It is an active and dynamic layer supporting life since it is an exchange zone for chemical compounds between the abiotic and biotic part of the ecosystem.

At the beginning, scientific interest on soil was linked to compound used to enhance plant growth, to improve crop yields. In contrast, nowadays' studies also focus on the role this layer poses on the ecosystem dynamics. Soil is described by the soil profile, a compilation of different layers (called *horizons*) distinguished based on physical, chemical, and biological properties. The overlaying layers are more strongly weathered, in

comparison with the lower horizons, which are more alike the parent material.

From a physical point of view, the soil is made of particles with different sizes, containing void spaces between them, called pores. Hence, *porosity* is a property of soil measuring its capacity to retain water or air. In contrast, the connectivity of these pores is described through the *hydraulic conductivity*. These two characteristics are relevant regarding the movement of elements over and within the soil layer. Surface runoff erodes the soil, retrieving and transporting particles within the ecosystem. In contrast, subsurface flow moves more slowly, and is responsible of soil *leaching*, the transport of compounds to lower layers of the soil, reaching the saprolite and parent material.

The soil particles react with water exchanging chemical compounds to form surface complexes. Not all the elements tend to associate equally, ions such as Ca^{2+}, Mg^{2+}, and Na^{+} are not strongly adsorbed, thus they tend to enter the biogeochemical cycles in the soil layer. The role of biology on soil conditions its evolution: micro and macrofauna in the rooting zone affects soil acidity, which has a profound impact on the chemical reactions given in it.

Because of the complexity of soil description, different classifications have been stated, being the *U.S. Soil Taxonomy* and the *FAO Soil groups* (by the United Nations), the most relevant a commonly used. Within the present PhD thesis, the FAO classification (FAO et al., 2012) will be used.

2.4 The water cycle

The diversity of water pathways through the environment driving the riverine matter transport reveals the relevance of the water cycle (or the hydrological cycle). Water is found in Earth close to the triple point–coexisting liquid, vapour, and solid phases–due to the energy received from the Sun and because of the polar characteristics of the H_2O molecule, water may dissolve compounds and act both as reservoir and vector of transport for matter and energy (Schaub & Turek, 2016). The largest water reservoir in

the Earth system is the ocean, where water receives solar energy and evaporates to the atmosphere (Stephens et al., 2020). Through wind transport and condensation, water precipitates over land or ocean and, when it falls on land, it enters the continental hydrological cycle. The *hydrological basin* concept is commonly used at this stage to assess the inland water movement towards other water bodies such as oceans or lakes.

2.4.1 The hydrological basin

A hydrological basin (or river basin) is a geographical unit delimited by a shared water routing network. It normally consists of an outlet which drains all waters reaching the surface of the basin, collected through a riverine network formed by tributaries and channels. Water is commonly a vector of transport for matter from land to ocean, hence the basin is usually regarded as an integrative approach to study the CZ and the matter cycles present within. Since the hydrological cycle is strongly affected by nowadays global change hazards, and its influence on other cycles is notorious (Stephens et al., 2020), many environmental assessments are performed at the river basin scale.

From the hydrological point of view, three main pathways may be described within a hydrological basin:

- *Surface runoff* appears when the amount of water the soil can retain—the soil's field capacity—is exceeded or the precipitation intensity is over the infiltration capacity. Precipitation water falling over these areas in these moments is transported over the ground surface, rather than infiltrated. Within a homogeneous soil, the capacity of the soil to retain water is characterised by the hydraulic conductivity and phreatic level. Normally, high phreatic levels are found when the slopes are low and there may appear a concavity within the downstream flowlines.
- *Sub-surficial runoff* (or lateral flow) happens when the horizontal hydraulic conductivity of a soil layer is larger than the vertical conductivity, which facilitates a lateral flux rather than a vertical movement.

- *Groundwater flow* (or baseflow) is related to the saturated zone of the CZ. Normally, precipitation water infiltrates down to the phreatic level, which normally determines the riverine baseflow during low flow periods. When the phreatic level meets the topographic height, baseflow is generated.

Conceptually, these fluxes are distributed vertically on the CZ, where sub-surficial runoff and groundwater flow are those in contact with the regolith, saprolite, and bedrock layers, and exchange ions which are later transported to the river. The residence time of each pathway has a great impact on the weathering process in the CZ, as shown by the composition of water found in rivers (Maher, 2011). Those residence times depend on several aspects of the hydrological basin, e.g. topography and vegetation, and they may vary from a few months or years in small headwater catchments to several decades in large watersheds (Maher, 2011).

2.4.2 Water as a vector of transport

Water interacts with many other cycles along the water cycle, both as reservoir and vector of transport. The later role implies that water transfer matter through continental, oceanic, and atmospheric environments. Focusing on the continental-to-ocean flux, rivers carry heterogeneous compounds spanning from solid matter in the form of particles or colloids to dissolved matter in ionic or aqueous forms (Bagnold, 1977; Meybeck, 1982). It may transport biology such as algae or other microorganisms as well (Ohte et al., 2007).

Recently, research studies have worked on evaluating riverine transport of suspended solids to assess soil loss through water erosion (Panagos et al., 2020), and to quantify carbon exports (Fabre et al., 2019), among other applications. They have also focused on dissolved exports to understand coastal plumes from riverine loads (Han et al., 2012; Horner-Devine et al., 2015). As stated before, the river water composition is conditioned by these loadings, which is commonly used as a proxy of the processes happening at

the basin scale.

Paying attention to the dissolved water chemistry, major composition is determined by the so-called *major ions* (Ca^{2+}, Mg^{2+}, Na^{+}, K^{+}, SO_4^{2-}, Cl^{-}, HCO_3^{-}, CO_3^{2-}, NO_3^{-}, PO_4^{3-}), which are those elements or compounds commonly presenting values over 1 $mg{\cdot}L^{-1}$ in solution, which commonly originate from rocks. At the global scale, PO_4^{3-} is studied in the phosphorus cycle, NO_3^{-} on the nitrogen cycle, (HCO_3^{-} + CO_3^{2-}) in the carbon cycle, and SO_4^{2-} in the sulphur cycle, but these elements share a strong relation to the inorganic part of the Earth system, derived from the geochemical cycle.

2.5 The geochemical cycle

Conceptually, the geochemical cycle comprises the chemical reactions involved with rocks, and it is commonly divided in two, depending on the where those processes occur: an internal geochemical cycle occurring within the Earth crust, and an external geochemical cycle happening over the crust. The external geochemical cycle has a more dynamic effect on surface water composition (Figure 2.2, Gucinski, 1999)

As stated before, the CZ spans from the soil surface to the bedrock, where weathering processes condition its evolution. Rocks are broken and dissolved releasing matter to soil and water, but all rocks don't react equally. The Jackson Silt and Clay Weathering Stages (Jackson et al., 1948) established a list of minerals depending on their sensibility to weathering, where gypsum and halite are the most susceptible to dissolve, while rutile, anatase, and ilmenite present the lowest sensibility (Bleam, 2017). A deeper explanation of weathering processes is present in section 2.5.2.

The dissolution of minerals is strongly determined by the environmental conditions of the CZ (water acidity, pressure, temperature, biodiversity) which enhance or impede water-rock interactions. Soil respiration–the decomposition of soil organic matter by biological activity–produces CO_2 ,which is dissolved into carbonic acid and later dissolves primary minerals. Not all minerals react equally, and some of them produce secondary

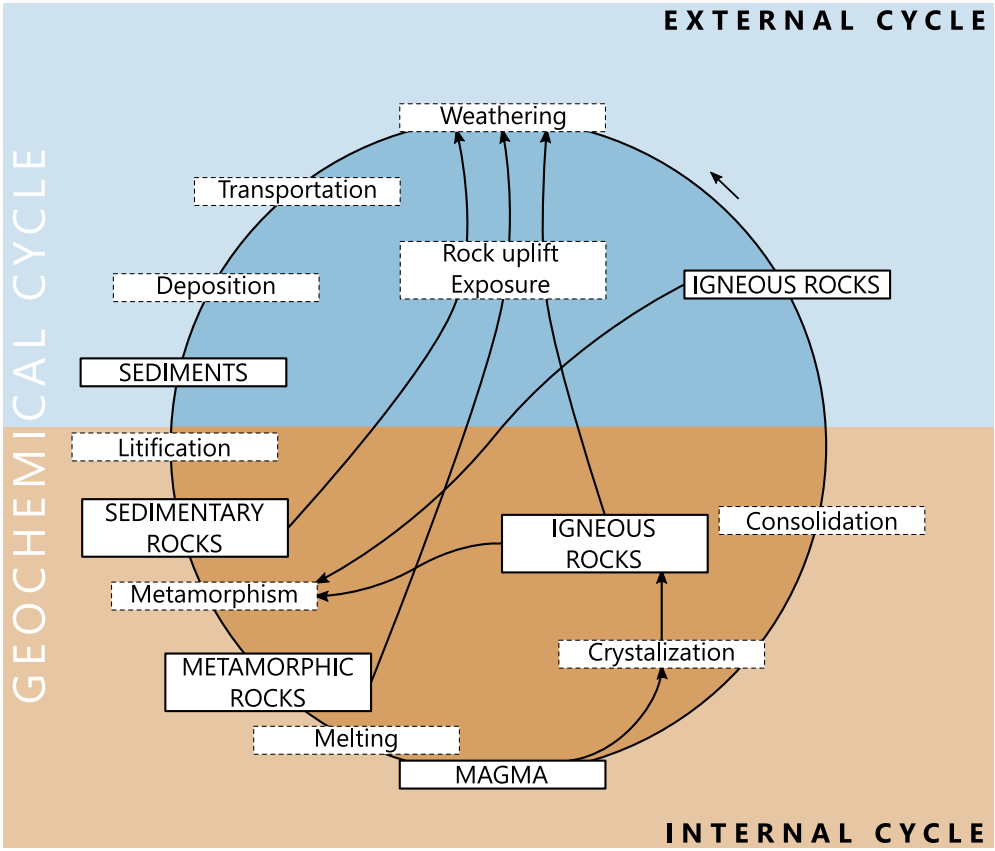

Figure 2.2: Conceptualization of the geochemical cycle. Modified from Bleam, 2017; Monroe et al., 1992.

minerals, the chemical processes are later discussed in section 2.5.2.

One of the most studied areas in this field is the implication of weathering on the carbon cycle, since the role of weathering on the carbon sequestration and on the long-term climate, has long been discussed (Amiotte Suchet & Probst, 1993b, 1995; Drake et al., 2018; Gaillardet et al., 1999; Hartmann et al., 2009; Velbel, 1993). Understanding and assessing weathering in the framework of the CZ at the global scale is of interest for biogeochemical cycling research, especially for the carbon cycle.

2.6 Rock weathering

The transformation of bedrock into soil needs together biological, physical, and chemical processes at the Earth's surface, and causes direct responses to the geosphere, the hydrosphere, and the atmosphere (S. P. Anderson et al., 2004; Schaub & Turek, 2016). The consequences of these complex processes include nutrients being fed to the ecosystem, components being transported between reservoirs, landscapes being shaped along a wide range of temporal and spatial scales, and carbon being sequestered conditioning long-term climate (S. P. Anderson et al., 2004; S. P. Anderson et al., 2007). Despite of the relevant consequences of weathering in the environment, there are large knowledge gaps to be fulfilled in order to understand *"how does the Earth weathering engine break down rock to nourish ecosystems, carve terrestrial landscapes, and control carbon dioxide in the global atmosphere"* (S. P. Anderson et al., 2004).

Weathering is the decay of rocks into soil under the influence of air, water, within biological activities, yielding residual minerals in soil and exporting solutes in water (Brantley et al., 2011; Keller, 2019; Riebe et al., 2017). It may be classified in *physical* weathering when the continuous rock is broken into smaller particles maintaining the original mineralogical composition, or *chemical* weathering when primary minerals are changed to secondary chemical compounds, exchanging matter with other physical phases such as water or air (Bleam, 2017). Weathering plays a fundamental role on the geochemical cycles and then on the global biogeochemical cycles. Thus understanding weathering is necessary to improve our knowledge on the Earth system and perform forecasts of the ecosystem evolution under different scenarios (Brantley et al., 2011).

S. P. Anderson et al., 2004 proposed several research questions to fuel the discussion on weathering processes, and some of the main challenges in this research field are included within these questions:

1. *"How can the dominant factors controlling chemical weathering be identified and their effects be quantified in a given environment and at various scales?*

2. *How can we advance our ability to predict weathering processes over the range of pertinent spatial scales, including mineral surfaces, laboratory reactors, soil profiles, catchments, and global systems?*
3. *In what ways are physical, chemical, and biological weathering processes coupled, and how can these couplings be elucidated and quantified?"*

The identification of which factors control weathering (Question 1) has been an object of study of several researchers who, among all variables studied, have highlighted the role of hydrology (Amiotte Suchet & Probst, 1993b; Bluth & Kump, 1994; Hartmann et al., 2009), lithology (Bluth & Kump, 1994; Hartmann et al., 2009; Kempe, 1979; Meybeck, 1987), temperature (Dessert et al., 2003; Hartmann, Moosdorf, et al., 2014), physical erosion (Syvitski et al., 2005), vegetation (Goddéris et al., 2006) (Gislason et al., 1996), and soil units (Hartmann, Moosdorf, et al., 2014). However, the spatial implications of these factors (Question 2) are not equally distributed (Hartmann, Moosdorf, et al., 2014). Thus, the coupling of physical, chemical, and biological processes (Question 3), as well as the prediction of weathering at different spatial and temporal scales, is still challenging.

Research has been done at different spatial scales, from the laboratory and catchment scales (Naisse et al., 2015; White et al., 2003) to global studies (Gaillardet et al., 1999; Syvitski et al., 2005). However, since the *in situ* evaluation of weathering is challenging, insights for these processes are commonly derived from proxy signals, such as riverine exports. Physical weathering is mostly responsible for suspended sediments (Millot et al., 2002) while chemical weathering releases dissolved matter (Minasny et al., 2008); thus the weathering implication on freshwater quality is notorious.

2.6.1 Physical weathering

Rocks are broken apart during physical weathering because of changes in temperature and pressure. The freeze-thaw process breaks rocks because of the expansion of water

when it freezes within the cracks and fractures. Exfoliation occurs because of changes in pressure due to erosion and rock uplift. Aeolian erosion is also common in places with windy weather and sandy terrain (Camuffo, 1995).

Most of the interest in physical weathering research is related to rock break and soil erosion, as well as in the production and transport of sediments through the riverine network (Borrelli et al., 2018; Panagos et al., 2020). It is expected that freeze-thaw cycles will become more frequent due to climate change, affecting soil and physical weathering rates (Henry, 2008). And one of the main consequences is that the smaller the rock grains are, the larger their reactive surface becomes, increasing chemical weathering rates and dissolved solid exports (Gaillardet et al., 1999).

2.6.2 Chemical weathering

Chemical weathering carries the transformation of primary minerals (gypsum, halite, calcite, dolomite, olivine, feldspar, etc.) into secondary minerals, releasing or precipitating matter, normally in the presence of water (Bleam, 2017). The dissolution of these minerals is strongly conditioned by the environmental conditions (water acidity, pressure, temperature, etc.) which enhance or impede water-rock interactions. Microorganisms in the upper-most layers of the CZ decay organic matter (CH_2O) through "soil respiration" (Reaction 2.1, combustion of the glucose) causing an increase of the CO_2 partial pressure (pCO_2) in soil. CO_2 is then dissolved by water (Reaction 2.2) creating carbonic acid (H_2CO_3), which decreases the pH conditions in water (Reaction 2.3), increasing acidity to better react with minerals.

$$CH_2(s) + O_2(g) \rightarrow CO_2(g) + H_2O(l) + ATP \quad (2.1)$$

$$CO_2(g) + H_2O(l) \rightarrow H_2CO_3(ac) \quad (2.2)$$

$$H_2CO_3(ac) \rightarrow HCO_3^-(ac) + H^+(ac) \quad (2.3)$$

Some of the primary minerals dissolve producing secondary minerals, such as in the case of the albite (Reaction 2.4), the orthoses (Reaction 2.5) or the anorthite (Reaction 2.6), however not all reactions produce them. In the case of the olivine (Reaction 2.7), the calcite (Reaction 2.8) or the halite (Reaction 2.9), the result of these reactions are soluble products such as major ions. These equations release anions and cations to the aqueous solution, conditioning the major ion composition and major ion chemistry of surface waters. Reaction 2.4 to Reaction 2.8 happen under acidic condition, generally affected by carbonic acid derived from soil respiration (Bleam, 2017). But not all the water-rock interaction is driven by acids, such as in the case of the halite (Reaction 2.9) or when oxidation is a relevant process, as in the case of the pyrite (Reaction 2.10).

$$2NaAlSi_3O_8(s) + 2HCO_3^-(aq) + 2H^+(aq) + 9H_2O(l) \rightarrow$$
$$\rightarrow \quad Al_2Si_2O_5(OH)_4(s) + 2Na^+(aq) + 2HCO_3^-(aq) + 4H_4SiO_4(aq) \qquad (2.4)$$

$$2KAlSi_3O_8(s) + 2CO_2 + 6H_2O(l) \rightarrow$$
$$\rightarrow \quad Al_2Si_4O_{10}(OH)_2(s) + 2K^+(aq) + 2HCO_3^-(aq) + 2H_4SiO_4(aq) \qquad (2.5)$$

$$CaAl_2Si_2O_8(s) + 2CO_2 + 2H_2O(l) \rightarrow$$
$$\rightarrow \quad Al_2Si_2O_5(OH)_4(s) + Ca^{2+}(aq) + 2HCO_3^-(aq) \qquad (2.6)$$

$$Mg_2SiO_4(s) + 4CO_2 + 4H_2O(l) \rightarrow$$
$$\rightarrow \quad 2Mg^{2+}(aq) + 4HCO_3^-(aq) + H_4SiO4(ac) \qquad (2.7)$$

$$CaCO_3(s) + CO_2 + H_2O(l) \quad \rightarrow \quad Ca^{2+}(aq) + 2HCO_3^-(aq) \qquad (2.8)$$

$$NaCl(s) + H_2O(l) \quad \rightarrow \quad Na^+(aq) + Cl^-(aq) + H_2O(l) \qquad (2.9)$$

$$2FeS_2(s) + 15/2O_2(g) + 4H_2O(l) \rightarrow Fe_2O_3(s) + 4SO_4^{2-}(aq) + 8H^+(aq) \quad (2.10)$$

These water-rock interactions are similar between groups of minerals, and some researchers have worked on mapping the abundance of minerals at different spatial scales. For instance, Amiotte Suchet et al. (2003) established a worldwide 1°x1° grid map where they classified the rock in six lithological classes (sand and sandstone, carbonate rocks, shales, shield rocks, acid volcanic rocks, and basalts) and ice. Later, Dürr et al. (2005) focused not on the geological characteristics of rocks, but on their susceptibility to chemical weathering, creating a 17 classes lithological map. Finally, the most recent global lithological map is that presented by Hartmann and Moosdorf (2012), where they followed a similar classification to that of Dürr et al. (2005) but considering three levels of rock characterisation. The development of this kind of maps reflects the research interest on the assessment of weathering at the global scale, where lithology is a dominant factor.

Traditionally, geochemists have been interested in understanding the origin and transformation of minerals, but chemical weathering has gained a more interdisciplinary interest nowadays. Physical geographers evaluate landscape evolution (S. P. Anderson et al., 2002; Slessarev et al., 2019; Whipple et al., 2000), biogeochemists focus on the biological use of the different elements (O. R. Anderson, 2016), oceanographers are interested in quantifying the riverine input to coastal zones (Sun et al., 2016), ecologists need the temporal and spatial evolution of salinity (Herbert et al., 2015), and water stakeholders need to know whether water complies to the quality standard for irrigation or drinking purposes (Meybeck, 2003). In addition, researchers are interested in the implications of chemical weathering on climate regulation at geological time scales (J. L. Probst, 1992).

In general, all these interests are related to biogeochemical cycles, i.e. the movement of matter between reservoirs in the environment. Weathering—and especially chemical weathering—is a process responsible for the matter transfer between rocks and water which determines the chemical composition of surface waters, conditioning the

amount of dissolved matter reaching the oceans. The estimation of the dissolved matter delivered from land to ocean has been a common subject of study for over a century, when the first rough estimation of Clarke (1924) quantified the delivery of dissolved matter to $2{,}735 \cdot 10^6$ Mg·y^{-1} after collecting data on numerous rivers and tributaries in the US continuum, and the results from other researches outside the United States. Almost 40 years later, Livingstone (1963) revised this estimate by proposing $3{,}905 \cdot 10^6$ Mg·y^{-1}, following a similar methodology to that presented by Clarke but modifying the hydrological description of river discharges. Later, Meybeck (1979) again modified this estimate and clarified the anthropogenic input, by accounting the natural exports at $3{,}718 \cdot 10^6$ Mg·y^{-1} and specifying the results by each ion. A similar value for the total dissolved matter and each major ion was estimated by J. L. Probst (1992), ranging from $3{,}981 \cdot 10^6$ to $4{,}080 \cdot 10^6$ Mg·y^{-1}. A diverging value was then estimated by Gaillardet et al. (1999) which estimated the chemical weathering derived flux in $2{,}131 \cdot 10^6$ Mg·y^{-1}, after considering the 60 largest rivers and extrapolating this value to the rest of the continuum. The last estimate is also the lowest, $1{,}439 \cdot 10^6$ Mg·y^{-1} estimated by Hartmann, Moosdorf, et al. (2014) after using a spatially explicit, empirical model fitted for a large number of samples, but all of them sited at the Japanese Archipelago.

The heterogeneity of the results presented along the last century highlights the large uncertainty existing on the dissolved exports estimation. Despite of the efforts put by previous researchers on assessing not only the total dissolved exports, but the individual ion exports, and even the reported relevance of assessing water quality at a global scale (Syvitski et al., 2005; Vörösmarty et al., 2010), any consensus has not been reached yet. The accurate estimation of this budget is necessary in the frame of the carbon cycle since, despite of not being the most important pathway on the global cycle, its influence on the long-term climate has been noticed (Amiotte Suchet & Probst, 1993b, 1995; Gaillardet et al., 1999; Hartmann et al., 2009; Velbel, 1993).

Recent approaches to estimate the dissolved solid exports at the global scale (Hartmann, Moosdorf, et al., 2014) have moved towards the development of spatially explicit models concerning the chemical weathering rates. This modelling exercise is challenging due to the amount of input data needed to perform the analysis, which is commonly

not available and the model configuration choice, which may carry large uncertainty on the estimates.

2.7 Hydro-geochemical modelling

A model is a simplification of the reality (Abbott et al., 1986) used to understand, describe, or assess systems. According to COX (2003) definition, "*(...) a water-quality model can mean anything from a simple empirical relationship, through a set of mass balance equations, to a complex software suite*". In Earth system analysis, and more specifically in cycling, the use of modelling approaches is common. Regarding the water and the geochemical cycles, there are numerous independent models, called respectively *hydrological* and *geochemical* models, but those that integrate these kind of cycles–commonly called *hydro-geochemical* models–are not so common.

2.7.1 Hydrological modelling

Hydrological modelling is the representation of real hydrologic systems and features by using small-scale physical models, mathematical models, and computer simulations (Allaby, 2020; Devi et al., 2015). In general, three steps are found when modelling a hydrological system: the conceptualization of the system, the mathematical model set up, and the numerical code application (Yu, 2015). The conceptualization—or simplification—of the hydrological system usually regards to the level of detail in the spatial description, yielding lumped, semi-distributed, or distributed models. Lumped models are usually applied at a single point (e.g. an outlet), and the parameters used are an average of the area studied (the basin); semi-distributed models spread the description of the model in homogeneous spatial units; and distributed models uniformly discretize the spatial area, usually following a grid-approach (Epelde Beraza, 2015).

The mathematical choice of the model represents how the physical processes are

represented: mechanistic models are based on physical laws, empirical models serve of correlations between output and input variables, and conceptual models semantically or graphically represent the conceptualization of the system. Because of the complexity of some systems, the mathematical models are normally implemented in numerical codes, where the input data are transformed in output results by means of several parameters and equations (M. P. Anderson et al., 2015).

Two other classifications exist for hydrological models: based on the type of their results, and the temporal scope of the phenomena. Based on the type of their outputs, models may be stochastics when they produce an estimation of the liability of the results, or deterministic if they yield a single result as a function of a single input. Considering the temporal scope, they may be event-based when considering a single moment, or continuous if the variables are expressed over a time series. A summary of these modelling classifications is shown in Figure 2.3. The choice of a model is based on the intended use of the results, the modelling objectives, and the performance expectations (ASABE, 2017), but in many occasions, the choice of a model is also conditioned by the input data and computational resource availability.

Numerical models, i.e. the implementation of the mathematical approach normally in software, is based on parameters and variables. Parameters are constant site-specific values which characterise the processes for the hydrological system of study. Examples of hydrological parameters could be the hydraulic conductivity or soil roughness. Variables are those describing the phenomena and may vary with time. Three types of variables are possible: input variables regarding the forcings of the model (e.g. precipitation, temperature, topography, etc.), output variables concerning the results of the models (discharge, erosion, exports, etc.), and the state variables, regarding several conditions of the model affecting the input and output variables (phreatic level, soil humidity, etc.) (Epelde Beraza, 2015).

Even though there are numerous numerical codes for hydrological modelling, the underlaying basis are commonly shared (Jajarmizadeh et al., 2012), thus their applicability is dependent on the previous characteristics indicated for model choice. A recent

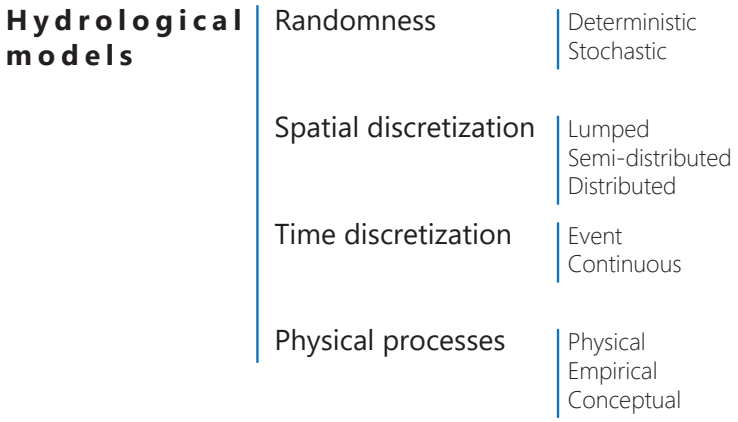

Figure 2.3: Classification of hydrological models, adapted from Epelde Beraza (2015) and Meaurio Arrate (2017).

review (Fu et al., 2019) on water quality modelling has shown that the Soil and Water Assessment Tool (SWAT) is the most used by researchers on catchment studies.

2.7.2 Geochemical modelling

Geochemical modelling studies the chemical processes (dissolution, redox, etc.) affecting geologic systems (solid Earth, rocks). The *low-temperature* systems are mostly focused on aqueous solutions assessments such as assessing the composition of natural waters, or understanding the formation and dissolution of rocks under external agents (acids, wastes, steam, etc.).

Historically, Garrels and Thompson (1962) first applied chemical modelling to geochemistry, developing an *equilibrium model* to predict species distributions and other properties without mass change (reversible reactions). Later, Garrels and Mackenzie (1967) simulated reactions with mass change (irreversible reactions), creating the first *reaction path model*. Soon, Helgeson et al. (1969) created the first software to solve equilibrium and reaction path problems, with which they studied weathering among other applications. Models' structures evolved from their formulation (differential equations

to algebraic) to their conceptualization (elements to compounds). Nowadays, there is a new kind of model: the *reactive transport model*, which cover the reaction path with transport processes through different porous media.

There are two approaches in geochemical modelling: *direct* and *inverse* modelling, whether the input data describe the initial phases or the final conditions, respectively. Commonly, the results are the other variables not used as input. There is a large list of processes covered in reaction-transport modelling, including geochemical reactions (dissolution/precipitation, acid/base, redox, etc.), mass transport (advection, diffusion, dispersion, etc.), heat transport (advection, conduction, convection, etc.), or medium transformation (compression/expansion, fracture, etc.).

There is a great challenge in reactive transport modelling: the large amount of detailed data needed to set up a project, regarding physical, chemical, hydrological, biological, and other characteristics of the field area and time of studies. This challenge commonly forces modellers to apply several simplifications and assumptions, creating uncertainty on the model results and insights derived from the modelling, while other times conditions the choice of the model.

Even though there are fewer geochemical than hydrological models, many numerical codes are available to conduct geochemical modelling, among them:

- **PHREEQC** (Parkhurst, 1995), designed for aqueous calculations (equilibrium and reaction path model for reversible and irreversible reactions, respectively) with transport modules to make direct or inverse calculations. Input data includes specification of the elements, reactions, mineral and gas phases, as well as rate expressions.
- **The Geochemist's workbench (GWB)** (Bethke & Yeakel, 2018), also designed for aqueous calculations (equilibrium and reaction path modelling) which may be coupled to hydrologic transport models to perform reactive-transport modelling. It may work coupled to MODFLOW. The input data also needs the initial elements and phases, as well as constraints regarding temperature, partial pressure, activi-

ties..., then depending on the program used, several processes are considered.

- **The MIN3P** (Mayer et al., 2011) is a reactive transport code designed to compute aqueous calculations between different phases.
- **CrunchFlow** (Steefel et al., 2015) is a reactive transport model where the input data includes identifying the elements and phases, temperature, reaction rates, reaction path or equilibrium modelling, how to compute the activity coefficients, etc.
- **HYDROGEOCHEM** (Yeh & Sun, 2004) is a reactive transport model issued to simulate aqueous solutions problems. It needs the initial elements, phases, and rates for all reactions. The boundary conditions are difficult to establish and need for a spatially explicit result.
- **PHAST** (Parkhurst et al., 2010) is a transport model with geochemical reaction modules. With input data identical to PHREEQC.
- **Reaktoro** (Leal & Saar, 2018) is reactive transport model designed with C++ and Python, which needs to define elements and phases, as well as system variables such as temperature and pressure, the reactions, and initial conditions.

In general, all these mechanistic models follow a similar approach regarding its model structure and input data requirements. These requirements are a barrier for large scale applications, such as global assessment.

Another mechanistic model designed for weathering assessments at the catchment scale is the WITCH model (Goddéris et al., 2006), which also uses elemental identification, phases characterisation, and initial boundary conditions for its modelling exercise. The main difference with previous models is its spatial characterisation, not distributed but lumped, at a basin scale. It has been used for soil water characterisation, but stream water description needs further refinement.

A different approach is present when studying chemical weathering and its implication on the C or P cycles, such as the empirical approach. Models such as the GEM-CO2

(Amiotte Suchet & Probst, 1995) or the CWR (Hartmann, Moosdorf, et al., 2014) have already been used to estimate a first large-scale snapshot of these processes. The main advantage of these model configurations is the lower input data demand, but the largest drawback is the large uncertainty on their results due to the simple structure of the model. Nonetheless, they have been shown as useful and capable of capturing large amounts of variance of the observed variables.

At the beginning of this PhD, such an empirical approach is the only one capable of assessing chemical weathering and the major ionic fluxes at the global scale, as well as estimating its role on other relevant cycles at large spatial scales.

2.7.3 Modelling chemical weathering

Chemical weathering, being the combination of all chemical reactions that transfer matter from rock to water to be eventually transported in rivers, may be assessed using hydro-geochemical modelling. Physically-based models may estimate the concentrations of water in the porous media underground, considering both equilibrium and kinetics, which eventually drives the development of the weathering front and the composition of riverine water. However, the main challenge in hydrogeochemical modelling is the application of physically-based models to large spatial or temporal scales, mainly derived from a mismatch between the input data needs and the input data availability, as well as the constraint of computational resources. A model is only useful and efficient if there is enough data to feed it.

The study of chemical weathering at local sites, such as that presented by Apollaro et al. (2019), is suitable for application of physically-based geochemical models since the input data (including mineral abundance, the initial composition of the aqueous solution, or other thermodynamic data) is available. A similar approach may be followed at the basin scale, as shown by the WITCH model (Goddéris et al., 2006) but needing the establishment of several hypotheses. In the WITCH model, the soil is conceptualized as “boxes” where the input data is similar as in the previous study (initial aqueous

solution, mineral abundance, and kinetic data). Another example of the integration of a geochemical model in a hydrological model is that recently presented by Bailey et al., 2019 where they based their calculation on the spatial conceptualization of the Soil and Water Assessment Tool (SWAT) (Arnold, Allen, et al., 1995) model, but again needing detailed input data description.

When considering larger approaches, such as the global scale, the application of physically-based models is not possible since there is no description of all mineralogical abundances, nor the data of the initial solution composition, nor possible consideration of all potential case-specific situations. At such scales, there is the need of a coarser simplification of the process, such as those presented by Meybeck (1987), Amiotte Suchet and Probst (1995), Gaillardet et al. (1999), or Hartmann, Moosdorf, et al. (2014). In these cases, the approach followed is the consideration of the key factors controlling the process which are available worldwide, such as the lithological description (not by means of minerals, but by rock types), the hydrological cycle, or the main contributions of relevant variables.

An interesting recent approach is that followed by Hartmann, Moosdorf, et al. (2014) since they assessed the main drivers of chemical weathering in several basins of the Japanese archipelago (Hartmann, 2009) and extrapolated these drivers to the world in the later study. Such an approach is based on the considerations that the parameters fitted at the Japanese Archipelago are suitable for worldwide applications. This modelling scheme has been proved valid for large scale studies to estimate the worldwide distribution of chemical weathering.

Regarding the temporal scale, biogeochemical and geochemical cycles are usually estimated at the annual scale. However, the kinetics of the reactions may require that geochemical models compute shorter periods of time to account not only for the reaction itself but for the residence time of the water within the porous media (Maher, 2010, 2011; Maher & Druhan, 2014). Riverine dissolved matter budgets may vary at lower timescales than the year, causing that annual average values may not be representative of the hot spots and hot moments regarding these processes. The estimation of such

places and moments is relevant for the understanding of the processes, and research should be focused on those moments and places (McClain et al., 2003).

2.8 Research question, hypotheses, and objectives

The present research work studies the field of hydro-geochemistry, understood as the group of geological processes happening on the critical zone where chemical reactions transfer matter between rocks and water, conditioning freshwater composition. More precisely, this PhD thesis focuses on the applied science of hydro-geochemical modelling, by aiming to develop a tool that is useful for researchers working on biogeochemical cycling at various spatial and temporal scales.

Hydro-geochemistry is the intersection of three established fields of modern science: hydrology, geology, and chemistry, i.e. the study of water, rocks, and matter. Research on this field has focused on identifying the factors conditioning the transfer of mass; on understanding the processes and pathways of this transfer; as well as on assessing those factors and processes within spatial and temporal contexts. Known how the matter is transferred and what affects this transfer, the fundamental basis of this field is set. Recent research efforts have focused on measuring when and where these processes occur, and on which are the impacts of these changes on the environment.

The assessments of when and where these processes occur are normally performed through field surveys (such as monitoring programs, sampling campaigns...) or modelling techniques, which have the advantage of being able to simulate scenarios to assess potential impacts. The main challenge for modellers is to find a compromise between the complexity of the modelling tools, and the scope of the study they are working on. Complexity in a model may be measured through the amount of input data and resources needed to yield results, small projects (in terms of spatial and temporal resolution) are suitable for complex models needing a large amount of detailed data for their performance, and yield results with higher accuracy and lower uncertainty. On

the contrary, the use of such complex techniques is constrained to the data availability or the computing resources, though they need to apply assumptions or less complex configurations to be able to accomplish their aims, yielding results with larger uncertainties. Thus, complex mechanistic models are less flexible in terms of model set up and application, while empirical models allow for useful insights even though their uncertainty, they are more flexible when setting them up.

2.8.1 Research question

The research question that we pose has been taken from S. P. Anderson et al. (2004): *"(...) how can the dominant factors controlling chemical weathering be identified and their effects be quantified in a given environment and at various scales?"*

2.8.2 Hypothesis and objectives

Previous literature on biogeochemical cycles has highlighted the relevance of weathering processes in the critical zone, emphasising the role of chemical weathering on the matter transfer from the geochemical cycles to other biogeochemical cycles by means of water. The scientific context presented in this chapter has recognised the gaps of knowledge present regarding the role of chemical weathering on the Earth system and, despite of the recent works performed at large scales, great effort is still needed on providing input data and developing tools to support field studies. In this sense, the main objective of the present PhD thesis is ***to assess the role of chemical weathering on biogeochemical cycling, paying special attention to the major ion fluxes derived from rocks, by means of modelling this process at different spatial and temporal scales.***

Considering the literature on the subject, several hypotheses (H) have been formulated or recuperated from previous works, for which partial objectives (O) are stated in the following lines:

H1 Annual average ionic fluxes derived from chemical weathering of rocks at the global scale may be described as a function of several main drivers regarding draining basin characteristics such as lithology, soil structure, climate, and hydrology.

O1 Identify main drivers on chemical weathering at the global scale, paying special attention to their influence for each of the major ion governing the surface water composition (*Chapter 4*).

O2 Develop a model to global annual average ionic fluxes derived from chemical weathering of rocks, based on the main drivers identified (*Chapter 4*).

H2 Within the annual scale, the main responsible of ionic fluxes temporal evolution is hydrology; thus, the downscaling of the global parameters at the regional and local scale is conditioned to the representativity of the hydrological cycle.

O3 Evaluate the global model and globally fitted parameters at different spatial and temporal scales on the estimation of ionic fluxes (*Chapter 5* and *Chapter 6*).

H3 Even though the current chemical weathering rates remain stable before 2100, hydrological changes would lead to a modification of the hot spots and hot moments regarding ionic fluxes delivery (Brantley et al., 2011), causing a shift on the carbon sequestration dynamics at the global scale.

O4 Apply the model to estimate the impact of chemical weathering on the global carbon sequestration (*Chapter 7*).

The results presented in this work are relevant for environmental scientists and modellers on biogeochemical cycling, especially for those working at large-scale studies or when the first snapshot of their system is needed, and the data availability or computing resources are limited.

Bibliography

Abbott, M. B., Bathurst, J. C., Cunge, J. A., O'Connell, P. E., & Rasmussen, J. (1986). An introduction to the European Hydrological system - systeme hydrologique europeen, "SHE", 1:History and Philosophy of a physically-based, distributed modelling system. *Journal of Hydrology*, *87*, 45–59. https://doi.org/10.1016/0022-1694(86)90114-9

Allaby, M. (2020). *A Dictionary of Geology and Earth Sciences* (5th ed.). Oxford Publisher Press. https://doi.org/10.1093/acref/9780198839033.001.0001

Amiotte Suchet, P., & Probst, J. L. (1993b). Modelling of atmospheric CO2 consumption by chemical weathering of rocks: Application to the Garonne, Congo and Amazon basins. *Chemical Geology*, *107*(3-4), 205–210. https://doi.org/10.1016/0009-2541(93)90174-H

Amiotte Suchet, P., & Probst, J. L. (1995). A global model for present-day atmospheric/soil CO2 consumption by chemical erosion of continental rocks (GEM-CO2). *Tellus B*, *47B*(1-2), 273–280. https://doi.org/10.1034/j.1600-0889.47.issue1.23.x

Amiotte Suchet, P., Probst, J. L., & Ludwig, W. (2003). Worldwide distribution of continental rock lithology: Implications for the atmospheric/soil CO2 uptake by continental weathering and alkalinity river transport to the oceans. *Global Biogeochemical Cycles*, *17*(2). https://doi.org/10.1029/2002GB001891

Anderson, M. P., Woessner, W. W., & Hunt, R. J. (Eds.). (2015). *Applied Groundwater Modelling*. Academic Press. https://doi.org/10.1016/C2009-0-21563-7

Anderson, O. R. (2016). The Role of Heterotrophic Microbial Communities in Estuarine C Budgets and the Biogeochemical C Cycle with Implications for Global Warming: Research Opportunities and Challenges. *The Journal of eukaryotic microbiology*, *63*(3), 394–409. https://doi.org/10.1111/jeu.12279

Anderson, S. P., Blum, J., Brantley, S. L., Chadwick, O., Chorover, J., Derry, L. A., Drever, J. I., Hering, J. G., Kirchner, J. W., Kump, L. R., Richter, D., & White, A. F. (2004). Proposed initiative would study Earth's weathering engine. *EOS*, *85*(28), 265–269. https://doi.org/10.1029/2004EO280001

Anderson, S. P., Dietrich, W. E., & Brimhall Jr, G. H. (2002). Weathering profiles, mass-balance analysis, and rates of solute loss: Linkages between weathering and erosion in a small, steep catchment. *GSA Bulletin*, *114*(9), 1143–1158. https://doi.org/10.1130/0016-7606(2002)114{\%}3C1143:WPMBAA{\%}3E2.0.CO;2

Anderson, S. P., von Blanckenburg, F., & White, A. (2007). Physical and Chemical Controls on the Critical Zone. *Elements*, *3*(5), 315–319. https://doi.org/10.2113/gselements.3.5.315

Apollaro, C., Perri, F., Le Pera, E., Fuoco, I., & Critelli, T. (2019). Chemical and minero-petrographical changes on granulite rocks affected by weathering processes. *Frontiers of Earth Science*, *13*(2), 247–261. https://doi.org/10.1007/s11707-018-0745-5

Arnold, J. G., Allen, P. M., Muttiah, R. S., & Bernhardt, G. (1995). Automated Base Flow Separation and Recession Analysis Techniques. *Ground Water*, *33*(6), 1010–1018. https://doi.org/10.1111/j.1745-6584.1995.tb00046.x

ASABE. (2017). Guidelines for calibrating, validating, and evaluating hydrologic and water quality (H/WQ) models. https://elibrary.asabe.org/abstract.asp?aid=47804

Bagnold, R. A. (1977). Bed load transport by natural rivers. *Water Resources Research*, *13*(2), 303–312. https://doi.org/10.1029/WR013i002p00303

Bailey, R. T., Tavakoli-Kivi, S., & Wei, X. (2019). A salinity module for SWAT to simulate salt ion fate and transport at the watershed scale. *Hydrology and Earth System Sciences*, *23*(7), 3155–3174. https://doi.org/10.5194/hess-23-3155-2019

Bethke, C. M., & Yeakel, S. (2018). GWB Essentials Guide. https://www.gwb.com/pdf/GWB11/GWBessentials.pdf

Bleam, W. (2017). *Soil and Environmental Chemistry*. Academic Press. https://doi.org/10.1016/C2015-0-01022-X

Bluth, G. J. S., & Kump, L. R. (1994). Lithologic and climatologic controls of river chemistry. *Geochimica et Cosmochimica Acta*, *58*(10), 2341–2359. https://doi.org/10.1016/0016-7037(94)90015-9

Borrelli, P., van Oost, K., Meusburger, K., Alewell, C., Lugato, E., & Panagos, P. (2018). A step towards a holistic assessment of soil degradation in Europe: Coupling on-

site erosion with sediment transfer and carbon fluxes. *Environmental research*, *161*, 291–298. https://doi.org/10.1016/j.envres.2017.11.009

Brantley, S. L., Megonigal, J. P., Scatena, F. N., Balogh-Brunstad, Z., Barnes, R. T., Bruns, M. A., van Cappellen, P., Dontsova, K., Hartnett, H. E., Hartshorn, A. S., Heimsath, A., Herndon, E., Jin, L., Keller, C. K., Leake, J. R., McDowell, W. H., Meinzer, F. C., Mozdzer, T. J., Petsch, S., … Yoo, K. (2011). Twelve testable hypotheses on the geobiology of weathering. *Geobiology*, *9*(2), 140–165. https://doi.org/10.1111/j.1472-4669.2010.00264.x

Camuffo, D. (1995). Physical weathering of stones. *The Science of the total environment*, *167*, 1–14. https://doi.org/10.1016/0048-9697(95)04565-I

Clarke, F. W. (1924). The data of geochemistry. https://doi.org/10.3133/b770

COX, B. (2003). A review of currently available in-stream water-quality models and their applicability for simulating dissolved oxygen in lowland rivers. *The Science of the total environment*, *314-316*, 335–377. https://doi.org/10.1016/S0048-9697(03)00063-9

Dessert, C., Dupré, B., Gaillardet, J., François, L. M., & Allègre, C. J. (2003). Basalt weathering laws and the impact of basalt weathering on the global carbon cycle. *Chemical Geology*, *202*(3-4), 257–273. https://doi.org/10.1016/j.chemgeo.2002.10.001

Devi, G. K., Ganasri, B. P., & Dwarakish, G. S. (2015). A Review on Hydrological Models. *Aquatic Procedia*, *4*, 1001–1007. https://doi.org/10.1016/j.aqpro.2015.02.126

Drake, T. W., Raymond, P. A., & Spencer, R. G. M. (2018). Terrestrial carbon inputs to inland waters: A current synthesis of estimates and uncertainty. *Limnology and Oceanography Letters*, *3*(3), 132–142. https://doi.org/10.1002/lol2.10055

Dürr, H. H., Meybeck, M., & Dürr, S. H. (2005). Lithologic composition of the Earth's continental surfaces derived from a new digital map emphasizing riverine material transfer. *Global Biogeochemical Cycles*, *19*(4). https://doi.org/10.1029/2005GB002515

Epelde Beraza, A. M. (2015). *Modelización de procesos hidrológicos y de contaminación por nitratos mediante dos códigos numéricos (SWAT y MOHID). Cuenca agrícola del río Alegria (País Vasco)* (Doctoral dissertation). Universidad del País

Vasco/Euskal Herriko Unibertsitatea. Leioa. http://hdl.handle.net/10810/15954

Fabre, C., Sauvage, S., Tananaev, N., Noël, G. E., Teisserenc, R., Probst, J. L., & Sánchez-Pérez, J. M. (2019). Assessment of sediment and organic carbon exports into the Arctic ocean: The case of the Yenisei River basin. *Water research*, *158*, 118–135. https://doi.org/10.1016/j.watres.2019.04.018

FAO, IIASA, ISRIC, ISS-CAS, & JRC. (2012). Harmonized World Soil Database (version 1.2). http://www.fao.org/soils-portal/soil-survey/soil-maps-and-databases/harmonized-world-soil-database-v12/en/

Fu, B., Merritt, W. S., Croke, B. F., Weber, T. R., & Jakeman, A. J. (2019). A review of catchment-scale water quality and erosion models and a synthesis of future prospects. *Environmental Modelling & Software*, *114*, 75–97. https://doi.org/10.1016/j.envsoft.2018.12.008

Gaillardet, J., Dupré, B., Louvat, P., & Allègre, C. J. (1999). Global silicate weathering and CO2 consumption rates deduced from the chemistry of large rivers. *Chemical Geology*, *159*, 3–30. https://doi.org/10.1016/S0009-2541(99)00031-5

Garrels, R. M., & Mackenzie, F. T. (1967). Origin of the Chemical Compositions of Some Springs and Lakes. *Advances in chemistry*, *67*, 222–242. https://doi.org/10.1021/ba-1967-0067.ch010

Garrels, R. M., & Thompson, M. E. (1962). A chemical model for sea water at 25ºC and one atmophere total pressure. *American Journal of Science*, *260*, 57–66. https://doi.org/10.2475/ajs.260.1.57

Goddéris, Y., & Brantley, S. L. (2013). Earthcasting the future Critical Zone. *Elementa: Science of the Anthropocene*, *1*, 000019. https://doi.org/10.12952/journal.elementa.000019

Goddéris, Y., François, L. M., Probst, A., Schott, J., Moncoulon, D., Labat, D., & Viville, D. (2006). Modelling weathering processes at the catchment scale: The WITCH numerical model. *Geochimica et Cosmochimica Acta*, *70*(5), 1128–1147. https://doi.org/10.1016/j.gca.2005.11.018

Gucinski, H. (1999). Cycles, geochemical. *Environmental Geology* (pp. 107–109). Springer Netherlands. https://doi.org/10.1007/1-4020-4494-1{\textunderscore}69

Guo, J., Ma, L., Gaillardet, J., Sak, P. B., Pereyra, Y., & Engel, J. (2020). Reconciling chemical weathering rates across scales: Application of uranium-series isotope systematics in volcanic weathering clasts from Basse-Terre Island (French Guadeloupe). *Earth and Planetary Science Letters*, *530*, 115874. https://doi.org/10.1016/j.epsl.2019.115874

Han, A., Dai, M., Kao, S.-J., Gan, J., Li, Q., Wang, L., Zhai, W., & Wang, L. (2012). Nutrient dynamics and biological consumption in a large continental shelf system under the influence of both a river plume and coastal upwelling. *Limnology and Oceanography*, *57*(2), 486–502. https://doi.org/10.4319/lo.2012.57.2.0486

Hartmann, J. (2009). Bicarbonate-fluxes and CO2-consumption by chemical weathering on the Japanese Archipelago — Application of a multi-lithological model framework. *Chemical Geology*, *265*(3-4), 237–271. https://doi.org/10.1016/j.chemgeo.2009.03.024

Hartmann, J., Jansen, N., Dürr, H. H., Kempe, S., & Köhler, P. (2009). Global CO2-consumption by chemical weathering: What is the contribution of highly active weathering regions? *Global and Planetary Change*, *69*(4), 185–194. https://doi.org/10.1016/j.gloplacha.2009.07.007

Hartmann, J., & Moosdorf, N. (2012). The new global lithological map database GLiM: A representation of rock properties at the Earth surface. *Geochemistry, Geophysics, Geosystems*, *13*(12). https://doi.org/10.1029/2012GC004370

Hartmann, J., Moosdorf, N., Lauerwald, R., Hinderer, M., & West, A. J. (2014). Global chemical weathering and associated P-release — The role of lithology, temperature and soil properties. *Chemical Geology*, *363*, 145–163. https://doi.org/10.1016/j.chemgeo.2013.10.025

Hedges, J. I. (1992). Global biogeochemical cycles: progress and problems. *Marine Chemistry*, *39*, 67–93. https://doi.org/10.1016/0304-4203(92)90096-S

Helgeson, H. C., Garrels, R. M., & Mackenzie, F. T. (1969). Evaluation of irreversible reactions in geochemical processes involving minerals and aqueous solutions-II Applications. *Geochimica et Cosmochimica Acta*, *33*, 455–481. https://doi.org/10.1016/0016-7037(69)90127-6

Henry, H. A. L. (2008). Climate change and soil freezing dynamics: historical trends and projected changes. *Climatic Change*, *87*(3-4), 421–434. https://doi.org/10.1007/s10584-007-9322-8

Herbert, E. R., Boon, P., Burgin, A. J., Neubauer, S. C., Franklin, R. B., Ardón, M., Hopfensperger, K. N., Lamers, L. P. M., & Gell, P. (2015). A global perspective on wetland salinization: ecological consequences of a growing threat to freshwater wetlands. *Ecosphere*, *6*(10), art206. https://doi.org/10.1890/ES14-00534.1

Horner-Devine, A. R., Hetland, R. D., & MacDonald, D. G. (2015). Mixing and Transport in Coastal River Plumes. *Annual Review of Fluid Mechanics*, *47*(1), 569–594. https://doi.org/10.1146/annurev-fluid-010313-141408

Jackson, M. L., Tyler, S. A., Willis, A. L., Bourbeau, G. A., & Pennington, R. P. (1948). Weathering sequence of clay-size minerals in soils and sediments. I. Fundamental Generalizations. *The Journal of Physical and Colloid Chemistry*, *52*(7), 1237–1260. https://doi.org/10.1021/j150463a015

Jajarmizadeh, M., Harum, S., & Salarpour, M. (2012). A review on theoretical consideration and types of models in hydrology. *Journal of environmental science and technology*, *5*(5), 249–261. https://doi.org/10.3923/jest.2012.249.261

Keller, C. K. (2019). Carbon Exports from Terrestrial Ecosystems: A Critical-Zone Framework. *Ecosystems*, *22*(8), 1691–1705. https://doi.org/10.1007/s10021-019-00375-9

Kempe, S. (1979). Carbon in the freshwater cycle. *The global carbon cycle*, 343–377. https://www.researchgate.net/publication/249313343_Carbon_in_the_freshwater_cycle

Leal, A., & Saar, M. (2018). Reaktoro, a unified framework for modeling chemically reactive systems and plans about its coupling with MOOSE. *Petrotherm Seminar 2018*.

Livingstone, D. A. (1963). Chemical composition of rivers and lakes (M. Fleischer, Ed.). https://doi.org/10.3133/pp440G

Maher, K. (2010). The dependence of chemical weathering rates on fluid residence time. *Earth and Planetary Science Letters*, *294*(1-2), 101–110. https://doi.org/10.1016/j.epsl.2010.03.010

Maher, K. (2011). The role of fluid residence time and topographic scales in determining chemical fluxes from landscapes. *Earth and Planetary Science Letters*, *312*(1-2), 48–58. https://doi.org/10.1016/j.epsl.2011.09.040

Maher, K., & Druhan, J. (2014). Relationships between the Transit Time of Water and the Fluxes of Weathered Elements through the Critical Zone. *Procedia Earth and Planetary Science*, *10*, 16–22. https://doi.org/10.1016/j.proeps.2014.08.004

Mayer, K. U., Amos, R. T., Molins, S., & Gérard, F. (2011). Reactive Transport Modeling in Variably Saturated Media with MIN3P: Basic Model Formulation and Model Enhancements. *Groundwater Reactive Transport Models*, 187–2112. https://doi.org/10.2174/978160805306311201010186

McClain, M. E., Boyer, E. W., Dent, C. L., Gergel, S. E., Grimm, N. B., Groffman, P. M., Hart, S. C., Harvey, J. W., Johnston, C. A., Mayorga, E., McDowell, W. H., & Pinay, G. (2003). Biogeochemical Hot Spots and Hot Moments at the Interface of Terrestrial and Aquatic Ecosystems. *Ecosystems*, *6*(4), 301–312. https://doi.org/10.1007/s10021-003-0161-9

Meaurio Arrate, M. (2017). *Assessing the hydrological response from an ensemble of climate projections in the transition zone of the Atlantic region (Bay of Biscay): Evaluation of SWAT model performance in small and forested catchments* (Doctoral dissertation). Universidad del País Vasco/Euskal Herriko Unibertsitatea. Leioa. http://hdl.handle.net/10810/23868

Meybeck, M. (1979). Concentrations des eaux fluviales en éléments majeurs et apports. *Revue de géologie dynamique et de géographie physique*, *21*(3), 215.

Meybeck, M. (1982). Carbon, nitrogen, and phosphorus transport by world rivers. *American Journal of Science*, *282*, 401–450. https://doi.org/10.2475/ajs.282.4.401

Meybeck, M. (1987). Global chemical weathering of surficial rocks estimated from river dissolved loads. *American Journal of Science*, *287*, 401–428. https://doi.org/10.2475/ajs.287.5.401

Meybeck, M. (2003). Global Occurrence of Major Elements in Rivers. In H. D. Holland & K. K. Turekian (Eds.), *Treatise on Geochemistry* (pp. 207–223). https://doi.org/10.1016/B0-08-043751-6/05164-1

Milliman, J. D., & Farnsworth, K. L. (2011). Runoff, erosion, and delivery to the coastal ocean. In J. D. Milliman & K. L. Farnsworth (Eds.), *River Discharge to the Coastal*

Ocean (pp. 13–69). Cambridge University Press. https://doi.org/10.1017/CBO9780511781247.004

Millot, R., Gaillardet, J., Dupré, B., & Allègre, C. J. (2002). The global control of silicate weathering rates and the coupling with physical erosion: new insights from rivers of the Canadian Shield. *Earth and Planetary Science Letters*, *196*, 83–98. https://doi.org/10.1016/S0012-821X(01)00599-4

Minasny, B., McBratney, A. B., & Salvador-Blanes, S. (2008). Quantitative models for pedogenesis — A review. *Geoderma*, *144*(1-2), 140–157. https://doi.org/10.1016/j.geoderma.2007.12.013

Monroe, J., Wicander, R., & Hazlett, R. (1992). *Physical Geology: Exploring the Earth* (1st ed.). West Publishing Co.

Naisse, C., Girardin, C., Lefevre, R., Pozzi, A., Maas, R., Stark, A., & Rumpel, C. (2015). Effect of physical weathering on the carbon sequestration potential of biochars and hydrochars in soil. *GCB Bioenergy*, *7*(3), 488–496. https://doi.org/10.1111/gcbb.12158

National Research Council. (2001). Basic Research Opportunities in Earth Science. https://doi.org/10.17226/9981

Ohte, N., Dahlgren, R. A., Silva, S. R., Kendall, C., Kratzer, C. R., & Doctor, D. H. (2007). Sources and transport of algae and nutrients in a Californian river in a semi-arid climate. *Freshwater Biology*, *52*(12), 2476–2493. https://doi.org/10.1111/j.1365-2427.2007.01849.x

Panagos, P., Ballabio, C., Poesen, J., Lugato, E., Scarpa, S., Montanarella, L., & Borrelli, P. (2020). A Soil Erosion Indicator for Supporting Agricultural, Environmental and Climate Policies in the European Union. *Remote Sensing*, *12*(9), 1365. https://doi.org/10.3390/rs12091365

Parkhurst, D. L. (1995). User's guide to PHREEQC - A computer program for speciation, reaction-path, advective-transport, and inverse geochemical calculations.

Parkhurst, D. L., Kipp, K. L., & Charlton, S. R. (2010). PHAST version 2-A program for simulating groundwater flow, solute transport, and multicomponent geochemical reactions. https://doi.org/10.3133/tm6A35

Probst, J. L. (1992). *Géochimie et hydrologie de l'érosion continentale. Mécanismes, bilan global actuel et fluctuations au cours des 500 derniers millions d'années.* (Doctoral

dissertation). Université Louis-Pasteur. Strasbourg, Institut de Géologie. www.persee.fr/doc/sgeol_0302-2684_1992_mon_94_1

Riebe, C. S., Hahm, W. J., & Brantley, S. L. (2017). Controls on deep critical zone architecture: a historical review and four testable hypotheses. *Earth Surface Processes and Landforms*, *42*(1), 128–156. https://doi.org/10.1002/esp.4052

Schaub, G., & Turek, T. (2016). *Energy Flows, Material Cycles and Global Development: A Process Engineering Approach to the Earth System* (Second Edition). Springer International Publishing. https://doi.org/10.1007/978-3-319-29495-7

Slessarev, E. W., Feng, X., Bingham, N. L., & Chadwick, O. (2019). Landscape Age as a Major Control on the Geography of Soil Weathering. *Global Biogeochemical Cycles*, *33*(12), 1513–1531. https://doi.org/10.1029/2019GB006266

Steefel, C. I., Appelo, C. A. J., Arora, B., Jacques, D., Kalbacher, T., Kolditz, O., Lagneau, V., Lichtner, P. C., Mayer, K. U., Meeussen, J. C. L., Molins, S., Moulton, D., Shao, H., Šimůnek, J., Spycher, N., Yabusaki, S. B., & Yeh, G. T. (2015). Reactive transport codes for subsurface environmental simulation. *Computational Geosciences*, *19*(3), 445–478. https://doi.org/10.1007/s10596-014-9443-x

Steffen, W., Richardson, K., Rockström, J., Cornell, S. E., Fetzer, I., Bennett, E. M., Biggs, R., Carpenter, S. R., de Vries, W., de Wit, C. A., Folke, C., Gerten, D., Heinke, J., Mace, G. M., Persson, L. M., Ramanathan, V., Reyers, B., & Sörlin, S. (2015). Sustainability. Planetary boundaries: guiding human development on a changing planet. *Science*, *347*(6223), 1259855. https://doi.org/10.1126/science.1259855

Stephens, G. L., Slingo, J. M., Rignot, E., Reager, J. T., Hakuba, M. Z., Durack, P. J., Worden, J., & Rocca, R. (2020). Earth's water reservoirs in a changing climate. *Proceedings. Mathematical, physical, and engineering sciences*, *476*(2236), 20190458. https://doi.org/10.1098/rspa.2019.0458

Sun, X., Higgins, J., & Turchyn, A. V. (2016). Diffusive cation fluxes in deep-sea sediments and insight into the global geochemical cycles of calcium, magnesium, sodium and potassium. *Marine Geology*, *373*, 64–77. https://doi.org/10.1016/j.margeo.2015.12.011

Syvitski, J. P. M., Vörösmarty, C. J., Kettner, A. J., & Green, P. A. (2005). Impact of humans on the flux of terrestrial sediment to the global coastal ocean. *Science*, *308*(5720), 376–380. https://doi.org/10.1126/science.1109454

Velbel, M. A. (1993). Temperature dependence of silicate weathering in nature: How strong a negative feedback on term accumulation of atmospheric CO2 and global greenhouse warming? *Geology*, *21*, 1059–1062. https://doi.org/10.1130/0091-7613(1993)021{\%}3C1059:TDOSWI{\%}3E2.3.CO;2

Vörösmarty, C. J., McIntyre, P. B., Gessner, M. O., Dudgeon, D., Prusevich, A., Green, P. A., Glidden, S., Bunn, S. E., Sullivan, C. A., Liermann, C. R., & Davies, P. M. (2010). Global threats to human water security and river biodiversity. *Nature*, *467*(7315), 555–561. https://doi.org/10.1038/nature09440

Whipple, K. X., Hancock, G. S., & Anderson, R. S. (2000). River incision into bedrock: Mechanics and relative efficacy of plucking, abrasion, and cavitation. *GSA Bulletin*, *112*(3), 490–503. https://doi.org/10.1130/0016-7606(2000)112{\%}3C490:RIIBMA{\%}3E2.0.CO;2

White, A. F., Blum, A. E., Schulz, M. S., Huntington, T. G., Peters, N. N., & Stonestrom, D. A. (2003). Chemical weathering of the Panola Granite: Solute and regolith elemental fluxes and the weathering rate of biotite. In R. Hellman & S. A. Wood (Eds.), *Water-Rock Interactions, Ore Deposits, and Environmental Geochemistry: A Tribute to David A. Crerar*.

Yeh, G.-T., & Sun, J. (2004). HYDROGEOCHEM 5.0: A three-dimensional model of coupled fluid flow, thermal transport, and HYDROGEOCHEMical transport through variably saturated conditions.

Yu, Z. (2015). Modeling and Prediction. *Encyclopedia of Atmospheric Sciences* (pp. 217–223). ELSEVIER. https://doi.org/10.1016/B978-0-12-382225-3.00172-9

Part II

MATERIALS AND METHODS

CHAPTER 3

Materials and Methods

This chapter presents all the materials, methods, and models used in the thesis. Three main sections are distinguished: an *Input data* section which describes the input data used throughout the work; a *Modelling* section explaining the models used throughout Chapter 4, Chapter 6, and Chapter 7; and a *Field and laboratory* section, which explains the materials and methods used on Chapter 5.

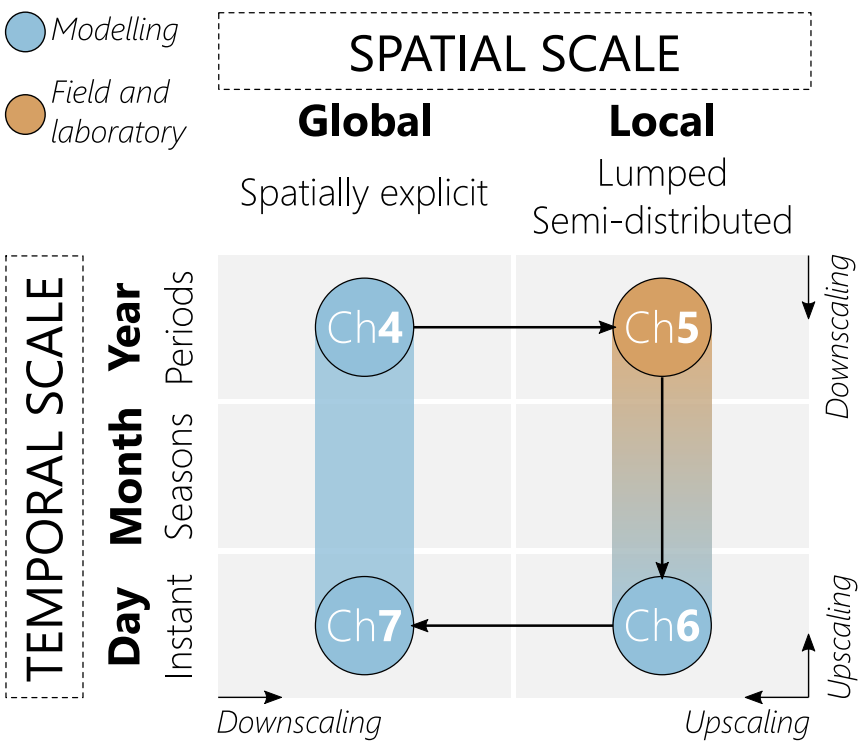

Figure 3.1: Conceptualization of the thesis chapters according to the spatial and temporal scale of the main results. Chapter 4 contains the chemical weathering model development and application at the global scale under static conditions (spatially explicit without temporal evolution). Chapter 5 contains an assessment of the hydrology and hydro-geochemical processes at a local case study (Deba basin), considering several sampling locations within the basin level. Chapter 5 and Chapter 6 are tightly linked, as the same location is chosen as a study case for the coupling of the empirical model on a physical hydrological model (SWAT). The results from all these chapters establish the basis for a global assessment of the chemical weathering's role on the carbon biogeochemical cycle under climate change scenarios, shown in Chapter 7 at different temporal resolutions.

3.1 Input data

The quality of input data determines the quality of the model's results as well as, in the case of empirical modelling, the robustness of the model's structure. At the *global scale*, the development of the empirical chemical weathering model shown in Chapter 4 uses the composition of river water as a proxy for the chemical weathering process (target variable), while the independent variables (potential descriptors) of this model are related to physical and hydrological characteristics of the draining basin. At the *local scale*, observed local data are used as reference.

3.1.1 Global scale

The input data at the **global scale** includes:

- The **Global River Chemistry** (**GLORICH**) database (Figure 3.2, Hartmann, Lauerwald, et al., 2014), which compiles information on two main types of variables at the global scale:
  - Regarding *river hydrochemistry*, it contains 1.27 million samples with data on instantaneous Q, punctual water temperature, and sample alkalinity and concentrations on HCO_3^-, Ca^{2+}, Mg^{2+}, Na^+, K^+, Cl^-, SO_4^{2-}, among other variables.
  - Concerning *catchment properties*, information on more than 17 thousand sampling locations and its draining catchment are described where the water samples were retrieved (Figure 3.2). It contains information on draining area, lithological abundance according to the GLIM dataset (Global lithological map, Hartmann and Moosdorf, 2012), land cover according to (GlobCover, Arino et al., 2007), annual and monthly average hydrological parameters such as runoff (UNH/GRDC composites, Fekete et al., 2002), precipitation, air temperature (according to WorldClim, Hijmans et al., 2005), and others.

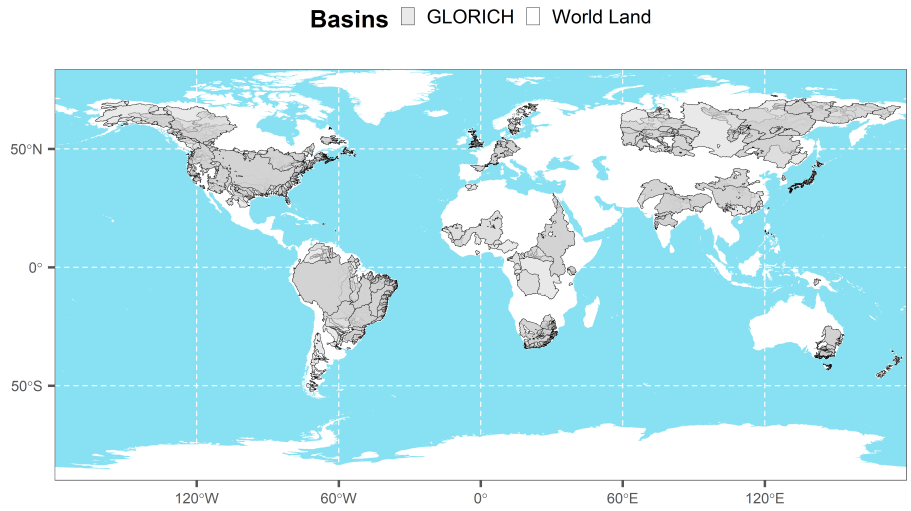

Figure 3.2: Basins contained in the GLORICH database by Hartmann, Lauerwald, et al., 2014.

- The **Global Lithological Map** (**GLIM**) (Figure3.3, Hartmann and Moosdorf, 2012), classifies the world land into a three-level hierarchy according to geochemical and physical properties of rocks. The first level contains 16 *lithological classes*: evaporites (ev), ice and glaciers (ig), metamorphics (mt), acid plutonic (pa), basic plutonic (pb), intermediate plutonic (pi), pyroclastics (py), carbonate sedimentary (sc), mixed sedimentary (sm), siliciclastic sedimentary (ss), unconsolidated sediments (su), acid volcanic (va), basic volcanic (vb), intermediate volcanic (vi), water bodies (wb), and no data (nd). This classification is based on the works by Dürr et al. (2005) and Hartmann and Moosdorf (2012) and is the only one considered in the present study. The scale of the map is on average 1:3,750,000.

- The **Harmonized Soil World Database** (**HWSD**, Figure 3.4, FAO et al., 2012) classifies the land in different soil units, depending on soil physical and chemical characteristics (e.g. organic matter content, water saturation, salinity, etc.). Those soil units are: acrisols, alisols, andosols, anthrosols, arenosols, calcisols, cambisols, chernozems, ferralsols, fluvisols, gleysols, greyzems, gypsisols, his-

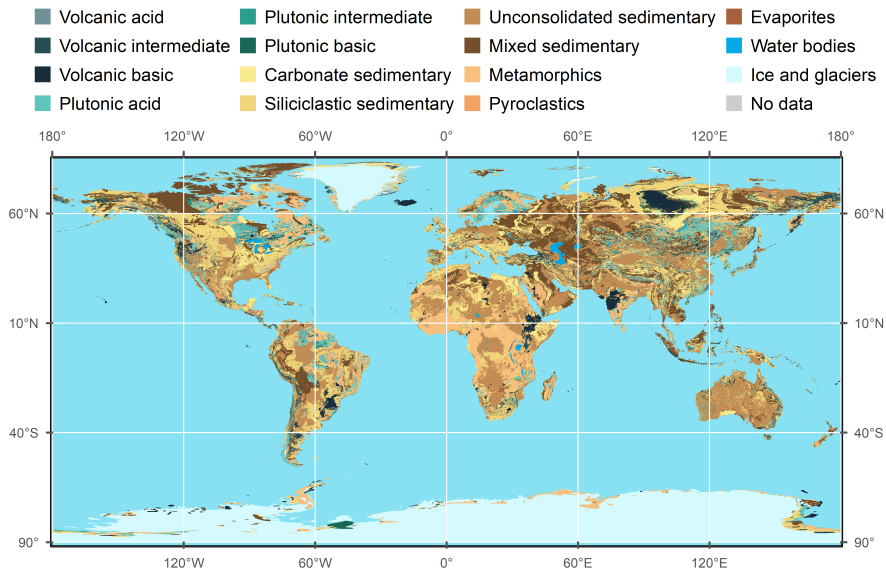

Figure 3.3: Lithological classification at the global scale according to the Global Lithological Map (GLIM), by Hartmann and Moosdorf, 2012

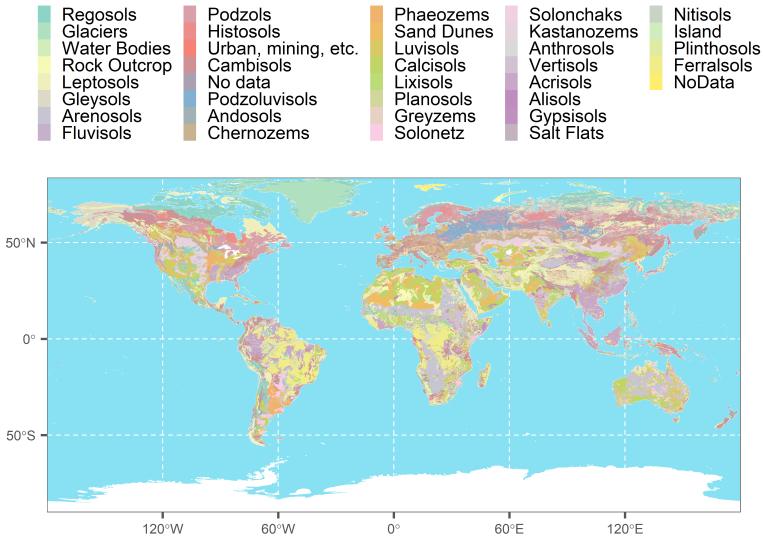

Figure 3.4: Soil classes contained in the Harmonized World Soil Database (HWSD) by FAO et al., 2012. Note that no data under 60ºS is present, thus the Antarctic continent in white colour.

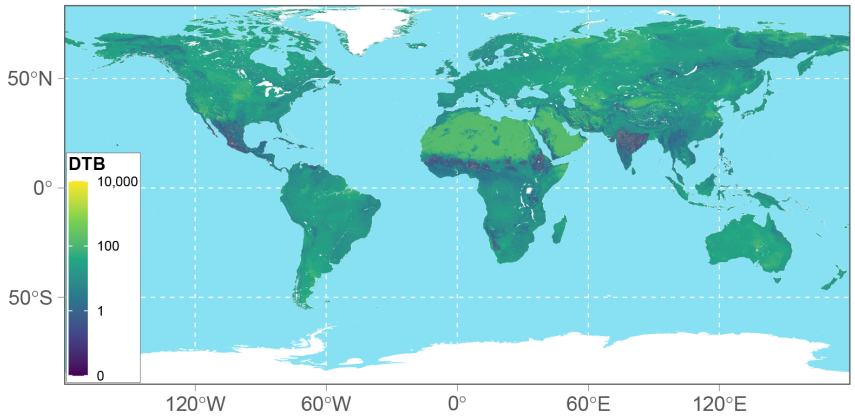

Figure 3.5: Regolith thickness derived from the depth-to-bedrock (DTB) map presented by Shangguan et al., 2017. For plotting purposes, the resolution has been reduced to 0.05x0.05° cell size.

tosols, kastanozems, leptosols, lixisols, nitisols, phaeozems, planosols, plinthosols, podzols, pozoluvisols, regosols, solonchaks, solonetz, and vertisols.

- The **regolith thickness** is derived from the Shangguan et al. (2017) depth-to-bedrock map (Figure 3.5), which continuously describes the depth from the ground surface to the bedrock (continuous rock), at a resolution of 250x250 m.

- The **permeability** map (**GLHYMPS 2.0**, Huscroft et al., 2018) which was used to derive the hydraulic conductivity at the basin scale (Figure 3.6).

- The **precipitation chemistry** (Vet et al., 2014) which describes the composition of meteoric water falling on the draining catchments, downloaded from the World Data Centre for Precipitation Chemistry (http://wdcpc.org). It estimates the seasalt deposition based on the data compiled from different rainfall stations (Figure 3.7).

- The global **annual average runoff** obtained from the composite runoff fields at 30' resolution (**UNH/GRDC**, Fekete et al., 2002).

- Global river discharge under climate change scenario (van Vliet et al., 2013).

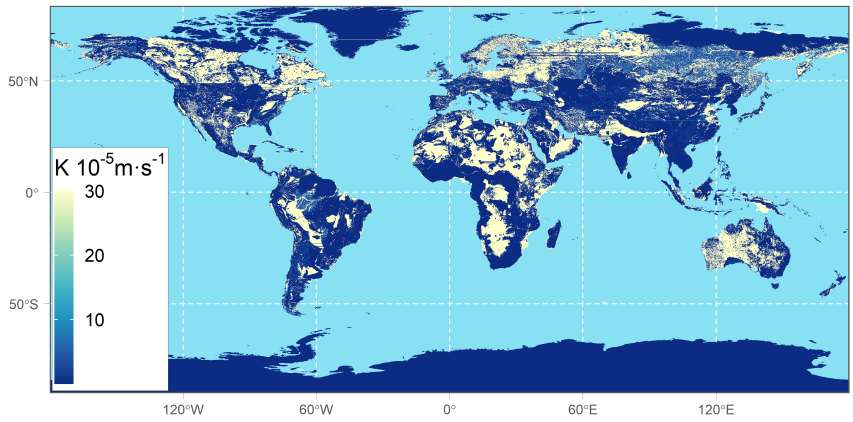

Figure 3.6: Hydraulic conductivity derived from the GLHYMPS 2.0 database, by Huscroft et al., 2018.

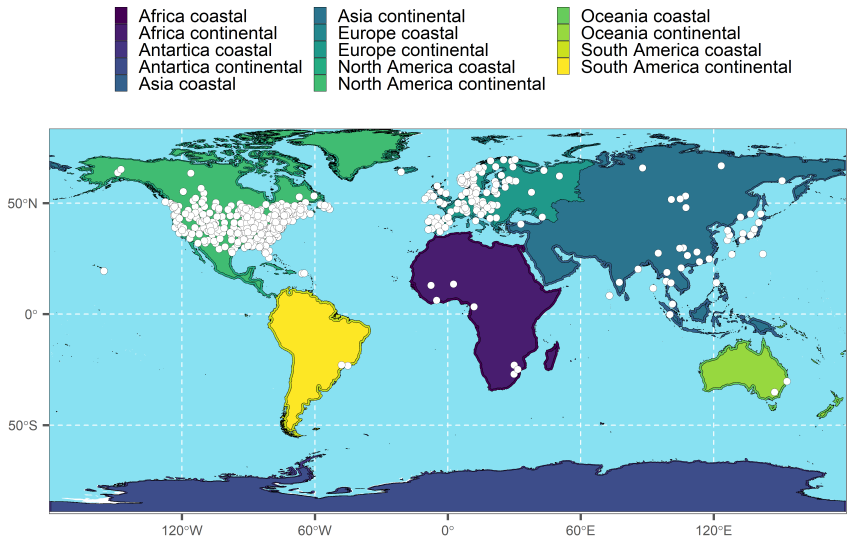

Figure 3.7: Rain chemical monitoring stations, after World Data Centre for Precipitation Chemistry (http://wdcpc.org/). Classified according to continent and coastal/continental depending on the distance to the coast (<100km for coastal).

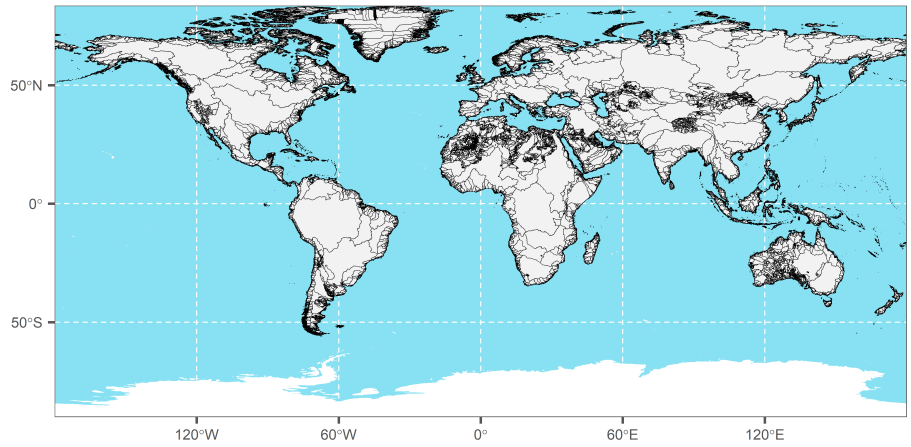

Figure 3.8: Basin delimitation from the HydroBASINS data on the HydroSHEDS dataset, by Lehner and Grill, 2013.

Derived from the coupling of physical models on climate, hydrology, and temperature. Containing daily time series over the land surface at 0.5x0.5º virtual stations, for 1960 to 2100, including projections of five different climate models.

3.1.2 Regional scale

At the regional scale, the input data counts with:

- **Basins borders** have been retrieved from the HydroSHEDS database (using the HydroBASINS data from Lehner and Grill, 2013), which has been delimitated using the high-resolution data from the NASA's Shuttle Radar Topography Mission (STRM). Basins are distributed worldwide except on the Antarctica (Figure 3.8).

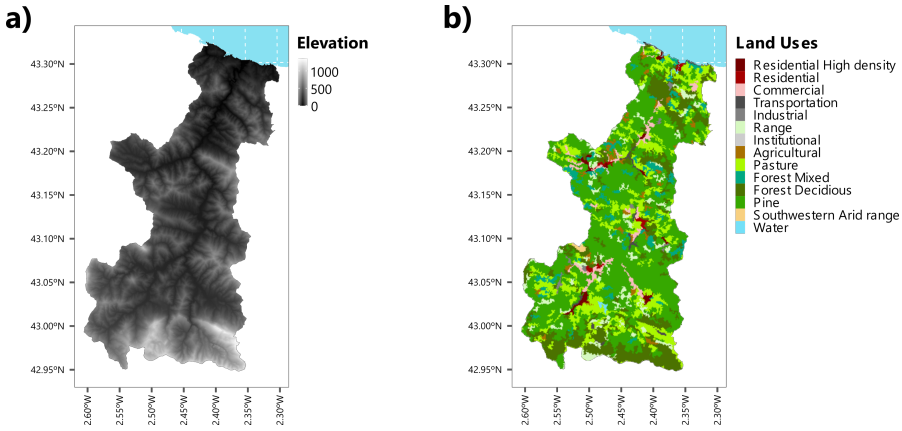

Figure 3.9: a) Digital Elevation Map (DEM) from the Deba catchment, at 25x25km resolution, and b) Land use cover on the Deba draining catchment.

3.1.3 Local scale

Lastly, for the local case study project set-up. These data correspond to the Deba basin located in the Basque Country (Spain, northern Iberian Peninsula) under temperate climate, further described on section 3.3.

- The **digital elevation map** (DEM, Figure 3.9a) derived from the Geoeuskadi portal with a resolution of 25x25m (www.geoeuskadi.eus, accessed on February 2019). The highest peak in this catchment is located in southwest, at 1320m over the sea level (Botraetiz peak) while the lowest is found in Deba city, at the outlet of the river basin.

- A **land use** map derived from the CORINE land cover project (EEA, 2012) with a resolution of 100x100m (Figure 3.9b). About 75% of the surface is covered by pine, forest, forest mixture, and pasture, while 7% of the surface is related to industrial and urban activities. Economic activity is linked to the industrial sector, largely located in Eibar, Elgoibar, Arrasate and Bergara cities.

- A **lithological map** retrieved from the Geoeuskadi portal (www.geoeuskadi.eus, accessed on February 2019), where the lithological classes (Figure 3.10) have

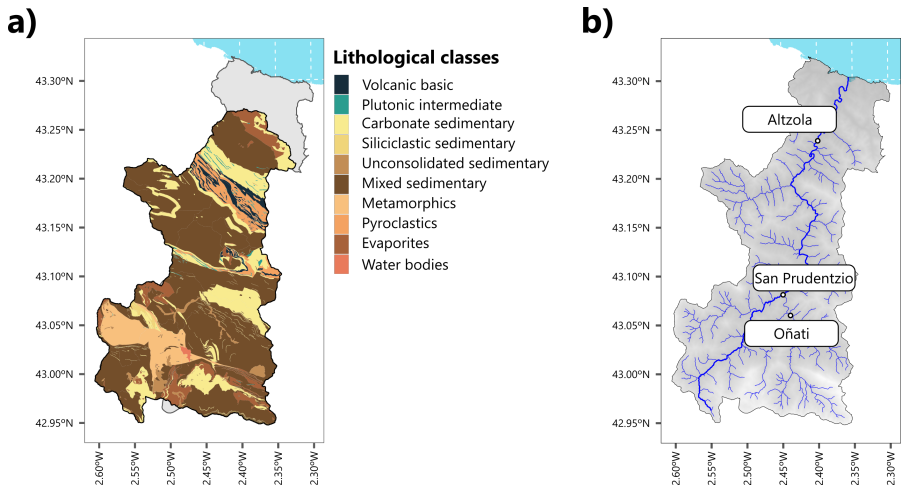

Figure 3.10: a) Lithological classification of the bedrock in the Deba basin, according to the Hartmann and Moosdorf, 2012 classification, b) Gauging stations located within the Deba river basin.

been adapted to those used in the GLIM classification (Hartmann & Moosdorf, 2012). The equivalence between original and adapted classes is shown in Table 3.1. The Deba basin is mainly a sedimentary complex with limestones, marls, and carbonate rocks. There are two relevant aspects regarding this basin's geology: the presence of evaporitic deposits in the southwest part of the catchment (gypsum and anhydrite) typical from the Wealden Facies (EVE - Ente Vasco de la Energía, 1989), and the presence of volcanic rocks in the mid-northern part of the basin, product of the Biscay Sinclinorium (Iribar & Ábalos, 2011). A larger description is found in section 3.3.

- Times series on **precipitation**, **air temperature**, **discharge** and **electrical conductivity** from three gauging stations (Altzola, San Prudentzio, and Oñati, Figure 3.10) located within the Deba basin were obtained from the Gipuzkoa Council (https://www.gipuzkoa.eus/es/inicio). These time series were recorded at 10min frequency, yielding an annual average precipitation and temperature (2008-2018) of 1425 mm and 13.7ºC. The coldest and wettest period is normally from November to March, and the driest from June to September. The average annual discharge at the outlet (Altzola) in that period was 12.3 $m^3 \cdot s^{-1}$.

Table 3.1: Equivalence between lithological classification used in the present study and the original classification present in the input data

Hartmann and Moosdorf, 2012 classification	**Original lithology**	**Original lithology**
Carbonate sediments	12 - Calizas	Limestones
	17 - Alternancia de margocalizas, margas calizas y calcarenitas	Alternance of limestones, marls, and calcarenites
Metamorphics	19 - Pizarras	Slates
Plutonic Basic	15 - Ofitas	Ophites
Plutonic intermediate	20 - Rocas ígneas	Igneous rocks
	24 - Rocas filonianas	Philonian rocks
Pyroclastics	13 - Rocas volcánicas piroclásticas	Pyroclastic rocks
Sediments mixed	10 - Margas	Marls
	11 - Calizas impuras y calcarenitas	Impure limestones and calcarenites
	16 - Arcillas con yesos y otras sales	Gypsum and others
Siliciclastics	02 - Rocas detríticas de grano grueso (Areniscas). Dominante	Detritic rocks with coarse grain (sandstones)
	03 - Rocas detríticas de grano medio (Limolitas). Dominante	Detritic rocks with medium grain (limolites)
	04 - Rocas detríticas de grano fino (Lutitas). Dominante	Detritic rocks with fine grain (lulites)
	08 - Detríticos alternantes	Alternance of detritic rocks
Unconsolidated sediments	01 - Depósitos superficiales	Alluvial deposits
Volcanic Basic	14 - Rocas volcánicas en coladas	Volcanic rocks
Water Bodies	00 - Embalses, ríos y cuerpos de agua	Rivers, ponds, and water bodies

3.1.4 Study area

3.1.4.1 Localisation

The Deba River urban catchment covers 538 km^2 of land in the northern part of the Iberian Peninsula (west Europe), most of it located in the Gipuzkoa province of the Basque Country (Spain). Born in the southwest part of the catchment, the Deba River collects the waters from the high slopes on the hills through a 62 km long river, reaching the mouth of the river in the Deba city, before arriving to the Cantabrian Sea (the Atlantic Ocean). Its topography spans from the sea level (0 m) to the Botreaitz peak (1320 m) in the southeast part of the catchment.

Headwaters, the river receives the influence of the saline springs in Leintz-Gatzaga and the Mazmela tributary before flowing through the towns of Eskoriatza and Aretxabaleta. Here it crosses the city of Arrasate-Mondragon before meeting one of the largest tributaries, the Oñati river, and flowing north to the Bergara city in the middle part of the catchment. Then, it moves to the northwest to meet the Ego tributary, before changing its course to the northeast to the town of Elgoibar, and the villages of Altzola and Medarozabal. Finally, it arrives to the Deba city, which names both the river and the draining catchment. Within this hydrological unit, there are other smaller streams draining to the river, not included in the present analysis.

3.1.4.2 Geological description

The Deba basin is located within the Basque Country, mainly limited by the Cantabrian Sea in the north, and the Ebro basin in the south. Two different watersheds are present within this area, the Atlantic Watershed containing all basins draining to the Cantabrian Sea, and the Mediterranean Watershed, compiling all catchments draining to the Ebro River, towards the Mediterranean Sea. The Deba basin is fully located in the Atlantic Watershed. From the geological perspective, it is located on the western part of the

Pyrenees with mainly carbonate rocks (EVE - Ente Vasco de la Energía, 1989). The rock ages outcropping in the Deba River vary from the Aptian-Albian to the Paleogene (Iribar & Ábalos, 2011), appearing between the Bilbao Anticlinorium and the Biscay Sinclinorium. The upper and middle part of the catchment is located within the Bilbao Anticlinorium, presenting several thrust and secondary faults exposing Cenomanian-Aastrichtian, Albian, Aptian-Albian, and Kimmeridgian-Barremian layers (EVE - Ente Vasco de la Energía, 1989; Iribar & Ábalos, 2011). From the Walden Facies found in the southwestern part of the catchment, there are several saline springs, which chemistry is conditioned by gypsum and evaporite sites. In contrast with the minerals found in these springs, the Deba catchment area is dominated by detritic rocks, interlayered with marls and clays. The southeast part of the catchment presents slates and the highest number of saline springs (Iribar & Ábalos, 2011), while the Ego tributary is mainly conformed by limestones. In the lower part of the catchment, there is a stripe with volcanic rocks crossing east-west.

3.2 Modelling

3.2.1 Modelling approach

Models are built based on observational data (empirical), on conceptualization of the phenomena (conceptual), or on physical laws (mechanistic or physical) (Epelde Beraza, 2015). In general, empirical models are computationally cost-efficient but their results carry a larger uncertainty, while physical models need more resources to yield more accurate results. The choice of the modelling approach is subjected to the processes to study, as well as the spatial and temporal scales aimed, and to the available resources.

The processes described in the present study through modelling may be classified in two groups: **hydro-geochemical** and **hydrological** processes. The main hydro-geochemical process is *chemical weathering*, the process by which bedrock is weathered to soil, releasing ions to water; while the main hydrological processes include *precip-*

itation, *evapotranspiration*, *infiltration*, and *routing*. Due to the wide range of spatial and temporal scales included in this PhD thesis, a combination of both physical and empirical modelling approaches is selected:

- An **empirical approach** is followed for the *hydro-geochemical processes*.
- Both **empirical** and **physical** models are used for the *hydrological processes* at the global and local scale, respectively.

Special mention is required for the empirical modelling approach as, in contrast to the physical model included in the present analysis, its development and evaluation is a central part of the methods used in this study. The development and evaluation of the empirical model for chemical weathering has followed a *global-to-local* and *static-to-dynamic* approach, trying to understand which are the main drivers controlling the average annual flux of ions derived from the chemical weathering of rocks at the global scale, and analysing the performance of the model at lower spatial and temporal scales (*downscaling*) before applying it to forecast potential impacts derived from climate change (*upscaling*). The reliability of the model results are contrasted against published literature at the global scale and against observed data obtained at the local scale (further explanation on the field and laboratory methods is included in section 3.3).

3.2.2 Empirical modelling

Empirical models (also called *metric*, *data based*, or *black-box* models) link target variables to descriptors, where there exists an unknown structure usually elucidated through statistical methods (such as correlation or regression). In hydro-geochemical modelling, a previous study of the chemical weathering process and its environmental context (Hartmann, 2009), as well as a review of previous literature (Amiotte Suchet & Probst, 1995; Hartmann, Moosdorf, et al., 2014; Meybeck, 1986) has allowed the selection of target variables and potential descriptors. Chemical weathering of rocks releases base cations and anions to groundwater, which are later routed to the river within a basin,

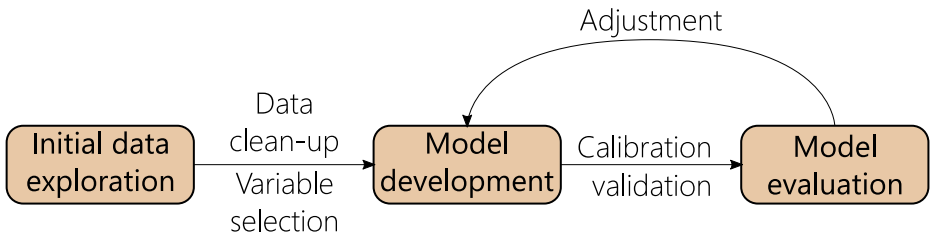

Figure 3.11: Three-step process for empirical model development.

conditioning the major ion composition of the streams. The riverine Ca^{2+}, Mg^{2+}, K^{+}, Na^{+}, SO_4^{2-}, Cl^{-} concentrations, alkalinity, and the annual hydrology on the draining basin are used to estimate the observed specific ionic flux. Those specific fluxes, after performing an atmospheric deposition correction, are used as target variables in the model development, while the description of physical parameters such as lithological abundance, soil classes, or regolith thickness are used as potential descriptors.

Commonly, large scale studies (large spatial or temporal scales) are carried using empirical modelling. In the case of hydro-geochemistry, two recent studies have set the basis for the present analysis (Hartmann, 2009; Hartmann, Moosdorf, et al., 2014). To elucidate which are those factors, a three-steps process has been followed (Figure 3.11).

Before beginning with the empirical model development, the input data must be collected, processed, and cleaned. In the present analysis, we have based our model on published and validated data described in the section 3.1. Then, during the *Initial data exploration* step, several techniques are used to understand the underlaying structure of the input data with regards to the process object of the study. Such techniques include data subset, aggregation, visualisation, correlation, and variable selection. Once the data has been explored, equations are proposed during the *Model development* step where, using the insights gained from the Initial data exploration and the knowledge of the process object of the development, several options to develop the equations are available, including linear and non-linear regression with one or multiple variables. In the present PhD thesis, a set of equations have been established, calibrated and validated

under the Model evaluation step. The initial dataset has been divided in two subsets, one for calibration (i.e. fit of the parameters of the equations), and other for validation (i.e. test of the robustness of the model and parameters). The *Model evaluation* phase compares the results from the simulation with observed data to test the accuracy of the model. These last two steps are an iterative process where the evaluation of the model generates new insights which may be used to develop a new equation to be tested. In the following sections, these steps are further described. The development of an empirical model for chemical weathering at the global scale has been carried out in Chapter 4.

3.2.2.1 Initial data exploration

The first step of the empirical model development process aims at preparing the input data for the model development. In the present study, the objective is to describe the specific fluxes of major ions derived from the chemical weathering of rocks, that is F_x where *x* represents Ca^{2+}, Mg^{2+}, K^+, Na^+, SO_4^{2-}, Cl^-, or alkalinity, expressed as unit of mass per unit of area and time, e.g. $mol \cdot km^{-2} \cdot y^{-1}$, $eq \cdot km^{-2} \cdot y^{-1}$, or $Mg \cdot km^{-2} \cdot y^{-1}$. The observed values of these specific fluxes are those computed as shown in Equation 3.1.

$$F_x = C_x \frac{Q}{A} \tag{3.1}$$

Where C_x represents the concentration of *x* ($mol \cdot L^{-1}$, $g \cdot L^{-1}$) under a discharge Q ($m^3 \cdot s^{-1}$) derived from a draining area A (km^2). Thus, the first step in the initial data exploration is to subset the samples in the GLORICH database (Hartmann, Moosdorf, et al., 2014) using the following criteria:

- A large heterogeneity in reported concentrations was present (missing values, only cations or anions reported, etc.), *thus those samples that contain all information for estimation of observed specific fluxes, i.e. concentration, were kept*.
- There exists a large heterogeneity among sampling locations regarding the number of samples included in the collected dataset, thus in order to diminish the

effect of highly monitored catchments and equalize it with those less monitored, a threshold has been established. *The minimum number of samples to consider a sampling location on the model development step was three, all those draining catchments with only one or two samples were discarded from the analysis*.

- To homogenize the weight of each outlet on the model development process, all individual samples were aggregated to an average value in each sampling location. This was performed using the median value as a non-normal distribution was found for most of the variables (according to a Shapiro-Wilk test, with samples showing $p<0.01$, thus non-normal distributions). *The nested catchments (sampling locations contained within other draining basin) were also excluded, so only independent basins with all physical descriptors (drainage area, lithological distribution...) were considered*.

These criteria were applied to subset the number of samples included in the model development step but, before moving to the following step a correction was needed. The target of this study is to estimate the specific flux of ions derived from the chemical weathering process of rocks but, even though this is the major source of these ions on the river streams, there are other sources that incorporate ions to the stream (see chapter 2), though a deconvolution of the fluxes (differentiation among sources) is needed to account only for those derived from rocks. This has been accomplished using precipitation chemical composition and the average specific precipitation over the basin. First, the seasalt deposition was computed using the Hemispheric Transport of Air Pollution database (HTAP, Vet et al., 2014) and then, the differentiation among ions was computed by different zones where the draining basin was located. Table 3.2 contains the different ionic distribution in rain derived from the observed data. Once the chemical dataset from the GLORICH database was treated and aggregated to the draining catchment basins, a set of 1751 sampling locations with annual average specific fluxes were used for model development.

According to literature, several variables have been reported as relevant regarding chemical weathering and the flux of ions in basins (Hartmann, 2009). Those variables

Table 3.2: Table of ionic chemical distribution by precipitation station classification. This classification has been made using the station contained in each zone, aggregating the data through the mean concentration for each element over the sum of cationic or anionic concentration.

Continent	Zone	Ca^{2+}	Mg^{2+}	Na^{+}	K^{+}	Cl^{-}	SO_4^{2-}
Africa	Continental	39%	6%	26%	29%	40%	60%
(n=182)	Coastal	19%	8%	62%	11%	30%	70%
Asia	Continental	51%	9%	19%	21%	51%	49%
(n=984)	Coastal	33%	6%	44%	16%	34%	66%
Europe	Continental	47%	8%	34%	10%	53%	47%
(n=2764)	Coastal	12%	11%	70%	7%	20%	80%
North America	Continental	65%	9%	18%	9%	80%	20%
(n=8154)	Coastal	18%	9%	67%	7%	39%	61%
Oceania	Continental	19%	13%	62%	6%	16%	84%
(n=104)	Coastal	7%	9%	81%	4%	31%	69%
South America	Continental	44%	9%	32%	15%	48%	52%
(n=27)	Coastal	23%	7%	47%	23%	26%	74%

include hydrology, lithology, temperature, soil properties, regolith depth, hydraulic conductivity, etc. Some of these variables were already included in the original GLORICH database (Hartmann, Lauerwald, et al., 2014), but others have been included for testing their effect on specific fluxes. The inclusion of these variables has been performed with an average value at the basin level for continuous data (regolith thickness and hydraulic conductivity) or relative abundance for categorical values (soil units or lithological classes).

3.2.2.2 Model development

The model development step is based on the establishment of the equations that describe the process based on mathematical relationships, through linear or non-linear regressions. A set of equations has been established based on the previous knowledge compiled in the literature review and the available information. The approach followed was from a simple equation to a more sophisticated one, through the inclusion of more variables or deriving factors that could explain the variability in the data. The starting point of the model development was the Equation 3.1 from which specific fluxes were computed. The empirical parameter to calibrate was the average concentration (M1). Secondly, lithology was included by considering that each lithological class may drain an average concentration for each ion (M2). Thirdly, this concentration was decreased

by a soil shielding effect factor derived for each ion depending on several soil classes (M3). Then, the soil shielding effect factor was replaced by a temperature effect factor (M4). Later on, the two previously tested factors were tested together (soil and temperature) (M5). Followingly, the soil shielding effect factor was changed by a factor regarding soil depth (M6). At the next step, this factor was changed by a hydraulic conductivity factor (M7). Finally, both the soil depth and hydraulic conductivity factor were included (M8).

$$F_x = q_{ann} \cdot c_x \tag{M1}$$

$$F_x = q_{ann} \sum (L_i \cdot c_x) \tag{M2}$$

$$F_x = q_{ann} \cdot f_{xs}(\text{soil}) \sum (L_i \cdot c_x) \tag{M3}$$

$$F_x = q_{ann} \cdot f_T(\text{temperature}) \sum (L_i \cdot c_x) \tag{M4}$$

$$F_x = q_{ann} \cdot f_{xs}(\text{soil}) \cdot f_T(\text{temperature}) \sum (L_i \cdot c_x) \tag{M5}$$

$$F_x = q_{ann} \cdot f_D(\text{soil depth}) \sum (L_i \cdot c_x) \tag{M6}$$

$$F_x = q_{ann} \cdot f_K(\text{hydraulic conductivity}) \sum (L_i \cdot c_x) \tag{M7}$$

$$F_x = q_{ann} \cdot f_{KD}(\text{soil depth, hydraulic conductivity}) \sum (L_i \cdot c_x) \tag{M8}$$

The definition of all factors (soil shielding, temperature, soil depth, hydraulic conductivity) was performed under a conceptual approach described below:

- The **soil shielding effect** factor ($f_{s,x}$, Equation 3.2) is a ratio of decrease in the specific flux, under the assumption that certain soil classes, the bedrock layer is "protected" from the chemical weathering process implying a lower ionic load. The value of this factor for each ion has been computed as follows: first, a threshold has been established to classify the basins where the soil shielding effect is relevant (50% of the drainage area covered by soil shielding classes), then the observed specific flux in these basins has been divided by the specific flux derived from the model not considering the soil shielding effect, obtaining a value varying from 0 to 1, different for each ion x. This factor has been computed under the assumption that the model considering hydrology and lithology (a similar configuration from that of Amiotte Suchet and Probst, 1995) is enough to estimate the loadings

where the soil shielding effect is not relevant.

$$f_{s,x} = \frac{F^*_{x(\text{shield}\geq 0.5)}}{F^*_{x(\text{M2,shield}\geq 0.5)}} \tag{3.2}$$

- The **temperature** factor (f_T, Equation 3.3) has been derived from an Arrhenius type equation, where higher temperatures imply a larger ion release, while a lower temperature suggest a lower chemical weathering process, thus a lower ion loading. This factor was inspired on the work of Hartmann, Moosdorf, et al., 2014.

$$f_T = \exp\left(\frac{1}{T} - \frac{1}{\overline{T}}\right) \tag{3.3}$$

- The **soil depth** factor (f_D, Equation 3.4) is presented here as an alternative to the soil shielding effect factor ($f_{s,x}$) where the driver of decrease in the specific fluxes is the regolith thickness (*Depth*). In this factor there was a parameter to be fit, *b*.

$$f_{s,x} = \frac{\text{Depth}}{\text{Depth}_{MAX} - b \cdot \text{Depth}} \tag{3.4}$$

- The **hydraulic conductivity** factor (f_K, Equation 3.5) is other alternative to the soil shielding effect, where the driver is not the regolith depth but the hydraulic conductivity (K_{hyd}). In this factor there is also a parameter to be fit, *b*.

$$f_K = \frac{K_{hyd}}{K_{hyd,MAX} - b \cdot K_{hyd}} \tag{3.5}$$

- The **soil depth and hydraulic conductivity** factor (f_{KD}, Equation 3.4) is a combination of the previous factors, under the assumption that a higher hydraulic conductivity in a thin regolith will decrease the residence time of water in contact with rocks decreasing the among of matter transferred from rock to water.

$$f_{KD} = \frac{\text{Depth}}{K_{hyd}} \tag{3.6}$$

All these model configurations and these factors have been tested on the dataset established, parameters were calibrated under 75% of the dataset ($n_{calibration}$ = 1313) and

validated under the remaining 25% of the dataset ($n_{validation}$ = 438) (Figure 3.12). The fit was carried out using the Levenberg-Marquardt algorithm, a method used to find the minimum of a function, in this case that is the error sum of squares (Moré, 1978), implemented in the package "minpack.lm" (Elzhov et al., 2016) for the R software (R Core Team, 2019). As the parameters to fit were interpreted as the concentration (c_x, $c_{x,i}$) of an element draining from water from each lithological group, a lower boundary of 0 was established.

3.2.2.3 Model evaluation

The models were calibrated and validated in an iterative sequence, as shown in Figure 3.11. And the evaluation was performed by comparing the observed and simulated specific fluxes for each ion. Two tests were used to evaluate the significance of the relation and the percentage of deviation. These tests are:

- The **Spearman's rank correlation** factor (ρ, Equation 3.7) is a non-parametric (used in non-normal distributions) which measures the rank correlation describing how well the two variables may be described using a monotonic function. It may vary from +1 to –1 depending on the degree of association towards a positive or negative trend, respectively.

$$\rho = \frac{\mathrm{cov}(rg_{Observed}, rg_{Simulated})}{\sigma_{rg,Observed}\sigma_{rg,Simulated}} \tag{3.7}$$

- The **average tendency** of the simulated values to be larger or smaller than the observed ones (PBIAS, Equation 3.8). The optimal is 0, with low values indicating a better representation of the simulated values. Positive PBIAS suggest overestimation of the simulation over the observations, while a negative indicates an underestimation.

$$\mathrm{PBIAS} = \frac{\sum(F_{Simulated} - F_{Observed})}{\sum(F_{Observed})} \tag{3.8}$$

  Where $\mathrm{cov}(rg_{Observed}, rg_{Simulated})$ is the covariance of the observed and simulated

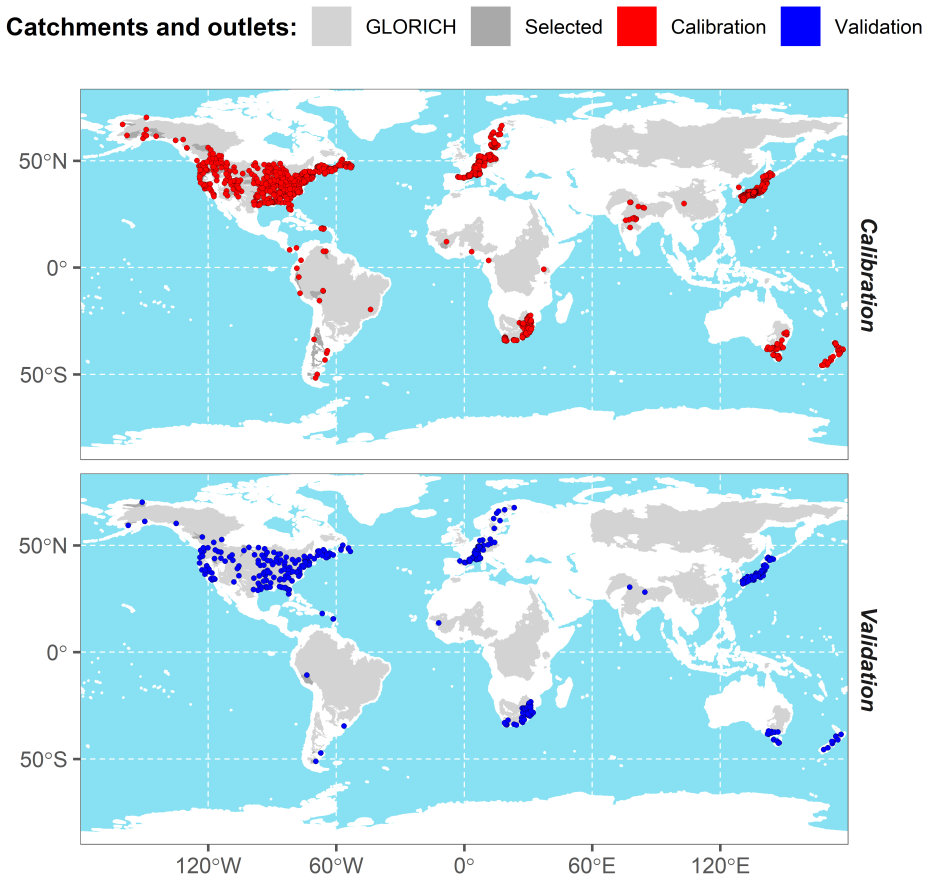

Figure 3.12: Original, subset, and classified sampling locations and draining catchments in the present study. Over the original GLORICH dataset (light grey), the darkest grey areas represents the selected draining catchments, for which the outlets are represented as red or black points depending on whether it has been used for calibration ($n_{calibration}$ = 1313) or validation ($n_{validation}$ = 438), respectively.

fluxes, σ_{rg} accounts for the standard deviation of the variables, and F represents the specific fluxes.

3.2.3 Physical modelling

The choice of a model for hydrological representation is conditioned by the objectives and conditions of the study (both at the temporal and spatial scales), as well as by the resources available and the level of abstraction needed. The scope of the present PhD thesis needs to cover a wide range of spatial and temporal scales, thus a model which is able to discretize the hydrological balance in these spatial scales is needed, specially one with the differentiation between surface, sub-surface, and groundwater fluxes. Given that, other than the hydrology, the lithological and soil characteristics of the draining basin are key for the determination of the ionic fluxes, a semi-distributed model is adapted to the needs, allowing to simplify the spatial and temporal variability according the soil and lithological characteristics, as well as represent a spatial and temporal variability in terms of basin and lower spatial units. For the present study, there is a need for a physically based model flexible enough to be applied at large and small scales which include the processes affecting the hydrological balance under different pedoclimatic conditions. In this context, and following a large used model, the choice is the Soil and Water Assessment Tool (SWAT).

3.2.3.1 SWAT Model

The United States Department of Agriculture (USDA), in the Agricultural Research Service, developed the Soil and Water Assessment Tool (SWAT) model to forecast the impacts of agricultural practices at the catchment scale, through a continuous, spatially semi-distributed hydrological and environmental code (Arnold et al., 1998). The SWAT model has been largely used (Fu et al., 2019) for a variety of purposes, including hydrological balance, erosion, nutrient loss, or pesticide loss.

The SWAT model is a compilation of different modules concerning different processes within the hydrological and other biogeochemical cycles. A graphical representation may be seen in Chapter 3.13, and a large description is found in Arnold et al. (2012). However, SWAT is not able to estimate the major ion composition in their simulation as it lacks a routine considering these processes. It has been considered an opportunity for the present study to include the ICWR model into a SWAT subroutine called *SWATLitho*, which is described in section 3.2.4.1, and on chapter 6. SWAT is a semi-distributed continuous model, based on land use, soil types, and topography for the discretization of the space in the Hydrological Response Units (HRU), the smallest unit where all processes are computed, and on meteorological data for its temporal evolution, written in FORTRAN, which has been used both in small and large-scale applications, at the basin and regional scale. SWAT uses text tables as input and yield text tables as output, and the set up of the input tables is done through Geographic Information System (GIS) plugins, such as ArcSWAT for ArcGIS, and QSWAT for QGIS.

3.2.3.2 Spatial discretization

The first step in SWAT modelling, after compiling all input data, is to prepare the input tables. This may be done using the ArcSWAT or QSWAT, as both use topographical information to delimitate the stream network, the basin boundaries, and the sub-basins. Then, spatial tools in these GIS systems are used to intersect slope, land use, and soil type maps which allow for the delimitation of the HRU (Figure 3.14). Finally, the meteorological information is incorporated to each of these units, yielding the SWAT input tables, ready for simulation.

In the present study, we have modified the spatial discretization of the SWAT model to include a fourth layer on the HRU discretization, the lithological map. This modification has been performed by modifying the QSWAT plugin, based on Python language, which may be found in (https://swat.tamu.edu/software/swat-litho/). This spatial discretization has allowed to estimate at a basin level, a spatially semi-distributed specific flux of ions. This is used to test the developed empirical model on a low scale approach

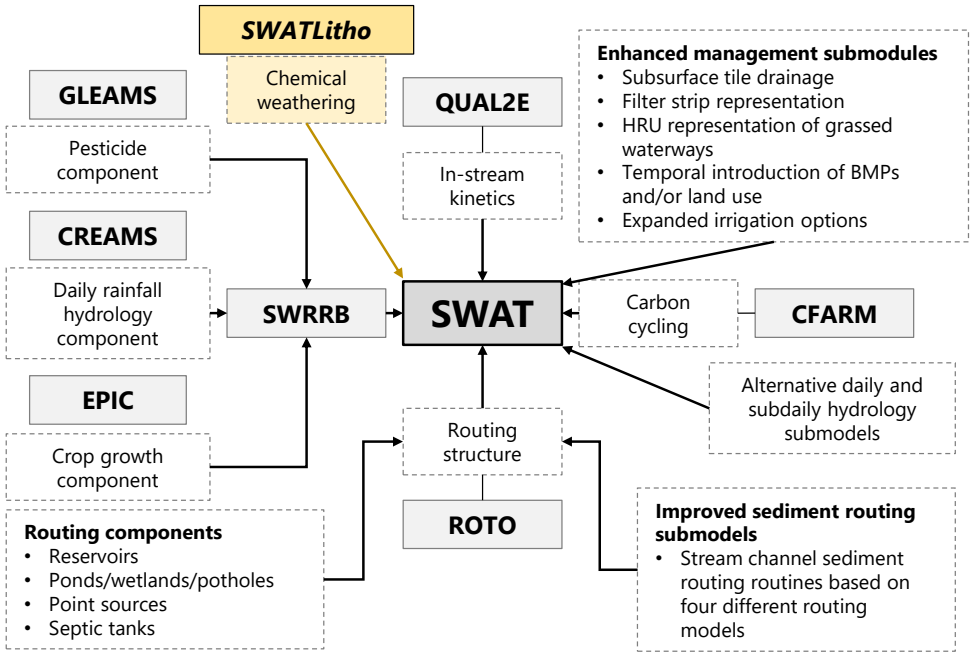

Figure 3.13: SWAT development schema adapted from Arnold et al., 2012. The different components of SWAT are the groundwaters through the Groundwater Loading Effects of Agricultural Management Systems (GLEAMS) by Leonard et al., 1987, the management of erosion and biogeochemical cycles with the model Chemicals, Runoff, and Erosion from the Agricultural Management Services (CREAMS) by Knisel, 1980, the management of meteorological data with the Environmental Policy Integrated Climate (EPIC) by Wang et al., 2011; Williams et al., 2008, which are aggregated into the Simulator for Water Resources in Rural Basins (SWRRB) by Arnold and Williams, 1987. Then, the hydrological routing is made through the Routing Outputs to Outlets model (ROTO) by Arnold, Allen, et al., 1995, the processes given within the river are computed using the QUAL2E by Brown et al., 1987 and the routing of organic carbon is done with the CFARM model by Kemanian et al., 2011. Lastly, the SWATLitho module developed in the present PhD thesis is included to simulate the chemical weathering processes between rocks and groundwater.

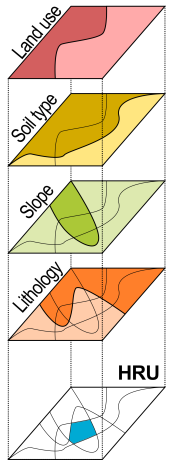

Figure 3.14: Spatial discretization applied in this study

and test its performance in a dynamic level (see section 3.2.4).

3.2.3.3 Hydrological simulation

SWAT simulates a land phase of the hydrologic cycle at the HRU scale based on the Equation 3.9 (Neitsch et al., 2011, Figure 3.15).

$$SW_t = SW_0 + \sum(R_{day} - Q_{surf} - E_a - w_{seep} - Q_{gw}) \tag{3.9}$$

Where SW_t is the soil water content at time t (mm), SW_0 is the soil water content at time, t is the time of simulation (days), R_{day} is the precipitation on day i (mm), Q_{surf} is the surface runoff on day i (mm), E_a is the evapotranspiration on day i (mm), w_{seep} is the percolation and bypass flow out of the soil profile on day i (mm), and Q_{gw} is the groundwater flow (return flow) on day i (mm).

The temporal driver of the simulation is established by the precipitation and air temperature time series, which in the present study are introduced at a daily time step, but sub-daily options are available. Water input in the simulation is through precipitation which, depending on the temperature may be in the form of rainwater or

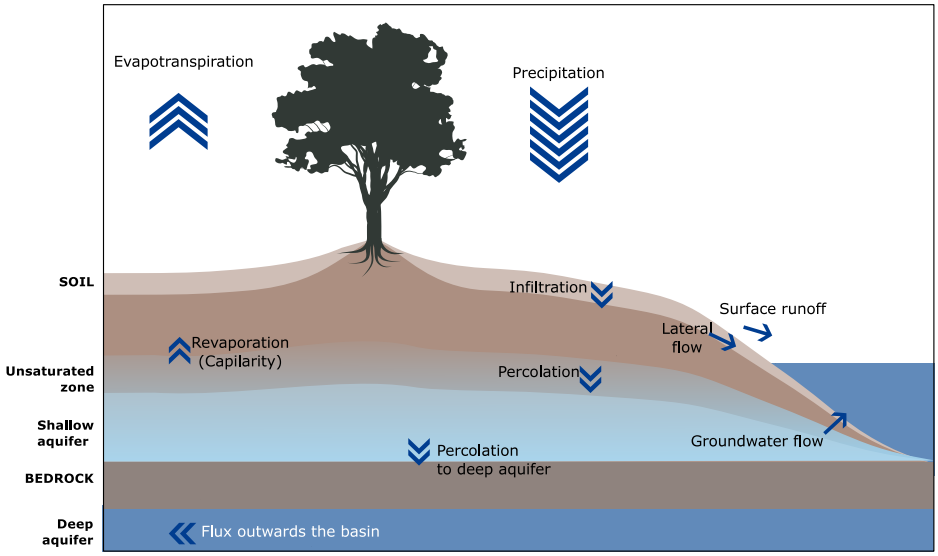

Figure 3.15: Conceptualization of the hydrological cycle within an HRU.

snow. According to the type of vegetation and crops, meteoric water may be intercepted by leaves and later evapotranspired or fall directly to the ground. Part of the water will be infiltrated to lower layers of the soil, while the remaining will be routed towards the reach at the HRU level as surface runoff. Infiltrated water may be retained in soil and later evapotranspired, taken by plants, drained to the reach as lateral (sub-surface) flow, or slowly move downwards to the shallow aquifer by underground paths. Water in the shallow aquifer composes the baseflow of the river in dry periods, but it may also be moved upwards to the upper soil layers or downwards to the deep aquifer, where water is not contributing to the basin routing.

In the present study we are interested on using the hydrological discretization between surface, lateral, and groundwater flow for the estimation of the ionic loadings draining to the main channel. For that, the assumption is that the groundwater and lateral flow are loaded with the ionic loadings while the surface runoff is diluted, this even though it increases the water discharge, it dilutes the concentration in the main channel and does not contribute to the loading export.

3.2.3.4 Calibration and validation

The performance of a SWAT project is tested by contrasting simulated outputs against observed values. For this purpose, a temporal calibration/validation is practiced. Three periods are distinguished in SWAT modelling: *warmup*, *calibration*, and *validation*. During the warmup period, the results of the model are skipped because initial conditions on all the variables need to be stabilized. Then, the simulation period is divided in other two independent periods: a calibration one where the observed values are used to estimate the real value of the parameters in this basin; and a validation period, where the parameters are no longer changed and the results are contrasted to observations under different circumstances. There are several ways to quantify the model's performance. In the present study, four tests are established:

- The **coefficient of determination** (r^2, Equation 3.10) measures the linear correlation existing between to series (Moriasi et al., 2007). This coefficient indicates the percentage of variation of the observed data explained by the model, varying from 0 (no fit) to 1 (perfect fit). In general, a threshold of 0.5 are considered as acceptable.

$$r^2 = \frac{\sum(obs_i - \overline{obs}) \cdot (sim_i - \overline{sim})}{\sqrt{\sum(obs_i - \overline{obs})^2} \cdot \sqrt{\sum(sim_i - \overline{sim})^2}} \tag{3.10}$$

- The **Nash-Sutcliffe Efficiency coefficient** (NSE, Equation 3.11) compares the "noise" (relative magnitude of the residual variance) against "information" (the variance of the data) (Moriasi et al., 2007; Nash & Sutcliffe, 1970). It ranges from $-\infty$ to 1, where values between 0 and 1 are generally viewed as acceptable.

$$NSE = 1 - \frac{\sum(obs_i - sim_i)^2}{\sum(obs_i - \overline{sim})^2} \tag{3.11}$$

- The **Percent of Bias** (PBIAS, Equation 3.12) indicates how the simulated results tend to over or underestimated with respect to the observations (H. Gupta et al., 1999). The closer the value is to 0, the closer the model results are to the

observations.

$$\text{PBIAS} = \frac{\sum(\text{sim}_i - \text{obs}_i) \cdot 100}{\sum(\text{obs}_i)} \tag{3.12}$$

- The **Kling-Gupta Efficiency** (KGE) is a decomposition of the NSE, with values ranging from $-\infty$ to 1, where 1 is the more accurate situation. It is computed as shown in Equation 3.13 (H. V. Gupta et al., 2009), where ED means Euclidean Distance and is computed as indicated in Equation 3.14, where r represents the potentially maximum value of KGE, α is a measurement of the variability in simulated and observed values computed as $\alpha = \sigma_s/\sigma_o$, or the ratio between the standard deviations of simulated (S) and observed values (O), and β is a measure of bias, computed as the ratio between simulated and observed means $\beta = \mu_s/\mu_o$.

$$\text{KGE} = 1 - \text{ED} \tag{3.13}$$

$$\text{ED} = \sqrt{(r-1)^2 + (\alpha-1)^2 + (\beta-1)^2} \tag{3.14}$$

The calibration process compiles two steps: manual and automatic calibration. The first one tries to establish a range for the parameters' values, while the second uses an algorithm to further find a better approximation of the parameters, as well as establish a Confidence Interval for each of them. The automatic calibration is accomplished by using the SWAT Calibration and Uncertainty Procedures (SWATCUP, Abbaspour, 2014), under the algorithm of Sequantial Uncertainty Fitting (SUFI2, Abbaspour et al., 2004).

3.2.4 Changing scales

One main challenge in modelling is the change of scale, specially on hydro-geochemical modelling. From a spatial perspective the possibility of using mechanistic models in large project is constrained by the computational resources and the data availability in space and time, while the use of the empirical models on small scale simulations may result on high PBIAS as processes are not well represented. From a temporal perspec-

tive, several hydro-geochemical models have focused on understanding the processes occurring in the past, at geological time scales, while there is a growing interest on understanding which are the potential changes expected in the Anthropocene, due to climate change or other drivers from the global change.

In this sense, the objective of the present study to develop a useful tool at large or small scales and at long or short time must deal with the change of scale challenge. Going from global to local (*downscaling*) allows to understand better the limits of the model development, while moving from local to global (*upscaling*) is an opportunity to understand global change approaches with an aggregation approach, where errors are commonly diluted.

The starting point in this PhD thesis is the global approach at a static level (Chapter 4), beginning at a basin scale extent spread worldwide to yield a spatially explicit (but static) result. Then, the downscaling of the model has allowed to move from a worldwide to a local approach, not only in a static but a dynamic way by understanding that the main driver is hydrology, and that a good spatial and temporal representation of the hydrological cycle is needed to compute the loadings from continental weathering. This is shown in Chapter 6. Then, understanding the limits of the model it is possible to couple it to physically based results to estimate global temporal potential evolutions under climate change scenarios (shown in Chapter 7).

This section explains how the change of scale has been performed from the spatially explicit model at a global scale.

3.2.4.1 Downscaling - SWATLitho

The incorporation of the lithological relative abundance (L_i) in the empirical model development (section 3.2.2) has been shown a key factor on improving the model's performance. This suggests that the spatial resolution of the lithological abundance is a key information regarding the ionic flux estimation. Downscaling the model to local

scales should be accompanied with a refinement of the lithological discretization and a finer representation of the hydrology. This has been accomplished by modifying the QSWAT discretization, using the hydrological representation of the SWAT model under the discretized HRUs including a local lithological map.

Regarding the temporal downscaling, it is important to note that, as lithology and soil are identified as the key physical characteristics conditioning the ionic fluxes at the river basin scale, and that these variables do not vary significantly on a daily, monthly or yearly basis, the hydrology has been considered as the main driver on temporal evolution of these fluxes. This has been tested on Chapter 6, though the comparison of observed data in a local basin with the simulated results. A Python script has been written to take the results from the SWAT simulation (regarding hydrology) and the physical description of the HRUs (see Chapter 6) and compute through the empirical model developed, the loadings at the outlet of the catchment (expressed as mass per unit of time, $Mg \cdot y^{-1}$ or $Mg \cdot d^{-1}$).

3.2.4.2 Upscaling

Upscaling from the spatial perspective implies lowering the spatial resolution of the results. Models may be classified based on their spatial resolution in distributed, semi-distributed, and lumped. Here, upscaling has been performed by changing from a semi-distributed approach to a lumped approach, considering the basin as the largest scale for spatial aggregation. This change may be seen in Chapter 6, where the spatially explicit global results obtained in the model development chapter has been moved to a basin scale approach.

The temporal aggregation has been performed according to the needs of the simulation. The finest resolution used in this analysis is the daily evolution, while the lowest resolution is the year. Seasonal aggregations have also been used in Chapter 7, where the climate change scenarios have been studied under annual and seasonal aggregations of the daily results.

3.2.4.3 Digital filter for hydrologic deconvolution

The application of a physically based model for the hydrological definition is not always possible due to large scale approaches or lack of input data. For these cases we have tested the use of a digital filter approach as an alternative, based on a continuous time series and the erase of the surface runoff (as done in Chapter 6). Such deconvolution is performed following the digital filter shown in Equation 3.15, as proposed by Eckhardt, 2005. Baseflow, *b(t)*, is computed through the digital filter using the total discharge, *Q(t)*, measured in the river, and two parameters: BFI_{mx} and a. In the present study, only interflow (lateral flow) and groundwater flow are considered as loaded with ions, while surface runoff is the main agent for dilution. A digital filter is selected, as it is based on the slopes of both the increasing and decreasing parts of the hydrographs, though being sensible to changes not only in the amount of water but in the seasonality and flood events. Nonetheless, this is a source of uncertainty as the infiltration process depends on a catchment-to-catchment properties, while this equation assumes linearity between the groundwater outflow (baseflow) and its storage (Eckhardt, 2005).

$$b(t) = \frac{(1 - BFM_{mx}) \cdot a \cdot b \cdot (t-1) + (1-a) \cdot BFI_{mx} \cdot Q(t)}{1 - a \cdot BFI_{mx}}, \text{ for } b(t) < Q(t) \qquad (3.15)$$

Where BFI_{mx} represents the long-term ratio of baseflow to total streamflow, and a is the filter parameter. When b(t)>Q(t), b(t) is replaced by Q(t). The parameters selected for the separation are $BFI_{mx} = 0.8$ and $a = 0.95$, as recommended by Xie et al. (2020).

3.3 Field and laboratory set up

The modelling approach described in the previous sections has a local scale modelling step, where the results of the model are compared to the observed values. In the present section, we describe the field and laboratory set up used to obtain the observed values dataset.

3.3.1 Field surveys

A monitoring program was established in the catchment to control chemical composition of water and sediments, as well as assess the potential anthropogenic effects. This monitoring program has two main aspects: a set of 11 sampling locations with monthly or bi-monthly sampling campaigns, and the control of the continuous registries collected in three gauging stations.

3.3.1.1 Sampling set up

A set of 11 sampling locations was established and sampled along the main channel and tributaries present in the Deba Basin since April 2014 to January 2017. The location of the sampling spots is shown in Figure 3.16 Sampling locations distributed along the main channel and tributaries in (a) the Deba catchment, and (b) at the confluence of Oñati with the main channel. D1 is considered to cover the control area (6.2 km^2) associated with low human impact. A tributary is incorporated to the main channel after this location, the Mazmela tributary, where the M1 (3.5 km^2) sampling location is established. The river flows through Aretxabaleta and Eskoriatza, after which the D2 sampling location (62.4 km^2 accumulated area) is placed, before arriving to Arrasate-Mondragon city. Passed this agglomeration, the river arrives to the confluence with Oñati, one of the largest tributaries in this basin. Two independent sampling locations are established here: one on the main river before the confluence (D3, 121 km^2), and other on the Oñati tributary (O1, 130 km^2). After the confluence, two sampling locations are closely placed: D4 (321 km^2) and D5 (329 km^2). At this point, the river changes its course towards the northwest to meet the last relevant tributary in this basin, the Ego river with two sampling locations: one of them in headwaters (E1, 2.4 km^2) and other one close to the confluence (E2, 55.5 km^2). After the confluence, the D6 sampling location collects the mixed waters (419 km^2), now faced to the northeast. Before the transition zone of the river to the ocean, the last sampling location is established (D7, 487 km^2). From this location to the sea there are no more sampling locations. Every

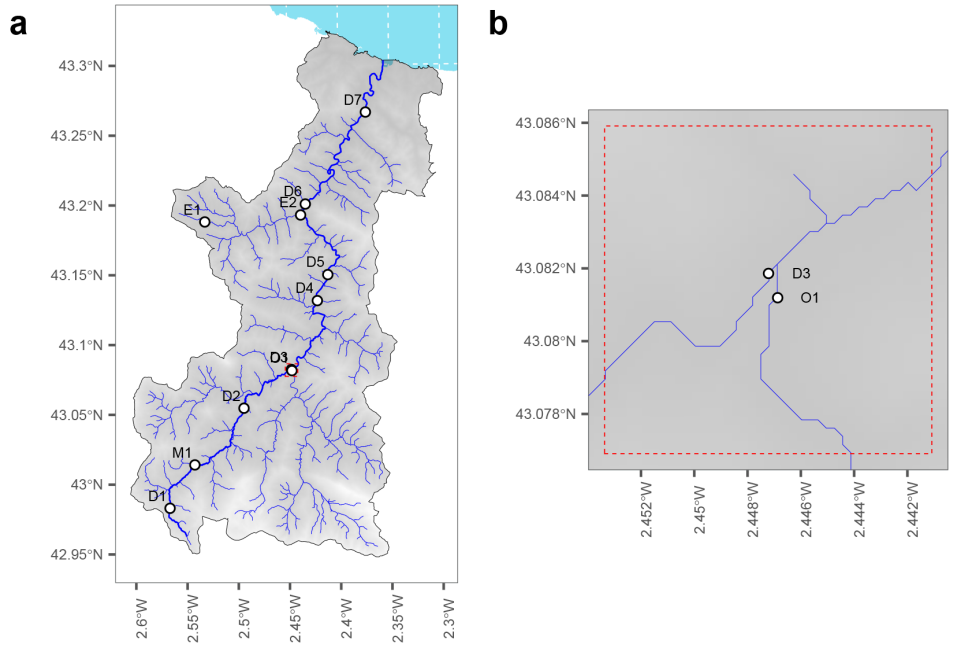

Figure 3.16: Sampling locations distributed along the main channel and tributaries in (a) the Deba catchment, and (b) at the confluence of Oñati with the main channel.

sampling point was sampled monthly or bimonthly between April 2014 and January 2017, covering two full hydrological years (October 2014-September 2015 and October 2015-September 2016) and part of the 2013-2014 and 2016-2017 hydrological years. Sampling campaigns consisted in water collection in all sampling locations within a single day, using 1L pre-cleaned polyethylene bottles to collect water samples on the middle part of the river. These samples were kept at 4ºC and taken to the laboratory in the Chemical and Environmental Engineering department of the Bilbao School of Engineering at the University of the Basque Country (UPV/EHU) to be analysed. In addition to the water sample, a Crison EC-Meter Basic 30+, and a Crison Micro pH 2000 sonde were used to measure *in situ* Electrical Conductivity (EC), Total Dissolved Solids (TDS), and pH, respectively.

3.3.1.2 Continuous registries

In addition to the punctual sampling methodology, three gauging stations measure hydrological (precipitation, discharge) and quality (turbidity, suspended sediment concentration, EC) variables at a 10-min frequency. EC is measured in flowing water pumped to the station from the river. The three gauging stations are San Prudentzio and Oñati in the upper part of the catchment, and Altzola near the outlet (Figure 3.10b). The Altzola gauging station, placed between D6 and D7 sampling locations in the lower part of the catchment, collects 464.25 km^2 of the area of the basin according to www.geoesukadi.eus. Inside this drainage area, San Prudentzio (121.78 km^2) and Oñati (105.78 km^2) are located close to D3 and O1 sampling locations, respectively, collecting independent draining surfaces (Figure 3.16). There is a relevant tributary in terms of discharge and chemical compounds which is not controlled by a gauging station: the Ego tributary in the western part of the catchment. The discharge in this sampling location has only been estimated through physical modelling in SWAT.

3.3.2 Laboratory analysis

Once in the laboratory (Figure 3.17), the raw water samples were filtered through 0.45µm filters to separate the suspended particles from the dissolved phase. Four replicates from the filtered water were separated for further analysis:

- One replicate of the filtered sample was acidified to 0.2% with HNO_3^- (68%) for base cations (Ca^{2+}, Mg^{2+}, Na^+, and K^+) analysis through Induced Coupled Plasma – Atomic Emission Spectroscopy (ICP-OES), using a Perkin Elmer Optima 2000.
- One replicated from the filtered sample was used to analyze base anions (Cl^-, NO_3^-, and SO_4^{2-}) by means of Ion Chromatography (IC), using a DIONEX ICS 3000.

- Alkalinity, Dissolved Organic Carbon (DOC), and Total Organic Carbon (TOC) were determined in the filtered sample using a Catalyst Combustion Oxidation, using a Total Organic Carbon Analyzer (TOC-L Shimadzu).
- One last filtered replicate was used to analyze phosphorus ($P\text{-}PO_4^{3-}$) following the method 4500-P E (APHA, 2015). To 5 mL of the water sample, 10µL of a phenolphthalein dissolution (0.1%) in ethanol. Then, 10textmu L of the H_2SO_4 dissolution (5N) were added for neutralization. Lastly, 0.75mL of a dissolution containing 50mL of H_2SO_4, 5mL of potassium-antimuonium tartrate (0.27%), 15mL of ammonium molybdate (4%), and 30mL of ascorbic acid (0.1M). After 10 min, absorbance was measured using ultraviolet spectrophotometry (λ=880nm).

Due to the pH ranges, the alkalinity values were converted to HCO_3^- concentration in ($mg{\cdot}L^{-1}$). Sample analysis was validated by computing the Ionic Charge Balance (ICB) between anions and cations for each sample following Equation 3.16.

$$ICB = \frac{[Z^+] - [Z^-]}{[Z^+] + [Z^-]} \tag{3.16}$$

Where $[Z^+]$ and $[Z^-]$ represents, respectively, the sum of all cation and all anion concentrations expressed in $meq{\cdot}L^{-1}$. Samples showing $|ICB| \geq 10\%$ were discarded from the analysis.

3.3.3 Data analysis methods

The analysis of the results has been performed following different statistical techniques, from exploratory analysis to statistical test. The techniques have been performed using the R software (R Core Team, 2019) using functions from different libraries or native functions.

- Exploratory analysis:
  - **Scatterplots** were used to visually elucidate patterns among the different

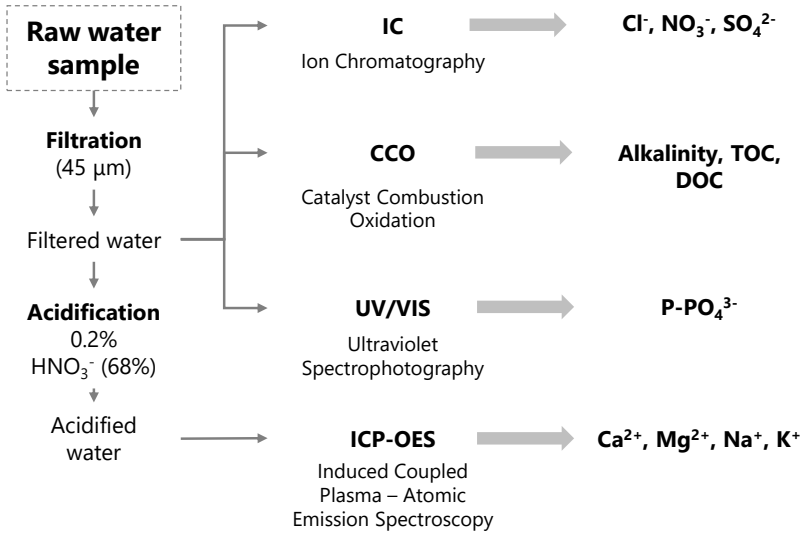

Figure 3.17: Schematic summary of laboratory analysis step and results.

variables in different cases, both using direct results or elemental ratios ("ggplot2" package, Wickham, 2016).

- **Boxplots** were used to evaluate spatial evolutions under different categories (sampling locations) considering the statistical distribution of the samples ("ggplot2" package, Wickham, 2016).
- **Piper Diagram**, used to classify the types of water according to its major composition, through the display of two ternary plots (one for anions, other for cations) and its projection towards the central diamond ("ggplot2" package).

- Statistical tests:
  - **Pearson correlation** test measures the correlation between two variables, based on the Pearson's product moment correlation (native function in the "stats" package, R Core Team, 2019).
  - **Shapiro-Wilk** test to determine the normality of the variables' distributions (native function in the "stats" package, R Core Team, 2019).
  - **Welch's t-test** used to determine whether two populations have equal means.

These two populations do not have equal variances, even though the normality assumption is maintained (native function in the "stats" package, R Core Team, 2019).

- Statistical methods:
  - **Cluster analysis** to group cases according to the similarity in the variables, using a Ward distance method in a hierarchical clustering (native function in the "stats" package, R Core Team, 2019).
  - **Principal Component Analysis** (PCA) to produce a set of factors that describe the variability among the cases. Only factors presenting an eigenvalue over 1 where considered. The principal components were orthogonally rotated using the Varimax rotation to maximize the variance captured by each factor, as well as to enhance correlations in these factors with several variables while reducing them with the others (native function in the "stats" package, R Core Team, 2019).
  - **Univariate** and **multivariate linear regression** was used to explore and quantify the linear dependency between one variable and other, or other group of variables. This technique was also used to develop the empirical model described in section 3.2. Model evaluation is explained in section 3.2.2. For the case of univariate linear regression, 95% prediction intervals were computed (native function in the "stats" package, R Core Team, 2019, and the "minpack.lm" package from Elzhov et al., 2016).

Bibliography

Abbaspour, K. C. (2014). SWAT-CUP 2012: SWAT Calibration and Uncertainty Programs. A user manual. https://swat.tamu.edu/media/114860/usermanual_swatcup.pdf

Abbaspour, K. C., Johnson, C. A., & van Genuchten, M. T. (2004). Estimating uncertain flow and transport parameters using a sequential uncertainty fitting procedure. *Vadose Zone Journal*, *3*(4), 1340–1352. https://doi.org/10.2113/3.4.1340

Amiotte Suchet, P., & Probst, J. L. (1995). A global model for present-day atmospheric/soil CO2 consumption by chemical erosion of continental rocks (GEM-CO2). *Tellus B*, *47B*(1-2), 273–280. https://doi.org/10.1034/j.1600-0889.47.issue1.23.x

APHA. (2015). Standard Methods for the Examination of Water and Wastewater. https://www.standardmethods.org/

Arino, O., Gross, D., Ranera, F., Leroy, M., Bicheron, P., Brockman, C., Defourny, P., Vancutsem, C., Achard, F., Durieux, L., Bourg, L., Latham, J., Di Gregorio, A., Witt, R., Herold, M., Sambale, J., Plummer, S., & Weber, J.-L. (2007). GlobCover: ESA service for Global Land Cover from MERIS. *2007 IEEE International Geoscience and Remote Sensing Symposium*, 2412–2415. https://doi.org/10.1109/IGARSS.2007.4423328

Arnold, J. G., Allen, P. M., Muttiah, R. S., & Bernhardt, G. (1995). Automated Base Flow Separation and Recession Analysis Techniques. *Ground Water*, *33*(6), 1010–1018. https://doi.org/10.1111/j.1745-6584.1995.tb00046.x

Arnold, J. G., Moriasi, D. N., Gassman, P. W., Abbaspour, K. C., White, M. J., Srinivasan, R., Santhi, C., Harmel, R. D., van Griensven, A., Van Liew, M. W., Kannan, N., & Jha, M. K. (2012). SWAT: Model use, calibration, and validation. *Transactions of the ASABE*, *55*(4), 1491–1508. https://doi.org/10.13031/2013.42256

Arnold, J. G., Srinivasan, R., Muttiah, R. S., & Williams, J. R. (1998). Large area hydrologic modeling and assessment: Part I: Model development. *Journal of the American Water Resources Association*, *34*(1), 73–89. https://doi.org/10.1111/j.1752-1688.1998.tb05961.x

Arnold, J. G., & Williams, J. (1987). Validation of SWRRB—Simulator for Water Resources in Rural Basins. *Journal of Water Resources Planning and Management*, *113*(243-256). https://doi.org/10.1061/(ASCE)0733-9496(1987)113:2(243)

Brown, L. C., Barnwell, T. O., & Barnwell, J. (1987). The enhanced stream water quality models QUAL2E and QUAL2E-UNCAS: Documentation and user manual.

Dürr, H. H., Meybeck, M., & Dürr, S. H. (2005). Lithologic composition of the Earth's continental surfaces derived from a new digital map emphasizing riverine material transfer. *Global Biogeochemical Cycles*, *19*(4). https://doi.org/10.1029/2005GB002515

Eckhardt, K. (2005). How to construct recursive digital filters for baseflow separation. *Hydrological Processes*, *19*(2), 507–515. https://doi.org/10.1002/hyp.5675

EEA. (2012). Corine Land Cover (CLC) 2012: Version 20. http://land.copernicus.eu/pan-european/corine-land-cover/clc-2012/view

Elzhov, T. V., Mullen, K. M., Spiess, A.-N., & Bolker, B. (2016). minpack.lm: R Interface to the Levenberg-Marquardt Nonlinear Least-Squares Algorithm Found in MINPACK, Plus Support for Bounds. https://CRAN.R-project.org/package=minpack.lm

Epelde Beraza, A. M. (2015). *Modelización de procesos hidrológicos y de contaminación por nitratos mediante dos códigos numéricos (SWAT y MOHID). Cuenca agrícola del río Alegria (País Vasco)* (Doctoral dissertation). Universidad del País Vasco/Euskal Herriko Unibertsitatea. Leioa. http://hdl.handle.net/10810/15954

EVE - Ente Vasco de la Energía. (1989). Mapa geológico del País Vasco a escala 1:25,000: 63-I, 63-III, 88-I, 88-III, planos.

FAO, IIASA, ISRIC, ISS-CAS, & JRC. (2012). Harmonized World Soil Database (version 1.2). http://www.fao.org/soils-portal/soil-survey/soil-maps-and-databases/harmonized-world-soil-database-v12/en/

Fekete, B. M., Vörösmarty, C. J., & Grabs, W. (2002). High-resolution fields of global runoff combining observed river discharge and simulated water balances. *Global Biogeochemical Cycles*, *16*(3), 15-1-15–10. https://doi.org/10.1029/1999GB001254

Fu, B., Merritt, W. S., Croke, B. F., Weber, T. R., & Jakeman, A. J. (2019). A review of catchment-scale water quality and erosion models and a synthesis of future

prospects. *Environmental Modelling & Software*, *114*, 75–97. https://doi.org/10.1016/j.envsoft.2018.12.008

Gupta, H., Sorooshian, S., & Yapo, P. (1999). Status of Automatic Calibration for Hydrologic Models: Comparison with Multilevel Expert Calibration. *Journal of Hydrologic Engineering*, *4*(2), 135–143. https://doi.org/10.1061/(ASCE)1084-0699(1999)4:2(135)

Gupta, H. V., Kling, H., Yilmaz, K. K., & Martinez, G. F. (2009). Decomposition of the mean squared error and NSE performance criteria: Implications for improving hydrological modelling. *Journal of Hydrology*, *377*(1-2), 80–91. https://doi.org/10.1016/j.jhydrol.2009.08.003

Hartmann, J. (2009). Bicarbonate-fluxes and CO2-consumption by chemical weathering on the Japanese Archipelago — Application of a multi-lithological model framework. *Chemical Geology*, *265*(3-4), 237–271. https://doi.org/10.1016/j.chemgeo.2009.03.024

Hartmann, J., Lauerwald, R., & Moosdorf, N. (2014). A Brief Overview of the GLObal RIver Chemistry Database, GLORICH. *Procedia Earth and Planetary Science*, *10*, 23–27. https://doi.org/10.1016/j.proeps.2014.08.005

Hartmann, J., & Moosdorf, N. (2012). The new global lithological map database GLiM: A representation of rock properties at the Earth surface. *Geochemistry, Geophysics, Geosystems*, *13*(12). https://doi.org/10.1029/2012GC004370

Hartmann, J., Moosdorf, N., Lauerwald, R., Hinderer, M., & West, A. J. (2014). Global chemical weathering and associated P-release — The role of lithology, temperature and soil properties. *Chemical Geology*, *363*, 145–163. https://doi.org/10.1016/j.chemgeo.2013.10.025

Hijmans, R. J., Cameron, S. E., Parra, J. L., Jones, P. G., & Jarvis, A. (2005). Very high resolution interpolated climate surfaces for global land areas. *International Journal of Climatology*, *25*(15), 1965–1978. https://doi.org/10.1002/joc.1276

Huscroft, J., Gleeson, T., Hartmann, J., & Börker, J. (2018). Compiling and Mapping Global Permeability of the Unconsolidated and Consolidated Earth: GLobal HYdrogeology MaPS 2.0 (GLHYMPS 2.0). *Geophysical Research Letters*, *45*(4), 1897–1904. https://doi.org/10.1002/2017GL075860

Iribar, V., & Ábalos, B. (2011). The geochemical and isotopic record of evaporite recycling in spas and salterns of the Basque Cantabrian basin, Spain | Elsevier Enhanced Reader. *Applied Geochemistry*, *26*, 1315–1329. https://doi.org/10.1016/j.apgeochem.2011.05.005

Kemanian, A. R., Julich, S., Manoranjan, V. S., & Arnold, J. R. (2011). Integrating soil carbon cycling with that of nitrogen and phosphorus in the watershed model SWAT: Theory and model testing. *Ecological Modelling*, *222*(12), 1913–1921. https://doi.org/10.1016/j.ecolmodel.2011.03.017

Knisel, W. G. (1980). *A field scale model for chemicals, runoff, and erosion from agricultural management systems*.

Lehner, B., & Grill, G. (2013). Global river hydrography and network routing: baseline data and new approaches to study the world's large river systems. *Hydrological Processes*, *27*(15), 2171–2186. https://doi.org/10.1002/hyp.9740

Leonard, R. A., Knisel, W. G., & Still, D. A. (1987). GLEAMS: Groundwater Loading Effects of Agricultural Management Systems. *Transactions of the ASAE - American Society of Agricultural Engineers (USA)*, 1403–1418. https://doi.org/10.13031/2013.30578

Meybeck, M. (1986). Composition chimique des ruisseaux non pollués de France. *Sciences Géologiques*, *39*(1), 3–77.

Moré, J. J. (1978). The Levenberg-Marquardt algorithm: Implementation and theory. In G. A. Watson (Ed.), *Numerical Analysis* (pp. 105–116). Springer Berlin Heidelberg. https://doi.org/10.1007/BFb0067700

Moriasi, D. N., Arnold, J. G., Van Liew, M. W., Bingner, R. L., Harmel, R. D., & Veith, T. L. (2007). Model evaluation guidelines for systematic quantification of accuracy in watershed simulations. *Transactions of the ASABE*, *50*(3), 885–900. https://doi.org/10.13031/2013.23153

Nash, J. E., & Sutcliffe, J. V. (1970). River flow forecasting through conceptual models part I - A discussion of principles. *Journal of Hydrology*, *10*(3), 282–290. https://doi.org/10.1016/0022-1694(70)90255-6

Neitsch, S. L., Arnold, J. G., Kiniry, J. R., & Williams, J. R. (2011). *Soil and Water Assessment Tool: Theoretical Documentation Version 2009*. https://swat.tamu.edu/docs/

R Core Team. (2019). R: A language and environment for statistical computing. https://www.R-project.org/

Shangguan, W., Hengl, T., Mendes de Jesus, J., Yuan, H., & Dai, Y. (2017). Mapping the global depth to bedrock for land surface modeling. *Journal of Advances in Modeling Earth Systems*, *9*(1), 65–88. https://doi.org/10.1002/2016MS000686

van Vliet, M. T. H., Franssen, W. H., Yearsley, J. R., Ludwig, F., Haddeland, I., Lettenmaier, D. P., & Kabat, P. (2013). Global river discharge and water temperature under climate change. *Global Environmental Change*, *23*(2), 450–464. https://doi.org/10.1016/j.gloenvcha.2012.11.002

Vet, R., Artz, R. S., Carou, S., Shaw, M., Ro, C.-U., Aas, W., Baker, A., van Bowersox, C., Dentener, F., Galy-Lacaux, C., Hou, A., Pienaar, J. J., Gillett, R., Forti, M. C., Gromov, S., Hara, H., Khodzher, T., Mahowald, N. M., Nickovic, S., … Reid, N. W. (2014). A global assessment of precipitation chemistry and deposition of sulfur, nitrogen, sea salt, base cations, organic acids, acidity and pH, and phosphorus. *Atmospheric Environment*, *93*, 3–100. https://doi.org/10.1016/j.atmosenv.2013.10.060

Wang, X., Kannan, N., Santhi, C., Potter, S. R., Williams, J. R., & Arnold, J. G. (2011). Integrating APEX output for cultivated cropland with SWAT simulation for regional modeling. *Transactions of the ASABE*, *54*(4), 1281–1298. https://doi.org/10.13031/2013.39031

Wickham, H. (2016). ggplot2: Elegant Graphics for Data Analysis. https://ggplot2.tidyverse.org

Williams, J. R., Arnold, J. G., Kiniry, J. R., Gassman, P. W., & Green, C. H. (2008). History of model development at Temple, Texas. *Hydrological Sciences Journal*, *53*(5), 948–960. https://doi.org/10.1623/hysj.53.5.948

Xie, J., Liu, X., Wang, K., Yang, T., Liang, K., & Liu, C. (2020). Evaluation of typical methods for baseflow separation in the contiguous United States. *Journal of Hydrology*, *583*, 124628. https://doi.org/10.1016/j.jhydrol.2020.124628

Part III

RESULTS AND DISCUSSION

CHAPTER 4

Model development

The present chapter contains the exploration of several worldwide database to elucidate the main drivers of the ionic flux derived from chemical weathering of rocks. With those drivers, a conceptual model is represented under different mathematical models, to test which of them yield lower discrepancies between simulated and observed values. The model is calibrated, validated, and applied at the annual scale to elucidate the globally spatial distribution of mean annual fluxes of major ions independently. The main results of the present chapter are contained in an published scientific article: Lechuga-Crespo, J.L., Sánchez-Pérez, J.M., Sauvage, S., Hartmann, J., Amiotte Suchet, P., Probst, J.L., Ruiz-Romera, E. (2020). **A model for evaluating continental chemical weathering from riverine transports of dissolved major elements at a global scale.** *Global and Planetary Change, 192*, Article 103226. https://doi.org/10.1016/j.gloplacha.2020.103226

4.1 Abstract

This study presents a process-based-empirical model for the assessment of ionic fluxes derived from chemical weathering of rocks (ICWR) at a global scale. The equations are designed and the parameters fitted using riverine transport of dissolved major ions Ca^{2+}, Mg^{2+}, K^{+}, Na^{+}, Cl^{-}, SO_4^{2-}, and alkalinity at a global scale by combining point sampling analysis with spatial descriptions of hydrology, climate, topography, lithology and soil variables such as mineral composition and regolith thickness. Different configurations of the model are considered and the results show that the previously reported "soil shielding" effect on chemical weathering (CW) of rocks presents different values for each of the ions considered. Overall, there is good agreement between median and ranges in observed and simulated data, but further analysis is required to downscale the model to catchment scale. Application to the global scale provides the first global ICWR map, resulting in an average cationic flux derived from chemical weathering of $734 \cdot 10^6$ $Mg \cdot y^{-1}$, where 58% is Ca^{2+}, 15% is Mg^{2+}, 24% is Na^{+} and 3% is K^{+}, and an average anionic flux derived from chemical weathering of $2640 \cdot 10^6$ $Mg \cdot y^{-1}$, where 74% is alkalinity, 18% is SO_4^{2-}, and 8% is Cl^{-}. Hyperactive and hot spot areas are elucidated and compared between ions.

4.2 Introduction

Freshwater chemical composition has long been used as a proxy to understand the processes occurring in a catchment (e.g. Amiotte Suchet and Probst, 1993a; Gibbs, 1970; Romero-Mujalli, Hartmann, and Börker, 2019). The insights obtained from these analyses are relevant for assessing biogeochemical cycles, since rivers are vectors of matter transport between land and oceans (J. L. Probst, 1992). Major ion riverine loads are linked to the mineralogical composition of the underlying bedrock and overlying soil, and to their sensitivity to chemical weathering (CW) (Hartmann, 2009). CW of rocks is the process responsible for transforming rock into saprolites and soils, i.e. soil

pedogenesis, in the Critical Zone (CZ) (Riebe et al., 2017), which releases dissolved compounds that are subsequently transported by rivers.

For several decades, evaluation and quantification of CW has been the focus of hydrogeochemical research (Di Figlia et al., 2007; Hartmann, Lauerwald, et al., 2014; Jansen et al., 2010; Livingstone, 1963; Raab et al., 2019; White & Blum, 1995) and in more recent years it has also been used to quantify trends in salt increases related to human activities (Guo et al., 2015; Kaushal et al., 2018; Meybeck, 2003; Moosdorf et al., 2011). Large-scale studies have focused CW analysis on its implications for atmosphere/land/ocean fluxes and the Earth's climate, in influencing the biogeochemical cycles of elements by regulating CO_2 consumption, or nutrient release (Amiotte Suchet & Probst, 1993b, 1995; Dupré et al., 2003; Hartmann, Lauerwald, et al., 2014). However, fewer studies have centred on individual ion analysis (e.g. Goddéris et al., 2006; Goddéris et al., 2009) and, to the authors' knowledge, there is no spatially explicit reference product for ionic fluxes derived from chemical weathering of rocks (ICWR) at a global scale that quantifies the natural rock fluxes of single ions.

Assessment of chemical weathering rates (CWR) at catchment-to-global scale has evolved over recent years due to improvements in laboratory experiments, the compilation of river water chemical databases, and the development of technical resources in modelling (Amiotte Suchet & Probst, 1993a, 1995; Biondino et al., 2020; Dong et al., 2019; Hartmann, Lauerwald, et al., 2014; Meybeck, 1987; Perri et al., 2016; J. L. Probst et al., 1994). A distinction can be drawn between two main approaches to hydrogeochemical modelling: mechanistic and empirical based models. On the one hand, mechanistic models such as WHAM (Tipping, 1994) or WITCH (Goddéris et al., 2006) base their calculation on distinguishing between several layers in the soil with different chemical weathering rates, integrating the chemical composition of soils and the drainage waters in a mass-balance where the dissolution of primary minerals is described through kinetic laws (Goddéris et al., 2006; Roelandt et al., 2010), though they require a large quantity of detailed data which is normally not available worldwide. On the other hand, empirical models relate CWR to environmental variables through linear and non-linear regression, using statistically fitted parameters (Amiotte Suchet

& Probst, 1995; Dessert et al., 2003; Hartmann, 2009; Meybeck, 1987), ignoring the physical dynamics behind the process. Despite their greater degree of abstraction, empirical laws have extensively been used to quantify global fluxes of matter (Hartmann, Lauerwald, et al., 2014) and CO_2 sequestration by rock weathering (Amiotte Suchet & Probst, 1995; Dessert et al., 2003; Hartmann et al., 2009; J. L. Probst et al., 1997), since they require less exhaustive input data and fewer computing resources while at the same time providing a useful product.

Given that, to the best of the authors' knowledge, there are no spatially explicit results at a global scale for the contribution of each major ion to the total CWR, and that this needs to be quantified before assessing the global anthropogenic inputs of major ions (Vörösmarty et al., 2010),the present study seeks to develop and apply an empirical model at a global scale to quantify the ICWR of major elements. The methodology pursued is based on that presented by Hartmann (2009), and the objectives are: *i)* to present the methodology used to develop a spatially explicit empirical model of ICWR; *ii)* to evaluate the limitations of this methodology and of application of the model; and *iii)* to present and contrast the preliminary results of the model at a global scale, including a discussion of spatial distribution and an assessment of hyperactive and hot spot areas.

4.3 Materials and methods

4.3.1 Conceptualization

Conceptualization of the CW process used in developing this model is explained in the following lines and shown in graphic form in the Supplementary Information, Figure S4.1. Major ion fluxes—i.e. Ca^{2+}, Mg^{2+}, K^{+}, Na^{+}, Cl^{-}, SO_4^{2-}, and alkalinity (HCO_3^{-} + CO_3^{2-})—in rivers have previously been used as a proxy of all the processes occurring in the upstream draining catchment (Garrels & Mackenzie, 1972; Hartmann & Moosdorf, 2011; Meybeck, 1984, 1986), and are also considered in the present study. Two sources

are established with regards to the spatial unit of the catchment: allochthonous, when the origin of the element lies outside the boundaries of the catchment (i.e. atmospheric dry and wet deposition); and autochthonous when the source of the element lies within the catchment area (i.e. bedrock chemical weathering). Human activity is a third source of ions in rivers, which may be: allochthonous when ions originating from anthropogenic activities are brought to the river by atmospheric deposition, e.g. acid rain (Likens et al., 1996; Mahowald et al., 2011; Schindler, 1988); or autochthonous when there are spot saline sources or diffuse input within the unit, such as effluents from wastewater treatment plants (Carey & Migliaccio, 2009), cropland fertilization, or road salting (Dailey et al., 2014; Moore et al., 2008). The conceptual schema of the major ion biogeochemical cycle adopted in this study is shown in the Supplementary Information (Figure S4.1).

Atmospheric deposition incorporates ions to the CZ (from above the ground through the soil and saprolite horizons to the bedrock, Keller, 2019) which are either concentrated in the soil surface by evapotranspiration and washed out of the catchment through surface and sub-surface runoffs; or infiltrated into the saprolite down to the unsaturated and saturated zones, reaching the groundwater reservoir. Soil processes—such as organic matter decay and root uptake followed by biomass storage—interact with these salts and may present synergies with the transport fluxes, altering the concentration of the salts present in the lateral flow (or subsurface runoff) and subsequently the river water (Keller, 2019). As regards the groundwater source, salts are derived from water interaction with rocks and later transported to the stream with groundwater flow (or baseflow).

CW has long been reported as a dominant process in major water composition, and several studies (Balagizi et al., 2015; Gaillardet et al., 1999; Garrels & Mackenzie, 1972; Stallard & Edmond, 1981; Velbel, 1993) have highlighted the relevance of lithology, hydrology, soil chemistry, and temperature, as variables that condition both CW and soil processes, while distance to the coast and altitude mostly affect atmospheric deposition (Meybeck, 1986; Vet et al., 2014). The combination of all these variables, in addition to human input, condition major ion loads leaving the catchment.

Other dissolved compounds may be found in the dissolved riverine loadings which may interact with major ions, such as SiO_2, NO_3^-, or PO_4^{3-}. However, these elements have not been included within the scope of the modelling, since their global biogeochemical cycles are more complex and more closely linked to biological interactions (c.f. Galloway et al., 2004; Hartmann, Lauerwald, et al., 2014) than those of the major ions selected, which are assumed to have more similar pathways between reservoirs and a more stable temporal evolution (Keller, 2019).

4.3.2 Workflow and data overview

In order to estimate the specific fluxes of major ions, i.e. Ca^{2+}, Mg^{2+}, K^+, Na^+, Cl^-, SO_4^{2-}, and alkalinity, linear regressions have been developed using global databases as input data, fitting the parameters of the equations to minimize the difference between modelled and observed data. The mathematical approach used to develop the equations and fit the parameters is based on previous literature (e.g. Amiotte Suchet and Probst, 1993a, 1993b; Hartmann, 2009; Meybeck, 1979).

The observed chemical concentrations used in this study were taken from the GLORICH database (Hartmann, Moosdorf, et al., 2014, retrieved from https://doi.pangaea.de/10.1594/PANGAEA.902360), which compiles over 1.2 million analyses of river waters around the world, as well as containing additional information on the draining catchments at the sampling locations. In order to focus on sampling locations mainly affected by atmospheric deposition and chemical weathering fluxes, a subset of the samples was created (see section 4.3.2.1). The specific chemical fluxes were derived from averaged chemical concentrations and specific discharge for each draining catchment, and the differentiation between the atmospheric and chemical weathering contribution was computed using an independent dataset to estimate the atmospheric deposition (see section 4.3.2.2). Additional variables were then included in the analysis, such as soil type abundance taken from the Harmonized World Soil Database (HSWD, FAO et al., 2012), regolith thickness (GSDE, Shangguan et al., 2017), and soil permeability

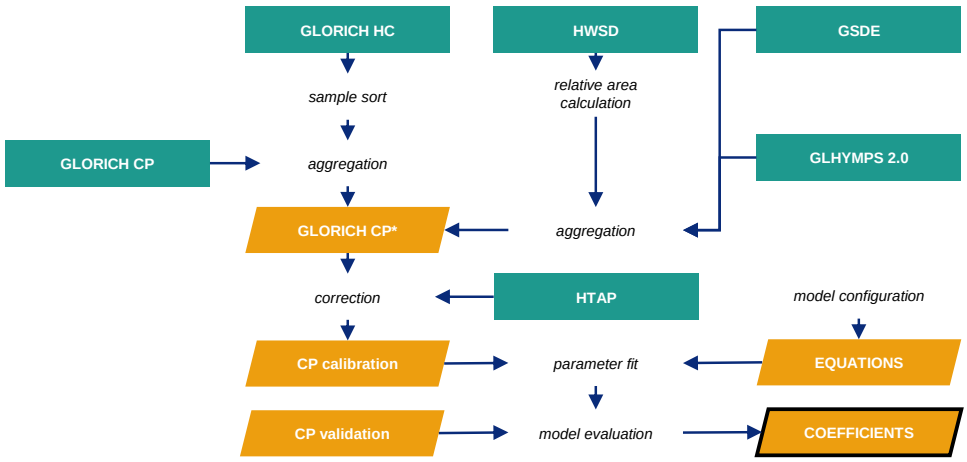

Figure 4.1: Workflow summary. The green rectangles represent the original databases included in the analysis, while the yellow boxes contain the datasets derived for the present analysis, and the arrows describe actions. The acronyms refer to: the GLORICH database (Hartmann, Moosdorf, et al., 2014) which contains information on hydrochemical analyses (HC) and catchment properties (CP); the Harmonized World Soil Database (HSWD, FAO et al., 2012); the global regolith thickness (GSDE, Shagguan et al., 2017); the soil permeability (GLHYMPS 2.0, Huscroft et al., 2018); and the world precipitation chemistry dataset (HTAP, Vet et al., 2014).

(GLHYMPS, Huscroft et al., 2018). The incorporation of these databases is described in section 4.3.2.3 and a summary of the uncertainties may be found in section 4.3.2.4. The workflow followed is shown in graphic form in Figure 4.1.

4.3.2.1 Data subset and estimation of atmospheric deposition

The original chemical data stored in the GLORICH HC was sorted to exclude samples with missing data for Ca^{2+}, Mg^{2+}, K^{+}, Na^{+}, Cl^{-}, SO_4^{2-}, and alkalinity, samples showing an ionic charge balance error over ±10% and sampling locations with <3 samples. Around 65% of the original 1,274,102 samples analysed in 18,897 locations between 1942 and 2011 were excluded. Chemical concentrations at the sampling location were aggregated through the median value since the distribution was non-normal according to a Shapiro-Wilk test ($p<0.01$). Not all sampling locations presented an associated draining catchment, and some were nested catchments; these were also excluded,

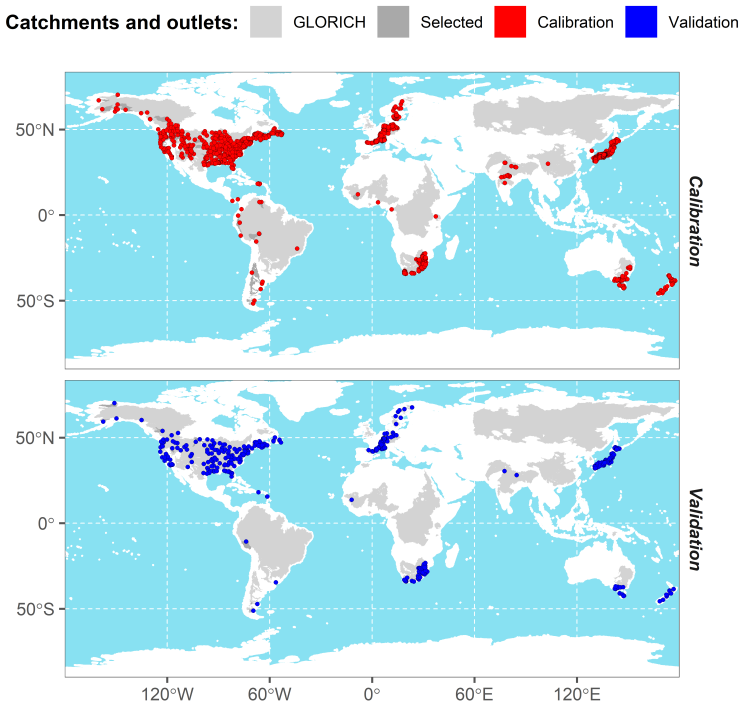

Figure 4.2: Original, subset, and classified sampling locations and draining catchments in the present study. Within the original GLORICH dataset (light grey), the darker grey areas represent the selected draining catchments, for which the outlets are represented as red or black points depending on whether they have been used for calibration (n = 1313) or validation (n = 438), respectively.

resulting in 1,751 catchments ranging from 1 to $2.9{\cdot}10^4$ km^2, with 3 to 1,220 samples, depending on the catchment. A map showing the selected sampling locations and associated areas may be seen in Figure 4.2.

4.3.2.2 Estimation of derived variables and atmospheric deposition

Due to the heterogeneity of the data on the number of samples in each sampling location and the frequent lack of instantaneous discharge, average riverine specific fluxes, F_x measured in $mol{\cdot}m^{-2}{\cdot}y^{-1}$, were estimated from riverine concentration and specific runoff

(computed as the discharge at the outlet of the catchment divided by the draining area, Fekete et al., 2002) using Equation 4.1. In this equation, specific runoff, q_{ann}, measured in $mm \cdot y^{-1}$, was multiplied by the average concentration C_x of the sampling location, measured in $mol \cdot L^{-1}$, for each ion *x*.

$$F_x = q_{ann} \cdot C_x \tag{4.1}$$

Riverine-specific fluxes include the mass departing the catchment from bedrock weathering, atmospheric deposits and other sources (including anthropogenic activities). In order to estimate ICWR, it was necessary to subtract the contribution of atmospheric deposition (Meybeck, 1983). Anthropogenic input could not be quantified since the extent of the anthropic influence differs between catchments; it was therefore assumed to be negligible for major cations and anions at the scale of application. However, further research on the impact of human pressure is needed (Vörösmarty et al., 2010).

Atmospheric flux was estimated using the results of Vet et al. (2014) (HTAP database) on atmospheric seasalt and sulphur deposition. First, the mean seasalt flux throughout the catchment was computed for each catchment using the "raster" package in R (Hijmans, 2019). In order to distinguish the contribution of each ion in the total salt deposition, an ionic concentration distribution profile was then calculated for coastal and continental zones in each continent. To compute these profiles, the raw data used in Vet et al. (2014), obtained from the World Data Precipitation Chemistry website (http://wdcpc.org/global-assessment-data) was classified by continents and into coastal/continental, based on distance from the coast. Average concentration values and ratios to the total salt concentration were then computed (see chemical distribution profiles in Supplementary Information Figure S4.2 and Figure S4.1).

Once the percentages of each element within the total concentration were obtained, the catchments were classified into zones according to the position of their centroid. This classification, together with the mean seasalt deposition flux, allowed us to quantify the specific atmospheric flux for each element in each catchment. CW fluxes were computed by subtracting the atmospheric deposition flux from the riverine flux.

4.3.2.3 Database integration

Spatial analysis was performed using ArcGIS 10.4 and mainly consisted of summarising raster files in the polygonal shapes of the draining catchment. All data was integrated using R software (R Core Team, 2019). Three worldwide databases were included in the original GLORICH catchment properties (CP) database. For each catchment, the cover percentage of each HSWD soil type (FAO et al., 2012) was computed, and the mean regolith depth (Shangguan et al., 2017) and mean hydraulic conductivity (Huscroft et al., 2018) were then summarised. The spatial resolution is different for each database included; the catchment borders were delimited using the Hydro1K database (c.f. Hartmann, Lauerwald, et al., 2014) at a 30 arc-second resolution, the same as for the HWSD soil type database (FAO et al., 2012) and hydraulic conductivity (Huscroft et al., 2018). However, finer resolution is found for the global soil depth database (Shangguan et al., 2017). Uncertainties in dataset collection are discussed in section 4.3.2.4. However, considering the global approach of the study and the relatively small size of some catchments (see Supplementary Information, Figure S4.3), the spatial resolution of the global databases was considered sufficient to represent the lithological and soil compositions, average soil depth, and hydraulic conductivity.

The data pre-process resulted in a database with over 180 variables, including chemical fluxes, morphological variables (i.e. altitude, area, slope, etc.), climate variables (monthly and annual temperature, precipitation, windspeed, etc.), land covers (forest, agricultural, managed percentages, etc.), soil types (Leptosols, Cambisols, Nitisols, etc.), soil descriptors (regolith thickness, hydraulic conductivity, pH, etc.), and lithology (Metamorphics, Plutonics Acids and Basics, Carbonate Sedimentary, etc.). This dataset was used to explore the relationships, calibrate the parameters of the equations, and test the residuals of the model created to further define the model.

4.3.2.4 Database uncertainties

The development, calibration, and validation steps of an empirical model rely on the data used for its construction. In this study, several types of data from different sources were included, selected following an assessment of their quality. Among chemical collection datasets, the GLORICH database (Hartmann, Moosdorf, et al., 2014) was chosen because it contained a larger amount of data located in a greater number of catchments. Moreover, it contains two types of data: spot data (related to the samples analysed in each river) and spatial data (relating to the physical description of the draining catchment). Spot data was gathered from different monitoring programs and scientific literature and tested to eliminate possible errors, although this dataset was considered to have been validated by its creators (Hartmann, Moosdorf, et al., 2014). The spatial data for both the GLORICH description of the draining basin characteristics and the added variables is based on contrasted spatial datasets. The lithological distribution was taken from the Global Lithological Map (GLIM, Hartmann and Moosdorf, 2012) which, to the best of the authors' knowledge, is the highest resolution lithological database at a global scale. Soil type abundance was computed using the polygons in the Harmonized World Soil Database (HSWD, FAO et al., 2012). The hydrology was taken from the 0.5ºx0.5º raster in the UNH/GRDC Composite Runoff Fields V1.0 (Fekete et al., 2002). Regolith thickness was taken from the 1x1km raster Global Soil Regolith Thickness (GSDE, Shagguan et al., 2017). Hydraulic conductivity was estimated from the polygons in Global Hydrogeology Maps (GLHYMPS, Huscroft et al., 2018). The seasalt atmospheric deposition was derived from 1ºx1º raster from the global assessment of precipitation chemistry (Vet et al., 2014). The uncertainties and limits for each dataset are set out in each of the publications, while in the present analysis the global results are modelled (using the soil, lithology, and specific runoff databases) at a resolution of 0.5ºx0.5º.

4.3.3 Modelling approach

Chemical weathering rates are mainly affected by hydrology, lithology of the underlying bedrock, the overlying soil, and water temperature (Hartmann, 2009; Hartmann, Lauerwald, et al., 2014). In order to analyse the effect of each one on all of the ion fluxes, it was proposed to test 8 linear equations. To design the equations, a physical interpretation of the estimates was considered, and the variables were added in the following order: lithology, soil shielding effect (further explained in the paragraphs below and in Hartmann, Lauerwald, et al., 2014), temperature, hydraulic conductivity and soil depth. The set of equations tested is as follows:

$$F_x = q_{ann} \cdot c_x \tag{M1}$$

$$F_x = q_{ann} \sum (L_i \cdot c_x) \tag{M2}$$

$$F_x = q_{ann} \cdot f_{xs}(\text{soil}) \sum (L_i \cdot c_x) \tag{M3}$$

$$F_x = q_{ann} \cdot f_T(\text{temperature}) \sum (L_i \cdot c_x) \tag{M4}$$

$$F_x = q_{ann} \cdot f_{xs}(\text{soil}) \cdot f_T(\text{temperature}) \sum (L_i \cdot c_x) \tag{M5}$$

$$F_x = q_{ann} \cdot f_D(\text{soil depth}) \sum (L_i \cdot c_x) \tag{M6}$$

$$F_x = q_{ann} \cdot f_K(\text{hydraulic conductivity}) \sum (L_i \cdot c_x) \tag{M7}$$

$$F_x = q_{ann} \cdot f_{KD}(\text{soil depth} + \text{hydraulic conductivity}) \sum (L_i \cdot c_x) \tag{M8}$$

$$f_{s,x} = \frac{F^*_{x(\text{shield} \geq 0.5)}}{F^*_{x(M2,\text{shield} \geq 0.5)}} \tag{4.2}$$

$$f_T = \exp\left(\frac{1}{T} - \frac{1}{\overline{T}}\right) \tag{4.3}$$

$$f_{s,x} = \frac{\text{Depth}}{\text{Depth}_{MAX} - b \cdot \text{Depth}} \tag{4.4}$$

$$f_K = \frac{K_{hyd}}{K_{hyd,MAX} - b \cdot K_{hyd}} \tag{4.5}$$

$$f_{KD} = \frac{\text{Depth}}{K_{hyd}} \tag{4.6}$$

Where F_x^* represents the ionic flux derived from chemical weathering of rocks (ICWR) of an element *x*, measured in $mol \cdot m^{-2} \cdot y^{-1}$; q_{ann} represents the annual average runoff composite of the catchment (computed as the discharge at the outlet of the catchment over the area of the draining surface), in $dm^3 \cdot m^{-2} \cdot y^{-1}$; L_i accounts for the percentage of the area covered by a lithological group i (see Figure S4.6); $f_{s,x}$ is the soil shielding effect factor, dimensionless; f_T represents the temperature effect factor, dimensionless; f_D is the soil depth factor, dimensionless; and the f_K considers the hydraulic conductivity factor, dimensionless; f_{KD} is the soil depth-hydraulic conductivity factor, dimensionless; $F^*_{x,M2}$ is the flux obtained with model M2, in $mol \cdot m^{-2} \cdot y^{-1}$; T is the average annual air temperature of the draining basin taken from the GLORICH database, computed from the WordClim (Hijmans et al., 2005) database, in K; $\overline{T}$ is the global average annual temperature, in K; Depth measures the soil depth, in cm; and K_{hyd} measures the mean hydraulic conductivity, in $m \cdot s^{-1}$. A further detail of the former three factors is set out in the following paragraphs. For all models tested here, the parameters are c_x, $c_{x,i}$, measured in $mol \cdot L^{-1}$, and b, dimensionless, and may be interpreted as the average concentration of an element x in the water draining from rock i (c_x and $c_{x,i}$) corrected for atmospheric inputs, and b as the function parameter. The parameters fitted at the calibration step are c_x, $c_{x,i}$, and b.

Soil cover over bedrock has been identified as an important factor to consider when analysing the CW at a global scale (Dupré et al., 2003; Hartmann, Lauerwald, et al., 2014). Some soil types with thick profiles, or high organic matter content, or low permeability may act as a buffer to the chemical flux arriving to the river stream, as shown by Boeglin and Probst (1998) for large river basins covered by lateritic soils, where the fluxes of bicarbonates supplied by silicate hydrolysis are half of the river fluxes produced in non-lateric basins. In this regard, Hartmann, Lauerwald, et al., 2014 estimated an average soil shielding factor of 0.1 for the following FAO soil types: Ferralsols, Acrisols, Nitisols, Lixisols, Histosols, and Gleysols. Here, we consider a similar factor, but differentiating between the values for each ion. In this study, 416

catchments showed a percentage of coverage of this kind of soil of 50% and were expected to be affected by the "soil shielding effect".

In order to include the soil shielding effect $f_{s,x}$ we established a threshold to differentiate between two groups of catchments: those in which 50% or more of the area was covered by the sum of the soil types Ferralsols, Acrisols, Nitisols, Lixisols, Histosols, and Gleysols (Hartmann, Lauerwald, et al., 2014), where the dominance of the soil shielding effect was expected; and those where this sum was under 50%. The mean values of the flux for each group and ion was computed and the ratio of atmospherically corrected observed flux to flux obtained with model M2, for soil-shield-affected affected catchments was computed, giving $f_{s,Ca}$=0.75; $f_{s,Mg}$=0.74; $f_{s,Na}$=0.46; $f_{s,K}$=0.78; $f_{s,Alkalinity}$=0.70; $f_{s,SO_4^{2-}}$=0.29; $f_{s,Cl}$=0.34.

As regards the temperature effect, catchments with higher average temperature were expected to drain higher fluxes of elements than those with lower temperatures. Annual air temperature was used as a proxy for groundwater mean temperature, which is responsible for changes in the solubility constants of certain minerals. Then, a similar temperature factor to Hartmann, Lauerwald, et al. (2014) with an Arrhenius type equation was then computed as f_T.

4.3.3.1 Calibration and model evaluation

The parameters from the equations were fitted using a 75% random subset of the data ($n_{calibration}$=1313) from the selected sites (Figure 4.2), while the remainder were used for validation ($n_{validation}$ = 438). The fit was carried out using the Levenberg-Marquardt algorithm, a method used to find the minimum of a function, in this case, a sum of squares (Moré, 1978), implemented in the "minpack.lm" package (Elzhov et al., 2016) for the R software (R Core Team, 2019). As the parameters to fit were interpreted as the concentration (c_x, $c_{x,i}$) of an element draining from water from each lithological group, a lower boundary of 0 was established. The performance of the model was evaluated by assessing the significance of the relation between observed and simulated values

using Spearman correlation (ϱ) and evaluation of the percentage of deviation (PBIAS), which measures the average tendency of the simulated values to be above or below the observed values.

$$\rho = \frac{\mathrm{cov}(\mathrm{rg}_{\mathrm{Observed}}, \mathrm{rg}_{\mathrm{Simulated}})}{\sigma_{\mathrm{rg,Observed}} \sigma_{\mathrm{rg,Simulated}}} \tag{4.7}$$

$$\mathrm{PBIAS} = \frac{\sum(\mathrm{F}_{\mathrm{Simulated}} - \mathrm{F}_{\mathrm{Observed}})}{\sum(\mathrm{F}_{\mathrm{Observed}})} \tag{4.8}$$

Where $\mathrm{cov}(\mathrm{rg}_{\mathrm{Observed}},\mathrm{rg}_{\mathrm{Simulated}})$ is the covariance of the observed and simulated fluxes, σ_{rg} accounts for the standard deviation of the variables, and F represents the specific fluxes. Finally, the model is applied over a grid with a cell size of 0.5x0.5° where superposition of the GLIM, HSWD, and UNH/GRDC (Fekete et al., 2002) datasets allowed for the generation of single combination cells where the M3 model estimates were applied.

4.4 Results

4.4.1 Assessment of model performance

Table 4.1 summarises the statistics used to evaluate performance of the model, all of which show a significant correlation ($p<0.01$). M1 only includes the average specific runoff and the fitted parameter represents the average concentration of element x in all catchments; it is used here as a starting point for model performance. As expected, the inclusion of lithology in the regression (M2) improved correlation of the model and decreased the difference between observed and simulated data. Inclusion of the "soil shielding" effect (M3) therefore has improved the correlation but also increased the difference between the data, as shown by the increase in PBIAS. The incorporation of temperature (M4) had no effect when compared to model M2, and neither did the combination of "soil shielding effect" and temperature (M5), while aggregation of soil depth (M6) decreased the correlation with regard to M2 and M3. M7 and M8 show

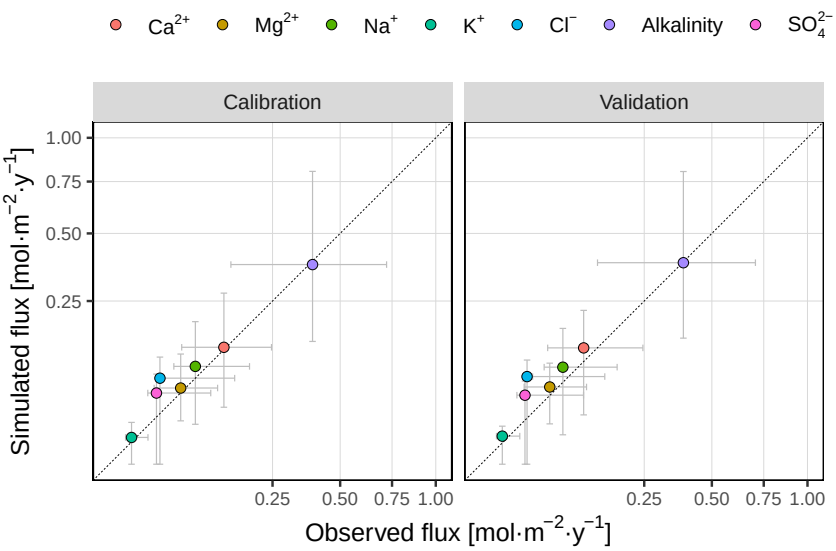

Figure 4.3: Scatterplot of simulated and observed data for calibration and validation, using model M3. Each point represents a median value for each ion considered in this study, and the bar expands over the first and third quartiles to show how the average ranges are captured by the model. The dashed line represents 1:1.

the lowest correlations and the highest PBIAS. It is important to note that there are almost no differences in the statistics from M2 to M5, although the best performance of the model, with the fewest explanatory variables, was achieved with M3, as further analysed in this study.

In general, there is a strong and significant correlation between the median observed and simulated values considering all catchments and ions included in the present study ($\rho_{Spearman}$=0.96, p<0.01), as shown in Figure 4.3. In addition, both observed and simulated fluxes expand over similar interquartilic ranges (IQR = 3^{rd}Q-1^{st}Q), suggesting that this model configuration is capable of estimating the median and ranges of ionic-specific fluxes in large scale studies. When each ion is evaluated independently, and site-specific fluxes are compared in observed-simulated pairs, two findings may be derived: there is a higher data scatter, as shown by lower µand a greater underestimation of the model, noted by a more negative PBIAS (Table 4.1). For M3, the best represented ions are Ca^{2+} and Alkalinity, with correlations of over 0.6 and a PBIAS of under 15%,

while the poorest are Na^+ and Cl^-, with correlation of under 0.3 and PBIAS >45% (Table 4.1). Nevertheless, the residuals display a normal distribution, centring on 0, suggesting a valid model configuration.

Application of the model to the validation dataset gives the result shown in Figure 4.3. Like the calibration dataset, the model shows better results for alkalinity, and worse results for Cl^-.

4.4.2 Application of the model

Model M3 has been considered to represent a fair starting point for assessing ICWR at large scales. Before applying it to smaller case studies, it should be contrasted in specific case studies with adapted data, such as observed average specific discharge, soil maps, and lithological distribution, with a finer resolution, instead of using globally derived products. Here, the model is applied to a grid with a cell size of 0.5º where superposition of the GLiM, HSWD, and UNH/GRDC datasets allowed for the generation of single combination cells in which the M3 model estimates were applied. The results of this application are displayed in Figure 4.4, which shows the spatial distribution of the ICWR, measured in $Mg \cdot km^2 \cdot y^{-1}$ for easier comparison with previous studies in Table 4.2.

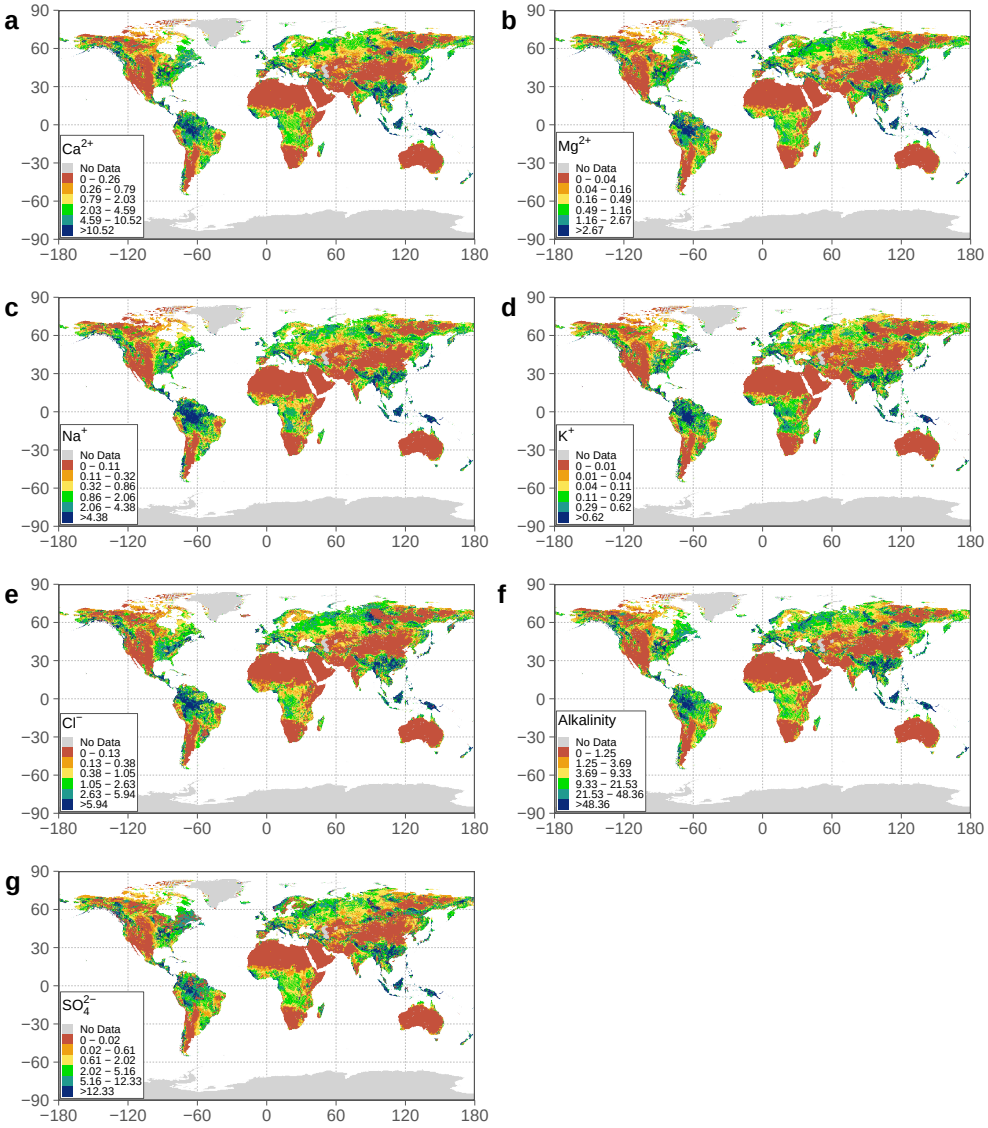

Figure 4.4: Holospheric distribution of Ionic fluxes derived from Chemical Weathering of Rocks (ICWR), all data expressed in $Mg \cdot km^2 \cdot y^{-1}$. The maps were obtained by applying the model to a global grid of 0.5º using the fitted parameters in model M3. Note that each ion presents a different colour range based on the global percentile distribution, using $P10^{th}$, $P25^{th}$, $P50^{th}$, $P75^{th}$, and $P90^{th}$ as breakpoints.

Table 4.1: Spearman correlation coefficients (ρ) and PBIAS values [%] for the eight models tested here (M1-M8, n=1313) in the calibration dataset. The last column ("MEAN") shows the mean value for all ion assessment in each model. All correlations are statistically significant ($p<0.01$). M3 is considered the best and analysed further in this text.

	Ca^{2+}		Mg^{2+}		Na^{+}		K^{+}		Cl^{-}		Alkalinity		SO_4^{2-}		MEAN	
	ρ	PBIAS	ρ	PBIAS	ρ	PBIAS	ρ	PBIAS	ρ	PBIAS	ρ	PBIAS	ρ	PBIAS	ρ	PBIAS
M1	0.41	-24.1	0.24	-34.7	0.31	-42.0	0.26	-24.0	0.13	-52.1	0.40	-26.5	0.32	-36.6	0.29	-34.3
M2	0.59	-13.7	0.39	-26.2	0.29	-41.3	0.43	-19.5	0.15	-48.6	0.66	-12.3	0.45	-26.5	0.42	-26.9
M3	0.60	-15.1	0.40	-28.0	0.29	-45.0	0.42	-20.8	0.16	-52.9	0.66	-13.4	0.50	-29.1	0.43	-29.2
M4	0.59	-13.7	0.39	-26.2	0.29	-41.3	0.43	-19.5	0.15	-48.6	0.66	-12.3	0.45	-26.5	0.42	-26.9
M5	0.60	-15.1	0.40	-28.0	0.29	-45.0	0.42	-20.8	0.16	-52.9	0.66	-13.4	0.50	-29.1	0.43	-29.2
M6	0.56	-16.2	0.41	-20.4	0.31	-25.7	0.36	-18.7	0.18	-28.4	0.66	-14.3	0.43	-26.3	0.41	-21.4
M7	0.15	-65.9	0.04	-71.2	0.12	-57.0	0.11	-60.8	0.06	-52.9	0.16	-72.5	0.20	-75.8	0.12	-65.2
M8	0.24	-81.4	0.23	-80.3	0.21	-83.0	0.18	-78.0	0.09	-84.8	0.30	-86.2	0.16	-88.4	0.20	-83.2

Table 4.2: Comparison between studies on of CWR at global scales. All values expressed at 10^6 $Mg \cdot y^{-1}$. ΣZ^+ represent the Ca^{2+}, Mg^{2+}, Na^+, and K^+ while ΣZ^- for Cl^-, SO_4^{2-}, and Alkalinity (expressed as HCO_3^-). Bracketed values represent a recalculation of ΣZ^+ adding a virtual contribution of SiO_2, considering a SiO_2/Ca^{2+} of 0.7.

Study	Code	Ca^{2+}	Mg^{2+}	Na^+	K^+	Alkalinity	SO_4^{2-}	SiO_2	Cl^-	ΣZ^+	ΣZ^-	Total flux from Chemical Weathering
This study	M1	374	100	223	25	1815	401	-	246	722 (984)	2642	3184 (3446)
	M2	484	121	202	29	2234	500	-	263	836 (1175)	2997	3833 (4172)
	M3	428	107	176	24	1954	465	-	221	734 (1034)	2640	3374 (3674)
	M4	527	132	221	31	2434	545	-	287	911 (1284)	3266	4177 (4550)
	M5	477	119	202	27	2139	490	-	241	825 (1159)	2870	3695 (4029)
Meybeck (1979)	Natural	502	126	192	48	1940	307	-	215	868	2462	3330
	Total	549	136	270	53	2040	431	388	308	1008	3167	4175
J. L. Probst (1992)		510	141	211	73	2013	455	355	223	935	3046	3981
Gaillardet et al. (1999)		-	-	-	-	-	-	-	-	-	-	2131
Hartmann, Lauerwald, et al. (2014)	Soil shielding applied	-	-	-	-	-	-	-	-	(1439)	-	-

Overall, higher ICWRs are obtained for alkalinity, SO_4^{2-}, and Ca^{2+}, in concordance with the dominant elements commonly found in freshwater environments, while the lowest ICWRs are found for K^+, which commonly accounts for a lower proportion of water chemistry. In general, higher ICWRs are found in latitudes between 15º S and 15º N for all ions, probably related to higher specific discharge and humid tropical climates. This is clearly shown for alkalinity, presenting highest values for the Amazon and the Congo basins, as well as the Polynesian Islands. Low median fluxes are found between 15ºN and 30ºN and 15ºS and 30ºS but probably affected by the Saharan and Australian deserts, in contrast, the south-eastern parts of Asia and Central America show higher ICWR. In this study, relevant fluxes are also found between 45º N and 75º N whose contribution to chemical fluxes had previously been assessed as not being relevant (Hartmann, Lauerwald, et al., 2014). In the GLORICH database and other input datasets, there is no catchment in the Antarctic and Greenland, though ICWRs in these areas are displayed as No Data, but they are probably affected by snow and ice processes not properly represented in this study, as described by Wadham et al. (2010) and St-Pierre et al. (2019).

4.5 Discussion

4.5.1 Overall

The present study shows the development of an inverse model for the assessment of ICWR at a global scale, based on aggregated chemical analysis of spot samples at a catchment level around the world, as well as on worldwide datasets. It is the first time that a map of the ionic flux derived from chemical weathering of rocks is presented, and represents an improvement on previously published similar models (Amiotte Suchet & Probst, 1995; Gaillardet et al., 1999; Hartmann, Lauerwald, et al., 2014; Ludwig et al., 2011; Meybeck, 1987). In order to discuss the results, three main points are established:

- A comparison is made between the results of the model and the last model presented on Chemical Weathering Rates (CWR, Hartmann, Lauerwald, et al., 2014) and other global studies, in order to validate the results obtained and contrast the differences.
- A framework of application of this model is established with regard to the spatial scale of application. In addition, the advantages that this configuration poses for potential users, and limitations regarding scales and conceptualization are also discussed.
- An identification and comparison of the hot spots among ions at a global scale is described, to highlight the role of ICWR in global biogeochemical cycles.

4.5.2 Model validation

The results of the present study are compared to previous studies in table 4.2, considering the individual ionic fluxes and their aggregations in cation, anion, and total fluxes. In general, the M3 model presents an average global CWR of ~3375·10^6 Mg·y^{-1}, which is lower than previous studies, e.g. ~4175·10^6 Mg·y^{-1} (Meybeck, 1979), ~4050·10^6 Mg·y^{-1} (J. L. Probst, 1992), but higher than more recent results ~2131·10^6 Mg·y^{-1} (Gaillardet et al., 1999). However, focusing specifically on the ~734·10^6 Mg·y^{-1} total cation flux (ΣZ^+), it has a lower value than a recent study at the same scale ~1439·10^6 Mg·y^{-1} (Hartmann, Lauerwald, et al., 2014). Differences in this result are attributed to three main causes: differences in the definition of CWR (inclusion of dissolved silica), the number and location of the reference sampling sites selected for the model calibration step, and the configuration of the model itself. According to results from Meybeck, 1979 and J. L. Probst, 1992, the SiO_2/Ca^{2+} ratio is ~0.7, which would yield a $\Sigma Z^+_{M3^*}$ of ~1034·10^6 Mg·y^{-1} closer to, but lower than, the study by Hartmann, Lauerwald, et al., 2014.

The CWR measurement shows discrepancies between research studies, given that several compute the total weathered matter from rocks through Total Dissolved Solids,

TDS (e.g. Dessert et al., 2003; Donnini et al., 2016) while others make different aggregations, i.e. cations (e.g. Balagizi et al., 2015; Dessert et al., 2003; Gaillardet et al., 1999) or cations plus SiO_2 (e.g. Hartmann, Lauerwald, et al., 2014). In the present study, each ion is computed independently to overcome these discrepancies, in a similar way to Braun et al. (2005) and Goddéris et al. (2009). Among the applications of these studies, a knowledge of CWR is of interest in assessing CO_2 consumption through rock dissolution (Amiotte Suchet and Probst, 1995; Amiotte Suchet et al., 2003; Hartmann, 2009), in studying the global biogeochemical cycles of P (c.f. Hartmann, Lauerwald, et al., 2014), and in characterising the riverine end-member in oceanic assessments (Sun et al., 2016). Assessing each ion independently offers an opportunity for a more detailed description of the CW process and the associated assessments at a global scale. In this regard, the present study will be a reference for future works, especially in large-scale applications (see discussion sections below). The ICWR model yields similar flux median and ranges values as compared to the observed data for alkalinity, but a poorer representation of Cl^-, linked to a predominantly atmospheric input and traces of evaporites located in other lithological groups that are not large enough to be mapped at a global scale but are large enough to have a significant impact on riverine loads.

Previous authors have attributed the overestimation of empirically-modelled CWR in tropical areas (such as the Amazon, Congo, and Orinoco basins) and its underestimation in northern latitudes to the small number of sampling locations included in development of the model (see discussion in Hartmann, Lauerwald, et al., 2014 and Goddéris et al., 2006). The recent study by Hartmann, Lauerwald, et al. (2014) extrapolated a regionally fitted model (using 381 sampling locations in the Japanese Archipelago, see Hartmann and Moosdorf, 2011) to the world, and further refined its formulation by considering 49 large river catchments in different locations worldwide, among which there are several tropical and Arctic basins. Gaillardet et al. (1999), on the other hand, initially included this kind of basin in their model fitting, taking the 60 largest rivers in the world as a reference. Here, 1313 sampling locations in large basins and small catchments in warm and cold climates around the world were used for the model fit step, reflecting greater variability in the parameter estimates and thus giving to more robust results, as supported by the residual normal distribution.

Nevertheless, even though the number of sampling locations is greater than in previous empirical model developments, they are spatially clustered in some areas, excluding relevant areas from the calibration and validation steps (Figure 4.2). Northern latitudes (the Arctic catchments), Polynesian sampling locations and a large quantity of data available from Asia are not included in the present analysis because of non-availability in the data source selected, or due to the subset criterion established (see section 4.3.2.1). Despite not including these areas, the calibration subset is considered to be representative of different climates, soils and lithological characteristics (see Supplementary Information, Figure S4.3 to Figure S4.7), allowing a flexible tool to be developed that is capable of capturing a great variability in catchment characteristics, albeit acknowledging its limitations (see section 4.5.3).

CW of rocks is a complex process that is controlled by several factors that vary with soil depth, e.g. the composition of minerals (Apollaro et al., 2019; Biondino et al., 2020), and the hydrology (S. P. Anderson et al., 2004; Gabet et al., 2006; Hartmann, 2009). Boeglin and Probst (1998) showed that for large river basins, the atmospheric/soil CO_2 consumed by silicate weathering and the associated bicarbonate river fluxes are 1.8 times lower when the bedrock is covered by deep lateritic soils. Oliva et al. (2003) noted that regolith depth shields the rocks from CW in areas where this layer is thicker, however Dong et al. (2019) reported that the highest CW occurs at an intermediate soil thickness. In this regard, we hypothesized that a larger regolith (soil+saprolite) layer would act as a proxy for erosion-product deposition, and in synergy with a low hydraulic conductivity, would result in a lower CWR (S. P. Anderson et al., 2004; Gabet et al., 2006).

However, inclusion of global regolith thickness (Shagguan et al., 2017) and hydraulic conductivity (Huscroft et al., 2018) in this study did not improve the results. We associate this finding with the model configuration and the scale of application. In addition, the GLHYMPS database (Huscroft et al., 2018) was computed from the GLiM database, which is already accounted in the model variables, although information may already have been included in the lithological group classification. In contrast with our study, Dong et al. (2019) succeeded in including of these variables using a physically

based model, by making a distinction between different soil layers. However, our data-driven model was not capable of including these variables within its context and the area of application poses a challenge in describing the required variables. Nonetheless, an improvement in performance of the model in relation to soil data can be found in the "soil shielding effect" factor (Dupré et al., 2003; Hartmann, Lauerwald, et al., 2014), computed for soil types classified based on their pedogenesis in the HSWD database (FAO et al., 2012). Soils with thick layers, low hydraulic conductivities, dominated by organic matter decay, or with a shallow ground water table (Hartmann, Lauerwald, et al., 2014) would have a stronger shielding effect. We attribute the improvement in the model's results to the soil shielding effect, and the lack of success in including new variables to the fact that the combination of the lithological and soil classification maps already takes into account the interaction of chemical fluxes with the soil layers overlying the bedrock zone, and the fact that the inclusion of regolith thickness and hydraulic conductivity requires a physically-based approach for inclusion in studies of chemical weathering studies.

Temperature is another variable initially considered to be relevant in CW (Dessert et al., 2003; Drever & Zobrist, 1992; Hartmann, Lauerwald, et al., 2014), since it reflects changes in the equilibrium constant of the dissolution reactions (Drever, 2012). An increase in water temperature would increase dissolution of rocks and augment biological activity, through respiration and pCO_2 in the soil, but it would also reduce the gas dissolution in the liquid. However, CO_2 is produced by ecosystem respiration, inducing acids responsible for chemical weathering; this is a two-factor dependence (soil water content and temperature) which explains why an Arrhenius-type factor for the model alone does not improve the results (Romero-Mujalli, Hartmann, Börker, et al., 2019). Dissolution takes place in the regolith water and groundwater, but we could find no database with worldwide spatially distributed temperature values. For this reason, air temperature is used as a proxy for this effect, but its inclusion does not provide any improvement in the model. This is related to two main factors: the different effect on the dissolution of each mineral and that the fact that, although groundwater temperature is dependent on annual average air surface temperature, this variable appears not to be a proxy related to the temperature effect on CW reactions.

Further research is needed to analyse the effect of water temperature on these fluxes worldwide.

At the conceptualization stage (see section 4.3.1), several other variables were considered, such as vegetation (land cover), evapotranspiration, or a finer definition of rocks (including rock ages), but after some consideration, these data were not included in the development stage. Vegetation fixes atmospheric C through photosynthesis, which is later exchanged by roots with microorganisms during soil respiration, increasing the CO_2 concentration in the soil pores, which would dissolve in water to generate carbonic acid and enhance rock dissolution, thus releasing ions into the water matrix (c.f. Keller, 2019). However, changes in the photosynthesis process, soil respiration and evapotranspiration are processes with a higher variability (posing a challenge in modelling them, c.f. Chen and Liu, 2020) than the annual mean value used in this study, although this variability could not be captured. Evapotranspiration, conditioned by climatic variables such as temperature and precipitation, affects the water balance by extracting water from the system (i.e. basin) causing an increase in the saline concentration found in rivers. However, its effect on CW is less pronounced than other characteristics, such as lithological classification (White & Blum, 1995). This suggests that a better representation of the effect of precipitation, air temperature and other climatic variables on chemical weathering rates is mainly related to an improvement in the water balance at a basin scale, which could be achieved by using more detailed models. Lastly, in comparison with previous similar studies (Amiotte Suchet & Probst, 1995; Meybeck, 1986) recent studies include a larger number of lithological classes (Hartmann, Lauerwald, et al., 2014, this study), involving a finer definition of minerals. Despite this larger number, further levels of classification of lithologies are available (c.f. Hartmann and Moosdorf, 2012), but given the number of sampling locations, it would have been a challenge to include all of them, as most of them would not vary in a wide enough range to calibrate the parameters in the model. Even with the classification used in this study, there are some lithological classes which do not span the entire spectrum (e.g. plutonic intermediate, see Supplementary Information, Figure S4.6), meaning that in the subset considered in this study, there are no catchments in which 100% of the draining area is covered by these lithologies. The inclusion of finer lithological classification should

focus on smaller-scale cases, where mechanistic models may be applied, or when the chemical data compilation includes cases spanning the entire range of values.

Despite the current assessment, the relative importance of these variables in chemical weathering may not be well represented in the selected modelling approach, since data-driven models describe the process based on correlations of the data and not on physical fundaments, as mechanistic models do (e.g. WITCH model, Goddéris et al., 2006). The uncertainty regarding this kind of model is large and difficult to quantify (Hartmann, Lauerwald, et al., 2014), and is strongly affected by the reference sampling locations and the pre-processing step, which may induce bias in the data used for model fitting. Strict criteria on sampling location selection excludes around 80% of the data included in the original database but excludes the bias introduced by isolated samples (catchments sampled only once or twice) or from heavily anthropogenically affected samples.

The greatest uncertainty in the pre-processing step is found in the separation of the riverine flux between atmospheric and bedrock fluxes, but its relevance is noted in previous literature (Dessert et al., 2003; Hartmann & Moosdorf, 2011; Meybeck, 1986; Stallard & Edmond, 1981). With regard to the ionic sources in streams, atmospheric deposition has been noted as being relevant with regard to the input of sea-salt derived Cl^- and Na^+, especially in catchments located close to the coast (E. K. Berner & Berner, 2012; Meybeck, 1986). In arid regions, the atmospheric input of Ca^{2+} and K^+ is related more to aeolian dust, biomass burning, or industrial emissions (Vet et al., 2014). Several publications show large scale deposition of base ions in the United States e.g. (e.g. Brahney et al., 2013) and other authors such as Lehmann et al., 2005) have studied the temporal evolution of these depositions. In this study, no temporal evolution has been studied, but an average spatial value has been derived from the data of Vet et al. (2014), which may differ for specific cases and requires further analysis when downscaling the model.

To the best of the authors' knowledge, no results of mechanistic models representing ICWR at a global scale have previously been published, as upscaling of this kind of

models is constrained to the data availability (creating a need for assumptions or simplifications when applying to large scales) and computing resources. In this context, the present study represents a step forward in the assessment, through modelling, of CW at a global scale in three main aspects: assessing CW at a global scale making a distinction of each ion; establishing a simple law that can be downscaled to catchment-level studies in later studies, and highlighting the need for physically-based principles in order to study the effect of variables such as regolith thickness, hydraulic conductivity, or water temperature.

4.5.3 Domain of application

In general, this kind of model has been applied at regional or global scale to perform several assessments, such as atmospheric CO_2 sequestration by rocks through dissolution of minerals (Amiotte Suchet & Probst, 1995; Amiotte Suchet et al., 2003; Balagizi et al., 2015; Ludwig et al., 1998; J. L. Probst, 1992), Si mobilization (Jansen et al., 2010) and analysis of the P-release (Hartmann, Lauerwald, et al., 2014). Alkalinity fluxes measured in rivers have commonly been used as a tracer of CO_2 sequestration by CW, and two main groups of rocks have been studied: carbonates and silicates. Following the reactions shown in Figure S4.1, alkalinity fluxes from silicate rocks come only from the atmospheric/soil CO_2, while for carbonates draining waters, 50% of the riverine flux is associated with lithogenic carbonate contribution (Amiotte Suchet & Probst, 1993a; Balagizi et al., 2015; Gaillardet et al., 1999; Hartmann et al., 2009; J. L. Probst et al., 1994). It is important to note that SiO_2 is not considered in this study, because its implication for the biogeochemical cycle is strongly affected by its accumulation on amorphous silica, or biogenic silica in living organisms (Conley, 2002) processes which proved complex to simulate at the present scale.

Here, the present model defines the CWR by its constituents, i.e. ions, analyses the weight of each one in the total flux and helps to assess the average specific flux. The poor representation of Na^+ fluxes is linked to different drivers governing the dissolution of

the rocks with this kind of elements, such as albite or volcanic glass, which are reported as large CO_2 sinks in a global context (Dessert et al., 2003). In order better to represent the Na^+ and SO_4^{2-} ions from an inverse modelling point of view, other variables should be taken into consideration, as their presence may be linked more to redox processes than to congruent dissolution by acids (E. K. Berner & Berner, 2012), like dissolved oxygen concentration or redox potential, which are commonly measured in the field. This finding highlights the importance of analysing all ions when considering CW and other associated processes, as since although the CWR has previously been quantified, the representation of all ions in this flux is not equally well defined, indicating that further research is needed to improve the representation of those elements and an understanding of the associated processes. Keller, 2019 shows an analysis of the Critical Zone and explains CW in its context; a relevant number of variables are tied up with this process (including denudation rate, rock age, etc.), and these variables should be taken into consideration in any further developments of these models and may be responsible for the variability not captured by the model. This study has shown that CWR is mostly conditioned by Ca^{2+} and alkalinity, though the other ions need further research to be properly represented.

A relevant factor in applying this model is the scale of application. The model has been applied at a global scale, but the initial data encapsulated catchments with different sizes. In general, basins draining an area between 10 and 10,000 km^2 were those that showed discrepancies of within ±20% between modelled and observed data (Table S4.3). Those two limits encompass most of the catchments considered in this study and are therefore, the best spatial scale for application of the model. Larger catchments are expected to drain water affected by more processes other than CW (such as cyclic salts and pollution) and have a more complex hydrology, while smaller catchments may not be well defined in terms of the lithological composition. A compromise between the scale of application and the level of detail needs to be found in order to apply a model, especially for large scale applications (Fu et al., 2019). This is a limitation for application of the model at this step; further analysis on the performance and variability captured by the model in larger or smaller catchments should be studied and considered in future studies.

In addition to the applications noted above, the model provides an opportunity to assess the natural major ionic composition of water, relevant in analysis of crop production (Wicke et al., 2011) and useful when analysing "river syndromes" (salinization, eutrophication, etc. see Meybeck, 2003) at the scales indicated. An initial snapshot for ICWR fluxes is presented in Figure 4.4. This data can be used as a reference for scarce data availability on water chemistry analysis and as a constraint for assessing anthropogenic influence in analysis of catchment water. Moreover, the method presented can be used as a guide for developing models with different lithological classifications if a different the lithological map exists, and enough data are available for parameter fitting.

Application of this model is tested for sampling locations with the characteristics summarised in the Supplementary Information (Figure S4.3 to Figure S4.7) and extrapolation of the model to a global scale yielded to a similar value to recent studies (see section 4.4.2). Nonetheless, constraints have been found for classification of the lithology and soil considered in the input dataset (see Figure S4.6 and Figure S4.7 for a summary). Temporal evolution has not been tested, as chemical data was summarised to a unique value per catchment, and hydrology was aggregated to a single annual value. Refinement of the model should focus on distinguishing the different hydrological fluxes (groundwater, surface, lateral flows, etc.) in order to take into account processes of dilution and concentration, apart from the improvements in representation of the CW process. As regard performance of the model, the main limitation of this model is the poorer representation of some ions (Na^+ and Cl^-) compared to others (Ca^{2+} and alkalinity).

4.5.4 Hot spots at a global scale

Previous literature (McClain et al., 2003) has called for an assessment of hot spots and hot moments in the study of biogeochemical cycles. Although the present analysis does not take temporal evolution into account, the results shown in Figure 4.4 may be used

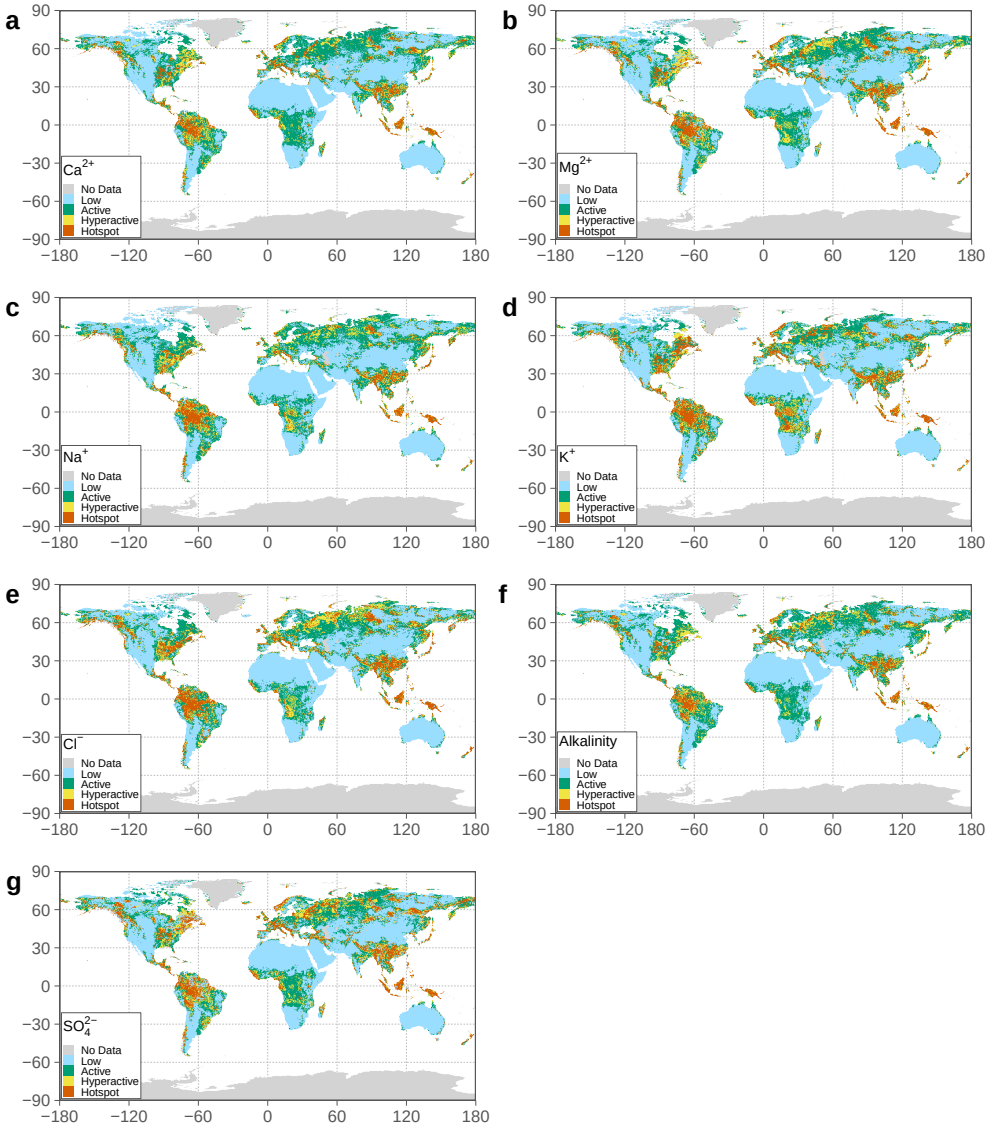

Figure 4.5: Holospheric distribution of low, active, hyperactive, and hot spot areas with regard to ICWR at a global scale. The classification is based on the global median value. Low activity areas (blue) are those that stand below the median global ICWR; Active areas (green) contain areas between the median and 5 times the median global ICWR; Hyperactive areas (yellow) include areas with between 5 and 10 times the global ICWR; and Hot spots (red) are those with over 10 times the global median value.

to assess relevant spatial locations with regard to the CW of the different ions, on which future research should focus. Taking the classification used in Hartmann et al. (2009) as a starting point, four zones have been established for inter-comparison between ions: low zones, where the ICWR is at most the global median value; active zones, where ICWRs range from the median value to five times the median value; hyperactive areas, where ICWRs range from five to ten times the median value; and hot spots, where ICWR crosses the median-x-10 threshold (Figure 4.5). In general, hot spots are located between 30ºN and 30ºS in the northern part of South America, Central America, south-eastern Asia and the Polynesian islands. They are also common in the north-west and eastern part of North America, Central Europe and some areas in northern Asia, New Zealand and the south-western part of South America. These hot spots are located in higher specific runoff areas (Fekete et al., 2002), mainly in tropical and temperate areas (Beck et al., 2018), which explain higher fluxes, but they are also linked to Acrisol, Ferralsol, Gleysol, Histosol, Lixisol, and Nitisol soils (FAO et al., 2012) which shield the underlying rocks from CW. The presence of soil shielding classes and the different effects found for each ion may explain the different spatial patterns among ions within these areas, especially noted for Na^+, Cl^-, and SO_4^{2-} (Figure 7.5).

A discussion of CW rates in northern latitudes, islands and areas of volcanic arcs may be found in Hartmann, Lauerwald, et al. (2014), which were found to be highly active with regard to chemical weathering rates. Such active areas in the northern latitudes (specially for Ca^{2+}, Mg^{2+}, and alkalinity) may be related to highly weatherable carbonate material, most common between 20ºN and 50ºN (Amiotte Suchet et al., 2003). The results of the present analysis support the maintenance of these areas as hot spots; however, differences were found between ions. The Congo basin contains several hot spot areas for Na^+, K^+, and Cl^-, related to areas with evaporitic presence or soils with lower shielding effect which are less present for Ca^{2+}, Mg^{2+}, or alkalinity. Similarly, hot spots for these ions are also found in the interior of the Amazon basin, which result from a high specific runoff in this area. In contrast, field studies in the Amazon basin (e.g. Moquet et al., 2016) have highlighted the role of the Andean mountain belt in the delivery of dissolved solutes in this tropical catchment, in opposition to the lowland area. In the present study, low active areas in the Andes are related to an

underestimation of the specific discharge in these areas, which has previously been noted (Hartmann, Lauerwald, et al., 2014). In contrast to the Andean mountain belt, the Himalayas are classified as hot spots for all ions considered in this study. The reasons for these differences in comparison to the study by Hartmann, Lauerwald, et al. (2014) may be explained by considering each ion independently for the establishment of ICWR and differentiating the soil shielding effect among elements. These findings suggests that, although CWR at a global scale may be dominated by alkalinity and Ca^{2+} because of their higher magnitudes, the contribution of each ion should be considered independently, since the implications for other biogeochemical cycles (C sequestration through CW, riverine end-member characterization regarding saline inputs, or land-ocean loadings) could be better delimited by considering this approach.

4.6 Conclusion and further developments

This study presents an assessment of the global ICWR for the major ions Ca^{2+}, Mg^{2+}, K^{+}, Na^{+}, SO_4^{2-}, Cl^{-} and alkalinity, together with its spatial distribution. Overall, although this kind of model contains an important degree of uncertainty, this study contributes to a closer step between empirical and mechanical approaches, since it improves the representation of CWR by separating the total fluxes into ionic fluxes (ICWR); it is based on a broader collection of sampling locations, and it has taken into consideration up-to-date worldwide databases, highlighting better representation of ions such as Ca^{2+} and alkalinity, and poorer representation of Na^{+} and Cl^{-}. The results of this analysis indicate that a regression including lithology, soil and hydrology is enough to estimate the average flux and ranges of major ion CWR at a global scale. The results also show that previous measurements of CWR are mainly determined by Ca^{2+} and alkalinity, though the other elements need to be analysed to understand the key variables dominating their geochemical cycles at a global scale. This study also supports the idea that the most relevant factors are lithological distribution, hydrological representation and the soil shielding effect. In contrast, temperature was not concluded as to be relevant, but its role remains uncertain. In addition, the results coincide with previous identification

of hot spots in temperate climate latitudes but reflect the importance of considering more northerly latitudes in global matter assessments. Further studies should focus on improving representation of the input data, as well as a more in-depth analysis the worst represented ions, and a shift in approach from a static model to a dynamic approach, considering the changes on these fluxes over time, and thus allowing forecasting studies to be applied.

4.7 Supplementary Information

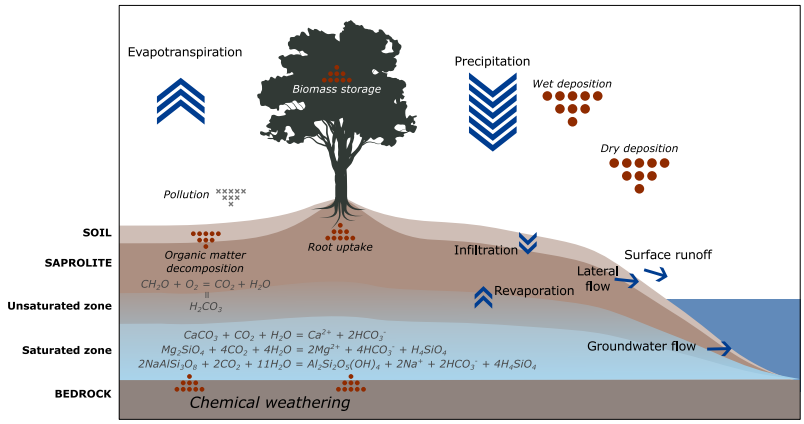

Figure S4.1: Conceptual schema of the biogeochemical cycle of the elements in the freshwater environments, dots indicate biogeochemical processes, arrows draw the water cycle and crosses represent human activities. Two main areas are differentiated in this schema, the atmospheric part where the water cycle is described by precipitation and evapotranspiration, and the land part where water moves between the root and vadose zones (through infiltration and revaporation, i.e. capillarity) and washes to the river into three main pathways: surface, lateral, and groundwater flows. Chemical processes in the atmospheric part include wet and dry deposition (A. Probst et al., 1990), where aerosols and particles migrate to the land area carried with or without water, respectively. In the land phase, organic matter decomposition (or soil respiration) enhances the production of CO_2, increasing the soil pCO_2 and the concentration of carbonic acid, which affects the dissolution of rocks in the chemical weathering process.

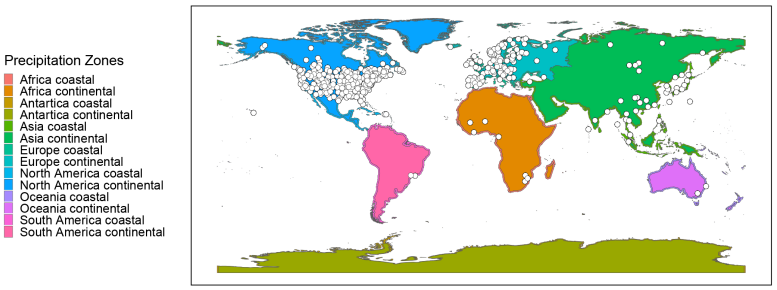

Figure S4.2: Rain chemical monitoring stations, after World Data Centre for Precipitation Chemistry (http://wdcpc.org/). Classified according to continent and coastal/continental depending on the distance to the coast (<100km for coastal).

Table S4.1: Table of ionic chemical distribution by precipitation station classification. This classification has been made using the station contained in each zone, aggregating the data through the mean concentration for each element over the sum of cationic or anionic concentration.

Continent	Zone	Ca^{2+}	Mg^{2+}	Na^{+}	K^{+}	Cl^{-}	SO_4^{2-}
Africa	Continental	39%	6%	26%	29%	40%	60%
	Coastal	19%	8%	62%	11%	30%	70%
Asia	Continental	51%	9%	19%	21%	51%	49%
	Coastal	33%	6%	44%	16%	34%	66%
Europe	Continental	47%	8%	34%	10%	53%	47%
	Coastal	12%	11%	70%	7%	20%	80%
North America	Continental	65%	9%	18%	9%	80%	20%
	Coastal	18%	9%	67%	7%	39%	61%
Oceania	Continental	19%	13%	62%	6%	16%	84%
	Coastal	7%	9%	81%	4%	31%	69%
South America	Continental	44%	9%	32%	15%	48%	52%
	Coastal	23%	7%	47%	23%	26%	74%

Table S4.2: Table of ionic chemical distribution by precipitation station classification. This classification has been made using the station contained in each zone, aggregating the data through the mean concentration for each element over the sum of cationic or anionic concentration.

	Ca^{2+}	Mg^{2+}	Na^{+}	K^{+}	Cl^{-}	Alkalinity	SO_4^{2-}
c_{ev}	1.19E-03	0.00E+00	0.00E+00	0.00E+00	0.00E+00	0.00E+00	1.40E-03
c_{ig}	1.77E-04	0.00E+00	0.00E+00	0.00E+00	0.00E+00	1.90E-04	0.00E+00
c_{mt}	2.96E-04	9.39E-05	7.01E-05	2.05E-05	7.24E-05	6.28E-04	1.24E-04
c_{nd}	9.14E-04	9.41E-05	0.00E+00	1.65E-05	0.00E+00	1.58E-03	2.67E-04
c_{pa}	9.49E-05	6.90E-06	9.58E-05	3.11E-06	3.03E-05	3.01E-04	0.00E+00
c_{pb}	6.35E-05	2.26E-04	1.35E-03	4.84E-06	1.77E-03	5.23E-04	0.00E+00
c_{pi}	1.27E-05	3.67E-05	1.44E-04	7.47E-06	1.89E-04	1.80E-04	1.70E-05
c_{py}	2.34E-04	3.40E-04	5.69E-04	9.54E-05	2.76E-04	1.54E-03	8.37E-05
c_{sc}	1.66E-03	6.61E-04	4.24E-04	5.19E-05	4.96E-04	4.54E-03	5.62E-04
c_{sm}	3.61E-04	1.59E-04	1.72E-04	1.17E-05	2.05E-04	1.63E-03	2.42E-04
c_{ss}	2.27E-04	1.03E-04	3.61E-04	1.06E-05	3.32E-04	5.29E-04	9.20E-05
c_{su}	2.40E-04	1.45E-04	3.86E-04	3.72E-05	1.92E-04	9.23E-04	9.26E-05
c_{va}	1.77E-04	2.03E-05	2.44E-04	4.79E-06	9.52E-05	2.93E-04	7.67E-05
c_{vb}	1.20E-04	4.71E-05	6.62E-05	0.00E+00	0.00E+00	3.39E-04	6.98E-05
c_{vi}	7.42E-04	1.42E-04	2.01E-04	2.14E-05	4.92E-05	8.42E-04	5.34E-04
c_{wb}	0.00E+00	0.00E+00	1.19E-03	1.97E-05	1.05E-04	0.00E+00	0.00E+00

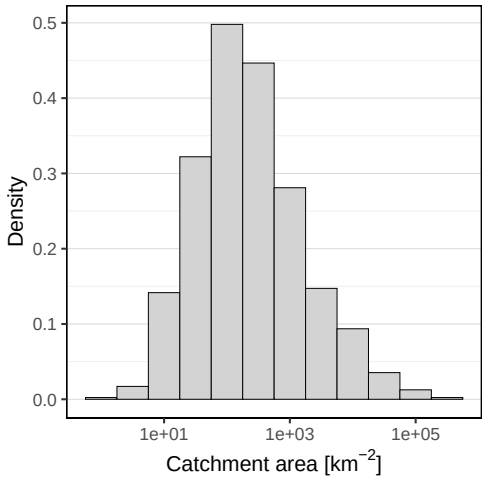

Figure S4.3: Catchment area histogram of the sampling locations. Note the logarithmic scale in the x axis

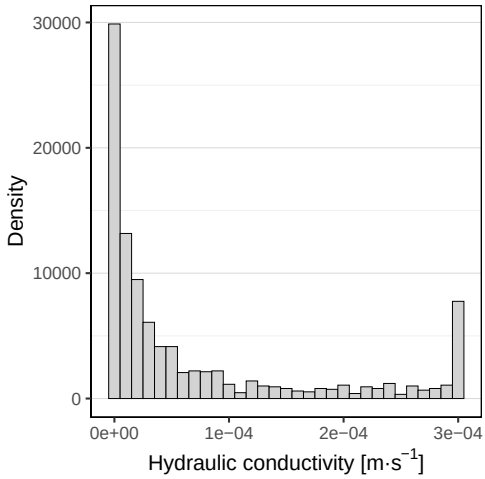

Figure S4.4: Mean hydraulic conductivity histogram on the selected catchments, according to the aggregated data from Huscroft et al., 2018.

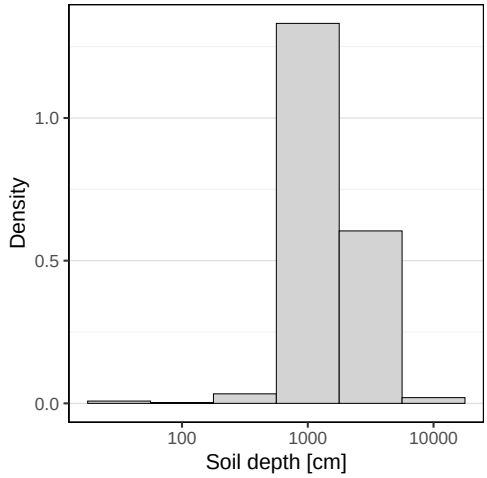

Figure S4.5: Mean soil depth of the sampling locations according to the aggregated data from Shangguan et al., 2017.

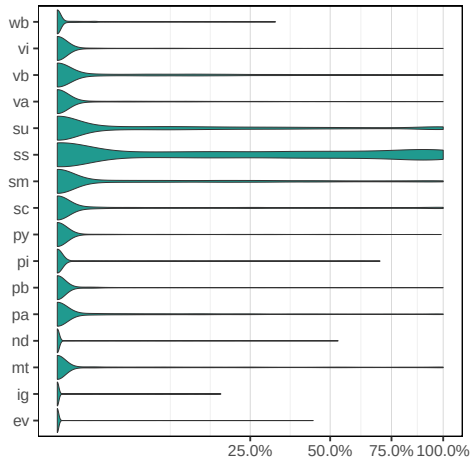

Figure S4.6: Lithological abundance distribution of the selected catchments. Each polygon represents one lithological group, the extend on the x axis of the shape represents the percentage of area of the catchment covered by such group, the top of the polygon indicates the maximum relative presence of a lithological group within a catchment, and the width of the polygon indicates the abundance of sampling locations with that percentage of cover of one lithological group. Lithological groups are, after Hartmann and Moosdorf, 2012 evaporites (ev), metamorphics (mt), no-data (nd), plutonic acid (pa), plutonic basic (pb), plutonic intermediate (pi), pyroclastics (py), carbonate sediments (sc), mixed sediments (sm), siliciclastic sediments (ss), unconsolidated sediments (su), volcanic acid (va), volcanic basic (vb), volcanic intermediate (vi). Two extra categories are present in the database: (ig) for ice and glaciers, and (wb) for water bodies.

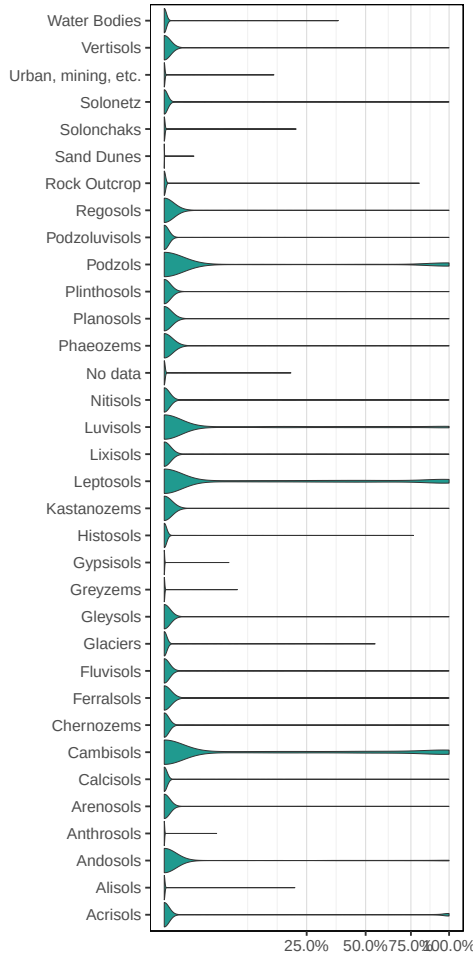

Figure S4.7: Soil abundance distribution in the selected catchments. Data is derived from the Harmonized World Database (HWSD, FAO et al., 2012).

Table S4.3: Table of ionic chemical distribution by precipitation station classification. This classification has been made using the station contained in each zone, aggregating the data through the mean concentration for each element over the sum of cationic or anionic concentration.

Area [km^2]	Ca^{2+}	Mg^{2+}	Na^{+}	K^{+}	Alkalinity	Cl^{-}	SO_4^{2-}	Mean	n
<10	10%	25%	-60%	-34%	-22%	-65%	-16%	-23%	53
10-10^2	-4%	-15%	2%	-36%	-9%	-8%	29%	-6%	565
10^2-10^3	12%	16%	29%	-10%	-6%	7%	46%	14%	780
10^3-10^4	-24%	-39%	-22%	-49%	-34%	11%	34%	-18%	269
10^5-10^6	-44%	-60%	-67%	-66%	-60%	-48%	-47%	-56%	77
>10^6	-13%	31%	-36%	11%	2%	23%	30%	7%	7

Bibliography

Amiotte Suchet, P., & Probst, J. L. (1993a). Flux de CO2 consommé par altération chimique continentale: influences du drainage et de la lithologie. *317*. https://oatao.univ-toulouse.fr/3544/

Amiotte Suchet, P., & Probst, J. L. (1993b). Modelling of atmospheric CO2 consumption by chemical weathering of rocks: Application to the Garonne, Congo and Amazon basins. *Chemical Geology*, *107*(3-4), 205–210. https://doi.org/10.1016/0009-2541(93)90174-H

Amiotte Suchet, P., & Probst, J. L. (1995). A global model for present-day atmospheric/soil CO2 consumption by chemical erosion of continental rocks (GEM-CO2). *Tellus B*, *47B*(1-2), 273–280. https://doi.org/10.1034/j.1600-0889.47.issue1.23.x

Amiotte Suchet, P., Probst, J. L., & Ludwig, W. (2003). Worldwide distribution of continental rock lithology: Implications for the atmospheric/soil CO2 uptake by continental weathering and alkalinity river transport to the oceans. *Global Biogeochemical Cycles*, *17*(2). https://doi.org/10.1029/2002GB001891

Anderson, S. P., Blum, J., Brantley, S. L., Chadwick, O., Chorover, J., Derry, L. A., Drever, J. I., Hering, J. G., Kirchner, J. W., Kump, L. R., Richter, D., & White, A. F. (2004). Proposed initiative would study Earth's weathering engine. *EOS*, *85*(28), 265–269. https://doi.org/10.1029/2004EO280001

Apollaro, C., Perri, F., Le Pera, E., Fuoco, I., & Critelli, T. (2019). Chemical and mineropetrographical changes on granulite rocks affected by weathering processes. *Frontiers of Earth Science*, *13*(2), 247–261. https://doi.org/10.1007/s11707-018-0745-5

Balagizi, C. M., Darchambeau, F., Bouillon, S., Yalire, M. M., Lambert, T., & Borges, A. V. (2015). River geochemistry, chemical weathering, and atmospheric CO 2 consumption rates in the Virunga Volcanic Province (East Africa). *Geochemistry, Geophysics, Geosystems*, *16*(8), 2637–2660. https://doi.org/10.1002/2015GC005999

Beck, H. E., Zimmermann, N. E., McVicar, T. R., Vergopolan, N., Berg, A., & Wood, E. F. (2018). Present and future Köppen-Geiger climate classification maps at 1-km resolution. *Scientific data*, *5*, 180214. https://doi.org/10.1038/sdata.2018.214

Berner, E. K., & Berner, R. A. (2012). *Global Environment: Water, Air, and Geochemical cycles* (2nd ed.). Princeton. http://refhub.elsevier.com/S0921-8181(20)30117-X/rf0045

Biondino, D., Borrelli, L., Critelli, S., Muto, F., Apollaro, C., Coniglio, S., Tripodi, V., & Perri, F. (2020). A multidisciplinary approach to investigate weathering processes affecting gneissic rocks (Calabria, southern Italy). *CATENA*, *187*, 104372. https://doi.org/10.1016/j.catena.2019.104372

Boeglin, J. L., & Probst, J. L. (1998). Physical and chemical weathering rates and CO2 consumption in a tropical lateritic environment: the upper Niger basin. *Chemical Geology*, *148*. https://doi.org/10.1016/S0009-2541(98)00025-4

Brahney, J., Ballantyne, A. P., Sievers, C., & Neff, J. C. (2013). Increasing Ca2+ deposition in the western US: The role of mineral aerosols. *Aeolian Research*, *10*, 77–87. https://doi.org/10.1016/j.aeolia.2013.04.003

Braun, J. J., Ngoupayou, J. R. N., Viers, J., Dupré, B., Bedimo Bedimo, J.-P., Boeling, J. L., Robain, H., Nyeck, B., Freydier, R., Nkamdjou, L. S., Rouiller, J., & Muller, J.-P. (2005). Present weathering rates in a humid tropical watershed: Nsimi, South Cameroon. *Geochimica et Cosmochimica Acta*, *69*(2), 357–387. https://doi.org/10.1016/j.gca.2004.06.022

Carey, R. O., & Migliaccio, K. W. (2009). Contribution of wastewater treatment plant effluents to nutrient dynamics in aquatic systems: a review. *Environmental management*, *44*(2), 205–217. https://doi.org/10.1007/s00267-009-9309-5

Chen, J. M., & Liu, J. (2020). Evolution of evapotranspiration models using thermal and shortwave remote sensing data. *Remote Sensing of Environment*, *237*, 111594. https://doi.org/10.1016/j.rse.2019.111594

Conley, D. J. (2002). Terrestrial ecosystems and the global biogeochemical silica cycle. *Global Biogeochemical Cycles*, *16*(4), 68-1-68–8. https://doi.org/10.1029/2002GB001894

Dailey, K. R., Welch, K. A., & Lyons, W. B. (2014). Evaluating the influence of road salt on water quality of Ohio rivers over time. *Applied Geochemistry*, *47*, 25–35. https://doi.org/10.1016/j.apgeochem.2014.05.006

Dessert, C., Dupré, B., Gaillardet, J., François, L. M., & Allègre, C. J. (2003). Basalt weathering laws and the impact of basalt weathering on the global carbon cycle. *Chemical Geology*, *202*(3-4), 257–273. https://doi.org/10.1016/j.chemgeo.2002.10.001

Di Figlia, M. G., Bellanca, A., Neri, R., & Stefansson, A. (2007). Chemical weathering of volcanic rocks at the island of Pantelleria, Italy: Information from soil profile and soil solution investigations. *Chemical Geology*, *246*(1-2), 1–18. https://doi.org/10.1016/j.chemgeo.2007.07.025

Dong, X., Cohen, M. J., Martin, J. B., McLaughlin, D. L., Murray, A. B., Ward, N. D., Flint, M. K., & Heffernan, J. B. (2019). Ecohydrologic processes and soil thickness feedbacks control limestone-weathering rates in a karst landscape. *Chemical Geology*, *527*, 118774. https://doi.org/10.1016/j.chemgeo.2018.05.021

Donnini, M., Frondini, F., Probst, J. L., Probst, A., Cardellini, C., Marchesini, I., & Guzzetti, F. (2016). Chemical weathering and consumption of atmospheric carbon dioxide in the Alpine region. *Global and Planetary Change*, *136*, 65–81. https://doi.org/10.1016/j.gloplacha.2015.10.017

Drever, J. I. (2012). *The chemistry of weathering*.

Drever, J. I., & Zobrist, J. (1992). Chemical weathering of silicate rocks as a function of elevation in the southern Swiss Alps. *Geochimica et Cosmochimica Acta*, *56*, 3209–3216. https://doi.org/10.1016/0016-7037(92)90298-W

Dupré, B., Dessert, C., Oliva, P., Goddéris, Y., Viers, J., François, L. M., Millot, R., & Gaillardet, J. (2003). Rivers, chemical weathering and Earth's climate. *Comptes Rendus Geoscience*, *335*(16), 1141–1160. https://doi.org/10.1016/j.crte.2003.09.015

Elzhov, T. V., Mullen, K. M., Spiess, A.-N., & Bolker, B. (2016). minpack.lm: R Interface to the Levenberg-Marquardt Nonlinear Least-Squares Algorithm Found in MINPACK, Plus Support for Bounds. https://CRAN.R-project.org/package=minpack.lm

FAO, IIASA, ISRIC, ISS-CAS, & JRC. (2012). Harmonized World Soil Database (version 1.2). http://www.fao.org/soils-portal/soil-survey/soil-maps-and-databases/harmonized-world-soil-database-v12/en/

Fekete, B. M., Vörösmarty, C. J., & Grabs, W. (2002). High-resolution fields of global runoff combining observed river discharge and simulated water balances. *Global Biogeochemical Cycles*, *16*(3), 15-1-15–10. https://doi.org/10.1029/1999GB001254

Fu, B., Merritt, W. S., Croke, B. F., Weber, T. R., & Jakeman, A. J. (2019). A review of catchment-scale water quality and erosion models and a synthesis of future prospects. *Environmental Modelling & Software*, *114*, 75–97. https://doi.org/10.1016/j.envsoft.2018.12.008

Gabet, E. J., Edelman, R., & Langner, H. (2006). Hydrological controls on chemical weathering rates at the soil-bedrock interface. *Geology*, *34*(12), 1065–1068. https://doi.org/10.1130/G23085A.1

Gaillardet, J., Dupré, B., Louvat, P., & Allègre, C. J. (1999). Global silicate weathering and CO2 consumption rates deduced from the chemistry of large rivers. *Chemical Geology*, *159*, 3–30. https://doi.org/10.1016/S0009-2541(99)00031-5

Galloway, J. N., Dentener, F., Capone, D. G., Boyer, E. W., Howarth, R. W., Seitzinger, S. P., Asner, G. P., Cleveland, C. C., Green, P. A., Holland, E. A., Karl, D. M., Michaels, A. F., Porter, J. H., Townsend, A. R., & Vörösmarty, C. J. (2004). Nitrogen Cycles: Past, Present, and Future. *Biogeochemistry*, *70*, 153–226. https://doi.org/10.1007/s10533-004-0370-0

Garrels, R. M., & Mackenzie, F. T. (1972). A quantitative model for the sedimentary rock cycle. *Marine Chemistry*, *1*, 27–41. https://doi.org/10.1016/0304-4203(72)90004-7

Gibbs, R. J. (1970). Mechanisms controlling world water chemistry. *Science*, *170*(3962), 1088–1090. https://www.jstor.org/stable/1730827

Goddéris, Y., François, L. M., Probst, A., Schott, J., Moncoulon, D., Labat, D., & Viville, D. (2006). Modelling weathering processes at the catchment scale: The WITCH numerical model. *Geochimica et Cosmochimica Acta*, *70*(5), 1128–1147. https://doi.org/10.1016/j.gca.2005.11.018

Goddéris, Y., Roelandt, C., Schott, J., Pierret, M.-C., & Francois, L. M. (2009). Towards an Integrated Model of Weathering, Climate, and Biospheric Processes. *Reviews*

in Mineralogy and Geochemistry, *70*(1), 411–434. https://doi.org/10.2138/rmg.2009.70.9

Guo, J., Wang, F., Vogt, R. D., Zhang, Y., & Liu, C.-Q. (2015). Anthropogenically enhanced chemical weathering and carbon evasion in the Yangtze Basin. *Scientific reports*, *5*, 11941. https://doi.org/10.1038/srep11941

Hartmann, J. (2009). Bicarbonate-fluxes and CO2-consumption by chemical weathering on the Japanese Archipelago — Application of a multi-lithological model framework. *Chemical Geology*, *265*(3-4), 237–271. https://doi.org/10.1016/j.chemgeo.2009.03.024

Hartmann, J., Jansen, N., Dürr, H. H., Kempe, S., & Köhler, P. (2009). Global CO2-consumption by chemical weathering: What is the contribution of highly active weathering regions? *Global and Planetary Change*, *69*(4), 185–194. https://doi.org/10.1016/j.gloplacha.2009.07.007

Hartmann, J., Lauerwald, R., & Moosdorf, N. (2014). A Brief Overview of the GLObal RIver Chemistry Database, GLORICH. *Procedia Earth and Planetary Science*, *10*, 23–27. https://doi.org/10.1016/j.proeps.2014.08.005

Hartmann, J., & Moosdorf, N. (2011). Chemical weathering rates of silicate-dominated lithological classes and associated liberation rates of phosphorus on the Japanese Archipelago—Implications for global scale analysis. *Chemical Geology*, *287*(3-4), 125–157. https://doi.org/10.1016/j.chemgeo.2010.12.004

Hartmann, J., & Moosdorf, N. (2012). The new global lithological map database GLiM: A representation of rock properties at the Earth surface. *Geochemistry, Geophysics, Geosystems*, *13*(12). https://doi.org/10.1029/2012GC004370

Hartmann, J., Moosdorf, N., Lauerwald, R., Hinderer, M., & West, A. J. (2014). Global chemical weathering and associated P-release — The role of lithology, temperature and soil properties. *Chemical Geology*, *363*, 145–163. https://doi.org/10.1016/j.chemgeo.2013.10.025

Hijmans, R. J. (2019). Raster: Geographic Data Analysis and Modeling: R package. https://CRAN.R-project.org/package=raster

Hijmans, R. J., Cameron, S. E., Parra, J. L., Jones, P. G., & Jarvis, A. (2005). Very high resolution interpolated climate surfaces for global land areas. *International Journal of Climatology*, *25*(15), 1965–1978. https://doi.org/10.1002/joc.1276

Huscroft, J., Gleeson, T., Hartmann, J., & Börker, J. (2018). Compiling and Mapping Global Permeability of the Unconsolidated and Consolidated Earth: GLobal HYdrogeology MaPS 2.0 (GLHYMPS 2.0). *Geophysical Research Letters*, *45*(4), 1897–1904. https://doi.org/10.1002/2017GL075860

Jansen, N., Hartmann, J., Lauerwald, R., Dürr, H. H., Kempe, S., Loos, S., & Middelkoop, H. (2010). Dissolved silica mobilization in the conterminous USA. *Chemical Geology*, *270*(1-4), 90–109. https://doi.org/10.1016/j.chemgeo.2009.11.008

Kaushal, S. S., Likens, G. E., Pace, M. L., Utz, R. M., Haq, S., Gorman, J., & Grese, M. (2018). Freshwater salinization syndrome on a continental scale. *Proceedings of the National Academy of Sciences of the United States of America*, *115*(4), E574–E583. https://doi.org/10.1073/pnas.1711234115

Keller, C. K. (2019). Carbon Exports from Terrestrial Ecosystems: A Critical-Zone Framework. *Ecosystems*, *22*(8), 1691–1705. https://doi.org/10.1007/s10021-019-00375-9

Lehmann, C. M. B., van Bowersox, C., & Larson, S. M. (2005). Spatial and temporal trends of precipitation chemistry in the United States, 1985-2002. *Environmental pollution (Barking, Essex : 1987)*, *135*(3), 347–361. https://doi.org/10.1016/j.envpol.2004.11.016

Likens, G. E., Driscoll, C. T., & Buso, D. C. (1996). Long-Term Effects of Acid Rain: Response and Recovery of a Forest Ecosystem. *Science*, *272*(5259), 244–246. https://doi.org/10.1126/science.272.5259.244

Livingstone, D. A. (1963). Chemical composition of rivers and lakes (M. Fleischer, Ed.). https://doi.org/10.3133/pp440G

Ludwig, W., Amiotte Suchet, P., Munhoven, G., & Probst, J. L. (1998). Atmospheric CO2 consumption by continental erosion: present-day controls and implications for the last glacial maximum. *Global and Planetary Change*, *16-17*, 107–120. https://doi.org/10.1016/S0921-8181(98)00016-2

Ludwig, W., Amiotte Suchet, P., & Probst, J. L. (2011). ISLSCP II Atmospheric Carbon Dioxide Consumption by Continental Erosion. In F. G. Hall, G. Collatz, B. Meeson, S. Los, E. Brown de Colstoun, & D. Landis (Eds.), *ISLSCP Initiative II Collection*. https://doi.org/10.3334/ORNLDAAC/1019

Mahowald, N., Ward, D. S., Kloster, S., Flanner, M. G., Heald, C. L., Heavens, N. G., Hess, P. G., Lamarque, J.-F., & Chuang, P. Y. (2011). Aerosol Impacts on Climate and Biogeochemistry. *Annual Review of Environment and Resources*, *36*(1), 45–74. https://doi.org/10.1146/annurev-environ-042009-094507

McClain, M. E., Boyer, E. W., Dent, C. L., Gergel, S. E., Grimm, N. B., Groffman, P. M., Hart, S. C., Harvey, J. W., Johnston, C. A., Mayorga, E., McDowell, W. H., & Pinay, G. (2003). Biogeochemical Hot Spots and Hot Moments at the Interface of Terrestrial and Aquatic Ecosystems. *Ecosystems*, *6*(4), 301–312. https://doi.org/10.1007/s10021-003-0161-9

Meybeck, M. (1979). Concentrations des eaux fluviales en éléments majeurs et apports. *Revue de géologie dynamique et de géographie physique*, *21*(3), 215.

Meybeck, M. (1983). Atmospheric inputs and river transport of dissolved substances. *IAHS*, *141*. http://hydrologie.org/redbooks/a141/iahs_141_0173.pdf

Meybeck, M. (1984). *Les fleuves et le cycle géochimique des éléments* (Doctoral dissertation).

Meybeck, M. (1986). Composition chimique des ruisseaux non pollués de France. *Sciences Géologiques*, *39*(1), 3–77.

Meybeck, M. (1987). Global chemical weathering of surficial rocks estimated from river dissolved loads. *American Journal of Science*, *287*, 401–428. https://doi.org/10.2475/ajs.287.5.401

Meybeck, M. (2003). Global Occurrence of Major Elements in Rivers. In H. D. Holland & K. K. Turekian (Eds.), *Treatise on Geochemistry* (pp. 207–223). https://doi.org/10.1016/B0-08-043751-6/05164-1

Moore, S. J., Bassett, R. L., Liu, B., Wolf, C. P., & Doremus, D. (2008). Geochemical tracers to evaluate hydrogeologic controls on river salinization. *Ground Water*, *46*(3), 489–501. https://doi.org/10.1111/j.1745-6584.2007.00420.x

Moosdorf, N., Hartmann, J., Lauerwald, R., Hagedorn, B., & Kempe, S. (2011). Atmospheric CO2 consumption by chemical weathering in North America. *Geochimica et Cosmochimica Acta*, *75*(24), 7829–7854. https://doi.org/10.1016/j.gca.2011.10.007

Moquet, J.-S., Guyot, J.-L., Crave, A., Viers, J., Filizola, N., Martinez, J.-M., Oliveira, T. C., Sánchez, L. S. H., Lagane, C., Casimiro, W. S. L., Noriega, L., & Pombosa, R.

(2016). Amazon River dissolved load: temporal dynamics and annual budget from the Andes to the ocean. *Environmental science and pollution research international*, *23*(12), 11405–11429. https://doi.org/10.1007/s11356-015-5503-6

Moré, J. J. (1978). The Levenberg-Marquardt algorithm: Implementation and theory. In G. A. Watson (Ed.), *Numerical Analysis* (pp. 105–116). Springer Berlin Heidelberg. https://doi.org/10.1007/BFb0067700

Oliva, P., Villa, I. M., & Dupré, B. (2003). Chemical weathering in granitic environments. *Chemical Geology*, *202*(3-4), 225–256. https://doi.org/10.1016/j.chemgeo.2002.08.001

Perri, F., Ietto, F., Le Pera, E., & Apollaro, C. (2016). Weathering processes affecting granitoid profiles of Capo Vaticano (Calabria, southern Italy) based on petrographic, mineralogic and reaction path modelling approaches. *Geological Journal*, *51*(3), 368–386. https://doi.org/10.1002/gj.2635

Probst, A., Dambrine, E., Viville, D., & Fritz, B. (1990). Influence of acid atmospheric inputs on surface water chemistry and mineral fluxex in a declining spruce stand within a small granitic catchment (Vosges massif, France). *Journal of Hydrology*, *116*, 101–124. https://doi.org/10.1016/0022-1694(90)90118-H

Probst, J. L. (1992). *Géochimie et hydrologie de l'érosion continentale. Mécanismes, bilan global actuel et fluctuations au cours des 500 derniers millions d'années.* (Doctoral dissertation). Université Louis-Pasteur. Strasbourg, Institut de Géologie. www.persee.fr/doc/sgeol_0302-2684_1992_mon_94_1

Probst, J. L., Ludwig, W., & Amiotte Suchet, P. (1997). Global modeling of CO2 uptake by continental erosion and of carbon river transport to the oceans. / Modélisation à l'échelle globale des flux de CO2 consommé par l'érosion continentale et des transports fluviaux de carbone vers les océans. *Sciences Géologiques. Bulletin*, *50*(1), 131–156. https://doi.org/10.3406/sgeol.1997.1950

Probst, J. L., Mortatti, J., & Tardy, Y. (1994). Carbon river fluxes and weathering CO2 consumption in the Congo and Amazon river basins. *Applied Geochemistry*, *9*, 1–13. https://doi.org/10.1016/0883-2927(94)90047-7

R Core Team. (2019). R: A language and environment for statistical computing. https://www.R-project.org/

Raab, G., Egli, M., Norton, K., Dahms, D., Brandová, D., Christl, M., & Scarciglia, F. (2019). Climate and relief–induced controls on the temporal variability of denudation rates in a granitic upland. *Earth Surface Processes and Landforms*, *44*(13), 2570–2586. https://doi.org/10.1002/esp.4681

Riebe, C. S., Hahm, W. J., & Brantley, S. L. (2017). Controls on deep critical zone architecture: a historical review and four testable hypotheses. *Earth Surface Processes and Landforms*, *42*(1), 128–156. https://doi.org/10.1002/esp.4052

Roelandt, C., Goddéris, Y., Bonnet, M.-P., & Sondag, F. (2010). Coupled modeling of biospheric and chemical weathering processes at the continental scale. *Global Biogeochemical Cycles*, *24*(2), n/a–n/a. https://doi.org/10.1029/2008GB003420

Romero-Mujalli, G., Hartmann, J., Börker, J., Gaillardet, J., & Calmels, D. (2019). Ecosystem controlled soil-rock pCO2 and carbonate weathering – Constraints by temperature and soil water content. *Chemical Geology*, *527*, 118634. https://doi.org/10.1016/j.chemgeo.2018.01.030

Romero-Mujalli, G., Hartmann, J., & Börker, J. (2019). Temperature and CO2 dependency of global carbonate weathering fluxes – Implications for future carbonate weathering research. *Chemical Geology*, *527*, 118874. https://doi.org/10.1016/j.chemgeo.2018.08.010

Schindler, D. W. (1988). Effects of acid rain on freshwater ecosystems. *Science*, *239*(4836), 149–157. https://doi.org/10.1126/science.239.4836.149

Shagguan, W., Hengl, T., Mendes de Jesus, J., Yuan, H., & Dai, Y. (2017). Mapping the global depth to bedrock for land surface modeling. *Journal of Advances in Modeling Earth Systems*, *9*(1), 65–88. https://doi.org/10.1002/2016MS000686

Shangguan, W., Hengl, T., Mendes de Jesus, J., Yuan, H., & Dai, Y. (2017). Mapping the global depth to bedrock for land surface modeling. *Journal of Advances in Modeling Earth Systems*, *9*(1), 65–88. https://doi.org/10.1002/2016MS000686

Stallard, R. F., & Edmond, J. M. (1981). Geochemistry of the Amazon: 1. Precipitation chemistry and the marine contribution to the dissolved load at the time of peak discharge. *Journal of Geophysical Research*, *86*(C10), 9844–9858. https://doi.org/10.1029/JC086iC10p09844

St-Pierre, M., Theriault, J. M., & Paquin, D. (2019). Influence of the Model Horizontal Resolution on Atmospheric Conditions Leading to Freezing Rain in Regional

Climate Simulations. *Atmosphere-Ocean*, *57*(2), 101–119. https://doi.org/10.1080/07055900.2019.1583088

Sun, X., Higgins, J., & Turchyn, A. V. (2016). Diffusive cation fluxes in deep-sea sediments and insight into the global geochemical cycles of calcium, magnesium, sodium and potassium. *Marine Geology*, *373*, 64–77. https://doi.org/10.1016/j.margeo.2015.12.011

Tipping, E. (1994). WHAMC—A chemical equilibrium model and computer code for waters, sediments, and soils incorporating a discrete site/electrostatic model of ion-binding by humic substances. *Computers & Geosciences*, *20*(6), 973–1023. https://doi.org/10.1016/0098-3004(94)90038-8

Velbel, M. A. (1993). Temperature dependence of silicate weathering in nature: How strong a negative feedback on term accumulation of atmospheric CO2 and global greenhouse warming? *Geology*, *21*, 1059–1062. https://doi.org/10.1130/0091-7613(1993)021{\%}3C1059:TDOSWI{\%}3E2.3.CO;2

Vet, R., Artz, R. S., Carou, S., Shaw, M., Ro, C.-U., Aas, W., Baker, A., van Bowersox, C., Dentener, F., Galy-Lacaux, C., Hou, A., Pienaar, J. J., Gillett, R., Forti, M. C., Gromov, S., Hara, H., Khodzher, T., Mahowald, N. M., Nickovic, S., … Reid, N. W. (2014). A global assessment of precipitation chemistry and deposition of sulfur, nitrogen, sea salt, base cations, organic acids, acidity and pH, and phosphorus. *Atmospheric Environment*, *93*, 3–100. https://doi.org/10.1016/j.atmosenv.2013.10.060

Vörösmarty, C. J., McIntyre, P. B., Gessner, M. O., Dudgeon, D., Prusevich, A., Green, P. A., Glidden, S., Bunn, S. E., Sullivan, C. A., Liermann, C. R., & Davies, P. M. (2010). Global threats to human water security and river biodiversity. *Nature*, *467*(7315), 555–561. https://doi.org/10.1038/nature09440

Wadham, J. L., Tranter, M., Skidmore, M., Hodson, A. J., Priscu, J., Lyons, W. B., Sharp, M. J., Wynn, P., & Jackson, M. (2010). Biogeochemical weathering under ice: Size matters. *Global Biogeochemical Cycles*, *24*(3), n/a–n/a. https://doi.org/10.1029/2009GB003688

White, A. F., & Blum, A. E. (1995). Effects of climate on chemical weathering in watersheds. *Geochimica et Cosmochimica Acta*, *59*(9), 1729–1747. https://doi.org/10.1016/0016-7037(95)00078-E

Wicke, B., Smeets, E., Dornburg, V., Vashev, B., Gaiser, T., Turkenburg, W., & Faaij, A. (2011). The global technical and economic potential of bioenergy from salt-affected soils. *Energy & Environmental Science*, *4*(8), 2669. https://doi.org/10.1039/c1ee01029h

CHAPTER 5

Case study

This chapter introduces the local case study used to test the global model performance at different spatial scales in the following chapter. Here, the local case study is introduced through the evaluation of the results from a monitoring program established in the catchment, where several sampling locations were distributed along the main channel and tributaries. Main geochemical processes are evaluated, as well as the potential of integrating spot sampling data from the monitoring program with continuous registries from gauging stations. The results from the present chapter are already published in: Lechuga-Crespo, J. L., Ruiz-Romera, E., Probst, J.-L., Unda-Calvo, J., Cuervo-Fuentes, Z. C., Sánchez-Pérez, J. M. (2020). **Combining punctual and high frequency data for the spatiotemporal assessment of main geochemical processes and dissolved exports in an urban river catchment**. *Science of the Total Environment, 727*, 138644. https://doi.org/10.1016/j.scitotenv.2020.138644

5.1 Abstract

The assessment of dissolved loadings and the sources of these elements in urban catchments' rivers is usually measured by punctual sampling or through high frequency sensors. Nevertheless, the combination of both methodologies has been less common even though the information they give is complementary. Major ion (Ca^{2+}, Mg^{2+}, Na^{+}, K^{+}, Cl^{-}, SO_4^{2-}, and alkalinity), organic matter (expressed as Dissolved Organic Carbon, DOC), and nutrients (NO_3^{-}, and PO_4^{3-}) are punctually measured in the Deba river urban catchment (538 km^2), in the northern part of the Iberian Peninsula (draining to the Bay of Biscay). Discharge, precipitation, and Electrical Conductivity (EC) are registered with a high frequency (10-minutes) in three gauging stations. The combination of both methodologies has allowed the assessment of major geochemical processes and the extent of impact of anthropogenic input on major composition of riverine water, as well as its spatial and temporal evolution. Three methodologies for loading estimation have been assessed and the error committed in the temporal aggregation is quantified. Results have shown that, even though carbonates dominate the draining area, the water major ion chemistry is governed by an evaporitic spring in the upper part of the catchment, while anthropogenic input is specially noted downstream of three wastewater treatment plants, in all nutrients and organic matter. The results of the present work illustrate how the combination of two monitoring methodologies allows for a better assessment of the spatial and temporal evolution on the major water quality in an urban catchment.

5.2 Introduction

Due to global population growth prospects in the following years (Ghanem, 2018), temporal and spatial assessments of anthropogenic influences on the ecosystem are of increasing interest. Among others, anthropogenic activity has influenced the delivery of elements (sediments, nutrients, organic matter, salts, etc.) to streams both through

point sources like facilities effluents, and diffusive sources like agriculture. Rivers act as a vector of transport for matter in the land to ocean continuum, though anthropogenic elements eventually arrive to coastal wetlands and the ocean, altering both freshwater and wetland ecosystems (Herbert et al., 2015; Nielsen et al., 2003; Vörösmarty et al., 2010). In the future, demographic growth is likely to keep on increasing human activities, and climate change is expected to alter hydrological regimes (Graham et al., 2007) causing moments of lower discharge, which would imply increases in dissolved solids concentration, threatening aquatic ecosystems (Cañedo-Argüelles et al., 2013; Vörösmarty et al., 2010). Understanding the extents of such hazards' effect on ecosystem services and goods is needed to forecast potential consequences of these impacts, as well as evaluating the effects of management actions taken to reduce them (Cañedo-Argüelles et al., 2013).

Focusing on the dissolved composition of water, the increase of dissolved inorganic solids (Ca^{2+}, Mg^{2+}, Na^{+}, K^{+}, HCO_3^{-}, CO_3^{2-}, Cl^{-}, and SO_4^{2-}) concentration in streams is called salinization (Nielsen et al., 2003). Increases of ionic concentration caused by natural (primary salinization) or anthropogenic (secondary salinization) sources are potential hazards to freshwater environments (Kaushal et al., 2017). In the absence of anthropogenic influences, freshwater salinity originates from three sources: (1) weathering of the catchment, which is a function of both geology of the catchment and precipitation; (2) sea spray, although this is only important in coastal locations, and (3) wet deposition caused by the evaporation of seawater (Cañedo-Argüelles et al., 2013). Organic matter and nutrients are commonly linked to the carbon, nitrogen, sulphur and phosphorus cycles, as complex interactions among biotic and abiotic elements in the riverine ecosystem are found (O. R. Anderson, 2016; Vitousek et al., 1997; Vitousek et al., 2009). When human inputs are present (through fertilization, wastewater effluents, road salt application, etc.), increased dissolved loadings alter the natural cycles (Herbert et al., 2015; Vitousek et al., 2009). Usually, evaluations regarding dissolved solid loadings focus on agricultural catchments (e.g. Merchán et al., 2019; Merchán et al., 2020; Vitousek et al., 2009) and less on urban environments (Khatri & Tyagi, 2015; Launay et al., 2016), where the saline input is in the form of point source. Commonly, the origin of these inputs are urban wastewater effluents (Álvarez-Vázquez et al., 2016),

systems where nutrients and turbidity are removed from water but where not act over major ion composition is taken unless tertiary treatment is present. In this sense, we ask the following question: which spatial and temporal influence have point sources on the streams?

To answer this question, a case study has been selected, and a monitoring program of the catchment has been established. Setting up a monitoring program within a system needs to capture the spatial and temporal variability of the processes given within a catchment and, with this purpose, punctual sampling campaigns are commonly taken with finer or lower temporal resolutions in the outlet, or spatially distributed in the catchment. Recently, the use of *in situ* sensors for the monitoring of water quality variables has become more common in these assessments (Rode et al., 2016), which allow for high-frequency measurements performed in specific sites within a system (commonly a gauging station). However, such sensors are not capable of quantifying all variables that can be assessed within a laboratory, though each of these methodologies has present advantages and drawbacks for the assessment. Nevertheless, the combination of both punctual results and continuous registries poses an opportunity to better understand the processes given and to assess their influences within a catchment as recently shown by Ponnou-Delaffon et al., 2020, who highlighted nycthemeral cycles due to biological impact on nitrate concentrations and carbonate precipitation in streamwaters.

The urban catchment selected in this study is a medium size catchment where previous studies of surface water quality have identified physicochemical variables (EC, DOC, PO_4^{3-}, NO_3^-, NO_2^-, NH_4^+) and specific pollutants (Cu, Zn, Pb, Ni, Cr) as main explainers of water pollution (Unda-Calvo et al., 2020), however none of the previous studies has focused on the major ion composition, thus the study of major geochemical processes and the assessment of anthropogenic inputs on major chemistry remains unstudied. Both a monitoring program with punctual samplings and continuous registries are present in this catchment, posing an opportunity to evaluate the combination of both methodologies on the assessment of the anthropogenic impact on salinity. Previous studies in the area (Ábalos et al., 2008; Iribar & Ábalos, 2011; Martínez-Santos et al., 2015) have highlighted the geological structures and the effect they have on the

water chemistry of this river. Saline springs are common in this area, as noted by Iribar and Ábalos, 2011 and its influence on the Deba river catchment, found in the Lenitz-Gatzaga area, has also been identified as relevant in the major ion composition of the water. Wastewater Treatment Plants (WWTP) effluents have also been found as major point sources of nutrients to the river streams, and the use of chemical compounds has been noted for phosphorus removal (Martínez-Santos et al., 2018). However, the spatial and temporal extent of the WWTP effluents impact, and the influence of natural saline springs on water chemistry in this urban catchment have not been evaluated yet. Understanding the present-state dynamics gives a starting point for forecasting studies. Other studies have shown that the Deba river catchment has a low capacity to absorb precipitation, making it vulnerable to extreme precipitation events, which are more likely to occur in climate change scenarios (Mendizabal et al., 2014). Considering hydrology as the main driver of suspended sediments (García-García et al., 2019) and being sediments a vector of transport of pollutants (Unda-Calvo, 2019) in this catchment, the relevance of including the temporal analysis is justified. In this sense, the integration of punctual data from a monitoring program to the high frequency registries of the gauging stations in this catchment poses an opportunity on highlighting the hot spots and times regarding hazards to the water chemistry.

Then, for the assessment of geochemical and anthropogenic inputs into the Deba river urban catchment, we propose of the following hypothesis: a) the geochemical processes responsible of major ion characteristics of the Deba River are mainly affected by the headwater southwestern part of the catchment due to the presence of a saline spring, and its influence is noted downstream to the outlet; and b) the urban and industrial treated and untreated waters have a greater impact in the middle part of the catchment, causing a shift in major ion composition and nutrients. In order to test these hypotheses, the aim of this study is to evaluate the dominant geochemical processes governing the major ion chemistry of the Deba river urban catchment, as well as assess the dissolved loadings to the estuary by combining punctual and continuous data. More specifically, the objectives of this study are: *i*) to identify the major geochemical processes controlling major ion chemistry along the main channel and tributaries, *ii*) to evaluate the possibilities of integrating punctual data on continuous registries for the

estimation of dissolved loadings, *iii*) to assess the role of temporal resolution on the estimation of dissolved loadings. The results from this study are expected to improve the understanding of human impacts on urban environments with relevant geological influence, as well as to present a methodology for the integration of punctual samplings on continuous registries.

5.3 Materials and Methods

5.3.1 Study area and sampling set up

The Deba catchment (538 km^2) is located in the northern part of the Iberian Peninsula (West Europe), in the middle part of Donostia-San Sebastian and Bilbao cities, mainly located in the Gipuzkoa province territory (Figure 5.1). High slopes both in the hills and in the stream channel drain water to the Cantabrian Sea (part of the Atlantic Ocean) in the Bay of Biscay through a 62 km long river born in the southwest part of the catchment. Close to the Leintz-Gatzaga saline springs, the Deba river receives the influent of the Mazmela tributary before flowing through the towns of Eskoriatza and Aretxabaleta and the city of Arrasate-Mondragon, after which it receives the influent of the Oñati tributary to continue through Bergara city towards the lower part of the catchment, where the Ego tributary incorporates to the main channel before Elgoibar town and the villages of Alzola and Mendarozabal, reaching the ocean in the Deba city, which names both the river and the draining catchment. Within this hydrologic unit, there are other streams draining to the ocean which are not included in the present analysis, like the one outflowing in the city Mutriku.

Together with the cities, there are several industries in the area (Figure 5.1b), which have made the Deba river the most polluted in the Gipuzkoa province (https://www.gipuzkoa.eus/es/web/obrahidraulikoak, accessed on November 2019). In the last years, the stakeholders have taken some management actions related to the treatment of the urban wastewaters, achieving a good ecological status in the last campaign of 2018 for

most of the sampling locations, except for the lower part of the catchment and the lower part of the Ego tributary (URA, 2019). Among those actions, special mention is needed for the incorporation of three wastewater treatment plants (WWTP) between 2008 and 2012: the Epele WWTP in the southwest part of the catchment, before the confluence with the Oñati tributary; the Mekolalde WWTP, in the middle part of the catchment; and the Apraitz WWTP, in the lowest part of the catchment, after the incorporation of the Ego tributary (Figure 5.1a,b).

The Epele WWTP collects the wastewaters from Eskoriatza, Aretxabaleta, Arrasate, and Oñati cities, treating an approximate load of 90,000 equivalent habitants; the Mekolalde WWTP takes the water from Bergara, and it is expected to be connected with Antzuola and other villages in the area, treating about 35,000 equivalent habitants; while the Apraitz WWTP treats the waters from Ermua, Eibar, and Elgoibar, the highest load of all the three (around 95,000 equivalent habitants) before draining the waters to the river. Both Epele and Mekolalde WWTP count with activated sludge and biological elimination of nitrogen but, while Epele WWTP uses biological elimination of phosphorus, Mekolalde WWTP uses a chemical procedure. In contrast, the Apraitz WWTP uses a sequential biological reactor (SBR), counting with biological elimination of nitrogen and chemical for phosphorus (www.gipuzkoakour.eus).

Before the set up of the WWTP, a monitoring program was established in the area with the installation of three gauging stations measuring a high frequency time series (every 10 min) variables such as accumulated precipitation, air and water temperature, discharge, electrical conductivity, among others. Registries have shown that, due to the latitude of the province and the placement in the Bay of Biscay, there is a high pluviometry (1384 $mm \cdot y^{-1}$) and a soft temperature (13ºC), with a seasonal distribution of the rainfall (https://www.gipuzkoa.eus/es/web/obrahidraulikoak, accessed on November 2019). This, together with the low ability of the Deba catchment system to infiltrate water (Mendizabal et al., 2014), causes periods with high discharge and very dry periods, yielding an annual average of 12.56 $m^3 \cdot s^{-1}$ (https://www.gipuzkoa.eus/es/web/obrahidraulikoak, accessed on November 2019). Even though the Deba river catchment has be noted as the most polluted in the area (Martínez-

Santos et al., 2015), most of the land is covered by forest or pasture (Figure 5.1d), where only 2% of the territory is dedicated to agricultural purposes (according to the CORINE Land Cover database, 2012, available via the Copernicus Land Monitoring Service of the European Union). Though, most of the anthropogenic influence over the water quality and composition is expected to be related to the industrial and urban effluents from the WWTP and industries (Martínez-Santos et al., 2015).

Due to the small distance from the coast, and the relatively homogeneous land use in contrast to the heterogeneous lithological groups in the area, the "natural" (not including the anthropogenic inputs) Deba river major ion composition is expected to be influenced mostly by geochemical processes related to water-rock interaction, i.e. chemical weathering. Regarding the geological context, this catchment is located between the Bilbao Anticlinorium and the Biscay Sinclinorium, with rock ages varying from the Aptian-Albian to the Paleogene (Iribar & Ábalos, 2011). Within the Bilbao Anticlinorium area, which is located in the upper and middle part of the catchment, there are some thrust faults and secondary faults showing Cenomanian-Aastrichtian, Albian, Aptian-Albian, and Kimmeridgian-Barremian layers (EVE - Ente Vasco de la Energía, 1989; Iribar & Ábalos, 2011). Scattered around this southwestern part of the catchment, there are several saline water springs, gypsum and evaporites sites (Figure 5.1b) related to Walden Facies, which are expected to have an effect on the major ion composition of the groundwater and surface water in the Deba river catchment. It is important to note that the official lithological map lacks the representation of these gypsum and evaporitic sites.

Regarding the geochemistry of the underlying rocks, the Deba catchment area is dominated by detritic rocks, mixed with alternate marls and clays, presenting different lithological configurations for three sections: the southwest part (draining to San Prudentzio gauging station, Figure 5.1b); the southeast part (draining to Oñati gauging station, Figure 5.1b), and the Ego tributary in the middle-west part of the catchment. The southwest part presents slates and is the most related to the saline springs and gypsum sites (Iribar & Ábalos, 2011), the southeast part drains mainly detritic rocks, while the Ego tributary is mainly conformed by limestones. The mid-lower part of the

catchment presents a stripe with volcanic rocks.

5.3.2 Field and laboratory methods

In order to control the major chemical composition of the catchment, and assess the potential anthropogenic effect, a set of 11 sampling locations has been established and sampled along the main channel and tributaries, since April 2014 to January 2017. The location of the sampling spots is shown in Figure 5.1a: along the main channel, D1 was considered as the control area associated with low human impact, this sampling location is placed before the input of any spring and drains 6.2 km^2. The Deba river flows downstream until it receives the waters from the Mazmela tributary, where a sampling location is also present, M1 (3.5 km^2). After Eskoriatza and Aretxabaleta, the sampling location D2 is placed in the main channel (62.4 km^2, accumulated area), before the river crosses Arrasate-Mondragon. Before the river gets to the confluence with Oñati (where one sampling location is placed: O1, 130 km^2), other sampling location is established, D3 (121 km^2). After the confluence, D4 (321 km^2) and D5 (329 km^2) are closely placed, before the river changes its course towards the northwest to meet the Ego tributary confluence. In the Ego tributary, due to its polluted characteristics, two sampling locations are placed, E1 in the upper part of the catchment (2.4 km^2), and E2 before the confluence with the main channel (55.5 km^2). After the confluence, the D6 sampling location collects the mixed water (419 km^2) now directed to the northeast part, where D7 is placed close to the transition zone of the river to the ocean (486 km^2). From the anthropogenic influence assessment point of view, there are four sampling locations with special interest: D3 receives the influence of the Epele WWTP, D5 registries the Mekolalde WWTP effect, E2 accounts for the Ermua and Eibar influence, and the D7 covers the Apraitz WWTP impact.

Every sampling location was sampled monthly or bimonthly between April 2014 and January 2017, covering two full hydrological years: 2014-2015 and 2015-2016, both beginning in October 1st, and part of the 2013-2014 and 2016-2017 hydrological years.

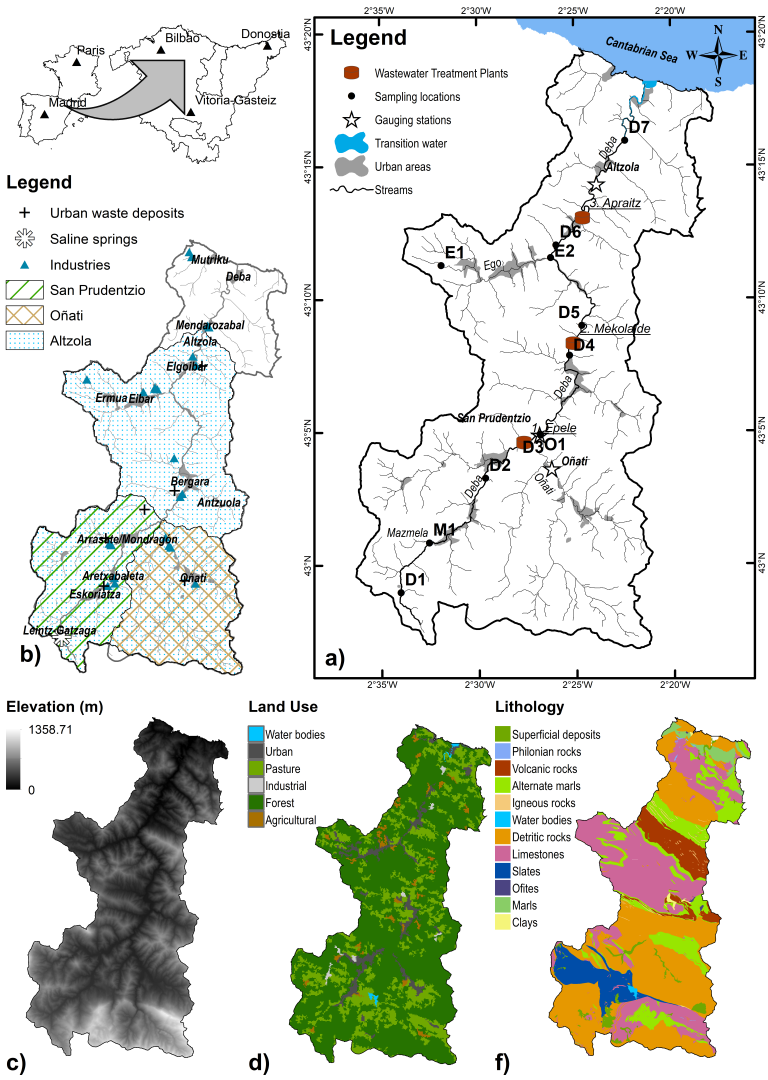

Figure 5.1: Study area localization and description: a) catchment extent and borders, together with main channel and tributaries, sampling locations, urban areas, wastewater treatment plants, and gauging stations; b) main human settlements, with principal industries, urban waste deposits, saline springs and main subasins, shaded for each gauging station; c) digital elevation model (DEM) showing orography; d) lithological groups derived from official maps; e) soil types according to FAO classification (HSWD), by FAO et al., 2012; and f) relevant land uses derived from the CORINE Land Cover map by EEA, 2012.

All eleven sampling locations were sampled within a day, where waters were taken from the middle part of the river in 1L pre-cleaned polyethylene bottles which were later taken at 4ºC to the laboratory in the Chemical and Environmental Engineering department of the University of the Basque Country (UPV/EHU), to be analyzed. In addition to the water sample, a Crison EC-Meter Basic 30+, and a Crison Micro pH 2000 sonde were used to measure *in situ* Electrical Conductivity (EC), Total Dissolved Solids (TDS), and pH, respectively.

Once in the laboratory, samples were filtered through 0.45µm filters to separate the suspended particles from the dissolved phase. One replicate of the filtered sample was acidified to 0.2% with HNO_3^- (68%) for base cations (Ca^{2+}, Mg^{2+}, Na^+, and K^+) analysis using ICP-OES (Perkin Elmer Optima 2000). One replicated of the filtered sample (non-acidified) was used to analyze (Cl^-, NO_3^-, and SO_4^{2-}) using ion chromatography (DIONEX ICS 3000). Alkalinity was determined using a Total Organic Carbon Analyzer (TOC-L Shimadzu). Due to the pH ranges, the alkalinity values were converted to HCO_3^- concentration in ($mg \cdot L^{-1}$). Sample analysis was validated by computing the Ionic Charge Balance (ICB) between anions and cations for each sample following $ICB = (([Z^+]-[Z^-]))/(([Z^+]+[Z^-]))$, where $[Z^+]$ and $[Z^-]$ represents the sum of all cation and all anion concentrations expressed in $meq \cdot L^{-1}$. Samples showing $|ICB| > 10\%$ were discarded from the analysis. A summary of all the results of these analysis is shown in Table 5.1.

Table 5.1: Summary of physicochemical characteristics for each sampling location in the main channel and tributaries. Values are presented as mean, minimum (Min) and maximum (Max) for each place. The number of samples for each variable is represented by n, when some values were missing, superscripts were added in the mean cell ([a] means 1 missing value, [b] represents 2, and [c] represents 3). Measured variables are pH (unitless), Alkalinity (meq·L^{-1}), Electrical Conductivity in field (EC_{field}, µS·cm^{-1}), Total Dissolved Solids in field (TDS_{field}, mg·L^{-1}), organic matter expressed as Dissolved Organic Carbon (DOC, mg·L^{-1}), nutrients concentrations including NO_3^- and P-PO_4^{3-}, as well as major anions (Cl^-, SO_4^{2-}) and cations (Ca^{2+}, Mg^{2+}, Na^+, and K^+) concentrations (mg·L^{-1}).

Sampling location		pH	Alkalinity	EC_{field}	TDS_{field}	DOC	NO_3^-	P-PO_4^{3-}	Cl^-	SO_4^{2-}	Ca^{2+}	Mg^{2+}	Na^+	K^+
Main channel														
D1	Mean	7.9	1.8	474.6	281.2[b]	1.8	1.1	2.1	67.1	35.3	43.8[a]	6.0[a]	35.6[a]	1.5[a]
n = 11	Min	7.5	1.1	203.4	110.8	0.2	0.6	0.9	17.3	15.4	22.7	3.0	9.1	0.9
	Max	8.2	3.0	1153.0	622.8	3.9	2.6	4.1	190.2	84.5	83.2	12.1	93.9	3.6
D2	Mean	8.2	2.9	1050.9	569.2[b]	3.6	2.0	20.0[a]	151.9	148.4	97.7[a]	14.1[a]	86.6[a]	4.2[a]
n = 23	Min	7.5	1.5	343.5	182.9	0.6	0.3	3.1	14.7	57.9	44.1	5.7	9.5	1.3
	Max	8.9	3.8	2015.0	1090.0	5.8	5.1	118.3	379.7	223.3	138.6	20.8	217.4	11.3
D3	Mean	8.1	2.7	716.3	386.5[b]	4.1	7.4	168.2[a]	74.5	104.9	80.2[a]	9.6[a]	43.5[a]	5.9[a]
n = 24	Min	7.1	1.7	330.1	176.0	0.4	1.0	6.0	12.8	48.4	45.4	4.9	8.2	1.2
	Max	8.8	3.6	1123.0	607.3	6.8	23.7	694.4	158.9	138.0	103.0	13.1	86.8	15.1
D4	Mean	8.1	2.6	462.3	250.7[b]	3.2	4.2	58.8[a]	33.8	50.9	60.7[a]	5.7[a]	21.0[a]	2.9[a]
n = 23	Min	7.2	1.6	288.6	152.6	0.7	1.4	7.2	9.3	23.5	37.6	3.1	5.7	1.0
	Max	8.8	4.2	712.3	382.3	5.1	9.3	250.4	90.7	86.4	83.6	8.3	67.0	7.2
D5	Mean	8.3	2.5	430.4	242.0[c]	3.0	5.8	88.9[a]	29.6	51.1	60.0[a]	5.5[a]	18.1[a]	2.8[a]
n = 12	Min	7.8	2.1	291.6	159.2	0.1	1.6	17.2	10.5	30.3	46.1	3.9	7.2	1.4
	Max	8.9	3.1	651.7	349.9	5.3	11.2	346.4	73.8	74.8	76.3	7.4	41.2	6.8
D6	Mean	8.1	2.6	427.3	230.1[b]	3.5	4.5	67.3[a]	28.4	40.3	59.2[a]	5.0[a]	17.5[a]	2.9[a]

...continued

Sampling location		pH	Alkalinity	EC_{field}	TDS_{field}	DOC	NO_3^-	$P\text{-}PO_4^{3-}$	Cl^-	SO_4^{2-}	Ca^{2+}	Mg^{2+}	Na^+	K^+
n = 23	Min	7.3	1.7	286.7	152.4	1.1	1.3	14.7	9.5	20.0	38.7	2.9	6.0	1.0
	Max	8.6	3.3	689.6	355.5	6.4	9.1	216.8	69.5	67.6	79.1	7.3	37.9	7.1
D7	Mean	8.1	2.5	407.3	226.3[b]	3.5	6.6	85.7	28.0	41.7	57.4[a]	4.9[a]	16.9[a]	3.1[a]
n = 11	Min	7.6	2.2	298.1	162.7	0.4	2.0	21.9	12.1	26.3	49.8	4.1	9.2	1.5
	Max	8.6	3.0	586.8	314.4	6.6	11.4	247.3	59.9	59.5	73.0	5.9	36.8	7.0
Tributaries														
M1	Mean	7.9	3.2	777.4	402.7[b]	2.7	1.7	7.8[a]	30.1	207.2	101.8[a]	20.2[a]	33.2[a]	3.9[a]
n = 23	Min	7.4	1.0	330.5	173.7	0.8	0.2	0.1	14.8	60.6	35.6	6.1	12.8	1.5
	Max	8.5	5.2	1250.3	556.6	5.5	5.2	31.9	48.5	451.0	151.6	33.2	62.9	8.0
O1	Mean	8.1	2.1	259.2	139.6[b]	2.4	1.8	8.8[a]	6.1	15.5	44.2[a]	2.8[a]	4.3[a]	1.1[a]
n = 23	Min	7.2	1.4	185.9	98.9	0.6	0.3	0.4	3.5	7.7	30.3	1.7	2.2	0.7
	Max	8.7	2.8	356.4	184.5	5.2	4.5	58.9	9.2	30.3	59.0	4.4	7.3	2.2
E1	Mean	8.1	3.8	417.0	222.0[b]	3.0	1.7	12.3	11.1	13.1	73.4	5.0	6.6	1.3
n = 19	Min	7.7	2.0	266.8	142.0	0.4	0.3	1.7	8.0	7.0	38.7	2.4	3.3	1.0
	Max	8.6	4.7	488.4	252.9	6.2	6.6	27.1	14.1	18.5	87.3	6.0	10.9	2.7
E2	Mean	8.0	3.5	432.8	230.6[b]	4.5	5.7	167.0[a]	17.8	17.8	70.2[a]	3.7[a]	10.4[a]	2.7[a]
n=23	Min	7.6	2.5	323.0	169.9	0.4	1.3	30.0	10.1	11.1	52.0	2.1	4.8	1.1
	Max	8.6	4.2	542.1	285.5	7.2	10.0	431.6	32.0	27.3	80.0	5.7	22.1	5.6

In addition to the punctual sampling methodology, three gauging stations measure hydrological (precipitation, discharge) and quality (turbidity, suspended sediment concentration, EC) variables at a 10-min frequency. EC is measured through in flowing water pumped to the station from the river. The three gauging stations are San Prudentzio and Oñati in the upper part of the catchment, and Altzola near the outlet (Figure 5.1a,b). The Altzola gauging station, placed between D6 and D7 sampling locations in the lower part of the catchment, collects 464.25km^2 of the area of the basin according to www.geoesukadi.eus. Within this drainage area, San Prudentzio (121.78km^2) and Oñati (105.78km^2) are located close to D3 and O1 sampling locations, respectively, collecting independent draining surfaces. There is a relevant tributary in terms of discharge and chemical compounds which is not controlled by a gauging station: the Ego tributary in the western part of the catchment. At this moment, the contribution of this stream to the main channel may only be estimated qualitatively through the analysis of the chemical analysis carried in the monitoring program or through modelling, but hydrological modelling has not been performed for the present study.

5.3.3 Statistical analysis

All statistical analysis performed in the present study has been accomplished using R software (R Core Team, 2019) for handling the data. Four sections may be described for the data analysis followed: punctual data, regarding the study of the monitoring program results; continuous data, regarding the analysis of the gauging station registries; the punctual and continuous data integration, regarding the combination of the two sources of data; and the analysis of flood events.

Analysis of the punctual data. Once the water samples were brought to the laboratory, the results of the analysis were compiled in a database. Graphs including the Gibbs plot, Piper diagram, and ionic ratios were constructed using the "ggplot2" library (Wickham, 2016). Due to the non-normality, the database was log-transformed to reduce skewness before a correlation matrix was performed to see which variables were independent.

Later, a Principal Component Analysis (PCA) with a Varimax rotation of the factors was used to reduce the number of variables, in order to distinguish the geochemical groups and the anthropogenic influence in the sampling locations for the different sampling periods. Finally, a Cluster Analysis (CA) was also performed using Euclidean square distance and the Ward's aggregation method to evaluate the degree of similitude among sampling locations for the three sampling periods.

Analysis of the continuous data. From the three gauging stations registries, accumulated precipitation (mm), average discharge ($m^3 \cdot s^{-1}$), water temperature (ºC), pH (dimensionless), and average EC ($\mu S \cdot cm^{-1}$) were selected for further analysis. For the Altzola gauging station, the start of the time series is in 1995 (July the 12th), for the San Prudentzio is in 1996 (July the 9th), and for the Oñati is in 1995 (April the 19th). The time series were validated by erasing negative values of accumulated precipitation, discharge, pH, and EC, introducing missing values in the analysis. Then, the 10-min registries were time-aggregated to hourly by summing the accumulated precipitation and computing the arithmetic mean for discharge, temperature, pH, and EC. The hourly time series was then further aggregated to daily, monthly and yearly, following the same criteria.

Punctual and continuous data integration. Punctual data were integrated using the daily aggregated time series and considering the punctual sample as representative for the day of the sampling campaign. EC and major ion concentrations in D6, D3, and O1 were incorporated to the Altzola, San Prudentzio, and Oñati time series, respectively. The gauging station and field EC were compared by means of the Pearson correlation finding a strong and significant correlation ($r>0.9$, $p<0.01$), and the correlation between TDS_{field} and EC_{field} is also strong and significant ($r>0.99$, $p<0.01$), while the extrapolation of TDS and major ion composition to a continuous time series was performed by computing a regression between the laboratory ionic concentration vs the EC_{field}. Three kinds of regressions are included: linear, potential, and logarithmic. Estimates of the parameters are calculated using the "stats" package in R for linear regression, and "minpack.lm" package (Elzhov et al., 2016) for non-linear fit. Prediction intervals (PI, 95%) have been calculated checking normality within the samples of each

sampling location through a Shapiro-Wilk test ($p<0.01$ imply the rejection of the null hypothesis, data non-normally distributed).Non-linear fit has been accomplished by Levenberg-Marquardt algorithm, and PI are calculated using uncertainty propagation through Taylor expansion and Monte-Carlo simulation ($n=10^6$ simulations) contained in the "propagate" package (Spiess, 2018). Then, continuous registries from EC were used as a proxy for the continuous concentration calculation.

5.4 Results and discussion

5.4.1 Sampling campaigns' results

5.4.1.1 Overview

A summary of the results from the punctual monitoring campaigns is shown in Table 5.1. In general, the pH ranges from 7.1 (D3) to 8.9 (D5) yielding neutral to slightly alkaline characteristics to the waters in all the system, relevant changes are not found nor in the main channel or the tributaries, nor within sampling campaigns in each location. In contrast, the highest mean values for alkalinity are found in the Ego tributary, while the lowest in the upper part of the catchment (D1), finding all values between 1.1 and 5.2 meq·L^{-1}. EC spans over an order of magnitude from 185.9 (O1) to 2015.0 µS·cm^{-1} (D2), reaching a mean peak (1050.9 µS·cm^{-1}) in the southwest part of the catchment (D2) decreasing towards the outlet, being the waters from Oñati (O1) the most diluted (mean 259.2 µS·cm^{-1}). Similar trends are found for TDS, where headwater sampling locations on the southwest part of the catchment (D1, and M1) present a wider difference between minimum and maximum TDS concentration, in comparison with the other upper sampling locations, O1 and E1.

Regarding major ions at the catchment level, the cationic mean concentration predominance is $Ca^{2+}>Na^{+}>Mg^{2+}>K^{+}$, but their relative contribution to the TDS is differ-

ent among ions: one group (Ca^{2+}, Mg^{2+}, and Na^{+}) present the greatest concentration in D2, as occurred for EC and alkalinity, but K^{+} concentration evolves similarly to nutrients and organic matter, peaking in D3. Na^{+} presents the highest differences between minimum and maximum concentration in D2, spanning over two orders of magnitude, while in other sampling locations this range is lower. Similarly happens with major anions (Cl^{-} and SO_4^{2-}) for which peak concentrations are found in D2, but their spatial evolution is slightly different: Cl^{-} concentration decrease from D2 downstream, while SO_4^{2-} presents slightly increasing trends between D1-D2, D4-D5, and D6-D7.

Concerning dissolved organic carbon (DOC) and nutrients (NO_3^{-} and $P\text{-}PO_4^{3-}$) along the main channel, the lowest concentration are in the D1 sampling location, while the highest concentrations are found at D3, both in the southwest part of the catchment before the confluence of the Oñati stream. Relative to their own ranges, $P\text{-}PO_4^{3-}$ presents the widest differences between low and high concentration, specially at D3, as well as the greatest heterogeneity in extreme values among sampling spots, as shown in the Ego tributary, where the greatest concentration is found for E2 and it is around 20 times the highest concentration upstream, in E1.

Further punctual analysis has been taken in the present system, focusing on the metallic pollution both in water and sediments (Martínez-Santos et al., 2015; Unda-Calvo, 2019; Unda-Calvo et al., 2017; Unda-Calvo et al., 2020). Those studies have shown and assessed the influence of anthropogenic inputs in the waters and sediments within this catchment focusing on metallic pollution, however the assessment of whether these human activities affect the major ion composition of water is remaining. Martínez-Santos et al., 2015 suggested that partially treated or untreated wastewater effluents are the main source of organic matter in some specific sites of the catchment. Their study was based on the samples taken in 2011 and 2012, at the time when management actions were put in place, such as the commissioning of three wastewater treatment plants (WWTP, Figure 5.1a). In the present analysis, samples taken after the installation of these WWTPs are considered, and still different spatial and temporal patterns between saline concentrations and organic matter (in the form of DOC) and nutrients concentrations in the catchment are present. Further analysis is presented in the 5.4.1.1

and 5.4.1.4 sections regarding these spatial and temporal patterns.

5.4.1.2 Spatial evolution

The waters in the Deba river catchment are mixed along the main channel, receiving inputs from several tributaries (specially the Mazmela, Oñati, and Ego). Concerning TDS (Figure 5.2a) and saline concentrations (Figure 5.2b), the highest values for major ion concentrations are in D2, showing a decreasing trend towards the outlet of the catchment. In opposition, DOC, P-PO_4^{3-}, and NO_3^- peak in D3 (Figure 5.2a) and show increasing trends between D4-D5 and D6-D7. Among the tributaries, and paying special attention to the sampling locations close to the main stream (M1, O1, and E2), three different aspects are relevant: Mazmela (M1) presents the highest concentrations for Ca^{2+}, Mg^{2+}, and SO_4^{2-} in all the system, Oñati (O1) has the lowest saline concentrations, and the Ego tributary (E2) inputs a relevant amount of DOC, P-PO_4^{3-}, and NO_3^-. Previous studies in the area (Martínez-Santos et al., 2018; Unda-Calvo et al., 2020) have attributed the highest water quality index to all headwater sampling locations (D1, M1, O1, and E1) and the lowest to (D3, D5, and D7) suggesting that the later group is influenced by effluents from wastewater treatment plants (WWTPs) and untreated urban wastewater (UWW), this is shown in the increasing trends between D2-D3, D4-D5, and D6-D7 in organic matter (DOC) and nutrients (PO_4^{3-}, and NO_3^-). Other study (Iribar & Ábalos, 2011) has reported the influence of spring waters in the composition of river chemistry in this and surrounding catchments, and the presence of a saline spring in Leintz-Gatzaga (between D1 and D2, Figure 5.1b) seems to be responsible of the peak in saline concentration in D2 which is later noted downstream at the outlet. This is particularly important for Na^+ and Cl^-, which are the main ions drained by this evaporitic spring (Ábalos et al., 2008), and for SO_4^{2-}, which is mainly associated to gypsum intrusion deposits in the Walden Facies in the Mazmela subasin (M1) (Ábalos et al., 2008; Iribar & Ábalos, 2011; Martínez-Santos et al., 2015). D2 presents the highest saline concentration, reaching the oligohaline threshold (0.5 $mg \cdot L^{-1}$), which is later diluted till reaching freshwater characteristics in the mid and lower part of the catchment, suggesting that the saline spring is the dominant factor on the saline

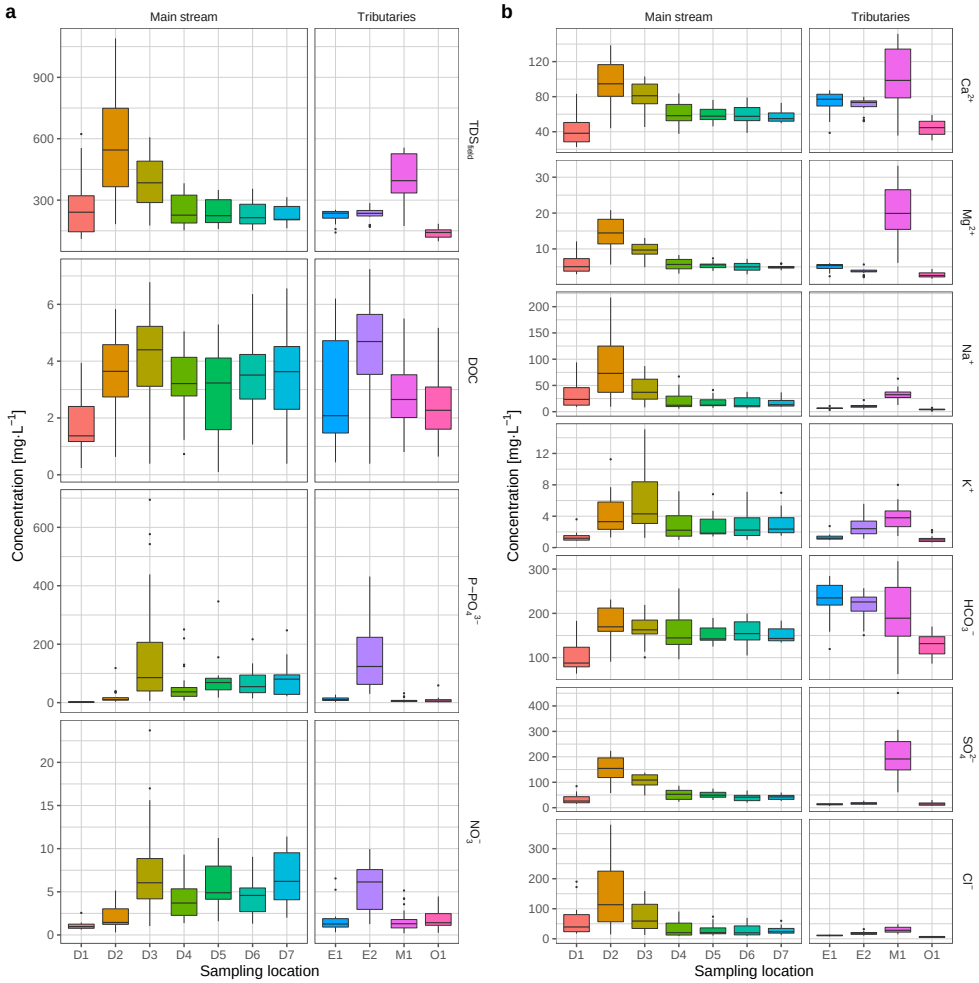

Figure 5.2: Boxplot spatial evolution for a) TDS, DOC, and nutrients, and b) major ion composition, expressed as concentration ($mg{\cdot}L^{-1}$). Two groups are present: main channel and tributaries.

composition and that downstream sampling locations are dilution water.

5.4.1.3 Sampling campaign classification

Each punctual sampling campaign was performed within a day for all sampling locations, and the results are considered as representative of that day, without taking in consideration diurnal cycles or sub-daily sampling, this assumption is later discussed on the section 5.4.2. Due to the differences found between the minimum and maximum values for each variable in each sampling location, a temporal assessment was considered necessary to understand the evolution of geochemical and WWTP influence on the water chemistry. In order to perform such assessment, a classification of the sampling campaigns regarding hydrological periods was included. This classification has been based on the daily mean discharge in the Altzola gauging station, and its relative value with regards to the 1st and 3rd quartiles of the October 2013 to September 2017 discharge time series. When the daily mean discharge was under the 1st quartile (P25th percentile, 1.8 $m^3 \cdot s^{-1}$) the sampling campaign was classified as "low discharge" period, when it was over the 3rd quartile (P75th percentile, 8.9 $m^3 \cdot s^{-1}$) it was attributed to "high discharge", and all other samples between were classified as "mid discharge". A potential source of uncertainty in this classification is not considering whether the sampling campaign was performed at the beginning or ending of a flood event, which is likely to condition the assessment of water and dissolved solid transports. These processes are taken in consideration and discussed in further sections (section 5.4.2). Nevertheless, precipitation and discharge between Altzola – San Prudentzio, and Altzola – Oñati show a strong and significant correlation ($r^2>0.8$, $p<0.01$) suggesting that, even though event characteristics are not considered, the dilution processes are expected to be uniform in all sampling stations, supporting the classification scheme. The Altzola discharge time series and the sampling classification is shown in Figure 5.3.

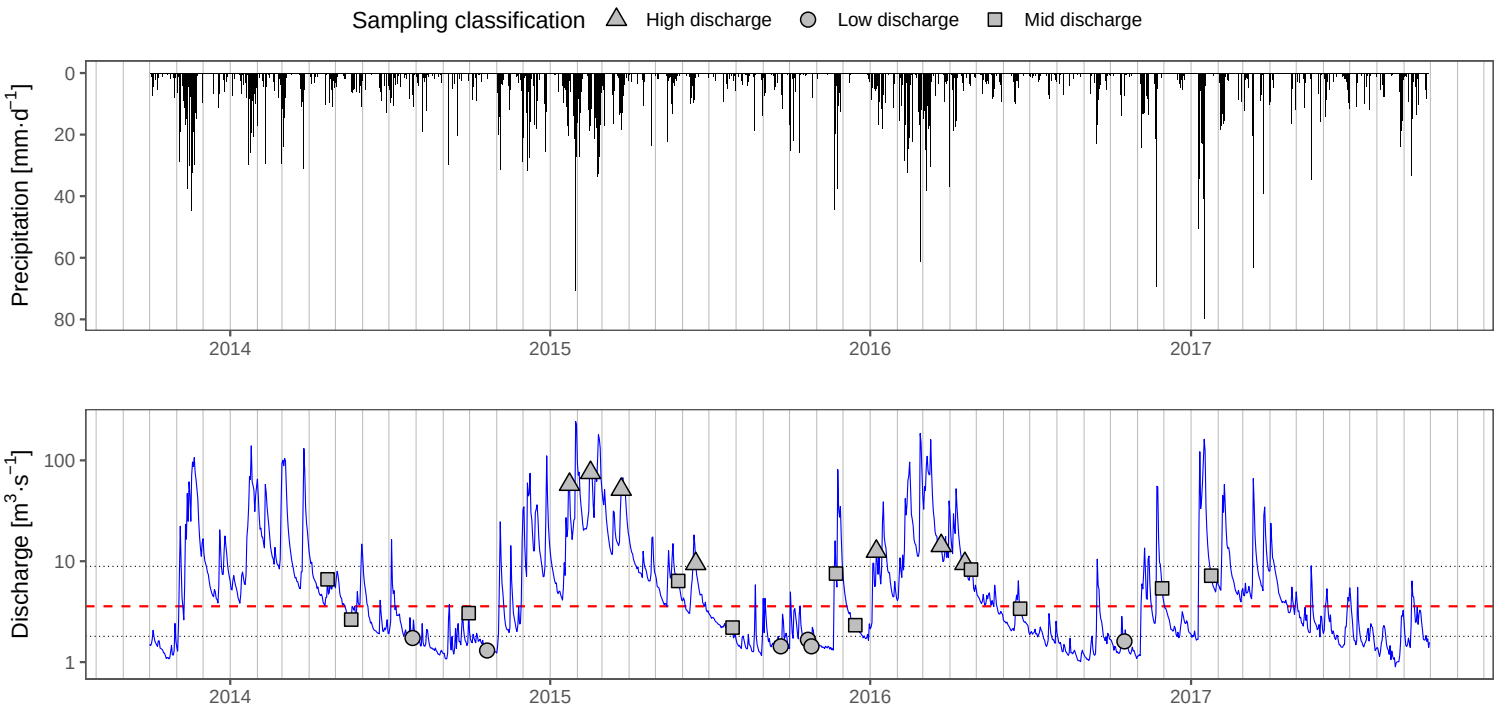

Figure 5.3: Daily accumulated precipitation and mean discharge time series at the outlet of the catchment (Altzola gauging station). Vertical axis in precipitation plot is in reverse order, while in the discharge plot it is presented in the logarithmic scale. The horizontal lines in the discharge plot represent the median (dashed line), 1st and 3rd quartiles (25th and 75th percentiles, respectively) used to classify the sampling campaigns into low discharge (triangles), mid discharge (squares), and high discharge (circles). Vertical black lines indicate the starting point of three flood events considered in the present study.

Table 5.2: Pearson correlation test performed on the log-transformed dataset from the punctual sampling for all sampling locations (n=175). Significance of the correlation is displayed through **bold** ($p<0.01$), *italics* ($0.01<p<0.05$), straight ($p>0.05$).

	pH	**TDS_{field}**	**EC_{field}**	**Ca^{2+}**	**Mg^{2+}**	**K^{+}**	**Na^{+}**	**Alkalinity**	**SO_4^{2-}**	**Cl^{-}**	**DOC**	**NO_3^{-}**	**P-PO_4^{3-}**
pH	1.00												
TDS_{field}	**0.25**	1.00											
EC_{field}	**0.20**	**1.00**	1.00										
Ca^{2+}	**0.22**	**0.89**	**0.90**	1.00									
Mg^{2+}	*0.14*	**0.89**	**0.89**	**0.82**	1.00								
K^{+}	0.09	**0.81**	**0.82**	**0.74**	**0.69**	1.00							
Na^{+}	*0.18*	**0.93**	**0.92**	**0.70**	**0.83**	**0.82**	1.00						
Alkalinity	**0.24**	**0.59**	**0.59**	**0.82**	**0.42**	**0.50**	**0.33**	1.00					
SO_4^{2-}	*0.15*	**0.81**	**0.81**	**0.66**	**0.92**	**0.72**	**0.85**	**0.19**	1.00				
Cl^{-}	**0.21**	**0.90**	**0.89**	**0.65**	**0.74**	**0.80**	**0.97**	**0.33**	**0.75**	1.00			
DOC	*-0.14*	0.09	*0.13*	0.07	-0.02	**0.25**	0.08	0.10	0.03	0.12	1.00		
NO_3^{-}	*0.15*	0.09	0.07	0.07	-0.08	**0.33**	*0.16*	0.10	0.07	**0.20**	*0.14*	1.00	
P-PO_4^{3-}	-0.03	0.12	0.12	0.11	-0.12	**0.42**	0.14	**0.23**	0.00	**0.20**	**0.38**	**0.66**	1.00

5.4.1.4 Temporal evolution

Sampling periods (low, mid, and high discharge) were compared among them, to test whether the catchment response was homogeneous under different hydrological conditions or there was some variation along time. Such comparison was performed making a Cluster Analysis (CA) on the sampling locations. Differences in the aggregation groups would indicate where and when there is a geochemical or anthropogenic influence on the water chemistry. Before performing a CA, a Shapiro-Wilk test for each of the variables has showed significant p-value ($p<0.01$) for every variable, allowing the rejection of the null hypothesis of normal-distribution of the variable, thus all variables are non-normally distributed. In light of the distribution, considering that all variables are continuous and positive and that the numeric ranges are dislike among variables, a log-transformation is applied before performing any other test. From the Pearson correlation matrix (Table 5.2) performed to the log-transformed punctual dataset, a set of 10 variables (pH, TDS_{field}, EC_{field}, Ca^{2+}, Mg^{2+}, Na^{+}, Alkalinity, SO_4^{2-}, Cl^{-}, $P\text{-}PO_4^{3-}$) which were, at least, non-correlated to one of the other variables were added to the CA. pH presents a non-significant ($p>0.05$) to very significant ($p<0.01$) but low correlation ($|r|<0.25$) to all variables, which in conjunction with the low variation in this variable suggests low influence of acidic inputs in this catchment. In contrast, TDS_{field} and EC_{field} present a very significant and perfect positive correlation ($r=1$) among them, and a very strong correlation to all major cations (Ca^{2+}, Mg^{2+}, Na^{+}, and K^{+}), supporting the findings on main influence of saline concentrations on the TDS found in the catchment. Ca^{2+} presents very significant but lower correlation to Na^{+} and K^{+} ($0.7<r<0.74$), indicating a different behaviour among these ions, which is also present on the relation of Alkalinity to all other variables, except for Ca^{2+} where the correlation is higher ($r>0.8$). Almost perfect fit is found between Na^{+} and Cl^{-} indicating a common origin in the catchment, which also present the highest correlation with EC_{field}, suggesting that among the saline concentrations in this catchment Na^{+} and Cl^{-} have the greatest influence on the EC_{field} and TDS_{field}. Among the organic matter and nutrients, there is a very significant correlation with K^{+}, but not a very strong correlation ($r<0.5$), which in contrast is found for NO_3^{-} and PO^{43-}. Three dendrograms are shown in Figure 5.4

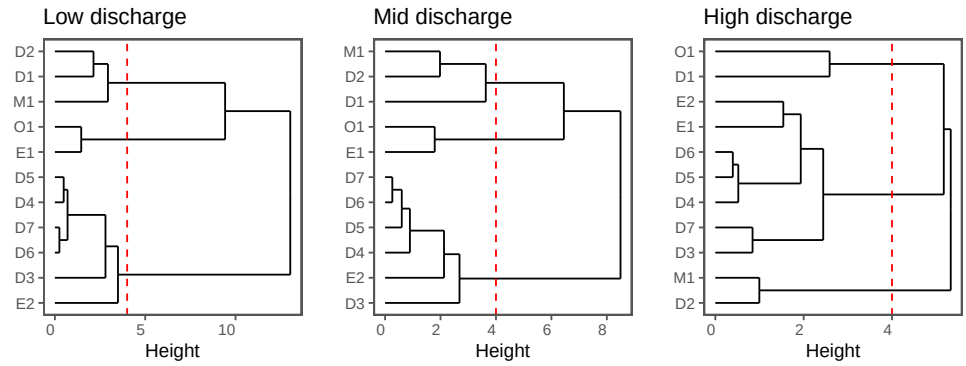

Figure 5.4: Cluster analysis of the sampling locations in this catchment considering pH, TDS_{field}, EC_{field}, Ca^{2+}, Mg^{2+}, Na^{+}, Alkalinity, SO_4^{2-}, Cl^{-}, and P-PO_4^{3-} in three different periods. Red dashed line represents a cutting line for three groups.

for each sampling periods. Within each dendrogram, three clusters have been identified for each hydrological period: D1-D2-M1, O1-E1, and D3-D4-D5-D6-D7-E2 for low and mid discharge periods; while D1-O1, D2-M1, and D3-D4-D5-D6-D7-E1-E2 for high discharge period. The greatest differences among groups are in the high discharge hydrological period, where the southern headwater sampling locations are split in two groups, and the Ego tributary presents more similar characteristics up and downstream. The lower Ward's distances among sampling locations is found in the high discharge period, suggesting lower differences within the catchment in periods with elevated discharge, indicating that discharge has a strong effect on the saline, organic matter, and nutrient concentrations, though dilution conditions the composition in the streams. In order to understand which variable has a stronger effect on each sampling location, a Principal Component Analysis (PCA) has been performed using the 10-variables dataset selected for the Pearson correlation matrix. Three components with an eigenvalue over 1 account for 79.4% of the total variance, as shown in Figure 5.5. Negative values of the F1 relate to sampling locations with high saline concentrations, where M1 and D2 samples stand out. M1 and D2 cluster together in the three sampling periods, representing a single group in the high discharge period, while grouping with D1 in low and mid discharge periods. It has been previously shown that these sampling locations have low nutrients and organic matter concentration, associated with lower anthropogenic input, while the saline characteristics are similar between M1 and D2 due to the strong

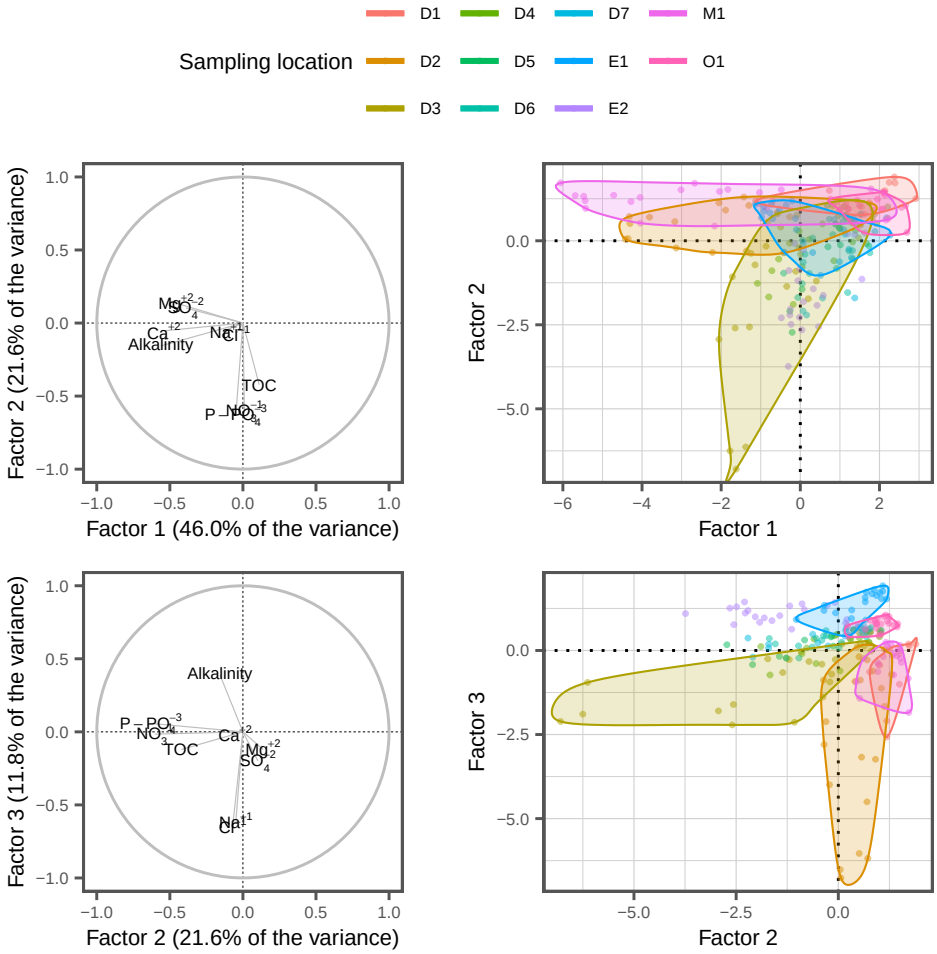

Figure 5.5: Principal Component Analysis (PCA) performed on the major ion, nutrients, and physicochemical variables of the samples. Left plots show the scores of the variables for Factors 1, 2, and 3 (explaining 79.4% of the variance), right plots represent the weights of the factors for each sample included in the analysis. Headwaters (D1, M1, E1, and O1) and D2 are circled to present the major differences.

influence of SO_4^{2-} and Ca^{2+} derived from the Mazmela tributary (M1) into this section of the main stream. Among the headwaters in this catchment (D1, M1, O1, and E1) M1 and D1 are the most alike in terms of SO_4^{2-} concentration, suggesting that the intrusions of gypsum deposits presented in the southwest part of the catchment (Ábalos et al., 2008; EVE - Ente Vasco de la Energía, 1989; Martínez-Santos et al., 2015) may be responsible of the relatively high concentration of this anion in this first cluster. Negative values of F2 relate to organic matter and nutrient concentrations, where D3 is strongly influenced together with D5, D7, and E2, to a lesser extent. The D3-D4-D5-D6-D7-E2 cluster seems to be strongly affected by nutrient loadings, specially in low and mid discharge sampling periods, where the two most impacted sampling locations (D3 and E2) stand over the mid and down part of the catchment (D4-D5-D6-D7 group). It seems that in D3 and E2, even after the implementation of management actions such as the Epele WWTP, there is a strong influence of the anthropogenic input, previously noted in the physicochemistry (Unda-Calvo et al., 2017) and microbial communities (Martínez-Santos et al., 2018; Unda-Calvo et al., 2019) in sediments, as well as in the ecological status linking water and sediments (Unda-Calvo et al., 2020). F3 allows for the discretization between two saline kinds of water, those draining halite (D2), and those draining gypsum (M1) waters. It is also relevant to note the clustering of O1 and E1, which is linked to the lower concentration of salts and nutrients in these two sampling locations.

Considering that the D1-D2-D3 and M1 group of sampling locations present both the highest saline and nutrients concentration, and that the main saline input in this area seems to be the evaporitic and stable flow spring located in Leintz-Gatzaga (Iribar & Ábalos, 2011). It is important to see how the relative influence of a constant input such as a spring is affecting the major ionic distribution in the catchment, while the hydrological conditions change through time. Further analysis on the temporal evolution is found in section 5.4.2.1.

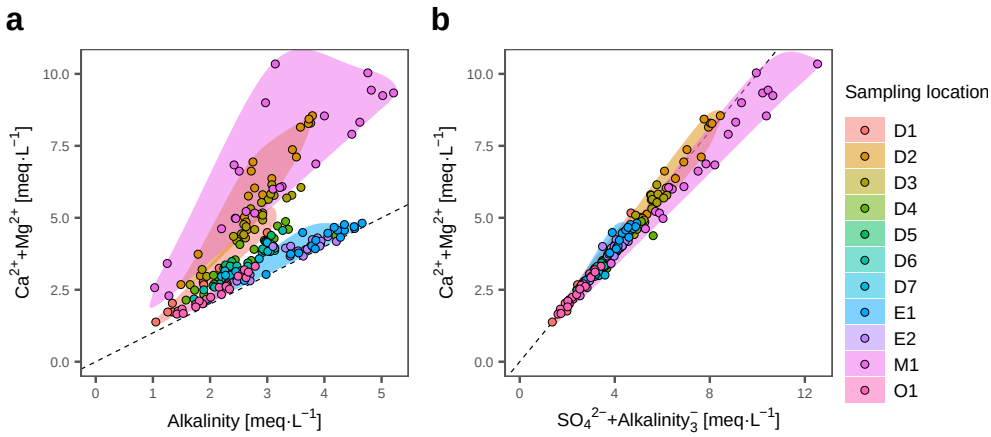

Figure 5.6: Ratio scatterplots for punctual sampling results for all sampling locations. Five sampling locations have been circled (D1, D2, M1, O1, and E1) in order to distinguish the different headwaters involved in this catchment, as well as D2. Dashed line represents 1:1 line.

5.4.1.5 Geochemical processes and water types

Once known that the anthropogenic influence is mainly noted on the nutrients and organic matter, and that major ion composition is dominated by lithology, an assessment on which are the main geochemical processes governing these inputs is performed. The water composition in the Deba river urban catchment varies from headwaters to the outlet of the catchment receiving waters from different tributaries draining influents with different water types and a varying degree of pollution from treated, partially treated, and untreated industrial and domestic effluents (Martínez-Santos et al., 2018; Martínez-Santos et al., 2015). In order to assess the main geochemical processes given in the catchment, the Gibbs plot (Gibbs, 1970) is used (Figure S5.1), according to which there are three main processes governing the river water composition: crystallization and evaporation, water-rock interaction, and precipitation. For this catchment, the Gibbs plot suggests water-rock interaction, together with crystallization and evaporation as the main geochemical processes governing major ion composition. The Oñati (O1) and Ego tributaries (E1 and E2) present a low ionic ratio, falling in the left side of the plot, suggesting a strong water-rock interaction in this area, related to the low

concentration of Na^+ in comparison with the Ca^{2+}, which is probably originated by the carbonate material of the area. The samples from the southeast tributary of Mazmela (M1) cluster around an ionic ratio of 0.25 while presenting a relatively high dissolved solid concentration, specially in the low and mid discharge sampling periods. This suggests a slight tendency towards the crystallization and evaporation zone, but more influenced by the high Ca^{2+} concentration, responsible for a lower value of the ionic ratio. The group D1-D2-D3 is pulled to the evaporation-crystallization area of the plot which is normally related to seawater intrusion, but in this case is attributed to a saline spring located in Leintz-Gatzaga (between D1 and D2, Figure 5.1b), which drains water from a deep evaporitic reservoir, as noted by Iribar and Ábalos (2011).

Carbonates is the dominant lithological formation in the catchment, thus an equivalent ratio $(Ca^{2+}+Mg^{2+})/(\text{Alkalinity}) = 1$ indicates that all Ca^{2+} and Mg^{2+} come from the dissolution of carbonate materials, while higher values suggest another lithological contribution for Ca^{2+} and Mg^{2+} than carbonate, i.e. evaporitic rocks (gypsum or epsomite). In this catchment, most of the samples present $(Ca^{2+}+Mg^{2+})/(\text{Alkalinity}) > 1$ (over the dashed line in Figure 5.6a), as well as an equivalent ratio $(SO_4^{2-})/(HCO_3^-) > 1$, while linear relationship between $Ca^{2+}+Mg^{2+}$ and SO_4^{2-}+Alkalinity (Figure 5.6b). The greatest deviation from linearity in these two relationships is found for the Mazmela tributary (M1) where there is a relevant amount of $Ca^{2+}+Mg^{2+}$ non-balanced by Alkalinity, while a slight predominance of SO_4^{2-}+Alkalinity over those two cations, suggesting a relevant input of SO_4^{2-}, confirming the existence of interlayered gypsum deposits (Qin et al., 2018), which are not included in the official map, but has been noted in previous studies (Iribar & Ábalos, 2011; Martínez-Santos et al., 2015; Orive et al., 1989).

The Piper Diagram shown in Figure 5.7 shows all the water samples collected in the monitoring program distinguished by sampling location and sampling period. It is possible to see that the Deba river and its tributaries samples span over four types of water, presenting higher differences for low and mid discharge sampling periods. Most of the samples are located in the magnesium-bicarbonate part of the upper diamond, being dominated mostly by Ca^{2+} concentrations, which presents the highest concentrations in the catchment (Table 5.1). The southwest part of the catchment is

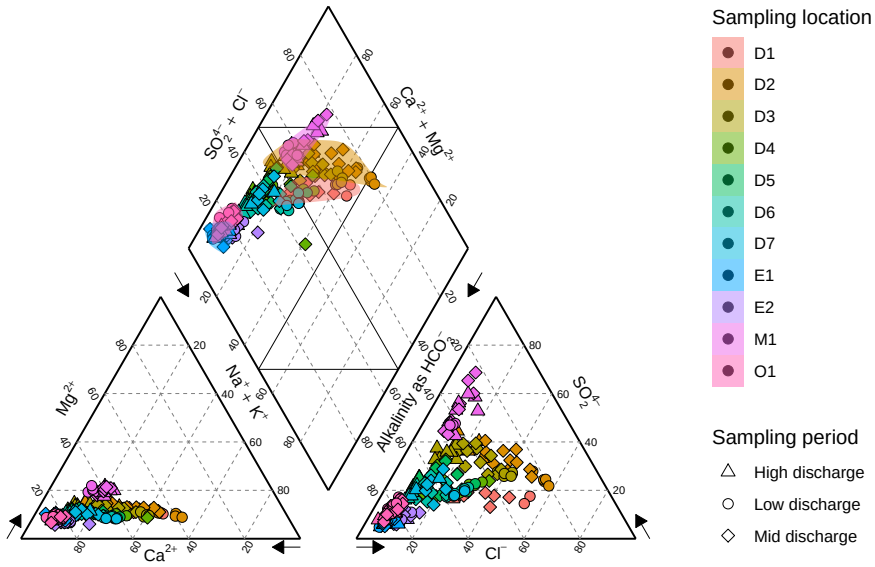

Figure 5.7: Piper diagram regarding water classification and geochemical mechanisms governing major ion chemistry at the catchment scale. Each colour represents a single sampling location (the reader is redirected to the web version of the article) while the shape represents the sampling period. Five sampling locations have been circled (D1, D2, M1, O1, and E1) in order to distinguish the different headwaters involved in this catchment, as well as D2 which presents a different kind of water.

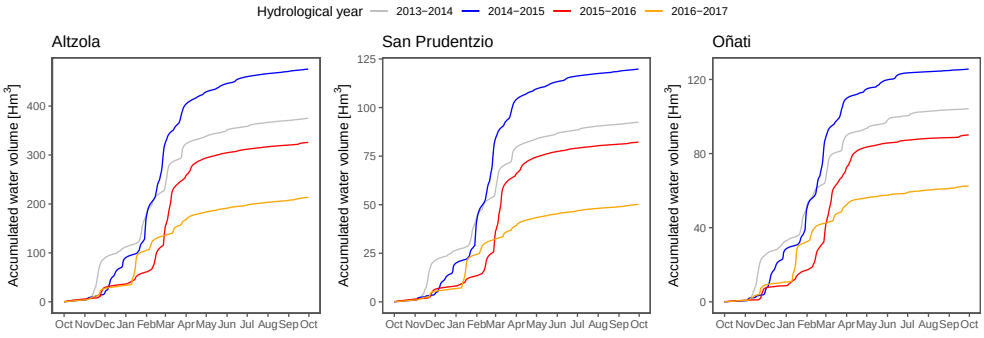

Figure 5.8: Accumulated water volume exported in the three gauging stations for the hydrological years (beginning October 1st, ending September 30th) between 2013 and 2017. Each line represents an independent hydrological year.

associated to the calcium-chloride (M1) and the sodium-chloride (D1-D2-D3) types of water, while the mid samples are more related to the mixed type. Regarding the anions, the lower right triangle separates the samples in clusters, explaining that M1 is dominated by sulphates supporting the gypsum deposits affecting water chemistry, while D1 and D2 are dragged towards the chloride type, due to the presence of the saline spring. In general, the alkaline earths exceed the alkalis, but the clustering of low and mid discharge samples in D2 and D1 towards the sodium-chloride part of the diamond indicates a different behavior of these spots. In D1-D2-M1 it seems that the strong acids (such as H_2SO_4 or HCl), related to sulphate and chloride dominate the water chemistry, while in the other sampling locations, the weak acids prevail (H_2CO_3).

5.4.2 Water and dissolved solid exports

Two assumptions on the classification of the sampling location have been performed: first, that the results from the punctual sampling campaigns are representative for the daily composition of the river in each location, and that daily mean discharge is enough for the hydrological classification, not taking in consideration previous hydrological conditions (accumulated precipitation, previous discharge, increasing or decreasing part of a flood event). These assumptions are discussed in the following sections. First, regressions are established using punctual data to estimate TDS using EC as proxy in the continuous data registered in three gauging stations (Figure 5.1a,b) in section 5.4.2.1. Second, the dissolved solid exports are compared taking in consideration different temporal aggregation methods to test the error committed in each time step. And finally, moments of relevant water and dissolved solid loads are evaluated to test which moments are more relevant in terms of TDS or water exports in the present system. All these analyses are performed covering four hydrological years (October 2013-September 2017).

The accumulated time series for water volume (Figure 5.8) show that the 2014-2015 was the wettest of the years, followed by 2015-2016 and 2013-2014, while 2016-2017

is the driest period. In general, the lowest discharge periods within these years are between June and November, while relevant flood events contribute to the total water volume exported between December and May. The 2015-2016 and 2016-2017 years overlap in March, before which month the 2015-2016 year was drier, but some flood events increased the total volume discharge. This is true for all three places, where Oñati and San Prudentzio yield comparable water volumes, about half of the total volume discharged on Altzola.

5.4.2.1 Continuous registries

The monitoring program set up in this catchment contains sampling locations close to the three gauging stations, all of them located within 5 km of the punctual spot: Altzola-D6, San Prudentzio-D3, and Oñati-O1. Due to their proximity and the lack of relevant contributions regarding water chemistry, it has been assumed that the EC in the gauging stations ($EC_{station}$) is a proxy for TDS and major ion composition in those locations. This assumption has been tested through linear regression between EC measurements in laboratory (EC_{lab}) and the EC_{field} measured in punctual sampling locations at the time of sampling, as well as evaluating the regressions between TDS_{field} and EC_{field}. In addition, as TDS_{field} and major ion composition are strongly and very significantly correlated (Table 5.3) it has been possible, following a similar approach to those of (Benettin & van Breukelen, 2017), to establish regressions between each element and EC_{lab} which may be used to deconvolute the $EC_{station}$ signal into its constituents. Table 5.3 summarize these regressions between laboratory and field measurements for each sampling location and its respective gauging station, and Figure 5.9 shows the scatterplots for those regressions, as well as the 95% prediction intervals (PI). Most of the samples lay within the PI, and the punctual EC_{field} strongly correlates to the daily mean $EC_{station}$, (Slope > 0.76, $r^2 > 0.81$, $p<0.01$), suggesting that these regressions may be used to extrapolate a continuous time series of dissolved solids concentrations, as well as major ion concentrations in the river stream. The agreement between the TDS_{field} and EC_{field} and the good correlation between each sampling location with its associated gauging station, allows for the use of the continuous $EC_{station}$ as proxy for

Table 5.3: Summary of regressions' estimates (A, B) and coefficients of determination (r^2) for each gauging station and corresponding sampling location (between brackets). Four types of regressions are displayed, with estimates shown for best fit: linear, potential, exponential, and logarithmic, along with the formulation. All regressions are fit using EC in $\mu S \cdot cm^{-1}$ and concentrations in $mg \cdot L^{-1}$, except alkalinity ($meq \cdot L^{-1}$). All regressions are significant ($p<0.01$). Only samples with all variables measured were taken in consideration (n = number of samples).

	Linear [Element]=A·EC+B		**Potential** [Element]=A·EC^B		**Logarithmic** [Element]=A·ln(EC)+B		
Element	**A**	**B**	**A**	**B**	**A**	**B**	**r^2**
Altzola (n=20)							
TDS_{field}~EC_{field}	0.5209	4.7026	-	-	-	-	1.00
EC_{field}~EC_{lab}	0.9686	36.647	-	-	-	-	0.98
Ca^{2+}~EC_{lab}	-	-	-	-	35.785	-154.81	0.96
Mg^{2+}~EC_{lab}	-	-	-	-	3.7524	-17.5	0.93
Na^{+}~EC_{lab}	-	-	0.00005	2.1135	-	-	0.98
K^{+}~EC_{lab}	-	-	0.00003	1.8696	-	-	0.88
Alkalinity~EC_{lab}	-	-	-	-	1.4177	-5.864	0.89
SO_4^{2-}~EC_{lab}	0.0992	-0.9197	-	-	-	-	0.81
Cl^{-}~EC_{lab}	0.00004	2.2131	-	-	-	-	0.95
San Prudentzio (n=23)							
TDS_{field}~EC_{field}	0.5305	1.876	-	-	-	-	1.00
EC_{field}~EC_{lab}	0.9855	30.624	-	-	-	-	1.00
Ca^{2+}~EC_{lab}	-	-	-	-	42.389	-195.79	0.96
Mg^{2+}~EC_{lab}	-	-	-	-	5.1368	-23.926	0.82
Na^{+}~EC_{lab}	-	-	0.0001	1.9335	-	-	0.99
K^{+}~EC_{lab}	-	-	0.00008	1.697	-	-	0.90
Alkalinity~EC_{lab}	-	-	-	-	1.2367	-5.3158	0.90
SO_4^{2-}~EC_{lab}	-	-	-	-	63.217	-307.89	0.84
Cl^{-}~EC_{lab}	-	-	0.00006	2.1204	-	-	0.97
Oñati (n=22)							
TDS_{field}~EC_{field}	0.5114	4.5188	-	-	-	-	0.97
EC_{field}~EC_{lab}	0.9498	31.938	-	-	-	-	0.91
Ca^{2+}~EC_{lab}	-	-	-	-	41.221	-181.52	0.91
Mg^{2+}~EC_{lab}	-	-	0.0026	1.2632	-	-	0.91
Na^{+}~EC_{lab}	0.012	1.3761	-	-	-	-	0.83
K^{+}~EC_{lab}	-	-	0.0019	1.1537	-	-	0.46
Alkalinity~EC_{lab}	-	-	-	-	1.8526	-8.02	0.90
SO_4^{2-}~EC_{lab}	0.1127	-11.769	-	-	-	-	0.73
Cl^{-}~EC_{lab}	0.0231	0.4847	-	-	-	-	0.41

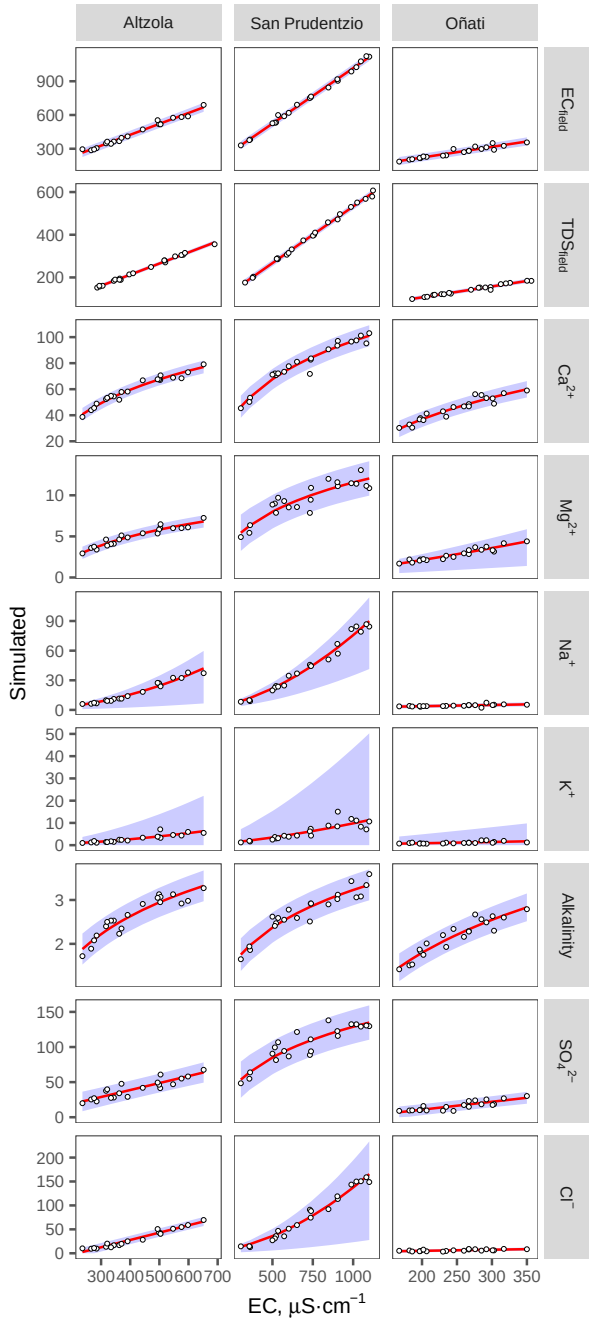

Figure 5.9: Scatter plot of ionic concentrations, TDS_{field} and EC_{field} vs EC_{lab} in each sampling location close to its associated gauging station. Points represent punctual samples; red line indicates simple linear regression (estimates and regression evaluation are shown in Table 5.3), and blue area indicate 95% prediction intervals.

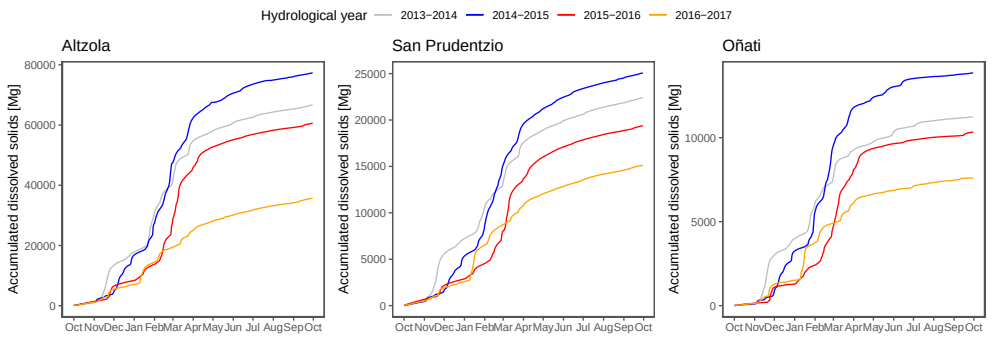

Figure 5.10: Accumulated dissolved solids exported in the three gauging stations for the hydrological years (beginning October 1st, ending September 30th) between 2013 and 2017. Each line represents an independent hydrological year.

the estimation of TDS concentration which, in combination with continuous discharge, allows for the estimation of dissolved loadings (Figure 5.10). Regarding the dissolved solids in the study period, the temporal trends are similar regarding periods, but the steepness of the curves are softer, especially for the case of San Prudentzio, suggesting a relevant contribution during low flow periods and a lower influence of the flood events on the dissolved solid exportation. In addition, the differences among the years are lower in San Prudentzio, suggesting a more stable load along the year. Regarding the ranges of the loadings, those of San Prudentzio are almost double the ones in Oñati, about a third of those measured in Altzola, suggesting a strong dependence of this area of the catchment on the loadings exported out of the basin. As expected, the combination of high frequency data from the gauging locations with the periodic sampling results have shown significant regressions between EC_{lab} and ionic concentrations. The obtained regression coefficients pose an opportunity for developing a time dependent analysis of the major ion loadings from the Deba river to the estuary, where the riverine end-member input is important when assessing the estuarine dynamics and the land pollutant estimation (Tueros et al., 2008). For this purpose, the continuous measurement of $EC_{station}$ in the Altzola gauging station is key, as it collects the waters for most part of the catchment. The knowledge of a continuous dissolved solids concentration and major ion chemical composition is of interest for biogeochemical modelling focusing in riverine loads to other water bodies (such as lakes, estuaries, or oceans) (Chapra

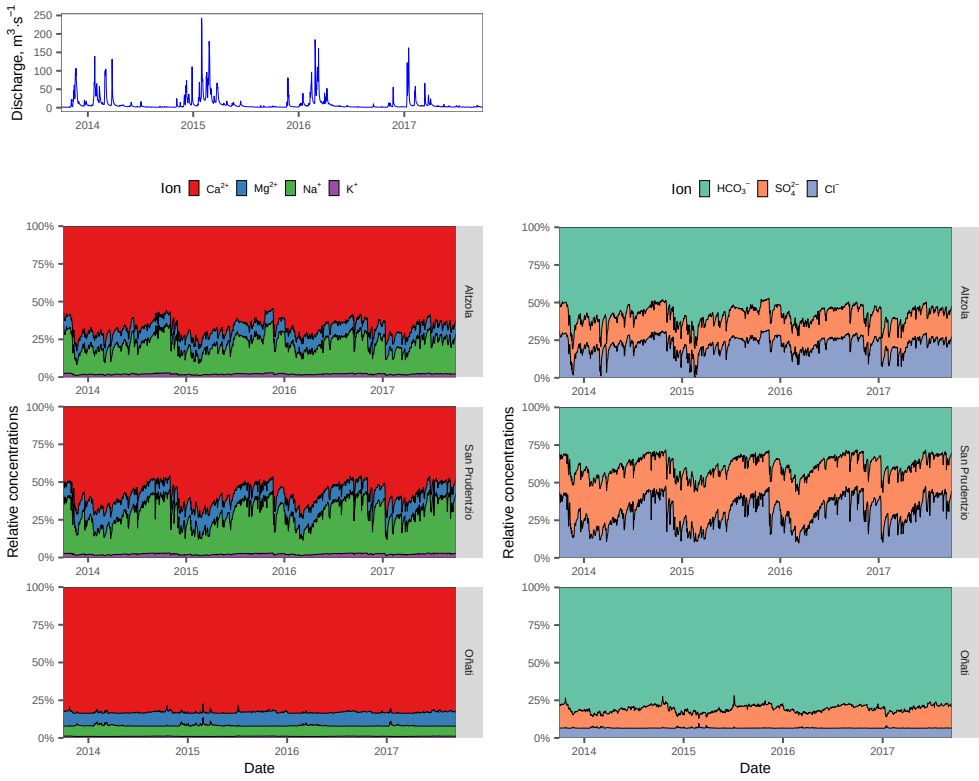

Figure 5.11: Major ion relative concentration time series for all three gauging stations. Areas represent the relative proportion of a ionic concentration respect the total cation ($(Z_i^+)/(\Sigma Z_i^+)$) or anion ($(Z_i^-)/(\Sigma Z_i^-)$) concentration, respectively. Percentages are calculated using equivalent concentrations

et al., 2012). In addition, it is possible to characterize these loadings in terms of their ionic concentration, as they show strong and significant correlations to EC_{lab}, the time series are shown in Figure 5.11.

5.4.2.2 Dissolved solid loadings

The obtained regressions from the punctual data have allowed us to compute the $TDS_{station}$ concentration temporal evolution, which is now used to estimate the annual loadings to the estuary of the Deba catchment, using Altzola gauging station as the outlet point. In this study, we have compared three methodologies (Table 5.4) on the

estimation of these loadings for the three gauging stations present in the system, taking into account different temporal steps. Method 1 is based on the mean discharge and mean concentration during all the period, Method 2 accounts for the moments with punctual samplings, while Method 3 used the integration of the daily mean discharge ($Q_{station}$) and $TDS_{station}$ concentration finding that, as finer the temporal resolution is, the lower the load becomes, suggesting that methods 1 and 2 overestimates the annual dissolved solid input. This insight highlights the advantages of establishing a continuous monitoring program with high frequency registries, which can improve this assessment through periodic monitoring program. Specially in systems such as the Deba river, where differences in river discharge span over two orders of magnitude between low flow period and high flow period. In such system like Deba, with a fast response to the precipitation, flood events are common (García-García et al., 2019) and floods have been studied as moments of wash-up of the catchment, becoming relevant events for matter transport from land to the ocean. The effect of these events on the major ion composition has not assessed in urban catchments such as the one in this study, where the anthropogenic activity could lead to the deposition of salts in the soil which are washed out during flood events. In this moment, we pose the following question: when are the moments where the exportation of dissolved solids is most relevant? To answer this question, we use the continuous registries in the Altzola gauging station, in combination with the regressions obtained (Table 5.3) to compute a time series of dissolved solids and compare which is the error committed when using lower temporal resolution data.

Table 5.4: Summary of Total Dissolved Solid exports in three sampling locations in the Deba river catchment. All units are expressed as $Mg \cdot y^{-1}$, computed as indicated in the Equation column. L_{annual} is mean annual load, k represents the unit conversion factor, TDS represents the Total Dissolved Solid concentration ($\overline{TDS}$ is the average concentration among all sampling campaigns, TDS represents instant concentration, and TDS' the obtained through linear regression with Electrical Conductivity, all expressed in $mg \cdot L^{-1}$), Q represents discharge (similar differences as for TDS, expressed in $m^3 \cdot s^{-1}$), Δt is the time span (measured in days), and dt represents the daily increment used for the integration.

	Equation	**D3**	**O1**	**D6**
		San Prudentzio	Oñati	Altzola
Method 1	$L_{annual} = k \cdot \overline{TDS} \cdot \overline{Q}$	36572	16414	92384
Method 2	$L_{annual} = \sum L_{i-(i+1)} = k \cdot \left(\frac{TDS_i + TDS_{i+1}}{2} \cdot \frac{Q_i + Q_{i+1}}{2} \cdot \Delta t \right)$	26940	13395	75579
Method 3	$L_{annual} = f(Q, TDS) = k \cdot \int_{i=1}^{i=365} Q(t) \cdot TDS'(t) \cdot dt$	15888	8383	46435

Table 5.5: Summary of Total Dissolved Solid exports in the Altzola gauging station using different aggregation methods for the continuous registries, and the sampling campaign data from sampling location D6. Errors among aggregation methods are shown for each hydrologic year covered in the present study. Only 2014-2015 and 2015-2016 hydrologic years are shown in the Samplings column, due to those are the only ones fully covered by the monitoring program.

Total dissolved solids (TDS) loadings ($Mg \cdot y^{-1}$)					
Hydrologic year	*10-minutes*	*1-hour*	*1-day*	*1-month*	*Samplings*
2013-2014	65888	66541	69183	79862	-
2014-2015	69337	69824	78034	94258	153763
2015-2016	58059	58197	63476	74909	37551
2016-2017	33401	33586	36236	50636	-
Error (%) = $(L\text{-}L_{10min})/L_{10min}$					
Hydrologic year	*10-minutes*	*1-hour*	*1-day*	*1-month*	*Samplings*
2013-2014	-	1.0%	5.0%	21.2%	-
2014-2015	-	0.7%	12.5%	35.9%	121.8%
2015-2016	-	0.2%	9.3%	29.0%	-35.3%
2016-2017	-	0.6%	8.5%	51.6%	-

Table 5.5 presents the TDS annual loadings (L_{annual}) using Method 3 from Table 5.4, and different temporal aggregations, and we compare them with those loadings obtained using only the punctual sampling locations. Note that only two full hydrological years are covered by the sampling program and are included in the analysis. In general, the finer the frequency, the lower the error committed, but no relevant errors (>15%) are found for 1-hour or 1-day aggregation, which could justify the use of the aggregated time series and the consideration of the punctual sampling results as representative of the mean daily concentration. Monthly aggregation implies a higher degree of error (>21%) reaching, in some hydrologic years an overestimation of 50%. Considering only the average discharge and TDS concentration between pairs of sampling campaigns (Method 2 in table) yielded higher uncertainties, with an overestimation of the load in 2014-2015 hydrologic year, and an underestimation of the load in 2015-2016. This suggests that, for the Deba river catchment, the response time of the catchment is fast (≤1 day), creating a need of continuous registries to quantify the exports of dissolved loads with an acceptable error. In this system, the use of punctual data as the daily average comprises greater uncertainty in period with higher discharge, but this error is under 15%.

5.4.2.3 Seasonality

Considering 1 day as the minimum threshold for dissolved matter exportation in the present catchment, an analysis for the study period has shown which are the moments of relevance for the total dissolved matter exportation and the saline concentration. Figure 5.12 contains the time series for discharge and the difference from the relative contribution between water volume and dissolved loadings. In such figure, it is possible to see that, depending on the increasing or decreasing branch of the flood event, the relative input of water volume or dissolved solids differs. The monthly evolution shows a seasonality occurring between February and March every year, as well as November, December and April some years, where the relative contribution of water prevails over the exportation of dissolved loadings, which is commonly higher in November 2015, and January 2017. This is associated to a higher number of flood events in these

periods, where diluted meteoric water decreases saline concentration while increasing water volume exports. Focusing on the daily time series (Figure 5.12b), the greater contribution of dissolved loads occurs at the end of those flood events, specially when the flood event occurs after a period of maintained low discharge (focus on November 2015 or January 2017). Such insight suggests that, in the present system, the greatest peaks of discharge are loaded with low concentrations of salts, decreasing the salinity in the estuary in periods of flood events (Ladouche et al., 2001), but the response of the soil and groundwater is fast, implying a rapid recovery of dissolved concentration, thus increasing the loadings in the decreasing part of the flood events.

The analysis of the hysteresis is relevant to understand the origin of water and the transport phenomena occurring in a system. With the aim of evaluating the dilution effect in this catchment, Figure 5.13 presents the daily and monthly $EC_{station}$ and discharge for the Altzola gauging station for the study period. In general, a linear relationship may be found for all years, with a slight clockwise pattern found for 2015-2016 year. Such pattern suggests that the response of the catchment to flood events is fast and homogeneous, where dilution occurs in all the catchment at the same time, and the water from the furthest part of the catchment reaches the outlet (Altzola gauging station) later than the water close to the station. As this water is already diluted, the lowest concentration in salts (here proxy as EC) is reached at the same time (linear) or after the peak discharge (clockwise). This confirms that the greatest donor of saline concentrations is lithology, and that human impact in this catchment does not has a relevant influence on major ion presence.

5.4.3 Punctual and continuous integration

The physicochemical analysis of water has commonly been performed through monitoring programs based on punctual samplings (e.g. Şener et al., 2017; Unda-Calvo, 2019). However, limitations on instantaneous and intermittent water sampling use for load estimation has been highlighted before (Cassidy & Jordan, 2011), as tempo-

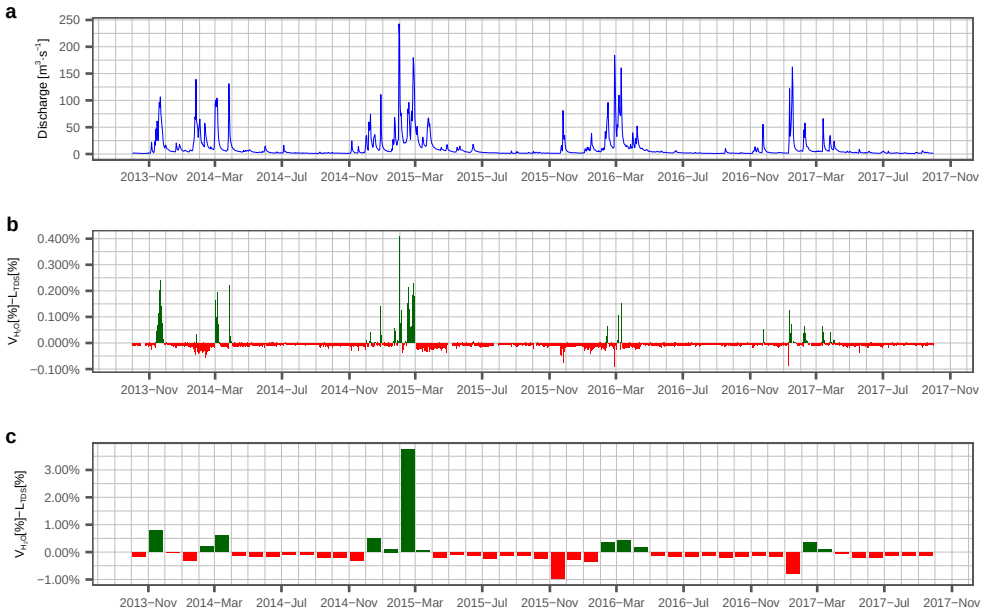

Figure 5.12: Temporal evolution of a) discharge, b) daily and c) monthly difference in the relative contribution of water volume (V_{H2O}) and dissolved load (L_{TDS}) to the total exports in the study period.

ral variability in daily or seasonal processes is not always fully captured by punctual sampling. Extrapolation of punctual measurements to continuous time series has long been performed, specially for the analysis of physical erosion and the quantification of sediment export yields (e.g. Peraza-Castro et al., 2015). However, such relationships are less common regarding dissolved solid concentrations, which allows the assessment of changes in salinity, conditioning which industrial or agricultural uses that water is plausible for (Ball et al., 2020), the characterization of the riverine endmember in estuarine dynamics (Franco et al., 2019), or the understanding of other physicochemical processes given in the water matrix (oxygen dissolution, flocculation, CO_2 exchange, carbonate precipitation, nitrate consumption, etc.), of interest for matter transport in biogeochemical cycles (Dessert et al., 2020; Ponnou-Delaffon et al., 2020). Here, the comparison among different frequencies used for dissolved saline loadings calculations (Table 5.5) has shown that the variability in this system, linked mainly to hydrological changes, needs at least a daily assessment for long-term loads. Then, even though

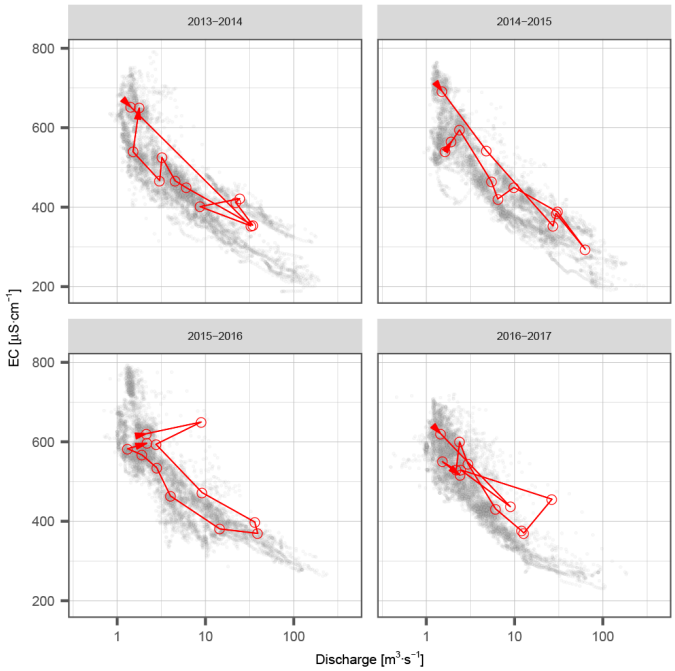

Figure 5.13: Monthly hysteresis in Altzola gauging station for each hydrologic year considered in the study. Grey points represent every daily record, while red lines and arrows indicate monthly averages.

the role of *in situ* sensors for ecological monitoring in rivers is being recognised more recently (Rode et al., 2016), the combination of both punctual and continuous methodologies has been needed for the present assessment, as continuous measurements of individual ions has not been possible.

As major ions, nutrients, and DOC have not been continuously monitored, the understanding of dissolved loading origin has been accomplished through the results of the punctual sampling. Here, the spatial distribution of the punctual samplings has allowed the understanding of which are the main geochemical processes, where are located, and which is their temporal evolution in the long-term. Even though it is an urban catchment which has long been considered as polluted due to industrial and urban effluents (Martínez-Santos et al., 2015; Unda-Calvo et al., 2020), anthropogenic activity exerts a greater impact on nutrients and metals than in major ion composition.

This is seen as D2 concentrations on all major ions is dominant in mostly all ions, suggesting that the saline spring input is the main responsible for the major composition of the main channel (Figures 5.2 and 5.8). Such influence over major ion composition is noted both in the punctual sampling campaigns as well as in the continuous integration, as the regressions for most of the ions are non-linear where, depending on the saline concentration, the ionic composition varies.

In summary, the two methodologies applied in the present analysis have given necessary and complementary information the present assessment: the spatial evaluation of main processes governing water chemistry, and its temporal evolution. The combination of both methodologies has recently allowed to evidence, for some elements, nycthemeral cycles due to biogeochemical processes (Ponnou-Delaffon et al., 2020). This combination has also been used to quantify dissolved loadings in urban environments (Viviano et al., 2014), and nutrient loadings in agricultural catchments (e.g. Ferrant et al., 2013), but in the present study it has allowed the estimation of saline loadings, as well as their characterisation among its major constituents. Alternatives to this combined method include the use of composite samples (e.g. Merchán et al., 2019) which give a single average daily value before computing daily loadings, or the use of frequent sampling for estimation of temporal variations (e.g. El Najjar et al., 2019). The fit of regressions with punctual data, and its application on continuous registries, allows not only for the approximation of the daily load, but also the establishment of a prediction interval (i.e. uncertainty assessment) in these loadings, as well as the quantification of the error committed when using temporal aggregations. The quantification of the uncertainty and the error committed in the temporal aggregation is a valuable information for stakeholders regarding the establishment of future monitoring programs and one way of optimizing the monitoring activities (Singh et al., 2004).

5.5 Conclusion

The major ion composition of the urban Deba river varies from headwaters to the outlet of the catchment while receiving effluents from tributaries, urban and industrial treated and untreated wastewaters. Punctual data has shown that the major ion composition is mainly affected by the natural geochemical processes given in the catchment, which are related to water-rock interaction and crystallization-evaporation, while nutrients remain related to treated and partially treated wastewater. The major source of Na^+ and Cl^- in the river is associated to evaporitic spring between D1 and D2, while Ca^{2+} and SO_4^{2-} are derived from gypsum deposits in M1, all these ions located in the southwest part of the catchment. The southeast, mid and down part of the catchment drains mainly sedimentary carbonate rocks, but the outlet chemical characteristics are mostly affected by the southwest part of the catchment. Only K^+ presents a different spatial pattern in the catchment, suggesting that anthropogenic input has a stronger effect on this major ion, and nutrients (NO_3^-, P-PO_4^{3-}), as peak concentrations are found downstream of the WWTP effluents. The inclusion of high-frequency registries has allowed for the extrapolation of punctual measures to continuous time series, which allow for the assessment of annual exports, as well as the evaluation of the error committed when considering low-resolution data on the assessment of such annual loadings. Continuous registries have allowed the identification of moments with higher influence of dissolved solids: the last part of the flood events, where the runoff is low and sub-surface and groundwater flow are dominant. In this system, errors under 15% are found when considering 1-day measurements, which carries high cost for punctual sampling. Such cost may be avoided by combining punctual sampling results with continuous registries, as has been done in the present analysis. Further research is needed on using these continuous data on the assessment of estuarine dynamics, as well as exploring the applicability of these continuous time series on the evaluation of modelling for the estimation of the continuum land-ocean matter exports, specially in the terms of Global Change.

5.6 Supplementary Information

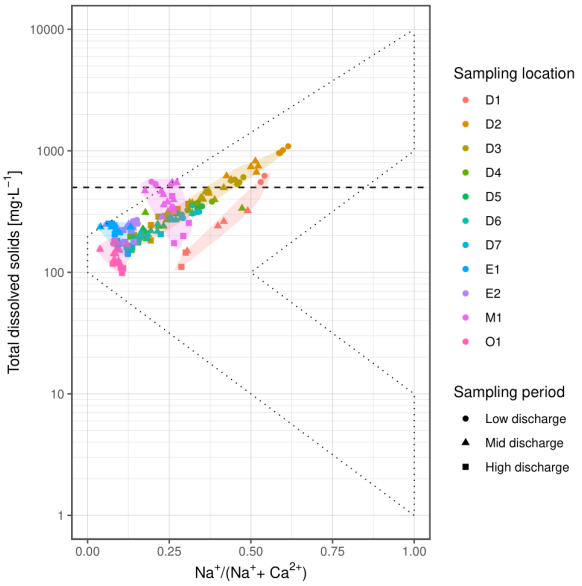

Figure S5.1: Gibbs diagram regarding water classification and geochemical mechanisms governing major ion chemistry at the catchment scale. Each colour represents a single sampling location (the reader is redirected to the web version of the article) while the shape represents the sampling period. Five sampling locations have been circled (D1, D2, M1, O1, and E1) in order to distinguish the different headwaters involved in this catchment, as well as D2 which presents a different kind of water. The dashed line represents the oligohaline limit (0.5 parts of solid per thousand, Montagna et al., 2013).

Bibliography

Ábalos, B., Alkorta, A., & Iribar, V. (2008). Geological and isotopic constraints on the structure of the Bilbao anticlinorium (Basque–Cantabrian basin, North Spain). *Journal of Structural Geology*, *30*(11), 1354–1367. https://doi.org/10.1016/j.jsg.2008.07.008

Álvarez-Vázquez, M. A., Prego, R., Ospina-Alvarez, N., Caetano, M., Bernárdez, P., Doval, M., Filgueiras, A. V., & Vale, C. (2016). Anthropogenic changes in the fluxes to estuaries: Wastewater discharges compared with river loads in small rias. *Estuarine, Coastal and Shelf Science*, *179*, 112–123. https://doi.org/10.1016/j.ecss.2015.08.022

Anderson, O. R. (2016). The Role of Heterotrophic Microbial Communities in Estuarine C Budgets and the Biogeochemical C Cycle with Implications for Global Warming: Research Opportunities and Challenges. *The Journal of eukaryotic microbiology*, *63*(3), 394–409. https://doi.org/10.1111/jeu.12279

Ball, L. B., Bedrosian, P. A., & Minsley, B. J. (2020). High-resolution mapping of the freshwater–brine interface using deterministic and Bayesian inversion of airborne electromagnetic data at Paradox Valley, USA. *Hydrogeology Journal*, *28*(3), 941–954. https://doi.org/10.1007/s10040-019-02102-z

Benettin, P., & van Breukelen, B. M. (2017). Decomposing the Bulk Electrical Conductivity of Streamflow To Recover Individual Solute Concentrations at High Frequency. *Environmental Science & Technology Letters*, *4*(12), 518–522. https://doi.org/10.1021/acs.estlett.7b00472

Cañedo-Argüelles, M., Kefford, B. J., Piscart, C., Prat, N., Schäfer, R. B., & Schulz, C.-J. (2013). Salinisation of rivers: an urgent ecological issue. *Environmental pollution*, *173*, 157–167. https://doi.org/10.1016/j.envpol.2012.10.011

Cassidy, R., & Jordan, P. (2011). Limitations of instantaneous water quality sampling in surface-water catchments: Comparison with near-continuous phosphorus time-series data. *Journal of Hydrology*, *405*(1-2), 182–193. https://doi.org/10.1016/j.jhydrol.2011.05.020

Chapra, S. C., Dove, A., & Warren, G. J. (2012). Long-term trends of Great Lakes major ion chemistry. *Journal of Great Lakes Research*, *38*(3), 550–560. https://doi.org/10.1016/j.jglr.2012.06.010

Dessert, C., Clergue, C., Rousteau, A., Crispi, O., & Benedetti, M. F. (2020). Atmospheric contribution to cations cycling in highly weathered catchment, Guadeloupe (Lesser Antilles). *Chemical Geology*, *531*, 119354. https://doi.org/10.1016/j.chemgeo.2019.119354

EEA. (2012). Corine Land Cover (CLC) 2012: Version 20. http://land.copernicus.eu/pan-european/corine-land-cover/clc-2012/view

El Najjar, P., Kassouf, A., Probst, A., Probst, J. L., Ouaini, N., Daou, C., & El Azzi, D. (2019). High-frequency monitoring of surface water quality at the outlet of the Ibrahim River (Lebanon): A multivariate assessment. *Ecological Indicators*, *104*, 13–23. https://doi.org/10.1016/j.ecolind.2019.04.061

Elzhov, T. V., Mullen, K. M., Spiess, A.-N., & Bolker, B. (2016). minpack.lm: R Interface to the Levenberg-Marquardt Nonlinear Least-Squares Algorithm Found in MINPACK, Plus Support for Bounds. https://CRAN.R-project.org/package=minpack.lm

EVE - Ente Vasco de la Energía. (1989). Mapa geológico del País Vasco a escala 1:25,000: 63-I, 63-III, 88-I, 88-III, planos.

FAO, IIASA, ISRIC, ISS-CAS, & JRC. (2012). Harmonized World Soil Database (version 1.2). http://www.fao.org/soils-portal/soil-survey/soil-maps-and-databases/harmonized-world-soil-database-v12/en/

Ferrant, S., Laplanche, C., Durbe, G., Probst, A., Dugast, P., Durand, P., Sánchez-Pérez, J. M., & Probst, J. L. (2013). Continuous measurement of nitrate concentration in a highly event-responsive agricultural catchment in south-west of France: is the gain of information useful? *Hydrological Processes*, *27*(12), 1751–1763. https://doi.org/10.1002/hyp.9324

Franco, T. P., Neves, L. M., & Araújo, F. G. (2019). Better with more or less salt? The association of fish assemblages in coastal lagoons with different salinity ranges. *Hydrobiologia*, *828*(1), 83–100. https://doi.org/10.1007/s10750-018-3804-8

García-García, J., Ruiz-Romera, E., Martínez-Santos, M., & Antigüedad Auzmendi, I. (2019). Temporal variability of metallic properties during flood events in the

Deba River urban catchment (Basque Country, Northern Spain) after the introduction of sewage treatment systems. *Environmental Earth Sciences*, *78*(1). https://doi.org/10.1007/s12665-018-8014-1

Ghanem, S. K. (2018). The relationship between population and the environment and its impact on sustainable development in Egypt using a multi-equation model. *Environment, Development and Sustainability*, *20*(1), 305–342. https://doi.org/10.1007/s10668-016-9882-8

Gibbs, R. J. (1970). Mechanisms controlling world water chemistry. *Science*, *170*(3962), 1088–1090. https://www.jstor.org/stable/1730827

Graham, L. P., Hagemann, S., Jaun, S., & Beniston, M. (2007). On interpreting hydrological change from regional climate models. *Climatic Change*, *81*(S1), 97–122. https://doi.org/10.1007/s10584-006-9217-0

Herbert, E. R., Boon, P., Burgin, A. J., Neubauer, S. C., Franklin, R. B., Ardón, M., Hopfensperger, K. N., Lamers, L. P. M., & Gell, P. (2015). A global perspective on wetland salinization: ecological consequences of a growing threat to freshwater wetlands. *Ecosphere*, *6*(10), art206. https://doi.org/10.1890/ES14-00534.1

Iribar, V., & Ábalos, B. (2011). The geochemical and isotopic record of evaporite recycling in spas and salterns of the Basque Cantabrian basin, Spain | Elsevier Enhanced Reader. *Applied Geochemistry*, *26*, 1315–1329. https://doi.org/10.1016/j.apgeochem.2011.05.005

Kaushal, S. S., Duan, S., Doody, T. R., Haq, S., Smith, R. M., Newcomer Johnson, T. A., Newcomb, K. D., Gorman, J., Bowman, N., Mayer, P. M., Wood, K. L., Belt, K. T., & Stack, W. P. (2017). Human-accelerated weathering increases salinization, major ions, and alkalinization in fresh water across land use. *Applied Geochemistry*, *83*, 121–135. https://doi.org/10.1016/j.apgeochem.2017.02.006

Khatri, N., & Tyagi, S. (2015). Influences of natural and anthropogenic factors on surface and groundwater quality in rural and urban areas. *Frontiers in Life Science*, *8*(1), 23–39. https://doi.org/10.1080/21553769.2014.933716

Ladouche, B., Probst, A., Viville, D., Idir, S., Baqué, D., Loubet, M., Probst, J. L., & Bariac, T. (2001). Hydrograph separation using isotopic, chemical and hydrological approaches (Strengbach catchment, France). *Journal of Hydrology*, *242*, 255–274. https://doi.org/10.1016/S0022-1694(00)00391-7

Launay, M. A., Dittmer, U., & Steinmetz, H. (2016). Organic micropollutants discharged by combined sewer overflows - Characterisation of pollutant sources and stormwater-related processes. *Water research*, *104*, 82–92. https://doi.org/10.1016/j.watres.2016.07.068

Martínez-Santos, M., Lanzén, A., Unda-Calvo, J., Martín, I., Garbisu, C., & Ruiz-Romera, E. (2018). Treated and untreated wastewater effluents alter river sediment bacterial communities involved in nitrogen and sulphur cycling. *The Science of the total environment*, *633*, 1051–1061. https://doi.org/10.1016/j.scitotenv.2018.03.229

Martínez-Santos, M., Probst, A., García-García, J., & Ruiz-Romera, E. (2015). Influence of anthropogenic inputs and a high-magnitude flood event on metal contamination pattern in surface bottom sediments from the Deba River urban catchment. *The Science of the total environment*, *514*, 10–25. https://doi.org/10.1016/j.scitotenv.2015.01.078

Mendizabal, M., Sepúlveda, J., & Torp, P. (2014). Climate change impacts on flood events and its consequences on human and in Deba River. *International Journal of Environmental Research*, *8*(1), 221–230.

Merchán, D., Luquin, E., Hernández-García, I., Campo-Bescós, M. A., Giménez, R., Casalí, J., & Del Valle de Lersundi, J. (2019). Dissolved solids and suspended sediment dynamics from five small agricultural watersheds in Navarre, Spain: A 10-year study. *CATENA*, *173*, 114–130. https://doi.org/10.1016/j.catena.2018.10.013

Merchán, D., Sanz, L., Alfaro, A., Pérez, I., Goñi, M., Solsona, F., Hernández-García, I., Pérez, C., & Casalí, J. (2020). Irrigation implementation promotes increases in salinity and nitrate concentration in the lower reaches of the Cidacos River (Navarre, Spain). *The Science of the total environment*, *706*, 135701. https://doi.org/10.1016/j.scitotenv.2019.135701

Montagna, P., Palmer, T. A., & Polack, J. (2013). *Hydrological Changes and Estuarine Dynamics* (1st ed., Vol. 8). Springer-Verlag New York. https://doi.org/10.1007/978-1-4614-5833-3

Nielsen, D. L., Brock, M. A., Rees, G. N., & Baldwin, D. S. (2003). Effects of increasing salinity on freshwater ecosystems in Australia. *Australian Journal of Botany*, *51*(6), 655. https://doi.org/10.1071/BT02115

Orive, E., Basaguren, A., G de Bikuña, B., & Cacho, M. (1989). A comparative study of water mineralization and nutrient status in the main water courses of biscay (Basque Country). *Water research*, *23*(6), 705–710. https://doi.org/10.1016/0043-1354(89)90203-0

Peraza-Castro, M., Ruiz-Romera, E., Montoya-Armenta, L. H., Sánchez-Pérez, J. M., & Sauvage, S. (2015). Evaluation of hydrology, suspended sediment and Nickel loads in a small watershed in Basque Country (Northern Spain) using eco-hydrological SWAT model. *Annales de Limnologie - International Journal of Limnology*, *51*(1), 59–70. https://doi.org/10.1051/limn/2015006

Ponnou-Delaffon, V., Probst, A., Payre-Suc, V., Granouillac, F., Ferrant, S., Perrin, A.-S., & Probst, J. L. (2020). Long and short-term trends of stream hydrochemistry and high frequency surveys as indicators of the influence of climate change, agricultural practices and internal processes (Aurade agricultural catchment, SW France). *Ecological Indicators*, *110*, 105894. https://doi.org/10.1016/j.ecolind.2019.105894

Qin, T., Yang, P., Groves, C., Chen, F., Xie, G., & Zhan, Z. (2018). Natural and anthropogenic factors affecting geochemistry of the Jialing and Yangtze Rivers in urban Chongqing, SW China. *Applied Geochemistry*, *98*, 448–458. https://doi.org/10.1016/j.apgeochem.2018.10.009

R Core Team. (2019). R: A language and environment for statistical computing. https://www.R-project.org/

Rode, M., Wade, A. J., Cohen, M. J., Hensley, R. T., Bowes, M. J., Kirchner, J. W., Arhonditsis, G. B., Jordan, P., Kronvang, B., Halliday, S. J., Skeffington, R. A., Rozemeijer, J. C., Aubert, A. H., Rinke, K., & Jomaa, S. (2016). Sensors in the Stream: The High-Frequency Wave of the Present. *Environmental science & technology*, *50*(19), 10297–10307. https://doi.org/10.1021/acs.est.6b02155

Şener, Ş., Şener, E., & Davraz, A. (2017). Evaluation of water quality using water quality index (WQI) method and GIS in Aksu River (SW-Turkey). *The Science of the*

total environment, *584-585*, 131–144. https://doi.org/10.1016/j.scitotenv.2017.01.102

Singh, K. P., Malik, A., Mohan, D., & Sinha, S. (2004). Multivariate statistical techniques for the evaluation of spatial and temporal variations in water quality of Gomti River (India)–a case study. *Water research*, *38*(18), 3980–3992. https://doi.org/10.1016/j.watres.2004.06.011

Spiess, A. N. (2018). Propagate: propagation of uncertainty. https://CRAN.R-project.org/package=propagate

Tueros, I., Rodríguez, J. G., Borja, A., Solaun, O., Valencia, V., & Millán, E. (2008). Dissolved metal background levels in marine waters, for the assessment of the physico-chemical status, within the European Water Framework Directive. *The Science of the total environment*, *407*(1), 40–52. https://doi.org/10.1016/j.scitotenv.2008.08.026

Unda-Calvo, J. (2019). *Sediment as tool for evaluating ecological status of a river basin: Physicochemical and biological quality indicators* (Doctoral dissertation). Universidad del País Vasco/Euskal Herriko Unibertsitatea. Bilbao. http://hdl.handle.net/10810/41887

Unda-Calvo, J., Martínez-Santos, M., & Ruiz-Romera, E. (2017). Chemical and physiological metal bioaccessibility assessment in surface bottom sediments from the Deba River urban catchment: Harmonization of PBET, TCLP and BCR sequential extraction methods. *Ecotoxicology and environmental safety*, *138*, 260–270. https://doi.org/10.1016/j.ecoenv.2016.12.029

Unda-Calvo, J., Martínez-Santos, M., Ruiz-Romera, E., & Lechuga-Crespo, J. L. (2019). Implications of denitrification in the ecological status of an urban river using enzymatic activities in sediments as an indicator. *Journal of environmental sciences (China)*, *75*, 255–268. https://doi.org/10.1016/j.jes.2018.03.037

Unda-Calvo, J., Ruiz-Romera, E., Martínez-Santos, M., Vidal, M., & Antigüedad Auzmendi, I. (2020). Multivariate statistical analyses for water and sediment quality index development: A study of susceptibility in an urban river. *The Science of the total environment*, *711*, 135026. https://doi.org/10.1016/j.scitotenv.2019.135026

URA. (2019). Red de seguimiento del estado biológico de los ríos de la Comunidad Autónoma del País Vasco. https://uragentzia.euskadi.eus

Vitousek, P. M., Aber, J. D., Howarth, R. W., Likens, G. E., Matson, P. A., Schindler, D. W., Schlesinger, W. H., & Tilman, D. G. (1997). Human alteration of the global nitrogen cycle: sources and consequences. *Ecological Applications*, *7*(3), 737–750. https://doi.org/10.1890/1051-0761(1997)007[0737:HAOTGN]2.0.CO;2

Vitousek, P. M., Naylor, R., Crews, T., David, M. B., Drinkwater, L. E., Holland, E., Johnes, P. J., Katzenberger, J., Martinelli, L. A., Matson, P. A., Nziguheba, G., Ojima, D., Palm, C. A., Robertson, G. P., Sanchez, P. A., Townsend, A. R., & Zhang, F. S. (2009). Agriculture. Nutrient imbalances in agricultural development. *Science*, *324*(5934), 1519–1520. https://doi.org/10.1126/science.1170261

Vörösmarty, C. J., McIntyre, P. B., Gessner, M. O., Dudgeon, D., Prusevich, A., Green, P. A., Glidden, S., Bunn, S. E., Sullivan, C. A., Liermann, C. R., & Davies, P. M. (2010). Global threats to human water security and river biodiversity. *Nature*, *467*(7315), 555–561. https://doi.org/10.1038/nature09440

Wickham, H. (2016). ggplot2: Elegant Graphics for Data Analysis. https://ggplot2.tidyverse.org

CHAPTER 6

Downscaling the model

Once the local study has been presented and the geochemical processes are elucidated in the system, this chapter contains the implementation of the Ionic fluxes derived from Chemical Weathering of Rocks (ICWR) model on the hydrological model Soil and Water Assessment Tool (SWAT), which has yielded two main products: a modified version of the input data plugin (QSWATLitho) which takes into account the lithological layer when delimiting the spatial units for calculation, and the SWATLitho module, a script to compute the ionic fluxes from rocks considering the spatially explicit distribution of the hydrology performed in SWAT. The results from the present chapter are prepared in a scientific article to be submitted to *Environmental Modelling & Software (EMS)*: Lechuga-Crespo, J. L., Sauvage, S., Ruiz-Romera, E., George, C., Sánchez-Pérez, J.M. (Under Review) **SWATLitho: a hydrogeochemical model to estimate daily geochemical loads at the catchment scale**. *Environmental Modelling and Software*

6.1 Abstract

The increase in water salinisation in catchments has led to increased concern in assessing major ion loadings in freshwater environments. In this study, we couple a globally fitted model on chemical weathering to the Soil and Water Assessment Tool (SWAT) for the estimation of daily geochemical loadings at the catchment scale, "SWATLitho". The enhancements include *i)* a modification on the discretisation of the catchment area by integrating a layer describing lithology (QSWATLitho), and *ii)* the development of an extra module to compute the ionic loads derived from the chemical weathering of rocks. The model is sensitive to input data resolution, yielding the best results when including local data. Larger spatial and temporal discrepancies are found in one tributary, associated with point sources impacting the main channel loadings; while these discrepancies are lower at headwater subbasins. Results suggest that, despite of these discrepancies, the average simulation of the daily ionic loadings is reasonable.

6.2 Introduction

Chemical quality assessment of river waters is crucial for understanding and assessing the potential impacts of threats to biodiversity, drinking water safety, and crop yields (Cañedo-Argüelles et al., 2018; Kaushal et al., 2017). One of these threats is the rise in major ion concentration, i.e. salinisation (Meybeck, 1989), which, despite having a relevant role in efficient ecosystem management (Cañedo-Argüelles et al., 2018), has received little attention in the past. Traditionally, two approaches tackling freshwater chemical assessments exist: the analysis of water samples framed within a monitoring program (e.g. Martínez-Santos et al., 2015), and the use of hydrogeochemical models to simulate the study area and possible scenarios (e.g. M'Nassri et al., 2019). Water sampling is a common practice in many places, yielding real valuable data, but spatially and temporally homogeneous information is obtained through modelling. The integration of these two approaches complements the assessment of chemical threats.

Models may be based on physical laws or data-regression equations for representing the system object of the study, being classified as mechanistic or empirical, respectively. Nowadays, there exists a number of mechanistic hydrogeochemical models, such as PHREEQC (Version 3 in Parkhurst and Appelo, 2013), MINTEQA2 (Allison et al., 1991), or WITCH (Goddéris et al., 2006), but their applicability is commonly limited to areas where extensive necessary data (mineral abundance, the chemical profile of soil water, initial boundary condition, etc.) is available as input. In other cases, simplifications or assumptions are needed in order to apply this kind of model, increasing the model's prediction uncertainty. A different solution is to develop simpler models to replace these complex configurations (Schoups et al., 2006).

As an alternative to mechanistic models, several empirical models focusing on single-processes have been built, such as the Global Erosion Model for CO_2 (GEM-CO2, Amiotte Suchet and Probst, 1995), the Chemical Weathering Rate model (CWR, Hartmann, Moosdorf, et al., 2014) and Ionic fluxes derived from Chemical Weathering of Rocks model (ICWR, Lechuga-Crespo, Sánchez-Pérez, et al., 2020), which have yielded a static output over worldwide scale assessments, i.e. the annual average result, regarding chemical weathering rates and associated products (atmospheric CO_2 consumption, P-release, ionic loadings to rivers, etc.). To date and to the best of the authors' knowledge, none of them have been tested on a local scale and under a dynamic approach, while management decisions are usually taken at a catchment scale and need the temporal evolution within a year.

In the present study, an empirically-based model has been coupled to a physically-based hydrological model to compute daily geochemical loadings from the chemical weathering of rocks. The SWAT model has long been used to quantify the loads and concentrations of matter and nutrients from land to the catchment's outlet (Arnold et al., 2012; Fu et al., 2019), as well as its evolution at different time scales. However, it is not possible to estimate the geochemical loadings with this model, as there is no subroutine or module implemented with this purpose. In this sense, the ICWR model (Lechuga-Crespo, Sánchez-Pérez, et al., 2020) has been applied to the global scale. It has yielded the first map on average annual ionic fluxes, derived from the chemical

weathering of rocks to rivers. Nevertheless, its ability to simulate the dynamics of chemical weathering derived ionic loads and its performance on local catchments have not been tested yet.

In this sense, the coupling of the SWAT and ICWR models poses an opportunity to evaluate spatially-explicit geochemical fluxes, since a basin's hydrology in SWAT is described using the Hydrological Response Unit's (HRU) semi-distributed approach. Consequently, ionic loadings from chemical weathering may be assessed and, if the atmospheric contribution is known, this tool may work with observed data to estimate how much anthropogenic saline effluent found in a catchment. It is important to note that a similar approach has been recently published by Bailey et al. (2019), where they present the coupling of a mechanistic model for major ion chemical partitioning within the SWAT hydrological code. Such mechanistic methodology presents the same constraints in application as the other mechanistic approaches: the availability of input data and the establishment of boundary conditions for simulation.

The objective of this study is to downscale the ICWR model spatially and temporally as well as explore the performance in a case study where a geochemistry monitoring program has been taken. This case is exploratory, and the model objectives are to simulate the daily geochemical loads of major ions and their spatial distribution. Given the modelling framework and the constraints of both models, the processes to be simulated are chemical weathering of rocks, mass transport, and routing from catchment subbasins to the outlet. The model's spatial definition is conditioned by the HRU delimitation of the modified model (which is explained in section 6.3.2), while the simulation's time-step is daily. A chemical equilibrium is assumed between rock and water at the temporal scale of simulation. Then, loadings are expected to be dependent on the discharge distribution among groundwater, lateral, and surface fluxes; the lithological groups in the underlying rock; and the soil types.

6.3 Methods

6.3.1 Overview of the SWAT and the ICWR models

The Ionic fluxes derived from Chemical Weathering of Rocks (ICWR, Lechuga-Crespo, Sánchez-Pérez, et al., 2020) model is empirically-based and its parameters have been fitted at a global scale for the estimation of spatially explicit fluxes of chemical weathering of rocks F, measured in $mol \cdot m^{-2} \cdot y^{-1}$ for each major ion Ca^{2+}, Mg^{2+}, Na^{+}, K^{+}, SO_4^{2-}, Cl^{-}, and alkalinity (commonly associated with HCO_3^{-}). The model configuration is based on the multivariable regression shown in equation 6.1. The input data needed for this model includes the specific discharge q_{ann} measured in mm, the lithological composition of the rocks L_i expressed as the percentage of the catchment area covered by a lithological group, the soil covering the bedrock layer for the estimation of the soil shielding effect factor $f_{s,x}$, which is different for each ion x, and the parameter of the equation $C_{x,i}$, representing the water concentration on every ion. Further explanation of the development, calibration, and limitations of the model can be seen in Lechuga-Crespo, Sánchez-Pérez, et al. (2020). The output of this model is an annual average specific flux of major ion loads originating from the chemical weathering of rocks to rivers, which, together with atmospheric deposition and anthropogenic inputs, is the main reservoir of saline exports of a basin.

$$F_x = q_{ann} \cdot f_{s_x} \cdot \sum L_i \cdot C_{x_i} \tag{6.1}$$

The SWAT is a physically-based and semi-distributed model developed to assess water, sediments, and nutrients in agronomic catchments at yearly, monthly, daily, and sub-daily time steps (Arnold et al., 1998). Water, matter, and nutrient balances are simulated in homogeneous spatial units, HRUs, a combination of unique slope, land use, and soil type areas, which are then aggregated to the subbasin scale and routed through tributaries and channels towards the outlet of the catchment. The HRUs, together with the weather data (at least precipitation and temperature time series), provide the input

data for the simulation. A more detailed description of the model is available in the SWAT2012 theoretical handbook (Neitsch et al., 2011).

6.3.2 Coupling ICWR to SWAT

The approach to spatially discretising the catchment area in the SWAT model has been modified to include a fourth layer in the definition of the HRUs: the lithological groups. This modification has been performed in the QGIS geographic information system plugin used to set up the model, QSWAT (Dile et al., 2016); the modified version is hereby called QSWATLitho. The SWAT code has not been modified to maintain the possibility of using external software, such as SWAT CUP (Abbaspour et al., 2007), for autocalibration. Instead, an extra module (SWATLitho.py) has been written to read the QSWATLitho and SWAT outputs and compute the geochemical fluxes and loads. The workflow of the model's configuration is shown in Figure 6.1.

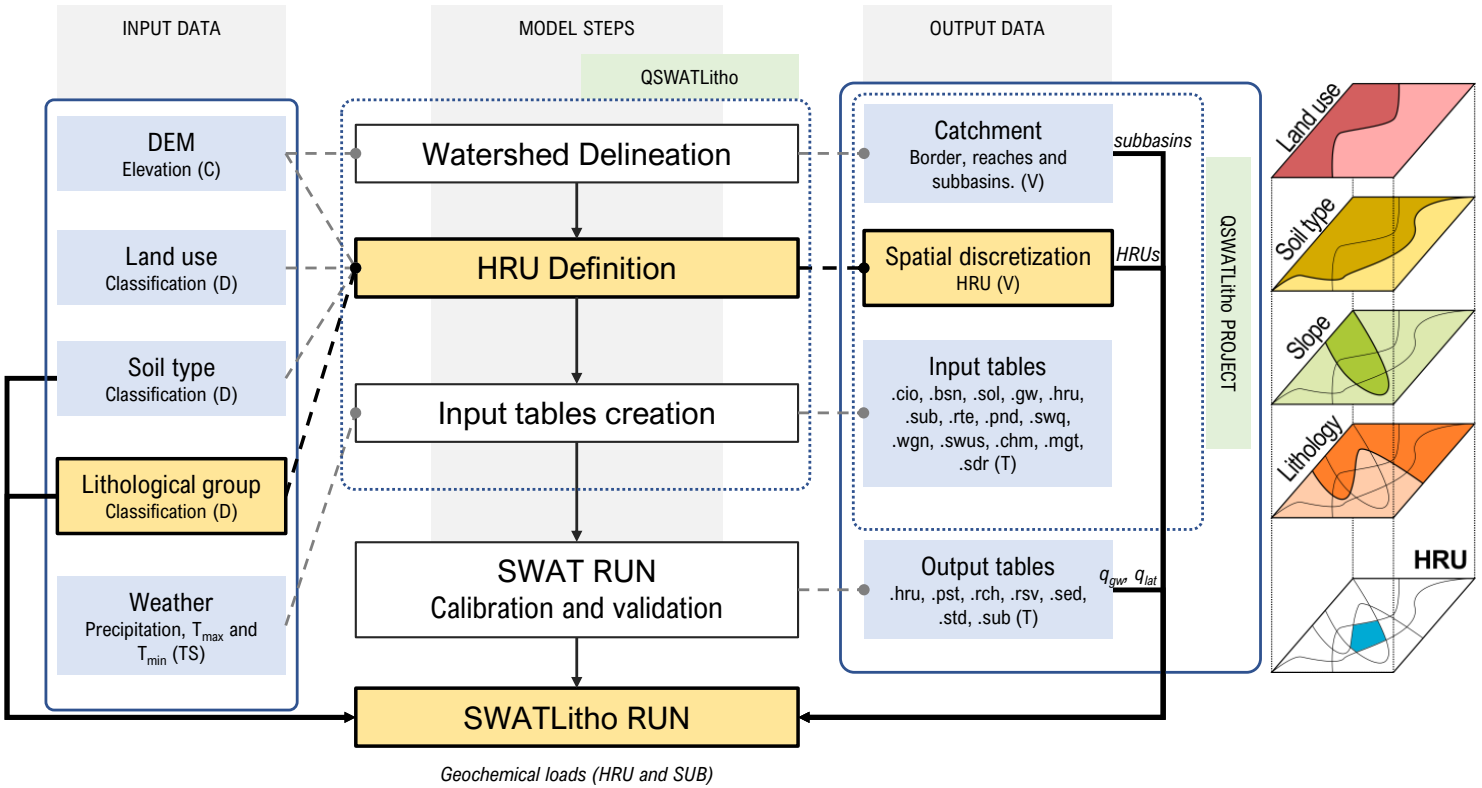

Figure 6.1: Workflow summary of the ICWR model implemented on the modified QSWAT. The modifications accomplished in the input data, model steps, and output data are highlighted in yellow (the reader is referred to the online version for the colour appreciation). Bold arrows indicate the input data for the SWATLitho module for the estimation of the geochemical loads. On the right side, there is a conceptual representation of the new delimitation of the HRUs.

6.3.2.1 QSWATLitho

Traditionally, a QSWAT model setup consists of three main phases: the delineation of the watershed and subbasins, the delimitation of the HRUs, and the write of the input tables for SWAT modelling. For the QSWATLitho implementation, the second step has been modified by changing the *hrus.py*, *DBUtils.py*, and *QSWATUtils.py* files in the original plugin, causing the inclusion of a new layer to the delimitation of the HRUs. Now, every HRU contains a unique combination of slope, land use, soil type, and lithological group, and the water balance is defined for each one of them. The first consequence of this change is an increased number of HRUs when setting up a project, causing a finer definition on the spatial distribution of the model outputs and an increase in the time used for the SWAT simulation. The QSWATLitho may be found and downloaded at https://swat.tamu.edu/software/swat-litho/.

6.3.2.2 ICWR module - SWATLitho

Once a QSWATLitho project has been set up, the calibration of the hydrology is needed, since this is the main dynamic input data for the ICWR model. Because the chemical weathering process occurs mainly in the vadose zone of the water cycle, the main water fluxes to be considered are groundwater (q_{gw}) and lateral flows (q_{lf}). The ICWR model has been adapted to include them ($q_{lf}+q_{gw}$) instead of the total average specific discharge (q_{ann}), which would also include runoff. Here, the runoff is considered as the main driver for the dilution of the total load rather than including it in the calculation of the daily geochemical loads. A new module has been created so that the user can use the SWAT results, in combination with the QSWATLitho tables, to obtain geochemical loadings' daily time series. The module consists of six main steps that are integrated into two loops. For each HRU, data like area, lithological group, and soil type is extracted from the *hrus_lithology.csv* file (a modified version of the *hrus* file in the *Project.mdb*) and, if necessary, used to set the soil shielding effect, $f_{s,x}$ (c.f. Lechuga-Crespo, Sánchez-Pérez, et al., 2020). Then, the *output.hru* file is read to obtain the specific discharge

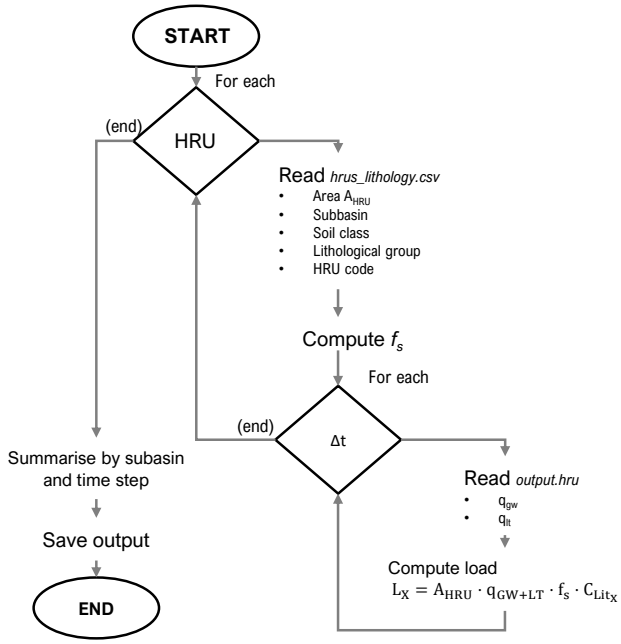

Figure 6.2: Workflow of the algorithm used to estimate the chemical weathering rates from the outputs of the QSWATLitho project calibrated for discharge. Ellipses indicate the start and end part of the algorithm, the diamonds represent the loops: one for each HRU in the project and other for each time step (Δt) simulated (year, month, day), arrows indicate the sequence of the actions.

in the lateral and groundwater fluxes to the river. With this information, together with the globally fitted parameters, the geochemical loads are calculated for each time step of the simulation and each HRU. This process generates a table with the loads of each HRU to the river stream for each time step. Then, all of the loadings are summarised at the subbasin scale in each time step and saved as output. The geochemical loadings are routed by adding the upstream loadings (if such exists) to the contribution of each subbasin draining area. A workflow summary is shown in Figure 6.2, and the modified version of the ICWR regression (Equation 6.1) is shown in Equation 6.2, where L_x represents the loading of ion x in each HRU (in $Mg \cdot d^{-1}$), A is the area of the catchment in m^2, q_{GW+LT} accounts for lateral and groundwater-specific discharge (mm), respectively, $f_{s,x}$ represents the soil shielding effect (dimensionless), and $C_{Lit,x}$ is the globally fitted parameter for each lithological unit and ion ($mol \cdot L^{-1}$). Note that units are adjusted depending on the ion that is being considered and that this modification considers each

HRU to be a monolithic unit to the river stream.

$$L_x = A_{HRU} \cdot q_{GW+LT} \cdot f_{s_x} \cdot C_{Lit_x} \tag{6.2}$$

The lithological groups used in the ICWR model development study are kept unaltered in the present development: evaporites (ev), metamorphics (mt), plutonic acid (pa), plutonic basic (pb), plutonic intermediate (pi), pyroclastics (py), sediment carbonates (sc), sediment mixed (sm), sediment siliciclastic (ss), sediment unconsolidated (su), volcanic acid (va), volcanic basic (vb), volcanic intermediate (vi), water bodies (wb), ice and glaciers (ig), and no data (nd), according to the description presented in Hartmann and Moosdorf (2012) and Dürr et al. (2005).

6.3.3 Case study: Deba river catchment

A case study is set up to explore the model's application. The validation comprises three steps: first, the annual comparison of the results to evaluate the model's sensitivity and select the input data among different combinations; second, the analysis of geochemical loadings in all subbasins derived from the QSWATLitho + SWATLitho combination (*spatial downscaling*); and last, the comparison of the daily representation in three gauging stations (*temporal downscaling*). The case study selected for this purpose is the Deba River catchment (Figure 6.3), on which numerous studies related to urban and industrial pollution on its sediments and waters have been conducted (García-García et al., 2019; Lechuga-Crespo, Ruiz-Romera, Probst, et al., 2020; Martínez-Santos et al., 2015; Unda-Calvo, 2019). There are eleven sampling locations along its main channel and tributaries, where a monitoring campaign was established between April 2014 and January 2017. Samples were taken in a monthly or bi-monthly time step. In addition, there are three gauging stations measuring, among other variables, discharge and electrical conductivity every 10 minutes.

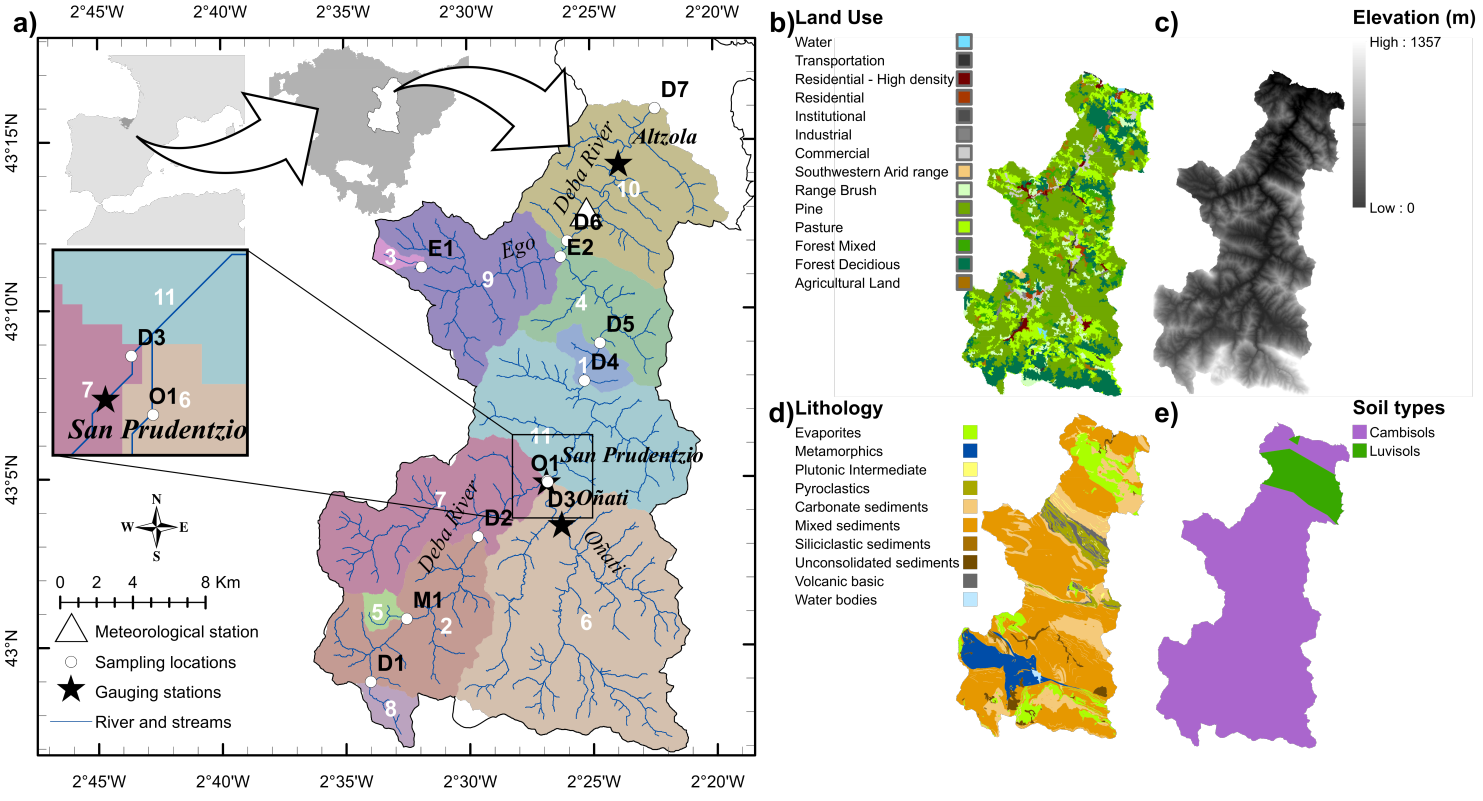

Figure 6.3: Deba River catchment description: a) localisation, main channel and tributaries, sampling locations, gauging stations and subbasins used in the present study; b) land use; c) digital elevation map; d) lithological units; e) soil types. Figures b), c), d), and e) are used for the setup of the model.

6.3.3.1 Study area

The Deba River Basin has a complete drainage area of 538 km^2 and 60 km of main stream, a maximum slope of 40%, and an elevation varying from 0 at sea level to 1320 m in Botreatiz (the highest mountain), which is located in the northern part of Spain, in the Gipuzkoa Province in the Basque Country (Figure 6.3). Regarding its hydrometeorology, there is a strong variation between humid and dry years, as well as a strong seasonal variability: about 30% of the total annual water volume is exported in December and January, and in dry summers, the specific discharge can reach 0.6 mm. The average annual precipitation is estimated to be 1613 mm, while the mean temperature is 12.7ºC, leading to the highest potential evapotranspiration (ETP) of the surrounding catchments at 871 mm. In terms of the occupation of this catchment, there is a strong presence of industries, with a population of 135000 inhabitants grouped into four important villages (Arrasate, Oñati, Bergara, Eibar, and Deba); 37% of the area is occupied by *Pinus spp*; 27% is covered by autochthonous forest, and 11% is given to farmlands and pastures. This catchment is commonly located over evaporitic rocks (gypsum and anhydrite deposits) included in detrital rocks, which, according to the classification proposed by Hartmann and Moosdorf (2012) and Dürr et al. (2005), correspond to a mix of siliciclastic, carbonate and mixed sediments, together with other lithological groups. A detailed description of the geology of the zone is addressed in Ábalos et al. (2008) and Iribar and Ábalos (2011). Historically, this catchment has suffered a strong urban and industrial pressure (Gipuzkoa Council, accessed on October 2019), and previous studies on the pollution in this catchment (García-García et al., 2019; Martínez-Santos et al., 2015; Unda-Calvo, 2019) have highlighted the inputs of urban and (residual) industrial effluents treated through wastewater treatment plants (WWTP) located in the middle of the catchment, where phosphorus is eliminated using Cl_3Fe (only from May 1st to October 15th), resulting in the presence of metals in the water and sediment matrixes. The analysis of this anthropogenic influence has been monitored from April 2014 to January 2017 in 11 sampling locations in the main channel and tributaries, highlighting the nutrients and metal input of urban and industrial effluents. Furthermore, a recent study on this catchment has focused on

the major ion chemistry of its waters, assessing the main geochemical processes input in relation to the anthropogenic input (Lechuga-Crespo, Ruiz-Romera, Probst, et al., 2020)while emphasising the influence of an evaporitic saline spring in the southwest part of the catchment, which exerts a great impact on the water chemistry downstream to the outlet of the catchment.

6.3.3.2 Set up of the QSWATLitho project

Table 6.1: Input data type, description and sources for the case study set up project used in the present study

Input data	Type	Description	Source
Digital Elevation Model (DEM)	Raster	A raster representing the elevations at 25x25m resolution	www.geoeuskadi.eus
Land Use	Raster	A raster representing the land uses of the catchment, at a resolution of 100x100m	https://land.copernicus.eu/pan-european/corine-land-cover
Soil Type	Raster	A raster representing the main types of catchment soil	http://webarchive.iiasa.ac.at/Research/LUC/External-World-soil-database/HTML/index.html?sb=1
Lithology	Raster	A derived raster representing the lithological classes of the catchment	www.geoeuskadi.eus
Precipitation and Temperature	Text File	Time series at one station with daily precipitation, maximum and minimum temperature	Spanish Agency of Meteorology (AEMET)

A local Digital Elevation Map (DEM, 25m resolution cell) was used to create the stream network, locate the outlet of the catchment, and delimit the drainage area. Sub-basins were merged to obtain their draining to the sampling locations of the monitoring campaigns. A European land use map from the CORINE Land Cover project (100m resolution), a soil map from the Harmonized World Database (a 30 arc-second resolu-

Table 6.2: Input data type, description and sources for the case study set up project used in the present study. Lithological clases: evaporites (ev), metamorphics (mt), plutonic intermediate (pi), pyroclastics (py), carbonate sediments (sc), mixed sediments (sm), siliciclastic sediments (ss), unconsolidated sediments (su), volcanic basic (vb), water bodies (wb)

	Main channel							**Tributaries**			
Lithology	D1	D2	D3	D4	D5	D6	D7	M1	O1	E1	E2
Area [km^2]	6.2	62.4	121.1	321.0	329.2	419.0	485.7	3.5	129.6	2.4	55.5
ev	4%	3%	7%	7%	7%	6%	7%		11%		
mt		25%	27%	11%	11%	9%	7%		3%		
pi							1%				
py				2%	2%	5%	5%				5%
sc	19%	11%	9%	16%	16%	15%	18%	3%	18%	2%	14%
sm	77%	54%	51%	60%	61%	61%	58%	97%	66%	98%	78%
ss		1%	1%	1%	1%						
su		6%	5%	3%	3%	2%		2%	3%		
vb				1%	1%	2%	3%				3%
wb									1%		

tion), and a local lithological map reclassified for the categories found in Hartmann and Moosdorf (2012) were combined with the DEM-derived slope map to create the HRUs (the description and source of the datasets may be seen in Table 6.1, Table 6.2, and Figure 6.3. While setting up the model, three slope ranges were established (0%-5%, 5%-10%, >10%) and no simplification was performed to reduce the number of HRUs. The weather input data was obtained from a hydrometeorological station located close to the outlet (Figure 6.3), consisting of precipitation as well as maximum and minimum temperature daily time series from January 1994 to December 2017. The observed data for discharge was covered from January 2004 to December 2017 for three gauging stations located close to the outlet and near the outlet of the two major subbasins of this catchment (see Figure 6.3). SWAT has been used to compute the hydrological representation of the case study, using the QSWATLitho HRU definition for the spatial discretization, but using the same water balance as the SWAT model.

Observed data for riverine chemical concentration ranged from April 2014 to January 2017. A monitoring program samples the river waters monthly or bimonthly using a pre-washed polypropylene bottle which was carried to the laboratory at 4ºC and filtered through 0.45µm filters. One replicate was acidified to 0.2% with HNO_3 (68%) for base cations (Ca^{2+}, Mg^{2+}, Na^{+}, and K^{+}) using ICP-OES (Perkin Elmer Optima

2000). The other non-acidified replicate was used to analyse anions (Cl^-, NO_3^-, SO_4^{2-}) through ion chromatography (DIONEX ICS 3000). Alkalinity was measured using a Total Organic Carbon Analyzer (TOC-L Shimadzu). The ionic charge balance (ICB) was within ±10% for all samples used in this study. For the modelling of the geochemical loads, groundwater and lateral flows from the SWAT hydrological representation have been used as a source of lithological chemical weathering derived loads, while runoff has been attributed to lower concentrations, inducing dilution in the stream's concentration.

Following the recommendations of ASABE (2017), three periods were defined in this project: a warmup period to reduce the effect of state variables' initial values (six years, January 1998-December 2003), a calibration period to optimise the parameters (ten years, January 2004-December 2013), and a validation period to test the model capabilities in an independent dataset (four years, January 2014-December 2017). The model's performance evaluation has been carried out for the calibration and validation periods independently, using graphical methods (time series between observed and simulated), and relative statistical measures (coefficient of determination, r^2, Nash-Sutcliffe Efficiency, NSE, PBIAS, and Kling-Gupta, KGE). The Moriasi et al. (2015) standard has been considered in this study to evaluate the model's performance. However, the authors have found no reference when comparing the daily loads of major ions, so the exploration of the results would yield the first reference for future similar analysis.

6.3.3.3 Discharge parameterization

The geochemical reactions responsible for ionic loads derived from rocks to the river are assumed to be in equilibrium at daily scales; however, other sources like human input or atmospheric deposition are expected to vary in these temporal ranges. Thus, the simulation (both calibration and validation) has been done at a daily time step. The first step is to calibrate the discharge (in surface runoff, lateral flow, and groundwater flow), which will be the main drivers in the temporal application of the ICWR model. The discharge has been calibrated using the parameters found in Table 6.3, through both manual calibration and autocalibration with the SUFI-2 algorithm in SWAT-CUP

Table 6.3: Parameters modified for calibration, type of change, description, and change adopted

File	Change type	Parameter name	Description	Best fit	Minimum	Maximum
gw	v	GW_DELAY	Groundwater delay time	240.5	200	500
	v	ALPHA_BF	Baseflow alpha factor	0.27	0.05	0.3
	v	GWQMN	Threshold depth of water in shallow aquifer required for return flow to occur	1081	600	1500
hru	v	LAT_TTIME	Lateral flow travel time	3.31	1	7
	r	HRU_SLP	Average HRU slope	↓ 15%	↓30%	0
	v	CANMX	Maximum canopy storage	17.8	5	20
mgt	r	CN2	Curve number for moisture condition II	↓ 26%	↓ 20%	0
sol	r	SOL_AWC	Available water capacity	↑11%	↓20%	↑30%
	r	SOL_K	Soil hydraulic conductivity	↑5%	0	↑30%

(Abbaspour et al., 2004). Three gauging stations have been used to evaluate the model performance on discharge calibration using four statistical criteria: the coefficient of determination (r^2), the Nash & Sutcliff Efficiency (NSE), the percent of bias (PBIAS), and the Kling-Gupta efficiency (KGE). All the statistics are applied to the simulated and observed values: r^2 focuses in the fit between the trends, varying from 0 (no fit) to 1 (perfect fit); PBIAS calculates the global over- (negative value) or underestimation (positive value); NSE evaluates the trends (similar to r^2, but varying from $-\infty$ to 1, perfect fit); and KGE is based on Pearson's coefficient "r", including bias and variability, ranging from $-\infty$ to 1 (perfect fit), where values >-0.41 could be considered as a reasonable performance (Knoben et al., 2019).

6.3.3.4 Downscaling the ICWR model

The original ICWR model (Lechuga-Crespo, Sánchez-Pérez, et al., 2020) was developed for an annual average specific flux output for which only the average specific discharge was needed for hydrology. To explore the possibilities of applying this model at lower spatial and temporal scales, three assessments have been performed: a model's sensi-

tivity analysis, a spatial evaluation, and a temporal assessment. The model's sensitivity to input data was evaluated by testing different global and local datasets combinations. Two lithological maps, one clipped from the Global Lithological Map (GLiM, Hartmann and Moosdorf (2012)), and a local one obtained from the Gipuzkoa Council (geoeuskadi.eus), together with two annual average specific discharges, one obtained from a global dataset (UNH/GRD, Fekete et al., 2002) and other from the Gipuzkoa Council Hydrological Department (www.gipuzkoa.eus), were combined to obtain four output datasets. The comparison with observed data indicated the best input data setup for building the QSWATLitho project. These results are shown and discussed in section *6.4.1 Model's sensitivity to input data*. Before applying the SWATLitho module, it is necessary to calibrate the water balance. The model setup and the calibration of hydrology are discussed in section *6.4.2 Case study*. Once the model was built and hydrology was calibrated, a simulation was conducted (period: January 2014 to December 2017). The application of the SWATLitho module allowed the evaluation of the model's spatial and temporal performance. No calibration of the ICWR parameters has been done, and globally fitted values were used (Lechuga-Crespo, Sánchez-Pérez, et al., 2020). The model's spatial downscaling evaluation was done by contrasting simulated geochemical loadings at the subbasin outlet with observed loadings at the corresponding sampling location (see Figure 6.3a). Results are presented in section *6.4.3 Spatial downscaling*. The temporal downscale was evaluated at three gauging stations, where daily loadings were derived from punctual data and continuous registries integration. The results are shown in section *6.4.4 Temporal downscaling*. Finally, model limitations, improvement suggestions, and alternatives are presented in section *6.4.5 SWATLitho limitations and alternatives*. Even though the wide applicability of the model makes this approach versatile, its setup may be constrained by input data availability.

A proposed alternative approach is the use of digital filters to deconvolute the hydrological signal between surface and groundwater fluxes. In this sense, we computed the hydrological deconvolution using the Eckhardt digital filter (Eckhardt, 2005; Xie et al., 2020). This test has been performed at the three gauging stations of the catchment.

Table 6.4: Average annual loadings obtained using the ICWR model in the Deba river catchment, with different input data. UNH represents the global hydrological dataset (UNH/GRDC, Fekete et al., 2002), the EUS indicates the local average data from the Gipuzkoa Council Hydrological Department (www.gipuzkoa.eus), the GLIM represents the global lithological map (GLIM, Hartmann and Moosdorf, 2012), and the GEUS implies the local lithological map (www.gipuzkoa.eus). All values expressed as mean annual load in [$Mg \cdot y^{-1}$].

Method	Ca^{2+}	Mg^{2+}	Na^{+}	K^{+}	Cl^{-}	HCO_3^{-}	SO_4^{2-}
Altzola							
UNH+GLIM	24783	5923	3707	755	6675	104465	20457
EUS+GLIM	22393	5352	3349	682	6031	94389	18484
UNH+GEUS	10492	2262	1991	348	3272	45897	14792
EUS+GEUS	9480	2044	1799	314	2957	41470	13365
Gauging station	20777	1755	6358	1050	10485	55244	14513
Oñati							
UNH+GLIM	6918	1651	1019	210	1842	28922	5640
EUS+GLIM	7233	1726	1066	220	1926	30238	5897
UNH+GEUS	2852	589	525	78	881	12565	4152
EUS+GEUS	2981	616	549	82	921	13137	4341
Gauging station	3894	294	314	84	381	10918	1861
San Prudentzio							
UNH+GLIM	5353	1287	861	164	1513	23340	4646
EUS+GLIM	4237	1019	681	130	1198	18473	3677
UNH+GEUS	2034	416	384	70	642	8871	2971
EUS+GEUS	1610	330	304	56	508	7021	2351
Gauging station	5691	497	2526	394	4266	14865	4381

6.4 Results and discussion

6.4.1 Model's sensitivity to input data

Average annual loadings obtained for the four input data combinations are shown in Table 6.4. The original ICWR model (Lechuga-Crespo, Sánchez-Pérez, et al., 2020) was calibrated and validated using global data (method UNH+GLIM in Table 6.4) and data on rivers worldwide from the GLORICH database. The highest values among all methods considered are found for the UNH+GLIM method, and the greatest differences are found not between the two hydrological datasets but between the lithological maps. This confirms that the lithological representation has a major impact on the loadings

computed by the model. Regarding the values obtained with the four datasets in comparison with the observed values (Gauging station in Table 6.4), the closest values are found for the EUS+GEUS method, the local data for hydrology and lithology. Nevertheless, the difference between the observed and the modelled values are different between ions and gauging stations. Both the Altzola and San Prudentzio gauging stations present the highest differences in Ca^{2+}, Na^{+}, K^{+} and Cl^{-}, while the differences between the observed and the simulated values are lower for other ions. Such differences are not found in the Oñati tributary, where the highest difference is found for Mg^{2+}, Cl^{-}, and SO_4^{2-}, but which is still lower than the Altzola and the San Prudentzio bias for the previously noted ions. The common pattern in the differences found for Altzola and San Prudentzio and the difference for the Oñati stream suggest that there is a common phenomenon not captured by the model's performance in the San Prudentzio draining basin, which affects downstream at the outlet of the catchment.

The monitoring program and previous studies in the area (Iribar & Ábalos, 2011; Martínez-Santos et al., 2015) have shown that the southwestern part of the catchment has the highest values of Ca^{2+}, Na^{+}, K^{+}, and Cl^{-}, which is related to the presence of gypsum intrusions and a spring, altering the local water's composition. In both lithological maps used, the intrusion of gypsum (evaporites) in the southwest part of the catchment seems to be underestimated. In addition, according to Iribar and Ábalos (2011), the southern part of the catchment contains a combination of different geological registries (Albian and Aptian-Albian) where there is a common presence of springs with saline waters. Within this catchment, the Leintz-Gatzaga spring contains one of the most concentrated effluents to the streams (230.6 $g{\cdot}L^{-1}$ according to Iribar and Ábalos, 2011). This suggests that the impact of the saline is not properly mapped in either the global or the local lithological maps, but that it exerts a strong influence on the chemical characteristics of this area downstream (Lechuga-Crespo, Ruiz-Romera, Probst, et al., 2020). For this reason, the observed data on Na^{+}, K^{+}, and Cl^{-} are higher than those modelled, especially in the San Prudentzio subbasin. The inclusion of a local lithological map, with a finer spatial resolution of lithology, has decreased the loads to around half of those obtained with the previous map. These new values are closer to reality when considering Mg^{2+}, HCO_3^{-}, and SO_4^{2-}, which are the elements less affected

by the spring inputs. The inclusion of a spatially distributed lithology has improved the results of the model, leading to the conclusion that increasing the spatial resolution of the lithology input data has a major effect on the output of the model.

From the model's sensitivity analysis, we conclude that when applying the ICWR model to local studies, local lithological data should be applied. Moreover, consideration of saline springs should be taken into account when evaluating the model's performance.

6.4.2 Case study

The combination of slope, land use, soil types, and lithological classes in this catchment leads to a spatial discretisation consisting of 11 subbasins and 985 HRUs. When building the same project considering land use, soil type, and slope layers in the HRU definition step, the number of spatial units reaches 286 HRUs. A more detailed project regarding spatial distribution increases the computation time, but the water balance calibration is more comprehensive, which is a key input for the geochemical loads' computation, and the model's temporal downscaling.

Regarding the calibration of hydrology at the daily time step (Figure 6.4), most of the parameterisation has been focused on calibrating groundwater and lateral flow, which account for almost 96% of the annual discharge at the catchment's outlet. The parameterisation of the model has yielded the results summarised in Table 6.5, and Moriasi et al. (2015) qualifies the simulation as "Satisfactory" for calibration and validation. According to these results, the model has been considered enough to represent the hydrology of the catchment studied. NSE is used based on its performance, which is better when the variable's range of variation is large. However, in low flows, the denominator tends towards 0, leading to higher values when the errors are small (Oeurng et al., 2011). The higher values for r^2 in comparison to the NSE suggest a good representation of the dynamic, but a worse depiction of the exact discharge value, indicating a difference between observed and simulated values which is stronger in lower flow periods. This can also be seen in the PBIAS, where the calibration for San Prudentzio

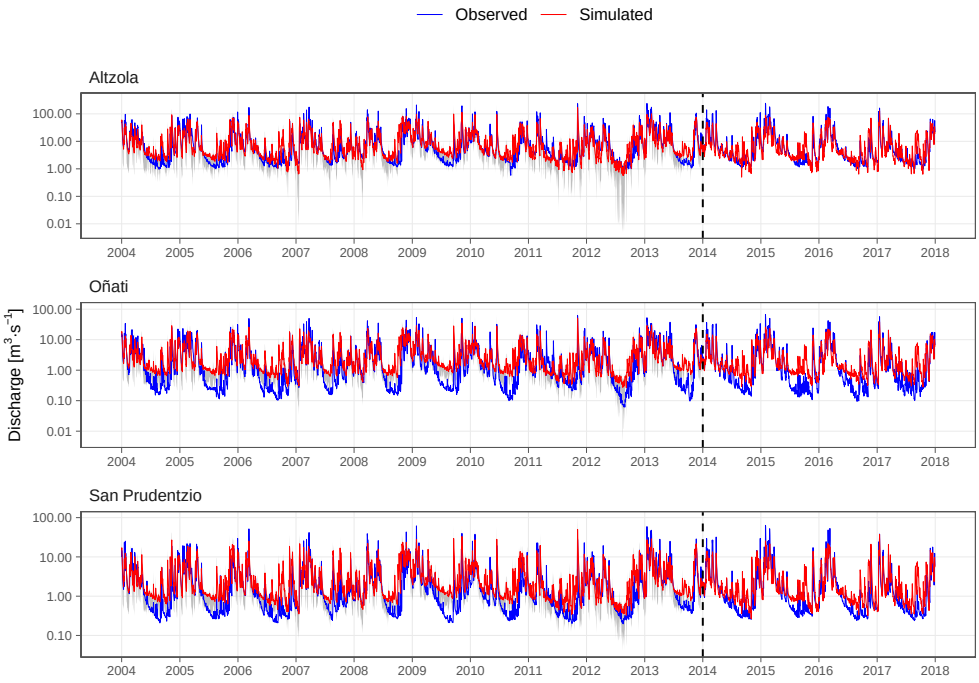

Figure 6.4: Time series of daily simulation and observation discharge in three sampling locations in the catchment. Dashed line separates calibration from validation period. As there is a relevant difference in discharge ranges between dry and wet periods, the vertical axis is plotted in logarithmic scale.

has yielded a value classified as "Non-Satisfactory" according to Moriasi et al. (2015). A negative value of the PBIAS proposes an underestimation of the model, which is attributed to peaks in the drier period of the simulation. Fluctuations are related to the way groundwater is calculated in SWAT, not using a spatially diffused flow, but pulses in each HRU (Bailey et al., 2019). Improvements in the model performance for hydrology may be expected by incorporating a more detailed soil map, as the present resolution seems too coarse for the needs of this modelling.

The most sensible parameters are the curve number (CN2.mgt), which was decreased to adjust the peak discharge in combination with the maximum canopy storage (CANMX.hru), the baseflow recession constant (ALPHA_BF.gw) and the lateral flow travel time (LAT_TTIME.hru).The lateral flow has a relevant role in the hydrology of

Table 6.5: Summary statistics of hydrological calibration

	Calibration					
	January 2004 - December 2013					
	r^2	NSE	PBIAS (%)	KGE	p-factor	r-factor
Altzola	0.72	0.71	-0.7	0.71	0.65	0.42
Oñati	0.64	0.64	-13.5	0.71	0.47	0.48
San Prudentzio	0.65	0.62	-28.4	0.64	0.57	0.50
	Validation					
	January 2014 - December 2017					
	r^2	NSE	PBIAS (%)	KGE		
Altzola	0.76	0.68	13.7	0.56		
Oñati	0.74	0.71	0.90	0.64		
San Prudentzio	0.70	0.66	-4.8	0.60		

this catchment. Baseflow was adjusted using the delay of water passing through the last soil layer (GWDELAY.gw) and the water threshold in the shallow aquifer needed for groundwater flow to occur (GWQMIN.gw). All specific changes are shown in Table 6.3.

6.4.3 Spatial downscaling

The geochemical loadings derived from rock's chemical weathering are carried out by the rivers to oceans and lakes. Disregarding instream transformation (outgassing, biological uptake, secondary precipitation, or ionic exchange processes) loadings are added along the river network. Figure 6.5 presents the comparison of these loadings at the outlet of each subbasin, which has a corresponding sampling location. Only fluxes from sampling campaigns are considered (c.f. Lechuga-Crespo, Ruiz-Romera, Probst, et al., 2020). As expected, there is a corresponding generally increasing trend between the two signals. Downstream sampling locations have higher exports than upstream subbasins. However, the trend is different for each ion.

Mg^{2+}, SO_4^{2-}, and HCO_3^- present the best spatial collinearity among all ions, and the mean loadings in each sampling location are scattered around the perfect fit line. The largest deviations are Na^+ and Cl^-, where observed values are higher than the

simulation ones. Nevertheless, since loadings are added through the routing network, upstream errors are carried downstream. Specific attention to the D2 and D3 sampling locations (subbasins 2 and 7, respectively) indicate underestimation for all ions, especially Na^+ and Cl^-. This suggests that this area contains an ionic point source loaded with these ions, which is not captured by the model. This results in the worst representation among all of the catchments.

Among the headwater sampling locations (D1, E1, M1, and O1) and subbasins (8, 3, 5, and 6, respectively), the Oñati stream presents the largest loadings, in which ions are commonly located close to the perfect fit line except for Mg^{2+} and SO_4^{2-}. This overestimation compensates for the underestimation found in D3 for these ions, improving the overall representation of the model. Further analysis of this stream's temporal evolution is found in section 6.4.4.

The application of the model to this case study supports that headwater locations present lower discrepancies than downstream subbasins. This spatial analysis indicates that point sources exert a great impact on the model's performance, since downstream locations are conditioned by incoming loadings.

6.4.4 Temporal downscaling

Figure 6.6 presents a graphical assessment of the SWATLitho performance, comparing the simulated and observed time series at three gauging stations (Altzola, San Prudentzio, and Oñati, Figure 6.3a). A visual evaluation shows that the global fitted parameters applied to the calibrated QSWATLitho project yield geochemical loads showing a varying degree of similarity between the simulated and the observed values, suggesting the model performs differently depending on the ion and drainage basin being considered. Besides, Table 6.6 contains the statistical results for each pair of time series and the average values for each gauging station. Considering Altzola results as representative of the catchment-scale performance of the model, the average statistics show a reasonable performance from the model (r^2 = 0.74 ± 0.02, PBIAS=-17.96 ±

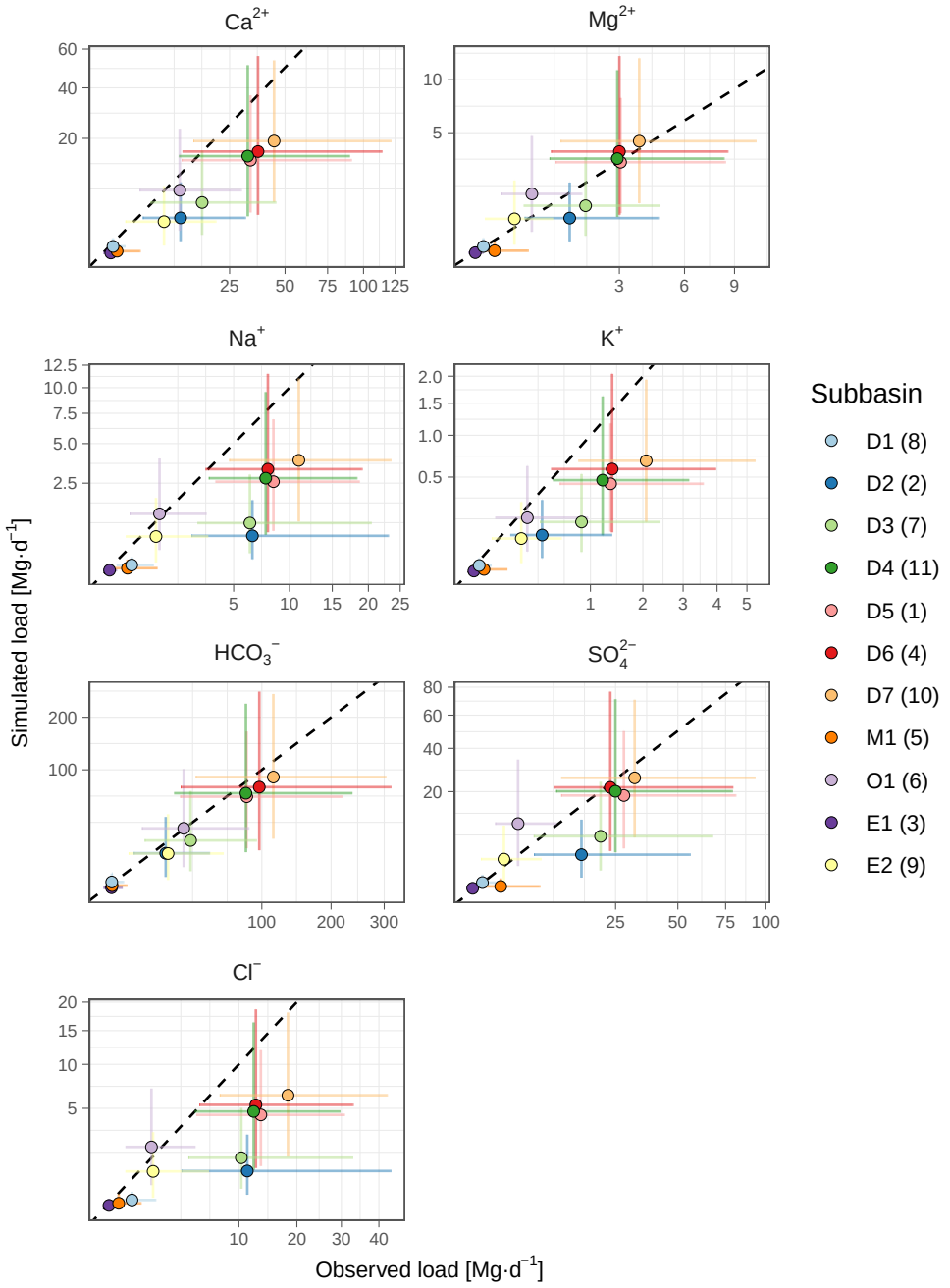

Figure 6.5: Simulated versus observed loadings for all sampling locations (subbasin number presented between brackets). The point represents the mean value for the daily loadings, considering only dates with *in situ* monitoring campaigns. Horizontal and vertical lines present minimum and maximum values for observed and simulated loadings.

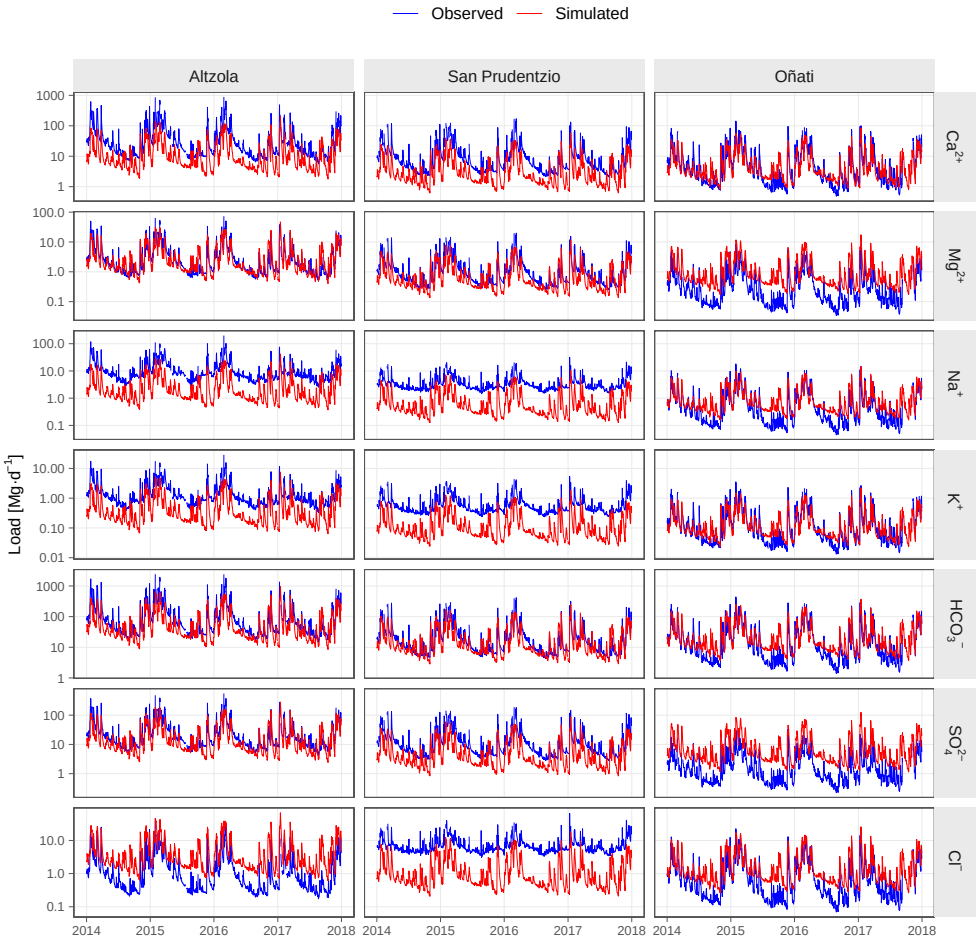

Figure 6.6: Time series (validation period: January 2014-December 2017) of daily simulated and observed loadings at three gauging stations, Altzola, San Prudentzio, and Oñati, of Ca^{2+}, Mg^{2+}, Na^{+}, K^{+}, SO_4^{2-}, Cl^{-}, and HCO_3^{-}. The gauging stations are located in the outlet of the catchment and in two tributaries. Note that the vertical axis is in logarithmic scale to better differentiate the results in dry and wet periods.

Table 6.6: Summary statistics of hydrological calibration

Station	**Ion**	**r^2**	**PBIAS [%]**	**KGE**
Altzola	Ca^{2+}	0.76	-67.70	-0.02
	Mg^{2+}	0.76	-9.80	0.68
	Na^{+}	0.70	-73.90	-0.04
	K^{+}	0.72	-66.60	0.05
	HCO_3^{-}	0.75	-44.30	0.26
	SO_4^{2-}	0.76	-31.10	0.46
	Cl^{-}	0.73	167.70	-0.84
	mean	0.74	-17.96	0.08
	sd	0.02	85.02	0.48
San Prudentzio	Ca^{2+}	0.75	-64.40	0.04
	Mg^{2+}	0.75	-38.40	0.38
	Na^{+}	0.70	-76.90	0.00
	K^{+}	0.73	-76.20	-0.02
	HCO_3^{-}	0.73	-28.30	0.47
	SO_4^{2-}	0.76	-58.10	0.15
	Cl^{-}	0.65	-80.50	-0.04
	mean	0.73	-60.40	0.14
	sd	0.04	20.26	0.21
Oñati	Ca^{2+}	0.74	-23.00	0.55
	Mg^{2+}	0.75	169.20	-1.10
	Na^{+}	0.75	25.40	0.70
	K^{+}	0.75	-13.80	0.64
	HCO_3^{-}	0.75	13.10	0.79
	SO_4^{2-}	0.67	284.30	-2.90
	Cl^{-}	0.75	64.40	0.29
	mean	0.74	74.23	-0.15
	sd	0.03	112.97	1.38

85.02, KGE=0.08 ± 0.48), according to the criterion presented by Knoben et al. (2019) regarding KGE.

Focusing on the subbasin-scale, each mean statistic yields a different pattern for the model's performance. The mean coefficient of determination (r^2) is comparable among gauging stations, suggesting that dynamic representation is homogeneous at the subbasin level. The mean percentage of deviation (PBIAS) indicates that the Altzola gauging station is the closest to reality, while Oñati presents the largest discrepancies; the Kling-Gupta Efficiency factor (KGE), as a summary statistic, is best for San Prudentzio and worst for Oñati. However, the analysis of the standard deviation highlights the presence of two outliers in Oñati: Mg^{2+} and $SO_4{}^{2-}$. Excluding these outliers from the analysis yields the best values for Oñati in all statistics (KGE = 0.59 ± 0.19, PBIAS[%] = 13.22 ± 34.68, and r^2 = 0.75 ± 0.01), and worst for San Prudentzio. The Altzola gauging station, which receives waters from Oñati, San Prudentzio and other tributaries in the main channel, presents intermediate statistics suggesting that the differences present in the upper part of the catchment are routed downstream to the outlet. This can also be seen in the times series in Figure 6.5, where the deviations between the observed and the simulated values are similar in Altzola and San Prudentzio, while they are independent at the Oñati stream. Using the KGE as an integrative measure of the model's performance, values >-0.41 are considered reasonable (Knoben et al., 2019). This criterion yields a valid representation of the average ionic loadings in all gauging stations.

Previous studies in the area using *in situ* samplings have highlighted the sulphate water composition in the Oñati stream of the catchment (Lechuga-Crespo, Ruiz-Romera, Probst, et al., 2020), which could be related to the evaporitic presence in the upper part of the catchment (Iribar & Ábalos, 2011). However, despite the evaporitic presence in the input data (largest percentage the in draining catchment, Table 6.2), a karstic presence has also been reported in the area (Iribar & Ábalos, 2011), which could be a source of diluted water to the system. A complex interaction of these saline and diluted water sources may be responsible for the discrepancies found between the simulated and the observed values for Mg^{2+} and $SO_4{}^{2-}$.

In addition, the presence of springs, i.e. wells with saline water, is common in the San Prudentzio stream (Iribar & Ábalos, 2011), particularly the Leintz-Gatzaga spring, which provides one of the most concentrated effluents, with 230.6 $g{\cdot}L^{-1}$ of total dissolved solids and over 85 $g{\cdot}L^{-1}$ of Cl^- (Iribar & Ábalos, 2011). The vertical pathway of this spring is over 384 m (Iribar & Ábalos, 2011), which explains the different dynamics of Cl^-, Na^+, and K^+ present in this area, as the input from the spring is steadier than the rapid response of the groundwater and the lateral flow of the remaining catchment, changing the relative contribution of these ions to the total cation concentration with time (Lechuga-Crespo, Ruiz-Romera, Probst, et al., 2020).

There are few models similar to this one, but a recent publication (Bailey et al., 2019) introduced a saline module based on physical equations at chemical equilibrium into the SWAT code to analyse of the fate and transport of the ions in catchments. In addition, the researchers in that study reported problems of underestimation of the model's value regarding unmapped mineral presence in the input data, which also occurred in the present study. Both studies have shown the importance of measured concentrations in rivers as a proxy for the geochemical minerals affecting the riverine loads. In the present case, the monitoring campaigns, together with the gauging station's data, have recorded the effect of the spring input, which the model did not capture.

6.4.5 SWATLitho limitations and alternatives

A recent study has presented a physically-based module for assessing the fate and transport of saline ions in catchments integrated on the SWAT model (Bailey et al., 2019). That model has been developed to evaluate the best irrigation management practices and their impacts on the salinisation of freshwater environments within a catchment. The setup requirements are a discharge calibrated SWAT project, the initial concentrations of the ions in the soil and the aquifer, and the percentage of five solid species present in each HRU to compute the chemical equilibrium (Bailey et al., 2019). In contrast, the model introduced in the present study focuses solely on the process of

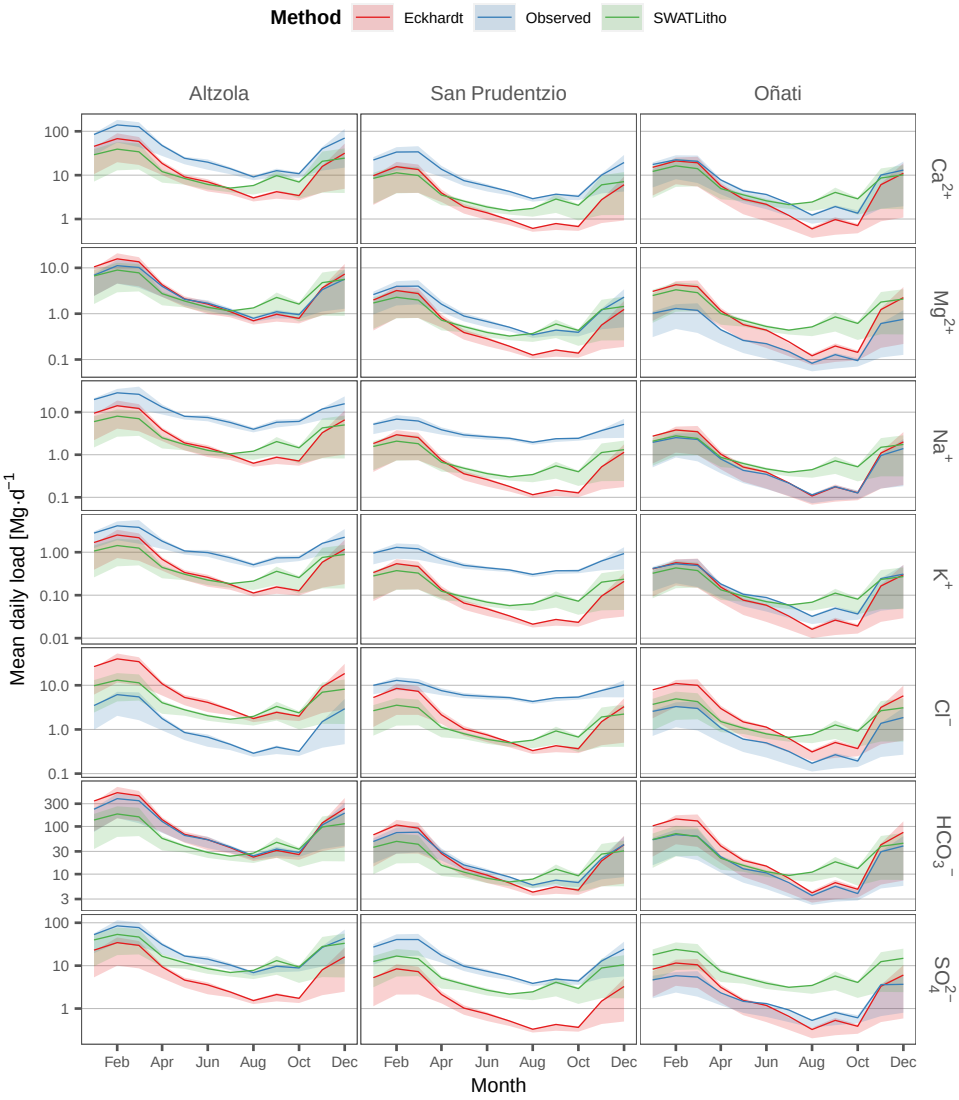

Figure 6.7: Average monthly inter-annual loading comparison among the observed, SWATLitho, and Eckhardt digital filter results. Lines indicate the mean value, while the shade represents the 1st and 3rd quartiles for the January 2014 to December 2017 time series. The vertical axis is shown in logarithmic scale.

chemical weathering. It computes the geochemical loadings derived from lithology to the river streams based on empirical equations; uses a lithological and soil description, as well as hydrology, as its input data. The SWATLitho model is not based on a spatial mineralogical representation but on lithological groups of minerals that are available worldwide (c.f. Hartmann & Moosdorf, 2012) or commonly available in finer resolution for local studies. However, it lacks point source data (for irrigation, saline springs, or other anthropogenic inputs). In fact, even though the SWAT model has been widely applied (Fu et al., 2019), there may be occasions when it is not possible to set up the model even though there is interest exists in assessing the chemical weathering derived geochemical loadings in a dynamic way.

Applying the SWATLitho model to evaluate daily loadings at a local scale has yielded reasonable results for representing the dynamic ($r^2 > 0.73$). However, applying the model to local-scale studies to quantify daily draining loads at the catchment's outlet is conditioned by a detailed representation of the area's lithology and the lack of other relevant salt sources. When considering the Altzola gauging station as a reference for the catchment-scale model application, the mean percentage of deviation of the model is ∼-17.96% (Table 6.6). The results shown here do not include any variation in the mineral dissolution constant ($c_{x,i}$ in Equation 6.1) which is likely to occur with changes in groundwater or lateral flow water temperature. A more mechanistic model is needed to account for this evolution, as well as the chemical equilibrium between phases (as done in Bailey et al., 2019). However, the more mechanistic a model is, the harder it is to find available input data.

In the present study, a digital filter to deconvolute the hydrograph –distinguish surface runoff from baseflow and lateral flow with the total discharge time series– has been tested as a potential alternative when it is not possible to set up QSWATLitho projects, either because of a lack of input data or computational resources constraints. Interannual daily loads (mean, first, and third quartiles) are shown monthly in Figure 6.7. Spatial and temporal limitations of the SWATLitho model have been discussed in previous sections (6.4.3 and 6.4.4), but all three results in the Oñati drainage catchment, observed, SWATLitho and Eckhardt, present a similar temporal pattern. However, the

SWATLitho presents a peak for all ions in September. This is not present in the other two methods, supporting the idea that the SWAT's groundwater flux computation is affected by pulses calculated in each HRU instead of a diffuse load, which is better represented by graphical separation in an Eckhardt model. Nonetheless, the variances of the two methods have yielded discrete values, though a Welch's test for the differences between the loadings SWATLitho and the Eckhardt module has yield a $p>0.05$, which does not demonstrate enough significance to indicate that the loadings are dissimilar. The visual inspection and the test demonstrate that the Eckhardt digital filter may be applied when a QSWATLitho project cannot be set up.

One of the limitations of the ICWR model is the presence of spring waters or point sources that alter the streams' composition. Those impacts are not presented in the model at this stage and should be considered when assessing the chemical loads from catchments with springs within their hydrogeological basin or groundwater inputs that are sourced outside the hydromorphological basin. When it comes to the model's performance from various input data, the greatest distinctions among results in the loadings have been found when changing the lithological map, yielding results closer to the observed values.

Future improvements of the SWATLitho model should allow the inclusion of saline point sources (which could represent natural saline springs or anthropogenic inputs), and permit the calibration of the $c_{x,i}$ parameters for each catchment (which could adjust the contribution of each lithology for each location) as done in the common SWAT calibration procedure.

6.5 Conclusion

An empirical model used to estimate the annual average geochemical loads to rivers through chemical weathering has been downscaled from global to local scale, and shifted from an annual average estimation to a daily dynamic output, based on the cou-

pling with SWAT, an extended hydrological model. The coupling method is described along with the case study, using different input datasets to check the influence of hydrology and lithology resolution in the outputs of the model. The use of globally fitted parameters for the model has yielded average loadings with a model underestimation of 17.96% with regards to the observed data, though the model's performance is "reasonable" on the representation of spatially explicit daily geochemical loadings to stream the a catchment level.

The limitations of the model have been addressed, such as the poor performance of the model when springs are present in the study area, or when the lithological input dataset does not contain information hydrogeochemically relevant units, such as gypsum intrusions, which are too small to be mapped but relevant enough to affect the water chemistry and loadings. An alternative has also been presented for those cases in which a QSWATLitho project cannot be set up: the application of a digital filter to measure data in a gauging station, together with the drainage basin description (lithology and soil classes). The results do not present significant differences from those of the SWATLitho, which suggests that both methods may be applied when it is not possible to set the first one up or that spatially explicit results are not in the scope of the modelling.

The present work introduces a hydrogeochemical tool which is useful for estimating dynamic chemical weathering loadings out of a catchment at a local scale and also for the estimating of ionic fluxes that derive from the chemical weathering of rocks in a spatiotemporal context.

6.6 Software availability

- The Soil and Water Assessment Tool (SWAT) is freely available in https://swat.tamu.edu/software/
- The QGIS plugin for SWAT (QSWAT) is freely available in https://swat.tamu.edu/software/

qswat/

- The modified QGIS plugin presented in this study (QSWATLitho) as well as the SWATLitho module written in Python is freely available in https://swat.tamu.edu/software/swat-litho/

6.7 Supplementary Information

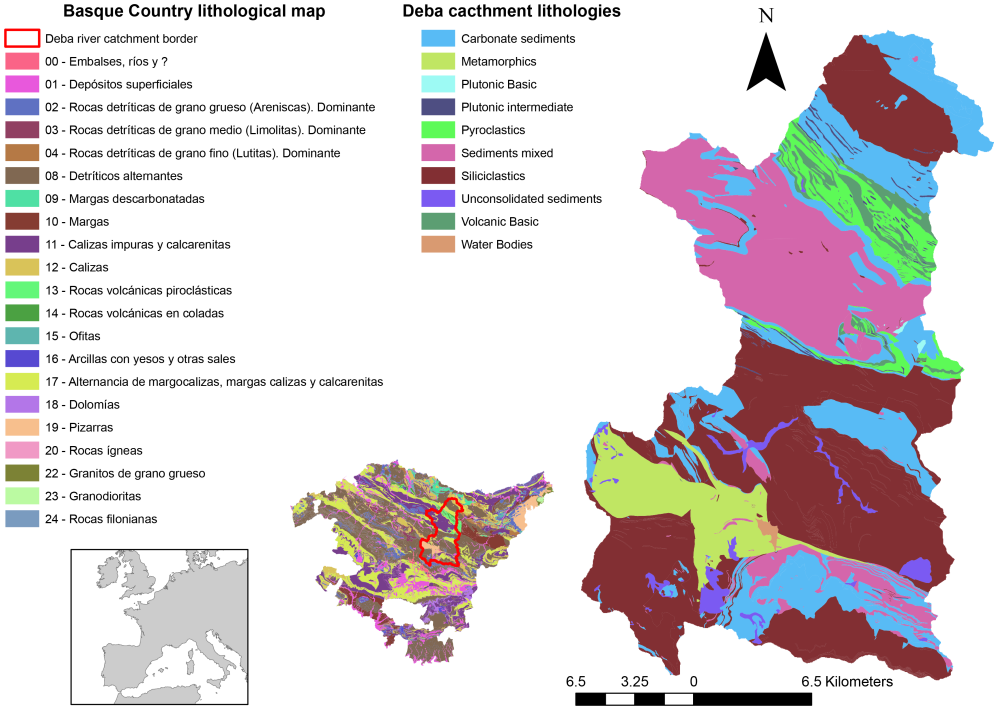

Figure S6.1: Original lithological classification of the Basque Country (north Spain) region based on the data published by the Basque Government (www.geoeuskadi.eus) and the classification according to Hartmann and Moosdorf, 2012 of the Deba River.

Table S6.1: Equivalence between lithological classification used in the present study and the original classification present in the input data

Hartmann and Moosdorf, 2012 classification	**Original lithology**	**Original lithology**
Carbonate sediments	12 - Calizas	Limestones
	17 - Alternancia de margocalizas, margas calizas y calcarenitas	Alternance of limestones, marls, and calcarenites
Metamorphics	19 - Pizarras	Slates
Plutonic Basic	15 - Ofitas	Ophites
Plutonic intermediate	20 - Rocas ígneas	Igneous rocks
	24 - Rocas filonianas	Philonian rocks
Pyroclastics	13 - Rocas volcánicas piroclásticas	Pyroclastic rocks
Sediments mixed	10 - Margas	Marls
	11 - Calizas impuras y calcarenitas	Impure limestones and calcarenites
	16 - Arcillas con yesos y otras sales	Gypsum and others
Siliciclastics	02 - Rocas detríticas de grano grueso (Areniscas). Dominante	Detritic rocks with coarse grain (sandstones)
	03 - Rocas detríticas de grano medio (Limolitas). Dominante	Detritic rocks with medium grain (limolites)
	04 - Rocas detríticas de grano fino (Lutitas). Dominante	Detritic rocks with fine grain (lulites)
	08 - Detríticos alternantes	Alternance of detritic rocks
Unconsolidated sediments	01 - Depósitos superficiales	Alluvial deposits
Volcanic Basic	14 - Rocas volcánicas en coladas	Volcanic rocks
Water Bodies	00 - Embalses, ríos y cuerpos de agua	Rivers, ponds, and water bodies

Bibliography

Ábalos, B., Alkorta, A., & Iribar, V. (2008). Geological and isotopic constraints on the structure of the Bilbao anticlinorium (Basque–Cantabrian basin, North Spain). *Journal of Structural Geology*, *30*(11), 1354–1367. https://doi.org/10.1016/j.jsg.2008.07.008

Abbaspour, K. C., Johnson, C. A., & van Genuchten, M. T. (2004). Estimating uncertain flow and transport parameters using a sequential uncertainty fitting procedure. *Vadose Zone Journal*, *3*(4), 1340–1352. https://doi.org/10.2113/3.4.1340

Abbaspour, K. C., Yang, J., Maximov, I., Siber, R., Bogner, K., Mieleitner, J., Zobrist, J., & Srinivasan, R. (2007). Modelling hydrology and water quality in the pre-alpine/alpine Thur watershed using SWAT. *Journal of Hydrology*, *333*(2-4), 413–430. https://doi.org/10.1016/j.jhydrol.2006.09.014

Allison, J. D., Brown, D. S., & Novo-Gradac, K. J. (1991).). MINTEQA2/PRODEFA2, A geochemical assessment model for environmental systems: version 3.0 user's manual.

Amiotte Suchet, P., & Probst, J. L. (1995). A global model for present-day atmospheric/soil CO2 consumption by chemical erosion of continental rocks (GEM-CO2). *Tellus B*, *47B*(1-2), 273–280. https://doi.org/10.1034/j.1600-0889.47.issue1.23.x

Arnold, J. G., Moriasi, D. N., Gassman, P. W., Abbaspour, K. C., White, M. J., Srinivasan, R., Santhi, C., Harmel, R. D., van Griensven, A., Van Liew, M. W., Kannan, N., & Jha, M. K. (2012). SWAT: Model use, calibration, and validation. *Transactions of the ASABE*, *55*(4), 1491–1508. https://doi.org/10.13031/2013.42256

Arnold, J. G., Srinivasan, R., Muttiah, R. S., & Williams, J. R. (1998). Large area hydrologic modeling and assessment: Part I: Model development. *Journal of the American Water Resources Association*, *34*(1), 73–89. https://doi.org/10.1111/j.1752-1688.1998.tb05961.x

ASABE. (2017). Guidelines for calibrating, validating, and evaluating hydrologic and water quality (H/WQ) models. https://elibrary.asabe.org/abstract.asp?aid=47804

Bailey, R. T., Tavakoli-Kivi, S., & Wei, X. (2019). A salinity module for SWAT to simulate salt ion fate and transport at the watershed scale. *Hydrology and Earth System Sciences*, *23*(7), 3155–3174. https://doi.org/10.5194/hess-23-3155-2019

Cañedo-Argüelles, M., Kefford, B. J., & Schäfer, R. B. (2018). Salt in freshwaters: causes, effects and prospects - introduction to the theme issue. *Philosophical transactions of the Royal Society of London. Series B, Biological sciences*, *374*(1764). https://doi.org/10.1098/rstb.2018.0002

Dile, Y., Daggupati, P., George, C., Srinivasan, R., & Arnold, J. G. (2016). Introducing a new open source GIS user interface for the SWAT model. *Environmental Modelling & Software*, *85*, 129–138. https://doi.org/10.1016/j.envsoft.2016.08.004

Dürr, H. H., Meybeck, M., & Dürr, S. H. (2005). Lithologic composition of the Earth's continental surfaces derived from a new digital map emphasizing riverine material transfer. *Global Biogeochemical Cycles*, *19*(4). https://doi.org/10.1029/2005GB002515

Eckhardt, K. (2005). How to construct recursive digital filters for baseflow separation. *Hydrological Processes*, *19*(2), 507–515. https://doi.org/10.1002/hyp.5675

Fekete, B. M., Vörösmarty, C. J., & Grabs, W. (2002). High-resolution fields of global runoff combining observed river discharge and simulated water balances. *Global Biogeochemical Cycles*, *16*(3), 15-1-15–10. https://doi.org/10.1029/1999GB001254

Fu, B., Merritt, W. S., Croke, B. F., Weber, T. R., & Jakeman, A. J. (2019). A review of catchment-scale water quality and erosion models and a synthesis of future prospects. *Environmental Modelling & Software*, *114*, 75–97. https://doi.org/10.1016/j.envsoft.2018.12.008

García-García, J., Ruiz-Romera, E., Martínez-Santos, M., & Antigüedad Auzmendi, I. (2019). Temporal variability of metallic properties during flood events in the Deba River urban catchment (Basque Country, Northern Spain) after the introduction of sewage treatment systems. *Environmental Earth Sciences*, *78*(1). https://doi.org/10.1007/s12665-018-8014-1

Goddéris, Y., François, L. M., Probst, A., Schott, J., Moncoulon, D., Labat, D., & Viville, D. (2006). Modelling weathering processes at the catchment scale: The WITCH

numerical model. *Geochimica et Cosmochimica Acta*, *70*(5), 1128–1147. https://doi.org/10.1016/j.gca.2005.11.018

Hartmann, J., & Moosdorf, N. (2012). The new global lithological map database GLiM: A representation of rock properties at the Earth surface. *Geochemistry, Geophysics, Geosystems*, *13*(12). https://doi.org/10.1029/2012GC004370

Hartmann, J., Moosdorf, N., Lauerwald, R., Hinderer, M., & West, A. J. (2014). Global chemical weathering and associated P-release — The role of lithology, temperature and soil properties. *Chemical Geology*, *363*, 145–163. https://doi.org/10.1016/j.chemgeo.2013.10.025

Iribar, V., & Ábalos, B. (2011). The geochemical and isotopic record of evaporite recycling in spas and salterns of the Basque Cantabrian basin, Spain | Elsevier Enhanced Reader. *Applied Geochemistry*, *26*, 1315–1329. https://doi.org/10.1016/j.apgeochem.2011.05.005

Kaushal, S. S., Duan, S., Doody, T. R., Haq, S., Smith, R. M., Newcomer Johnson, T. A., Newcomb, K. D., Gorman, J., Bowman, N., Mayer, P. M., Wood, K. L., Belt, K. T., & Stack, W. P. (2017). Human-accelerated weathering increases salinization, major ions, and alkalinization in fresh water across land use. *Applied Geochemistry*, *83*, 121–135. https://doi.org/10.1016/j.apgeochem.2017.02.006

Knoben, W. J. M., Freer, J. E., & Woods, R. A. (2019). Technical note: Inherent benchmark or not? Comparing Nash–Sutcliffe and Kling–Gupta efficiency scores. *Hydrology and Earth System Sciences*, *23*(10), 4323–4331. https://doi.org/10.5194/hess-23-4323-2019

Lechuga-Crespo, J. L., Ruiz-Romera, E., Probst, J. L., Unda-Calvo, J., Cuervo-Fuentes, Z. C., & Sánchez-Pérez, J. M. (2020). Combining punctual and high frequency data for the spatiotemporal assessment of main geochemical processes and dissolved exports in an urban river catchment. *Science of The Total Environment*, *727*, 138644. https://doi.org/10.1016/j.scitotenv.2020.138644

Lechuga-Crespo, J. L., Sánchez-Pérez, J. M., Sauvage, S., Hartmann, J., Amiotte Suchet, P., Probst, J. L., & Ruiz-Romera, E. (2020). A model to evaluate chemical weathering from riverine transports of dissolved major elements at global scale. *Global and Planetary Change*, *192*. https://doi.org/10.1016/j.gloplacha.2020.103226

Martínez-Santos, M., Probst, A., García-García, J., & Ruiz-Romera, E. (2015). Influence of anthropogenic inputs and a high-magnitude flood event on metal contamination pattern in surface bottom sediments from the Deba River urban catchment. *The Science of the total environment*, *514*, 10–25. https://doi.org/10.1016/j.scitotenv.2015.01.078

Meybeck, M. (1989). The quality of rivers: from pristine stage to global pollution. *Palaeogeography, Palaeoclimatology, Palaeoecology*, *75*, 283–309. https://doi.org/10.1016/0921-8181(89)90007-6

M'Nassri, S., Lucas, Y., Schäfer, G., Dridi, L., & Majdoub, R. (2019). Coupled hydrogeochemical modelling using KIRMAT to assess water-rock interaction in a saline aquifer in central-eastern Tunisia. *Applied Geochemistry*, *102*, 229–242. https://doi.org/10.1016/j.apgeochem.2019.01.018

Moriasi, D. N., Gitau, M. W., Pai, N., & Daggupati, P. (2015). Hydrologic and Water Quality Models: Performance Measures and Evaluation Criteria. *Transactions of the ASABE*, *58*(6), 1763–1785. https://doi.org/10.13031/trans.58.10715

Neitsch, S. L., Arnold, J. G., Kiniry, J. R., & Williams, J. R. (2011). *Soil and Water Assessment Tool: Theoretical Documentation Version 2009*. https://swat.tamu.edu/docs/

Oeurng, C., Sauvage, S., & Sánchez-Pérez, J. M. (2011). Assessment of hydrology, sediment and particulate organic carbon yield in a large agricultural catchment using the SWAT model. *Journal of Hydrology*, *401*(3-4), 145–153. https://doi.org/10.1016/j.jhydrol.2011.02.017

Parkhurst, D. L., & Appelo, C. A. J. (2013). Description of Input for PHREEQC Version 3—A Computer Program for Speciation, Batch-Reaction, One-Dimensional Transport, and Inverse Geochemical Calculations.

Schoups, G., Hopmans, J. W., & Tanji, K. K. (2006). Evaluation of model complexity and space–time resolution on the prediction of long-term soil salinity dynamics, western San Joaquin Valley, California. *Hydrological Processes*, *20*(13), 2647–2668. https://doi.org/10.1002/hyp.6082

Unda-Calvo, J. (2019). *Sediment as tool for evaluating ecological status of a river basin: Physicochemical and biological quality indicators* (Doctoral dissertation). Univer-

sidad del País Vasco/Euskal Herriko Unibertsitatea. Bilbao. http://hdl.handle.net/10810/41887

Xie, J., Liu, X., Wang, K., Yang, T., Liang, K., & Liu, C. (2020). Evaluation of typical methods for baseflow separation in the contiguous United States. *Journal of Hydrology*, *583*, 124628. https://doi.org/10.1016/j.jhydrol.2020.124628

CHAPTER 7

Global dynamic application

Once the performance of the model at different spatial and temporal scales has been evaluated, the model is applied at the global scale considering the watershed level as unit of calculus to evaluate the role of chemical weathering on the carbon sequestration at the global scale, paying special attention to the potential impact that hydrological shifts derived from climate change will have on the hot spots and hot moments of carbon sequestration. The results from the present chapter are prepared in a scientific article to be submitted to *Nature Climate Change*: Lechuga-Crespo, J. L., Sánchez-Pérez, J.M., Ruiz-Romera, E., Probst, J.L., van Vliet, M., Sauvage, S. **Potential impacts of hydrological shifts on carbon sequestration through chemical weathering under climate change.**

7.1 Introduction

Rivers link land and water bodies (estuaries, lakes, oceans, etc.) and transport terrestrial matter between reservoirs in the ecosystem. The role of rivers and their draining basins on the export of matter has long been object of study in biogeochemical cycling. Various of these studies (e.g. Amiotte Suchet and Probst, 1993b; Amiotte Suchet et al., 2003; Bhatt et al., 2018; Dupré et al., 2003; Gaillardet et al., 1999; Hartmann et al., 2009; J. L. Probst et al., 1997; J. L. Probst et al., 1994) have focused in the global CO_2 consumption through chemical weathering (CW) in the critical zone (S. P. Anderson et al., 2007), a process responsible of long-term climate regulation (Calabrese et al., 2017). In shorter timescales, soil respiration balances CO_2 presence in soils, conditioning soil acidification (Richter & Markewitz, 1995, 2001) by regulating pCO_2 in the topsoil layers (Kessler & Harvey, 2001) and increasing soil water acidity, hence enhancing chemical weathering of rocks. Carbonate and silicate rock weathering are the main geochemical mechanisms by which soil CO_2 is consumed, through the implication of carbonic acid in these dissolutions (R. A. Berner et al., 1983; Garrels & Mackenzie, 1971; Hartmann et al., 2009; Munhoven, 2002), being a relevant process on the carbon cycle. Most of the previously reported studies focus on current state or past evolution of this process, but few regards towards how this process influences future evolution of biogeochemical cycles.

Climate change scenarios forecast increases on atmospheric temperature and alteration on the hydrological cycles (IPCC, 2013), but the effect of this augmentation on chemical weathering and related CO_2 dynamics and dissolved solids exports is not clear (Liu et al., 2010). On one side, an increase in the microbial activity in the soils is expected, implying a rise in CO_2 production through respiration (Beaulieu et al., 2012; Conant et al., 2011). However, a growth in temperature may decrease CO_2 dissolution in water, as it has been shown that carbonate weathering follows a boomerang-shape evolution with increasing temperature (Gaillardet et al., 2019). On the other side, despite of the widely recognized role of water as a vector of matter transport and the forecasted changes derived from climate change scenarios (van Vliet et al., 2013), the

potential implication of these shifts remains unknown (Liu et al., 2010).

Typically, field surveys classify rivers and basins in three groups according to the concentration vs discharge relations: kinetically dominated, where the CW reaction is conditioned by the reaction equilibrium; transport dominated if the main condition is the input of carbonic acid drained from the top soil layer; and a mixture of those two (Calabrese et al., 2017). Such classification is mainly conditioned by the transition time of water, i.e. the time the water remains in the Critical Zone (CZ), since it determines the establishment of a thermodynamic equilibrium between the two phases (Maher & Chamberlain, 2014). Thus, hydrology has largely been noted as a relevant factor on biogeochemical cycling both of carbon and rock-derived ions and compounds (Maher & Chamberlain, 2014). In addition to field surveys, hydro-geochemical modelling has been a complementary approach to study these processes and perform simulations under different scenarios (e.g. Goddéris et al., 2006; Hartmann et al., 2009; Meybeck, 1987). Two main kind of models exist: mechanistic if based on physical principles, and empirical when built under parametrical laws, each kind presents its advantages and limitations.

Mechanistic models, such as B-WITCH (Beaulieu et al., 2012) and RT-Flux-PIHM (Bao et al., 2017; Li et al., 2017) models, have been working on linking the thermodynamic and transport processes to hydrology and vegetation. On the one hand, B-WITCH has been able to integrate dynamic vegetation model to a surface weathering model to estimate the cationic production and the CO_2 consumed by weathering in the Mackenzie River Basin (Beaulieu et al., 2012). They saw that 40% of the total increase in the CO_2 consumption would be related to direct effect of climate change on hydrology alteration, and the remaining is associated to the vegetation effect. On the other hand, the RT-Flux-PIHM model (Bao et al., 2017; Li et al., 2017) has been applied to establish the links between concentration and discharge (C-Q). They found that the riverine ionic mass was rather constant with time (chemostatic), suggesting a coupling of water flux with rock dissolution time, implying that water was in equilibrium with the mineral phases, thus changes on hydrological regime would condition the concentration in rivers. In contrast, empirical models have been commonly developed and applied at large spatial

scales (e.g. Amiotte Suchet and Probst, 1995; Hartmann et al., 2009) since despite of carrying a larger uncertainty, they are less input-data demanding and provide useful insights. They have been proved useful on assessing global biogeochemical cycles, and some of their results have been used in relevant assessments such as those carried by the EC Environment Climate Program ESCOBA (Aumont et al., 2003) and by the Intergovernmental Panel of Climate Change (IPCC) in their fifth Assessment Report (IPCC, 2013).

The amount of data required to apply numerical models prevents the assessments of these impacts of being carried at the global scale. It is here where the application of empirical laws brings an opportunity, yet they do not yield deeper understanding of the processes studied and their uncertainty is relevant, their lower data demanding structure allows for the establishment of a first snapshot on potential forecasts. In the present study, we work under part of the 9th hypothesis established by Brantley et al. (2011), where riverine solute fluxes were expected to be mainly conditioned by changes in the water fluxes, while secondly on changes through biologically mediated chemical weathering.

The objective of this study is to assess how climate change derived alteration of the hydrological regime will affect the CO_2 consumption at the global scale. To address this research objective, we couple an empirical model for the estimation of Ionic fluxes released by Chemical Weathering of Rocks (ICWR, Lechuga-Crespo, Sánchez-Pérez, et al., 2020) to a balance model for the estimation of CO_2 consumption (MEGA, Amiotte Suchet and Probst, 1996). In a next step, we force the coupled model system with hydrological time series simulations under changing climate from a previous literature(van Vliet et al., 2013; van Vliet, van Beek, et al., 2016; van Vliet, Wiberg, et al., 2016), and using lithological, and soil maps. Particularly, three targets are established: *i*) an estimation of the current annual and seasonal C sequestration through chemical weathering, *ii*) an evaluation of the potential relative changes derived from two climate change scenarios, and *iii*) a quantification of the uncertainty of the modelling approach. The results of the present analysis illustrate the effects of hydrological shifts on a part of the C cycle and present a starting point for future research in the area.

7.2 Datasets and methods

7.2.1 Climate scenarios and general circulation models

Four Representative Concentration Pathways (RCP) have been selected by the Intergovernmental Panel for Climate Change (IPCC) in their fifth report (IPCC, 2013) for the assessment of short-term (up to 2100) climate change impacts. From those four RCP, two have been included in the present analysis (RCP2.6 and RCP8.5) under two different assumptions. RCP2.6 considers that the radiative forcing (i.e. the strength of change drivers) will peak in 2100 at about 3 $W{\cdot}m^{-2}$ and then decline, while RCP8.5 considers that the radiative forcing will reach >8.5 $W{\cdot}m^{-2}$ by 2100. The Variable Infiltration Capacity (VIC) global hydrological model (Liang et al., 1994; Lohmann et al., 1998) was used to produce projections of daily discharge for 1961-2099 by using output from five global climate models under both RCP2.6 and RCP8.5: GFDL-ESM2M (Delworth et al., 2006; Donner et al., 2011), the HadGEM2-ES (Collins et al., 2011; Martin et al., 2011), the (Dufresne et al., 2013), the MIROC-ESM-CHEM (Watanabe et al., 2011), and the NorESM1-M (Iversen et al., 2013).

7.2.2 Modelling approach

7.2.2.1 Overview

The input data handling and modelling in the present study follow the workflow summarized in Figure 7.1. First, from the HydroBASINS dataset (Lehner & Grill, 2013) a subset of the 300 largest basins covering ~70% of the global land area were selected, including only exorheic river basins (Figures 7.2 and S7.1). The area of the catchments selected was derived from the HydroBASINS dataset. Secondly, the outlet from the VIC-RBM database was selected manually, exploring the time series for each sampling location and surrounding points (±0.5º) to select the correct outlet. When a catchment

presented several outlets (common for endoreic catchments draining to a lake or inner sea), all of them were considered, and their discharge was added, to account for all water flowing out the drainage surface. Secondly, a deconvolution of the daily discharge signal for each outlet is applied to distinguish between the surface runoff from the soil and groundwater flow. Thirdly, draining catchment characteristics are summarized for each basin, by considering the relative abundance of lithological classes contained in the Global Lithological Map (GLIM, Hartmann and Moosdorf, 2012), the soil classes as defined by the Harmonized World Soil Database (HWSD, FAO et al., 2012), and the climatic zones present according to the Köppen-Geiger classification presented by Beck et al. (2018). The modelling approach consists of two models in cascade, for each basin under each discharge time series. The flux of Ions derived from Chemical Weathering of Rocks (ICWR, Lechuga-Crespo, Sánchez-Pérez, et al., 2020) is computed at a daily time step. Then, the Major Element Geochemical Approach (MEGA, Amiotte Suchet and Probst, 1996; Donnini et al., 2016) uses these loadings to estimate the CO_2 consumed through chemical weathering.

From this set-up, a daily time series from 1965 to 2100 major ion loadings and CO_2 consumption through CW from 300 largest catchments is obtained. In order to estimate the potential effect of hydrological shift in the CO_2 consumption, two periods are established: the Historical (from October 1969 to September 1999) and the Projection (October 2069 to September 2099), and a comparison between the two periods is accomplished.

7.2.2.2 Hydrological modelling

Daily discharge values for the catchments selected have been taken from the modelling cascade results of the Variable Infiltration Capacity (VIC) (Liang et al., 1994) and the daily stream temperature model (RBM, Yearsley, 2009) used in previous studies of large basins (van Vliet et al., 2012) and global forecasts of climate change potential impacts (van Vliet et al., 2013). These results have been forced to two scenarios (SRES A2 and B1) from the IPCC under 5 Global Circulation Models (GCM). Daily discharges time

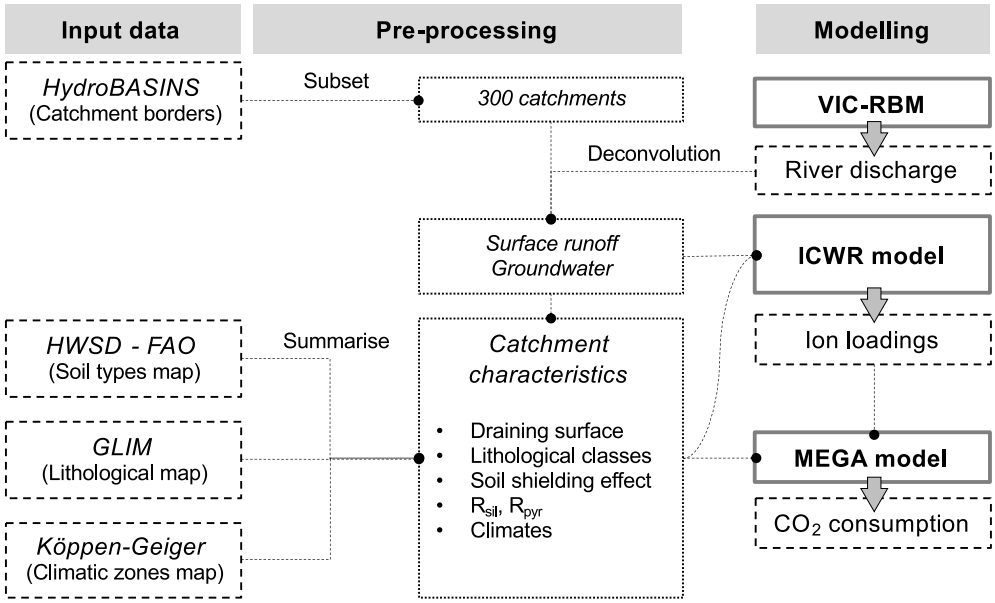

Figure 7.1: Workflow summary of the modelling-cascade approach. Input data includes the VIC-RBM database (van Vliet et al., 2013), the HydroBASINS Lehner and Grill, 2013, HWSD FAO et al., 2012, GLIM Hartmann and Moosdorf, 2012, and the Köppen-Geiger climate classification Beck et al., 2018. Subset is based on the draining area, deconvolution is performed following the Eckhardt, 2005 method, and summarisation is accomplished for each catchment by computing the relative area of the soil types, lithological classes and climatic zones. The VIC-RBM model estimates riverine discharges at a global scale van Vliet et al., 2013, the ICWR model evaluates the ionic fluxes derived from chemical weathering of rocks Lechuga-Crespo, Sánchez-Pérez, et al., 2020, the MEGA model balances the ionic loadings to the carbon uptake derived from chemical weathering Amiotte Suchet, 1995; Amiotte Suchet and Probst, 1996. Further description is found in the text

series have been taken from all of these scenario-model combinations, while temporal aggregation has been performed after applying the ICWR and MEGA models.

The discharge time series have been deconvoluted to separate the influence of the surface runoff, which has been considered as diluted with respect to the baseflow and interflow discharges. Such deconvolution is performed following the digital filter shown in Equation 7.1, as proposed by Eckhardt (2005). In the present study, only interflow and baseflow are considered as loaded with ions, while surface runoff is the main agent for dilution. A digital filter is selected, as it is based on the slopes of both the increasing and decreasing parts of the hydrographs, though being sensible to changes not only

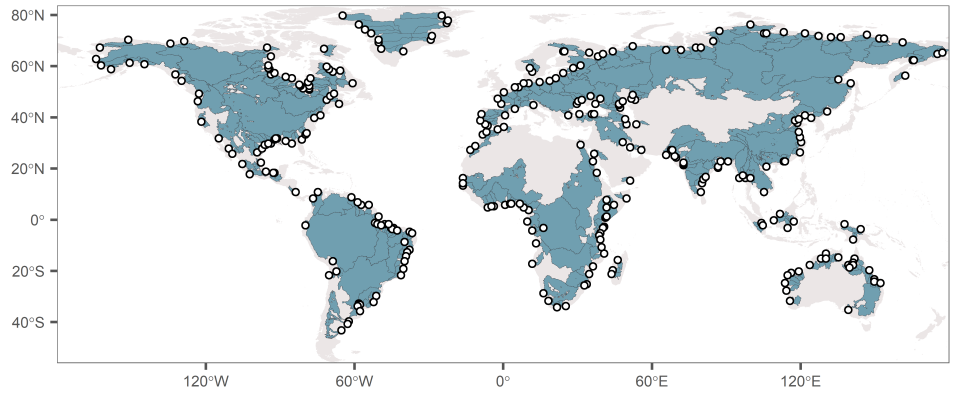

Figure 7.2: Map of selected basins and respective outlets.

in the amount of water but in the seasonality and flood events. Nonetheless, this is a source of uncertainty as the infiltration process depends on a catchment-to-catchment properties, while this equation assumes linearity between the groundwater outflow (baseflow) and its storage (Eckhardt, 2005).

$$b(t) = \frac{(1 - BFI_{mx} \cdot a \cdot b(t-1) + (a - a) \cdot BFI_{mx} \cdot Q(t)}{1 - a \cdot BFI_{mx}}, \text{ for} b(t) < Q(t) \qquad (7.1)$$

Where b(t) quantifies the baseflow, Q(t) de total discharge, BFI_{mx} represents the long-term ratio of baseflow to total discharge, and a is the filter parameter. When b(t)>Q(t), b(t) is replaced by Q(t). The parameters selected for the separation are $BFI_{mx} = 0.8$ and $a = 0.95$, as recommended by Xie et al. (2020). These parameters are kept constant in all catchments, also becoming a source of uncertainty.

7.2.2.3 Flux of Ions derived from Chemical Weathering of Rocks (ICWR)

The ICWR model is an empirical model developed under the major ion riverine fluxes at the global scale, based on Equation 7.2, which has been validated at the global scale under static situation (Lechuga-Crespo, Sánchez-Pérez, et al., 2020), and at the

local scale under dynamic evolution (Lechuga-Crespo et al., Under Review). For its computation, a description of the draining catchment is needed, regarding soil coverture and lithological distribution. The parameters of the equation regard the concentration for each ion x drained from a lithological class i. The calibration of the parameters on the ICWR model has been performed after the atmospheric correction, though the loadings computed from this equation are related to the chemical weathering process, which are the needed input for the MEGA model.

$$F_x(t) = b(t) \cdot f_{s,x} \cdot \sum \left(L_i \cdot C_{i,x} \right) \tag{7.2}$$

Where F_x represents the specific flux of ion x in mol·km^{-2}·y^{-1}, b represents the baseflow and interflow obtained from the deconvolution of the total discharge signal, $f_{s,x}$ is a factor considering the soil shielding effect on chemical weathering (adim), L_i is the relative abundance of a lithological class i with respect to the total area of the draining basin (expressed as percentage in 0-1), and $C_{i,x}$ is the calibrated parameter, representing the concentration of the ion x draining from the lithological class (expressed in mol·L^{-1}). This equation is applied to the time series of the deconvoluted discharge, including the baseflow+interflow part.

7.2.2.4 Major Element Geochemical Approach (MEGA)

The MEGA model is based on the mass balance showed in Figure 7.3 (Amiotte Suchet, 1995; Amiotte Suchet & Probst, 1996). The input data are the riverine molar loadings of each major ion, after the atmospheric correction and under the assumption that not anthropogenic influence is captured in the measurements of major ion concentrations, as well as the R_{pyr} and R_{sil} molar ratios for each catchment, which account for the $Ca^{2+}+Mg^{2+}$ loads coming from weathering of silicate rocks and the SO_4^{2-} originating from pyrite oxidation, respectively. The results from this model relates to the CO_2 consumed by the chemical weathering of rocks.

Considering the river loadings of all major ions, the CO_2 consumed is computed

as follows: first, the atmospheric deposition (wet and dry) must be removed from these loads, remaining the molar fluxes derived from chemical weathering. All Cl^- is associated to the dissolution of halite (NaCl), though remaining Na^+ is associated to Na-silicates. If the $Cl^- > Na^+$, the remaining Cl^- is linked to the dissolution of sylvite (KCl). Evaporites do not uptake any CO_2 when dissolving, while Na^+ and K^+ silicate rocks (e.g. albite $NaAl_3O_8$ and orthoses $KAlSi_3O_8$) require 1 mol CO_2 for each ion mol released to water. Then, using R_{pyr} it is possible to discriminate the SO_4^{2-} load released respectively by gypsum ($CaSO_4$) dissolution and pyrite (FeS_2) oxidation. Gypsum does not consume any CO_2 during dissolution, while pyrite releases 2 mol CO_2 for each SO_4^{2-} ion released. Later, the C_b (molar flux of Ca^{2+} and Mg^{2+} released by carbonates dissolution) is computed, using R_{sil}, to account how much Ca^{2+} and Mg^{2+} is derived from the weathering of the carbonates, a 60% of Ca^{2+} is linked to calcite ($CaCO_3$) dissolution while the remaining 40% is released by dolomite ($CaMgCO_3$) dissolution. The dissolution of calcite and dolomite also uptakes 1 mol of CO_2. The remaining Ca^{2+} and Mg^{2+} fluxes are linked to silicates which consume 2 mol CO_2. A further description of the model calculation is found in Amiotte Suchet (1995) and Amiotte Suchet and Probst (1996). The R_{pyr} and R_{sil} values used in the present study are compiled in Table 7.1.

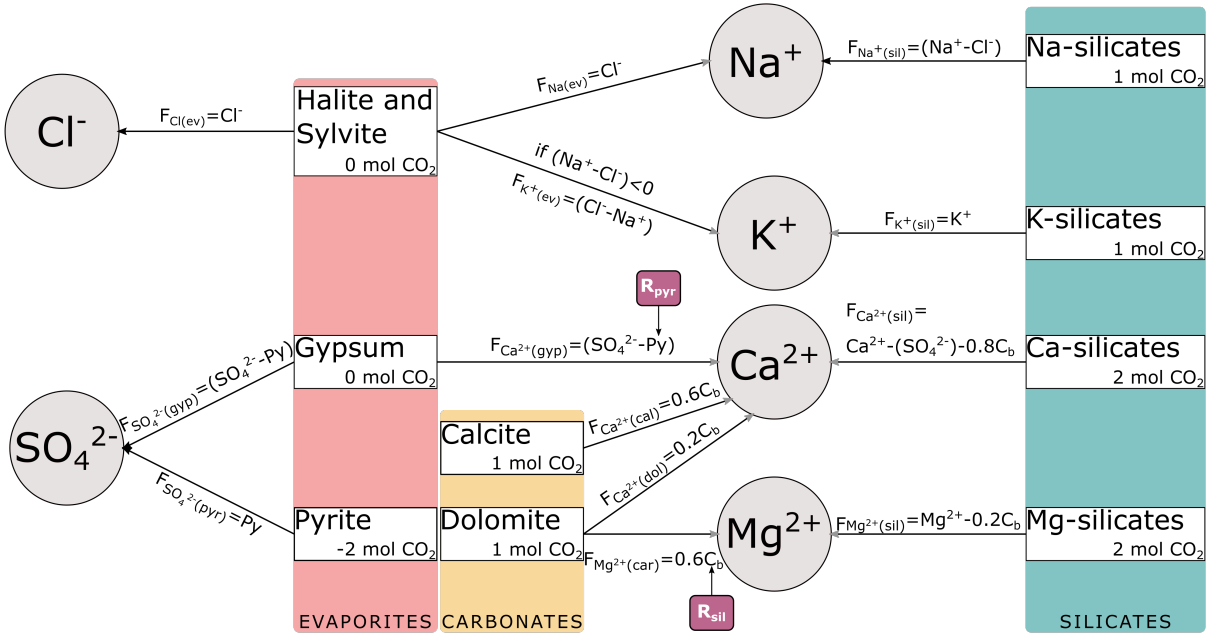

Figure 7.3: Mass balance followed in the MEGA model adapted from Amiotte Suchet, 1995. Carbon consumption by evaporites, carbonates, and silicates is estimated from a mass balance among the major ion composition found in river water. Further description in Amiotte Suchet and Probst, 1996 and Donnini et al., 2016

Table 7.1: R_{sil} and R_{pyr} molar ratios calculated for each lithological class and compared with Amiotte Suchet and Probst, 1996. R_{pyr}* relates to the actual values selected, due to the worse representation of the SO_4^{2-} in the ICWR model, these are taken from Amiotte Suchet and Probst, 1996.

Rock types	Source	R_{sil}	R_{pyr}	R_{pyr}*
Plutonic and metamorphics	Amiotte Suchet and Probst (1996)	1,50	0,15	–
Volcanic acid		1,20	0,02	–
Basalt		0,50	0,02	–
Sand and sandstones		1,30	0,24	–
Clay detrital rocks (Shales)		0,50	0,19	–
Evaporitic	Lechuga-Crespo, Sánchez-Pérez, et al. (2020)	–	–	–
Metamorphics		0,23	0,26	0,15
Plutonic Acid		0,97	0,00	0,15
Plutonic Basic		4,67	0,00	0,15
Plutonic Intermediate		3,06	0,08	0,15
Pyroclastics		1,16	0,07	0,02
Sedimentary carbonates				
Sedimentary mixed		0,35	0,34	0,19
Sedimentary siliciclastics		1,13	0,13	0,24
Sedimentary unconsolidated		1,10	0,11	0,24
Volcanic acid		1,26	0,17	0,02
Volcanic basic		0,40	0,30	0,02
Volcanic intermediate		0,25	0,48	0,02

R_{pyr} (mol·mol^{-1}) = $SO_4^{2-}/(Na^+ + K^+ + Ca^{2+} + Mg^{2+})$ and R_{sil} (mol·mol^{-1}) = $(Na^+ + K^+)/(Ca^{2+} + Mg^{2+})$ for water draining silicate rocks. R_{pyr} are taken from Amiotte Suchet and Probst (1996) considering the minerals conforming each lithological group by Hartmann and Moosdorf (2012)*

7.2.3 Potential impact estimation and assessment

Two 30-year periods are considered in the present study: an Historical (1969-1999) and a Projection (2069-2099), both of them computed at the daily time scale following the modelling approach described in section 7.3.1. The potential impacts derived from climate change are computed by quantifying the relative difference in the Projection period to the Historical period, following Equation 7.3. Where ΔCO_2 denotes the relative change for each basin (expressed in %), and L_{CO2} represents the mean amount

of CO_2 consumed through chemical weathering of rocks, during the Projection and Historical period, expressed in Mg C·y^{-1}. The analysis of these results is divided in two steps: at the annual scale, where L_{CO2} is the mean annual amount of CO_2 consumed in each period; and at the season scale, where L_{CO2} symbolizes the mean amount of CO_2 consumed during all January-February-March (JFM), April-May-June (AMJ), July-August-September(JAS), and October-November-September (ONS) of each period.

$$\Delta CO_2(\%) = \frac{L_{CO_2}^{Projection} - L_{CO_2}^{Historical}}{L_{CO_2}^{Historical}} \cdot 100 \tag{7.3}$$

7.3 Results and discussion

The present study compiles an assessment of the potential effects that shifts in the hydrological regimes–forecasted for two climate change scenarios (RCP2.6 and RCP8.5)–could cause in the carbon sequestration through chemical weathering of continental rocks. This section presents and discusses the results in three main points:

- An evaluation of the modelling approach, paying special attention to the deviations found in the ICWR model's results which are input to the MEGA model.
- An assessment of current global C sequestration through CW in comparison with previous studies, as well as the assessment of existing hot spots and hot moments.
- A description of potential shifts in two climate scenarios, both at the global scale and at the watershed scale.

7.3.1 Modelling approach evaluation

Forecasting changes at the global scale under the Earth system, i.e. "Earthcasting", is one of the current greatest challenges in environmental sciences (Brantley et al., 2011). This kind of studies may only be performed through modelling, with both empirical and

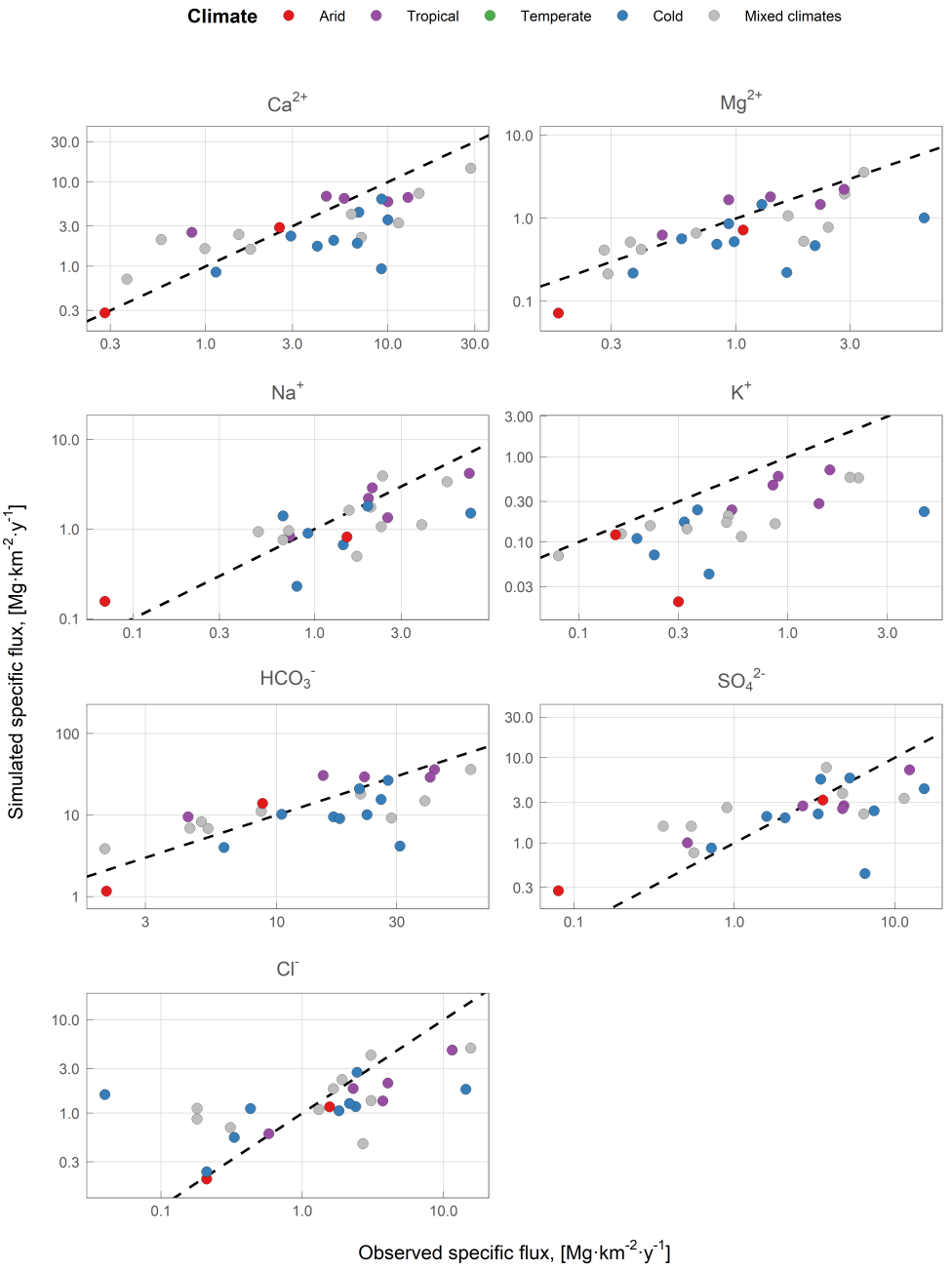

Figure 7.4: Comparison of simulated vs observed specific ion fluxes for large river basins. Simulated values were derived from the ICWR model, while observed fluxes were retrieved from a compilation found in J. L. Probst, 1992. Dashed line is the 1:1 line indicating perfect fit. Note that axes are displayed at the logarithmic scale. Larger figures with names for each location may be found in Figure S7.2 to Figure S7.8.

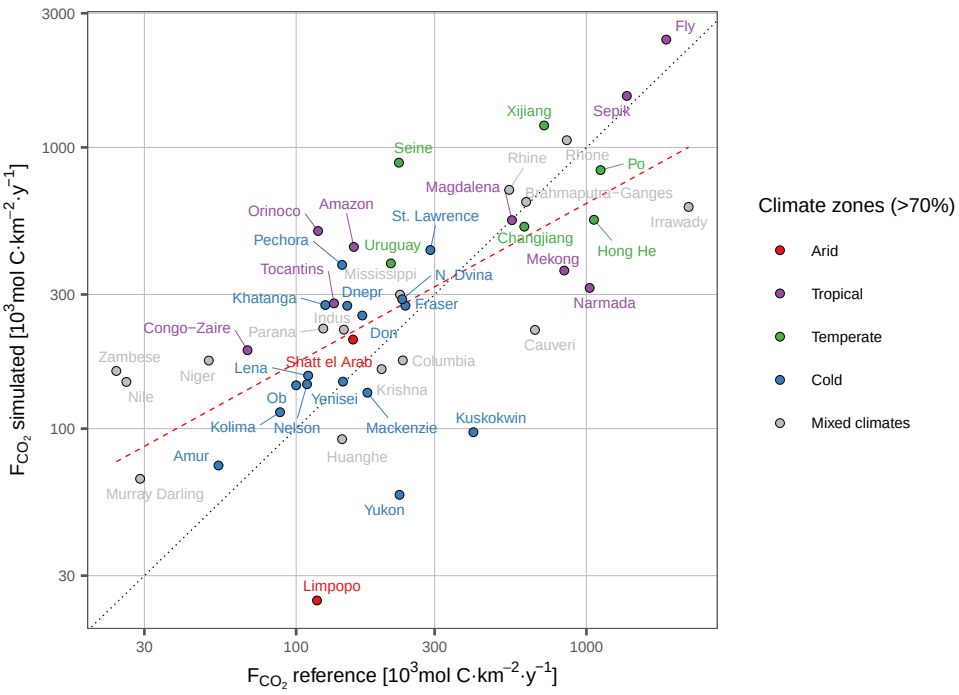

Figure 7.5: Comparison of annual simulated CO2 fluxes (in the Historical period, 1969-1999) with those derived from field studies, retrieved from Gaillardet et al., 1999. Dotted black line represents perfect fit line (1:1) while dashed red line is the regression between the reference and simulated values. Colours represent predominant current climatic zones, according to Köppen-Geiger classification presented by Beck et al., 2018 while grey dots are those basins with mixed climates. Axes are displayed at the logarithmic scale.

mechanistic basis. Empirical modelling, or parametric models, have been demonstrated as useful at the short time, but present the drawback of limited extrapolation on their applicability out of the development domain (both in space and time). On the contrary, physically-based models collect the relations among different processes. Their coupling allows for an integrative and adaptative assessment, but they require a large amount of data for their constrain and simulation. Apart from the mathematical description of the processes, studying several processes together requires the coupling of some models. Previous studies (Goddéris & Brantley, 2013) have recommended the use of a cascade modelling approach as the computation cost is more efficient. In the present analysis, we have used a such approach between the results of two physically based models on climate and infiltration, an empirically based model for chemical weathering, and a

mass balance model to estimate the CO_2 consumption.

The cascade modelling approach implies that errors are added and carried from one model to the following one, increasing uncertainty on the results. To account for these errors, we have assessed the uncertainties in the input data and the pre-processing step and compared the results from each modelling step with literature data.

The spatial resolution of the watershed boundaries is 15 arcseconds based on the STRM digital elevation map and performed consistently for the globe under the HydroSHEDS database (Lehner & Grill, 2013), which avoids the overlay of watershed boundaries. However, the quality of this dataset is lower for locations over 60ºN or 60ºS as no STRM is present. Some of the river basins included in the present analysis are in this area, thus their results are conditioned to the accuracy of their drainage area estimation. The VIC-RBM dataset is available at a coarser dataset (0.5x0.5º) than the HydroSHEDS, thus the selection of the corresponding outlet has been performed manually by exploring the time series near the outlet and choosing the one with the highest average discharge. In large river basins with relevant wetlands in their outlet, such as the Amazon, the estimation of this outlet has been done considering the last reach of the watershed by exploring the outlets and the surrounding locations, to choose the one with the largest discharge.

The GLIM database used for the lithological discretization has been used due to its global scale coverture, its resolution and because it has been used for the calibration of the ICWR parameters. Similarly, the soil classification has been performed using a 30 arc-second harmonized world soil classification. Considering that the smallest river basin included in the present analysis is $3.3 \cdot 10^4$ km^2, the resolution of the input data has been considered as enough for representing the physical characteristics of the drainage basins. It is relevant to note that the simulations presented in this study are based on the temporal digital deconvolution of the river discharge signal at one or several outlets, and not in spatially explicit runoff (defined as discharge over the drainage area) calculations as done in previous studies (e.g. Hartmann et al., 2009; Lechuga-Crespo, Sánchez-Pérez, et al., 2020). One of the methods to include the differentiation between

surface and groundwater discharges is the use of a digital filter on a continuous time series. The filter used in the present analysis has been chosen as it has been recently suggested to yield good representation of the baseflow in a broad set of basins (Xie et al., 2020).

The hydrological deconvolution, as well as the MEGA and the ICWR models have several parameters within their formulation. The establishment of these parameters has been performed using previous literature when available or estimated as explained in section 7.3.1. The BFI_{max} and the a parameters in the Eckhardt digital filter have been considered as constant for all river basins, acknowledging that these parameters may vary in a basin-to-basin case. Nevertheless, the values used have been demonstrated as useful in a wide range of hydrological conditions (Xie et al., 2020), thus considered acceptable for this assessment. Within the mass balance in the MEGA model, two parameters (R_{pyr} and R_{sil}) have been calculated for each basin considering the lithological distribution, based on the established values for each lithology depending on the chemical composition of their draining waters. R_{sil} values agree with previous results, but R_{pyr} presented several relevant discrepancies associated to a worse representation of some ion loadings, thus taken from literature (Amiotte Suchet & Probst, 1996). The parameters found in the ICWR model have been calibrated at the global scale in previous studies (Lechuga-Crespo, Sánchez-Pérez, et al., 2020) and validated at the local scale in a dynamic approach (Lechuga-Crespo et al., Under Review). The fitted values of these parameters have been calibrated using observational data in a broad set of draining basins with different lithological, soil, and hydrological conditions thus are expected to capture the variables influencing ionic fluxes derived from chemical weathering.

Concerning the modelling cascade, uncertainties related to the hydrological modelling are discussed in Yearsley (2009), and van Vliet et al. (2012) studies and uncertainties regarding the projections on global discharge are included in van Vliet et al. (2013). The ICWR model results were compared with a dataset compiled by J. L. Probst (1992) for each ion in several large river basins (Figure 7.4). Overall, the comparison of mean simulated vs observed data yields a very significant and positive correlation (ρ=0.83, p<0.01, n=173), but presenting a PBIAS of -31%, hence suggesting a general

underestimation of the specific fluxes by the ICWR model. Such underestimation is specially pronounced on the K^+ ion, where all simulated values are located under the 1:1 line. Focusing on the extreme deviations in the ionic fluxes, the Yukon river basin is commonly the most underestimated by the model. A recent study in this basin (Toohey et al., 2016) reported increasing trends on Ca^{2+}, Mg^{2+}, Na^+, and SO_4^{2-} loadings in this and other river basins on the Arctic, and that such trends are related to permafrost degradation, increasing the active layer where weathering occurs. The permafrost dynamics have not been included in the present model configuration; however, they play a relevant role on the weathering process when studying the cold river basins. The lack of including these processes in the model could explain why most of the "cold" river basins are located under the 1:1 line in Figure 7.4, i.e. underestimated by the ICWR model. In contrast, the Niger basin is commonly found overestimated by the model, which is associated to an overestimation of the discharge in this basin due to water extractions and complex wetland dynamics, as explained by van Vliet et al. (2013). Nevertheless, in tropical and mixed climates the model performance is better, where basins are scattered around the 1:1 line. Overall, the modelling approach carries a -31% error at the ICWR model step, which is consistent with the -29.2% PBIAS reported by Lechuga-Crespo, Sánchez-Pérez, et al. (2020) when calibration of the model was assessed.

The MEGA model results are contrasted with the results published by Gaillardet et al. (1999) in Figure 7.5. The comparison between simulated results and reference values yields a very significant correlation (ρ=0.71, p<0.01, n=48), and a mean PBIAS of 0.7% indicating a general good correlation between results and simulations. Focusing on specific river basins, the Limpopo is significantly underestimated by the model, but the similar scatter over and under the 1:1 line explains the low PBIAS, implying that at the global scale this modelling approach is suitable for performing a C uptake assessment by chemical weathering, but the results at the basin scale should be regarded with caution.

In summary, despite of the results from the ICWR model have a general underestimation of the ionic fluxes, the MEGA model has yielded a low overall PBIAS, implying

an overall fair representation of carbon consumption during chemical weathering at a global scale. In addition, the significant correlations found in both models suggest that the modelling cascade approach followed in the present analysis is suitable for describing carbon uptake by chemical weathering at the global scale during the Historical period.

7.3.2 Current hot spots and hot moments

The global annual carbon sequestration derived from CO_2 uptake by chemical weathering of continental surfaces ranges from 0.22 to 0.30 Pg C·y^{-1} (1 Pg = 10^{15} g) according to previous studies (Amiotte Suchet & Probst, 1995; Amiotte Suchet et al., 2003; R. A. Berner et al., 1983; Gaillardet et al., 1999; Hartmann et al., 2009; Meybeck, 1987; Munhoven, 2002; J. L. Probst, 1992; J. L. Probst et al., 1997), approximated to 0.30 Pg C·y^{-1} in the Fifth report of the Intergovernmental Panel of Climate Change (IPCC, 2013). In the present study, the covered drainage area yields 0.24 Pg C·y^{-1}, within the range of previous reports. Figure 7.6 shows the spatial distribution (at the basin unit) of the mean specific C flux consumed through chemical weathering for the Historical period (1969-1999) at the annual (Figure 7.6a) and seasonal times (Figure 7.6b). Ranges and spatial distribution at the annual and basin scales are comparable with the spatially explicit model results presented by Hartmann et al., 2009. Considering regional studies like the Amazon (Amiotte Suchet & Probst, 1993b; Moquet et al., 2016; Mortatti & Probst, 2003), Congo (Amiotte Suchet & Probst, 1995; J. L. Probst et al., 1994), Niger (Boeglin & Probst, 1998) and Garonne Amiotte Suchet and Probst, 1995, the Alps region (Donnini et al., 2016), or the United States continuum (Moosdorf et al., 2011), the values are also in the same range, even if the river basin draining lateritic soil covers have lower CO_2 uptake as shown by Boeglin and Probst, 1998.

Hot spots and hot moments are locations or moments with disproportional high loads or rates with respect to their surrounding matrix or moments (McClain et al., 2003). Their identification has been noted as relevant to understand the processes related to

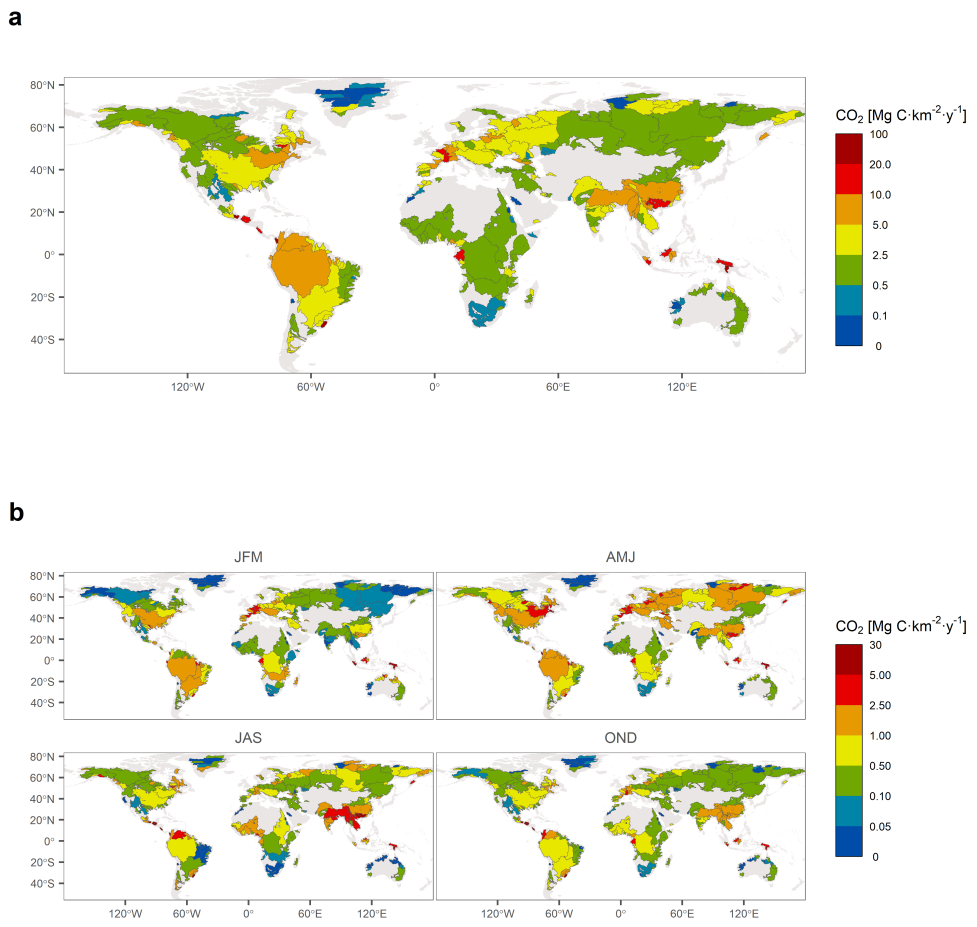

Figure 7.6: Simulation of the specific C-CO_2 fluxes (Mg C·km^{-2}·y^{-1}) consumed by chemical weathering of continental surfaces using the 400 largest river basins in the Historical period (1969-1999). Annual specific fluxes are shown in a), while seasonal periods (JFM for January-February-March, AMJ for April-May-June, JAS for July-August-September and OND for October-November-December) are shown in b). Basins are filled according the specific flux of CO_2 consumed during chemical weathering of rocks. Please, note different scales in a) and b).

the cycling of bioactive elements (e.g. carbon or phosphorus) (Hartmann, Moosdorf, et al., 2014; McClain et al., 2003), and their role in broader biogeochemical cycles. Under the assumption that the slow geochemical cycle is in steady state in timespans smaller than the geological times, alterations in the geological cycle are mainly linked to changes in the vector of matter transport: water. Figure 7.6 highlights several basins

(hot spots) with relevant contribution varying along the year, according to the season (hot moments).

Focusing on the spatial distribution, highest specific annual fluxes of C consumed through chemical weathering are found mainly in the tropics, particularly on the northern part of South America, the south-east part of Asia, and several catchments in the mid latitudes, probably related to carbonate outcrops as reported by Amiotte Suchet and Probst, 1995, who also reported a similar annual distribution as the one shown here, but spatially explicit. The analysis of the temporal evolution gives further insights on the seasonal spatial differences. Arc-islands are relevant sinks of C through chemical weathering along all year, as shown in the Polynesian islands and Central America (Amiotte Suchet & Probst, 1995; Hartmann et al., 2009), while the relative contribution of northern and southern latitudes vary to a greater extent.

During the period January to March (JFM), the northern latitudes (arctic and Siberian areas) present the lowest values, while the Amazon, and the river basins draining into the Mediterranean Sea present the highest sequestration rates. The period April to June (AMJ) brings a general increase of CO_2 specific fluxes for the basins of northern latitudes, while a decrease in the southern hemisphere, specially for the river basins draining South America, South Africa, and Australia. A decrease enhanced in the period July to September (JAS), when the tropics present their highest values, specially in the south-eastern part of Asia and the sub-Saharan river basins. Both in JAS and OND (October to December), the relative contribution of the Amazon basin—even though it is still relevant—is decreased, while an increase is captured for the Congo basin, particularly in OND, which can be related to the monsoon dynamics in this period and then, to the high flow period of tributaries (mainly the Ubangui river) of the northern hemisphere (Nkounkou & Probst, 1987)). Lastly, the period OND presents a middle point for both northern, southern, and mid-latitudes, where highest contributions are found for the tropics. Changes found among the load fluctuations in basins are in accordance with the hydrological variations, yielding higher exports in JFM and AMJ for northern latitudes where carbonates predominate (Amiotte Suchet et al., 2003; Hartmann & Moosdorf, 2012), while tropical catchments present higher exports in JAS, probably

linked to more pronounced hydrological dynamics related to cyclones (Rosentreter & Eyre, 2020) and to an active role of arc-islands on dissolved load exports and associated CO_2 sequestration (Hartmann et al., 2009).

7.3.3 Potential shifts

Considering that CO_2 sequestration through chemical weathering of rocks is at a "steady state" during the period included in the present analysis (1969-2099) changes are related to transport processes, i.e. hydrology. Figure 7.7 presents the comparison between the Historical (1969-1999, 0.24 Pg C·y^{-1}), and the two scenarios (2069-2099, 0.26 Pg C·y^{-1} for RCP2.6, and 0.27 Pg C·y^{-1} for RCP 8.5) regarding CO_2 sequestration for the different seasons. The annual changes only amount to 8 and 13%, respectively in RCP2.6 and RCP8.5 scenarios, which are larger than the predicted changes in hydrological discharge (4 and 9%, respectively). The overall growth in the CO2 sequestration is associated to an increase in the discharge found in the northern hemisphere, where several river basins—which significantly contribute to the total annual CO_2 flux—undergo an incrementation of their discharges derived of a greater precipitation (van Vliet et al., 2013). Considering the RCP8.5 potential emissions, the forecasted amount of C uptake by rocks in 2100 represents ~1% of anthropogenic CO_2 emissions (van Vuuren et al., 2011). However, these changes are not spatially distributed among seasons (Figure 7.8). Paying attention to JFM, a general increasing trend on the northern hemisphere is present, which is especially relevant on northern latitudes, such as in the Yenisei and the Ob' river basins. These two basins yielded similar values in the ICWR and MEGA model as those found in the reference data, as shown in Figure 7.5 and Figure S7.2 to Figure S7.8, the performance of the ICWR and MEGA model present similar values to the reference data during the Historical period. Here, positive changes over 25% are expected in this season, specially in the RCP8.5 scenario, where these changes grow over 75%. Increasing temperatures are expected to cause an acceleration on the snowmelt (van Vliet et al., 2013), which could justify the increase of these fluxes. In contrast, in the southern hemisphere these changes are more heterogeneous, yielding diverging

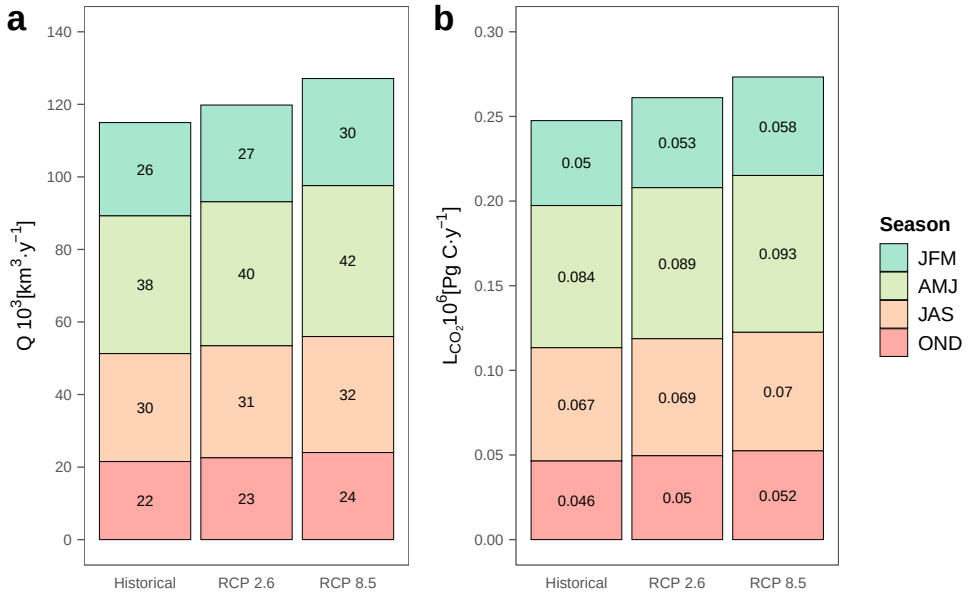

Figure 7.7: Mean annual distribution of a) water volume exported, and b) CO_2 uptake by chemical weathering of continental rocks at the global scale for the Historical and Projection periods, considering two climatic scenarios (RCP 2.6 and RCP 8.5). Colours represent different seasons (JFM for January-February-March, AMJ for April-May-June, JAS for July-August-September and OND for October-November-December).

changes between scenarios such as in the Murray-Darling river basin in Australia, or the Orange river in South Africa. Both these basins are located under mixed climatic zones (Beck et al., 2018), which could explain the heterogeneous results found between scenarios. The potential evolution in the hydrological seasonality in these areas may cause different fluxes derived from chemical weathering since a discharge decrease of >25% in low-flow period is expected (van Vliet et al., 2013), but further analysis is needed using mechanistic approaches to understand and assess potential changes in biogeochemical cycles.

Focusing on JAS season, the evolution pattern is different from the JFM season. Here, most of the area presents a negative change, suggesting a decrease of the CO_2 uptake by chemical weathering in this season. Again, this is mainly noted on the northern latitudes, where the dry season may cause a diminish of the hydrological

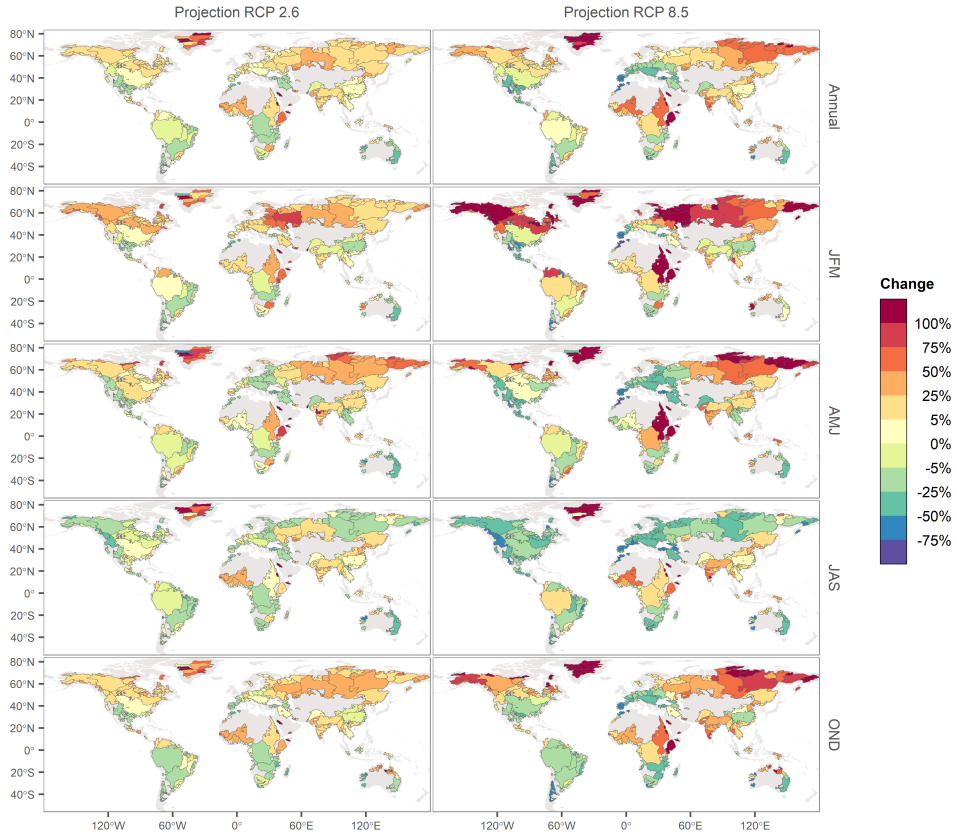

Figure 7.8: Projected relative changes (%) in C-CO_2 sequestration through chemical weathering of rock for the 400 largest river basins included in the analysis. Relative changes are computed as the mean value of 5 simulations, each simulation with each different GCM results for two scenarios (RCP 2.6 and RCP 8.5) for the Projection and Historical periods. Relative changes are computed through the absolute difference between modelled C-CO2 sequestration for the Projection and Historical periods over the C-CO_2 uptake in the Historical period. Negative values (red) imply a lower sequestration in the Projected period, while positive values (blue) suggest an increased sequestration in the forecasted period. JFM for January-February-March, AMJ for April-May-June, JAS for July-August-September and OND for October-November-December.

cycle, reducing the chemical weathering derived fluxes. Such diminish is more relevant on the RCP8.5 scenario in these areas, where the low flow period may experience decreases >25% as reported by van Vliet et al. (2013). The other two seasons (AMJ and OND) present "intermediate" states between the JFM and JAS seasons, which are the moments showing the largest relative changes.

Being discharge the key factor of change in short term assessments and the only one included in the present analysis, a comparison of the absolute changes on carbon uptake and discharge in a subset of river basins in the two scenarios (Figure 7.9) illustrates how river basins located in tropical climates present larger absolute differences both for carbon uptake and discharge, specially those basins with lower drainage area, located in active arc-islands in the Polynesian area. These changes illustrate how even though their smaller drainage area and discharges, the role of arc-island should be taken in consideration, and be a focus for future research, as their relative role on carbon sequestration through chemical weathering is relevant (Hartmann et al., 2009). In addition, potential impacts of climate change in this tropical areas is expected to be more relevant in this smaller basins than in larger watersheds like the Amazon and the Congo. On the other side, absolute change in carbon sequestration on cold basins is

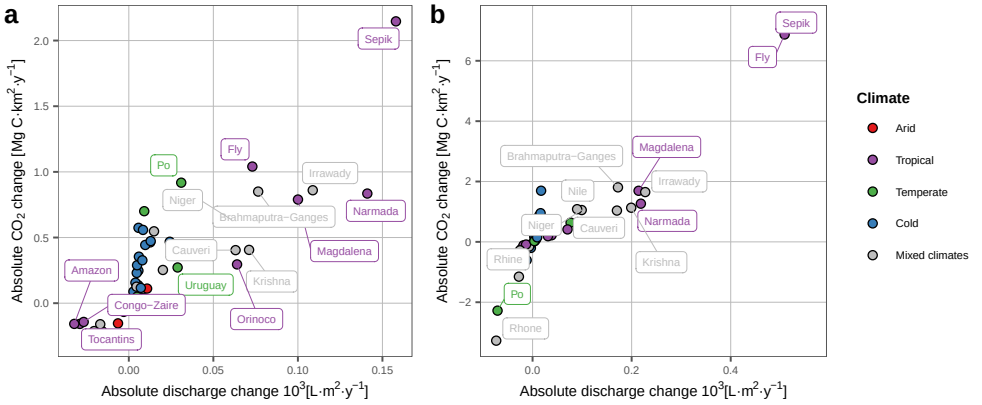

Figure 7.9: Absolute CO_2 uptake change vs absolute discharge variation in the basins used for MEGA model validation Gaillardet et al., 1999 for scenarios a) RCP2.6 and b) RCP8.5. Only relevant basins are labelled according to the dominant climate.

larger than changes in discharge for the future scenarios, which could be related to

larger amounts of carbonate sediments in these areas which uptake relevant amounts of CO_2 during weathering (Amiotte Suchet & Probst, 1996). Regarding the cold and polar basins, the permafrost processes are not included in the present analysis, which are expected to have a major impact on carbon sequestration and dissolved solid loadings in rivers (Streletskiy et al., 2015).

In summary, even though there are some relative changes noted at the annual scale, these differences are not kept during all the year, nor at the global, nor the river basin scale. Globally, JFM and OND periods present the largest differences between the two scenarios. These seasons should be more thoroughly a focus of interest for future research. At the river basin scale, those located in tropical arc islands, and cold climates are expected to suffer a greater impact according to the modelling results.

7.4 Conclusion

A modelling cascade approach is presented in this study to assess the potential impacts that shifts in hydrology may exert on the CO_2 sequestration through chemical weathering of continental rocks in the short term (before 2100). The results have shown that even though the global annual CO_2 weathering uptake may increase by about 8 to 13% depending on the scenario (RCP2.6 or RCP8.5), the seasonal changes derived from shifts on hydrology may reach a 16% increase during the JFM season. These relative changes are particularly relevant in river basins located in arc-island river basins, representing a current hot spot for CO_2 uptake through chemical weathering and showing larger absolute changes for carbon consumption and annual discharge. Cold basins also present a larger positive change in C sequestration than in water exports. The modelling approach followed in this study uses results from physically derived models to feed empirical approaches, yielding results with an absolute PBIAS of $\sim$0.7% for the Historical period. Despite of the large uncertainty, this modelling exercise provides relevant first results on the trends at the annual and seasonal scale for the global CO_2 rock weathering sequestration.

7.5 Supplementary Information

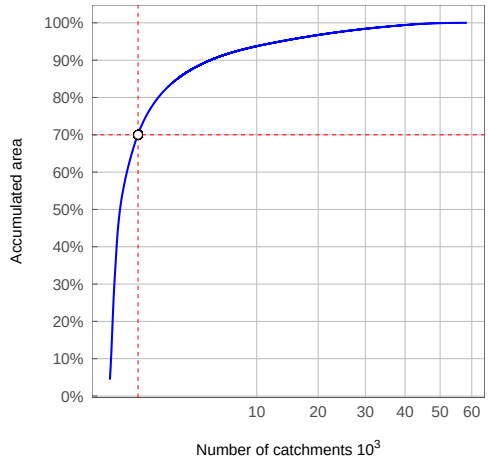

Figure S7.1: Accumulated area vs number of catchments. Dashed lines represent the 70% of the area covered under the 400 largest catchments. This computation does not take into account the Antartic continent, as this area is not included in the HydroBASINS dataset.

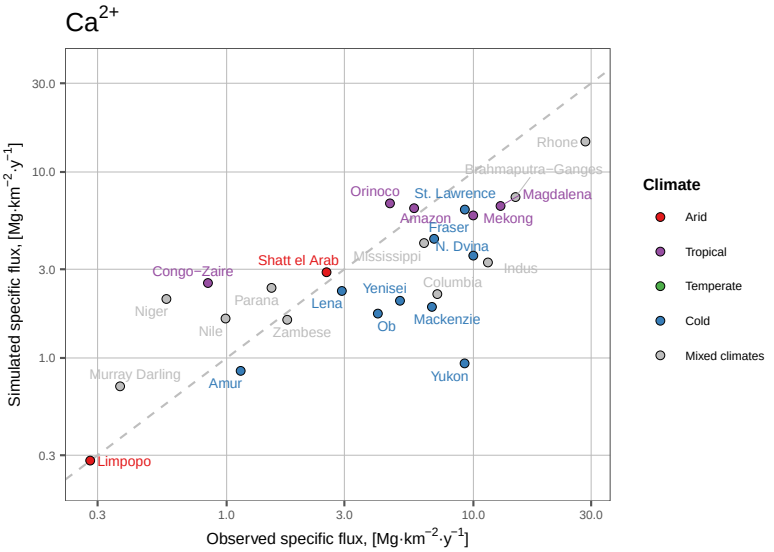

Figure S7.2: Comparison of observed and simulated Ca^{2+} specific fluxes, derived from ICWR modelling and J. L. Probst, 1992 compilation.

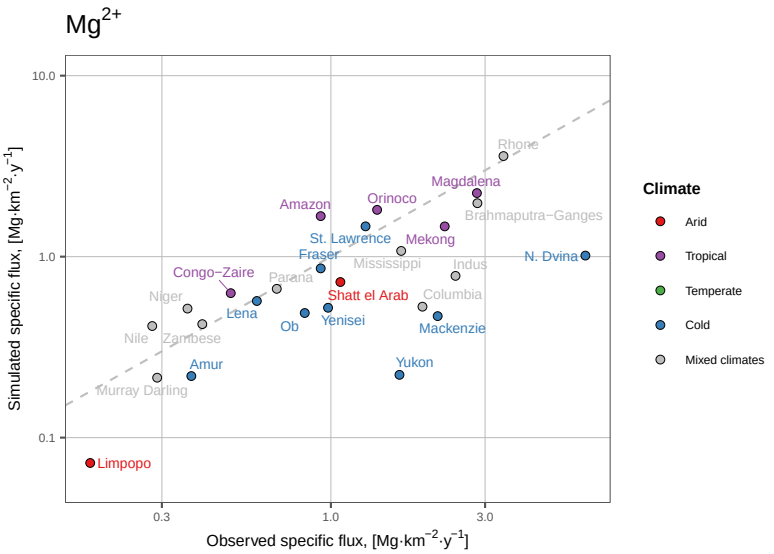

Figure S7.3: Comparison of observed and simulated Mg^{2+} specific fluxes, derived from ICWR modelling and J. L. Probst, 1992 compilation.

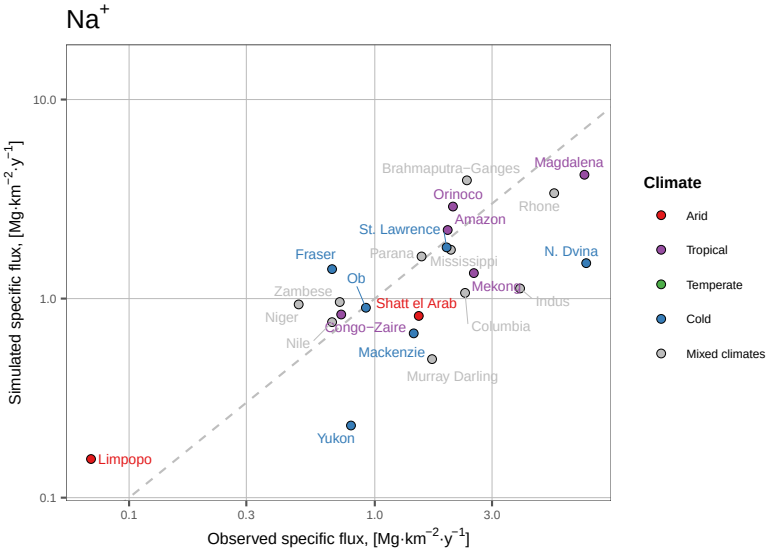

Figure S7.4: Comparison of observed and simulated Na^+ specific fluxes, derived from ICWR modelling and J. L. Probst, 1992 compilation.

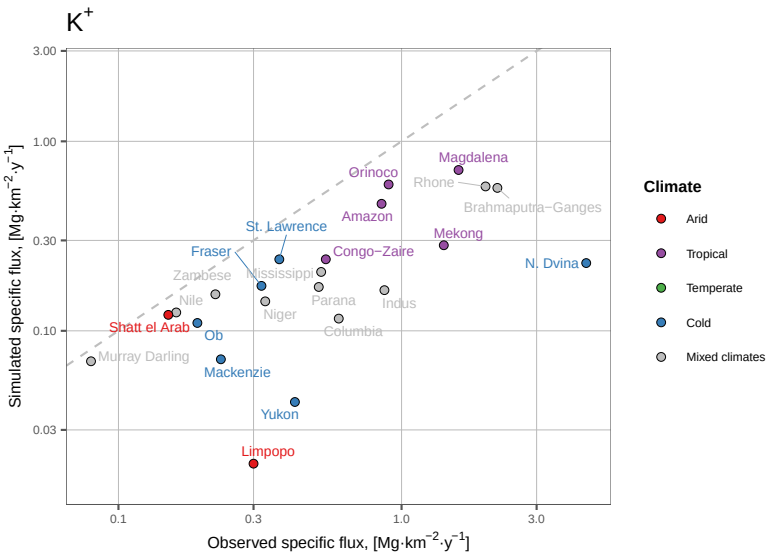

Figure S7.5: Comparison of observed and simulated K^+ specific fluxes, derived from ICWR modelling and J. L. Probst, 1992 compilation.

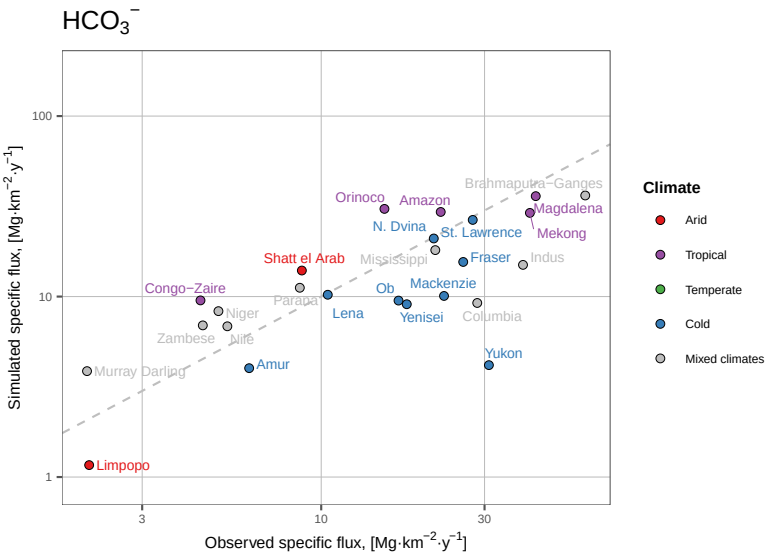

Figure S7.6: Comparison of observed and simulated HCO_3^- specific fluxes, derived from ICWR modelling and J. L. Probst, 1992 compilation.

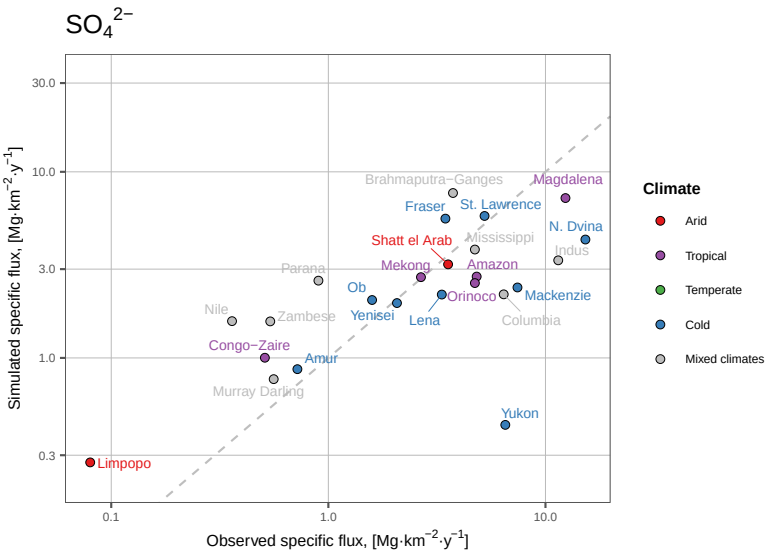

Figure S7.7: Comparison of observed and simulated SO_4^{2-} specific fluxes, derived from ICWR modelling and J. L. Probst, 1992 compilation.

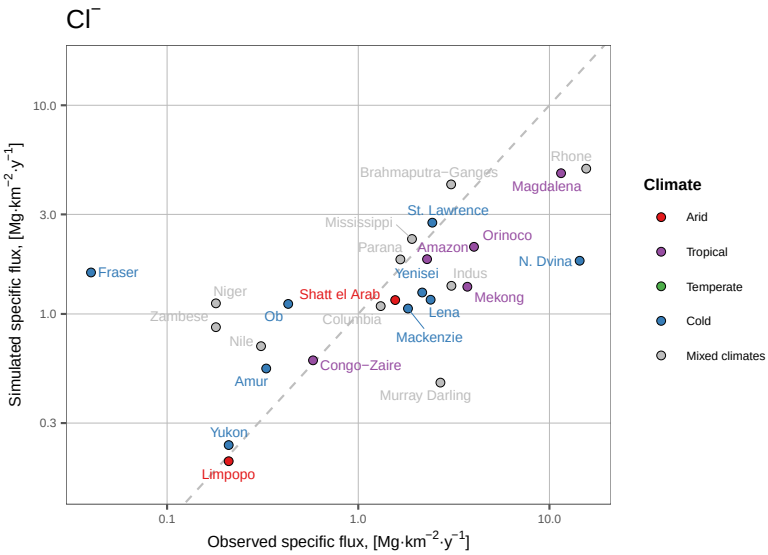

Figure S7.8: Comparison of observed and simulated Cl^- specific fluxes, derived from ICWR modelling and J. L. Probst, 1992 compilation.

Bibliography

Amiotte Suchet, P. (1995). *Cycle du carbone, érosion chimique des continents et transferts vers les océans* (Doctoral dissertation). Université Louis-Pasteur. Strasbourg, Institut de Géologie. https://www.persee.fr/doc/sgeol_0302-2684_1995_mon_97_1

Amiotte Suchet, P., & Probst, J. L. (1993b). Modelling of atmospheric CO2 consumption by chemical weathering of rocks: Application to the Garonne, Congo and Amazon basins. *Chemical Geology*, *107*(3-4), 205–210. https://doi.org/10.1016/0009-2541(93)90174-H

Amiotte Suchet, P., & Probst, J. L. (1995). A global model for present-day atmospheric/soil CO2 consumption by chemical erosion of continental rocks (GEM-CO2). *Tellus B*, *47B*(1-2), 273–280. https://doi.org/10.1034/j.1600-0889.47.issue1.23.x

Amiotte Suchet, P., & Probst, J. L. (1996). Origines du carbone inorganique dissous dans les eaux de la Garonne. Variations saisonnières et interannuelles. / Sources of dissolved inorganic carbon in the Garonne river water. Seasonal and inter

annual variations. *Sciences Géologiques. Bulletin*, *49*(1), 101–126. https://doi.org/10.3406/sgeol.1996.1938

Amiotte Suchet, P., Probst, J. L., & Ludwig, W. (2003). Worldwide distribution of continental rock lithology: Implications for the atmospheric/soil CO2 uptake by continental weathering and alkalinity river transport to the oceans. *Global Biogeochemical Cycles*, *17*(2). https://doi.org/10.1029/2002GB001891

Anderson, S. P., von Blanckenburg, F., & White, A. (2007). Physical and Chemical Controls on the Critical Zone. *Elements*, *3*(5), 315–319. https://doi.org/10.2113/gselements.3.5.315

Aumont, O., Maier-Reimer, E., Blain, S., & Monfray, P. (2003). An ecosystem model of the global ocean including Fe, Si, P colimitations. *Global Biogeochemical Cycles*, *17*(2). https://doi.org/10.1029/2001GB001745

Bao, C., Li, L., Shi, Y., & Duffy, C. (2017). Understanding watershed hydrogeochemistry: 1. Development of RT-Flux-PIHM. *Water Resources Research*, *53*(3), 2328–2345. https://doi.org/10.1002/2016WR018934

Beaulieu, E., Goddéris, Y., Donnadieu, Y., Labat, D., & Roelandt, C. (2012). High sensitivity of the continental-weathering carbon dioxide sink to future climate change. *Nature Climate Change*, *2*(5), 346–349. https://doi.org/10.1038/nclimate1419

Beck, H. E., Zimmermann, N. E., McVicar, T. R., Vergopolan, N., Berg, A., & Wood, E. F. (2018). Present and future Köppen-Geiger climate classification maps at 1-km resolution. *Scientific data*, *5*, 180214. https://doi.org/10.1038/sdata.2018.214

Berner, R. A., Lasaga, A. C., & Garrels, R. M. (1983). The carbonate-silicate geochemical cycle and its effect on atmospheric carbon dioxide over the past 100 million years. *American Journal of Science*, *283*, 641–683. https://doi.org/10.2475/ajs.283.7.641

Bhatt, M. P., Hartmann, J., & Acevedo, M. F. (2018). Seasonal variations of biogeochemical matter export along the Langtang-Narayani river system in central Himalaya. *Geochimica et Cosmochimica Acta*, *238*, 208–234. https://doi.org/10.1016/j.gca.2018.06.033

Boeglin, J. L., & Probst, J. L. (1998). Physical and chemical weathering rates and CO2 consumption in a tropical lateritic environment: the upper Niger basin. *Chemical Geology*, *148*. https://doi.org/10.1016/S0009-2541(98)00025-4

Brantley, S. L., Megonigal, J. P., Scatena, F. N., Balogh-Brunstad, Z., Barnes, R. T., Bruns, M. A., van Cappellen, P., Dontsova, K., Hartnett, H. E., Hartshorn, A. S., Heimsath, A., Herndon, E., Jin, L., Keller, C. K., Leake, J. R., McDowell, W. H., Meinzer, F. C., Mozdzer, T. J., Petsch, S., … Yoo, K. (2011). Twelve testable hypotheses on the geobiology of weathering. *Geobiology*, *9*(2), 140–165. https://doi.org/10.1111/j.1472-4669.2010.00264.x

Calabrese, S., Parolari, A. J., & Porporato, A. (2017). Hydrologic Transport of Dissolved Inorganic Carbon and Its Control on Chemical Weathering. *Journal of Geophysical Research: Earth Surface*, *122*(10), 2016–2032. https://doi.org/10.1002/2017JF004346

Collins, W. J., Bellouin, N., Doutriaux-Boucher, M., Gedney, N., Halloran, P., Hinton, T., Hughes, J., Jones, C. D., Joshi, M., Liddicoat, S., Martin, G., O'Connor, F., Rae, J., Senior, C., Sitch, S., Totterdell, I., Wiltshire, A., & Woodward, S. (2011). Development and evaluation of an Earth-system model – HadGEM2. *Geoscientific Model Development Discussions*, *4*(2), 997–1062. https://doi.org/10.5194/gmdd-4-997-2011

Conant, R. T., Ryan, M. G., Ågren, G. I., Birge, H. E., Davidson, E. A., Eliasson, P. E., Evans, S. E., Frey, S. D., Giardina, C. P., Hopkins, F. M., Hyvönen, R., Kirschbaum, M. U. F., Lavallee, J. M., Leifeld, J., Parton, W. J., Megan Steinweg, J., Wallenstein, M. D., Martin Wetterstedt, J. Å., & Bradford, M. A. (2011). Temperature and soil organic matter decomposition rates - synthesis of current knowledge and a way forward. *Global Change Biology*, *17*(11), 3392–3404. https://doi.org/10.1111/j.1365-2486.2011.02496.x

Delworth, T. L., Broccoli, A. J., Rosati, A., Stouffer, R. J., Balaji, V., Beesley, J. A., Cooke, W. F., Dixon, K. W., Dunne, J., Dunne, K. A., Durachta, J. W., Findell, K. L., Ginoux, P., Gnanadesikan, A., Gordon, C. T., Griffies, S. M., Gudgel, R., Harrison, M. J., Held, I. M., … Zhang, R. (2006). GFDL's CM2 Global coupled climate models. Part I: Formulation and Simulation Characteristics. *American Meteorological Society*, *19*(5), 643–674. https://doi.org/10.1175/JCLI3629.1

Donner, L. J., Wyman, B. L., Hemler, R. S., Horowitz, L. W., Ming, Y., Zhao, M., Golaz, J.-C., Ginoux, P., Lin, S.-J., Schwarzkopf, M. D., Austin, J., Alaka, G., Cooke, W. F., Delworth, T. L., Freidenreich, S. M., Gordon, C. T., Griffies, S. M., Held,

I. M., Hurlin, W. J., … Zeng, F. (2011). The Dynamical Core, Physical Parameterizations, and Basic Simulation Characteristics of the Atmospheric Component AM3 of the GFDL Global Coupled Model CM3. *Journal of Climate*, *24*(13), 3484–3519. https://doi.org/10.1175/2011JCLI3955.1

Donnini, M., Frondini, F., Probst, J. L., Probst, A., Cardellini, C., Marchesini, I., & Guzzetti, F. (2016). Chemical weathering and consumption of atmospheric carbon dioxide in the Alpine region. *Global and Planetary Change*, *136*, 65–81. https://doi.org/10.1016/j.gloplacha.2015.10.017

Dufresne, J.-L., Foujols, M.-A., Denvil, S., Caubel, A., Marti, O., Aumont, O., Balkanski, Y., Bekki, S., Bellenger, H., Benshila, R., Bony, S., Bopp, L., Braconnot, P., Brockmann, P., Cadule, P., Cheruy, F., Codron, F., Cozic, A., Cugnet, D., … Vuichard, N. (2013). Climate change projections using the IPSL-CM5 Earth System Model: from CMIP3 to CMIP5. *Climate Dynamics*, *40*(9-10), 2123–2165. https://doi.org/10.1007/s00382-012-1636-1

Dupré, B., Dessert, C., Oliva, P., Goddéris, Y., Viers, J., François, L. M., Millot, R., & Gaillardet, J. (2003). Rivers, chemical weathering and Earth's climate. *Comptes Rendus Geoscience*, *335*(16), 1141–1160. https://doi.org/10.1016/j.crte.2003.09.015

Eckhardt, K. (2005). How to construct recursive digital filters for baseflow separation. *Hydrological Processes*, *19*(2), 507–515. https://doi.org/10.1002/hyp.5675

FAO, IIASA, ISRIC, ISS-CAS, & JRC. (2012). Harmonized World Soil Database (version 1.2). http://www.fao.org/soils-portal/soil-survey/soil-maps-and-databases/harmonized-world-soil-database-v12/en/

Gaillardet, J., Calmels, D., Romero-Mujalli, G., Zakharova, E., & Hartmann, J. (2019). Global climate control on carbonate weathering intensity. *Chemical Geology*, *527*, 118762. https://doi.org/10.1016/j.chemgeo.2018.05.009

Gaillardet, J., Dupré, B., Louvat, P., & Allègre, C. J. (1999). Global silicate weathering and CO2 consumption rates deduced from the chemistry of large rivers. *Chemical Geology*, *159*, 3–30. https://doi.org/10.1016/S0009-2541(99)00031-5

Garrels, R. M., & Mackenzie, F. T. (1971). *Evolutions of sedimentary Rocks*. W.W. Norton, New York.

Goddéris, Y., & Brantley, S. L. (2013). Earthcasting the future Critical Zone. *Elementa: Science of the Anthropocene*, *1*, 000019. https://doi.org/10.12952/journal.elementa.000019

Goddéris, Y., François, L. M., Probst, A., Schott, J., Moncoulon, D., Labat, D., & Viville, D. (2006). Modelling weathering processes at the catchment scale: The WITCH numerical model. *Geochimica et Cosmochimica Acta*, *70*(5), 1128–1147. https://doi.org/10.1016/j.gca.2005.11.018

Hartmann, J., Jansen, N., Dürr, H. H., Kempe, S., & Köhler, P. (2009). Global CO2-consumption by chemical weathering: What is the contribution of highly active weathering regions? *Global and Planetary Change*, *69*(4), 185–194. https://doi.org/10.1016/j.gloplacha.2009.07.007

Hartmann, J., & Moosdorf, N. (2012). The new global lithological map database GLiM: A representation of rock properties at the Earth surface. *Geochemistry, Geophysics, Geosystems*, *13*(12). https://doi.org/10.1029/2012GC004370

Hartmann, J., Moosdorf, N., Lauerwald, R., Hinderer, M., & West, A. J. (2014). Global chemical weathering and associated P-release — The role of lithology, temperature and soil properties. *Chemical Geology*, *363*, 145–163. https://doi.org/10.1016/j.chemgeo.2013.10.025

IPCC. (2013). Climate Change 2013: The Physical Science Basis. Contribution of Working Group I to the Fifth Assessment Report of the Intergovernmental Panel on Climate Change (T. F. Stocker, D. Qin, G.-K. Plattner, M. Tignor, S. K. Allen, J. Boschung, A. Nauels, Y. Xia, V. Bex, & P. M. Midgley, Eds.). https://www.ipcc.ch/report/ar5/wg1/

Iversen, T., Bentsen, M., Bethke, I., Debernard, J. B., Kirkevåg, A., Seland, Ø., Drange, H., Kristjansson, J. E., Medhaug, I., Sand, M., et al. (2013). The Norwegian Earth System Model, NorESM1-M–Part 2: Climate response and scenario projections, Geosci. Model Dev., 6, 389–415.

Kessler, T. J., & Harvey, C. F. (2001). The global flux of carbon dioxide into groundwater. *Geophysical Research Letters*, *28*(2), 279–282. https://doi.org/10.1029/2000GL011505

Lechuga-Crespo, J. L., Ruiz-Romera, E., Sánchez-Pérez, J. M., George, C., & Sauvage, S. (Under Review). SWATLitho: a hydrogeochemical model to estimate daily geochemical loads at catchment scale.

Lechuga-Crespo, J. L., Sánchez-Pérez, J. M., Sauvage, S., Hartmann, J., Amiotte Suchet, P., Probst, J. L., & Ruiz-Romera, E. (2020). A model to evaluate chemical weathering from riverine transports of dissolved major elements at global scale. *Global and Planetary Change*, *192*. https://doi.org/10.1016/j.gloplacha.2020.103226

Lehner, B., & Grill, G. (2013). Global river hydrography and network routing: baseline data and new approaches to study the world's large river systems. *Hydrological Processes*, *27*(15), 2171–2186. https://doi.org/10.1002/hyp.9740

Li, L., Maher, K., Navarre-Sitchler, A., Druhan, J., Meile, C., Lawrence, C., Moore, J., Perdrial, J., Sullivan, P., Thompson, A., Jin, L., Bolton, E. W., Brantley, S. L., Dietrich, W. E., Mayer, K. U., Steefel, C. I., Valocchi, A., Zachara, J., Kocar, B., … Beisman, J. (2017). Expanding the role of reactive transport models in critical zone processes. *Earth-Science Reviews*, *165*, 280–301. https://doi.org/10.1016/j.earscirev.2016.09.001

Liang, X., Lettenmaier, D. P., Wood, E. F., & Burges, S. J. (1994). A simple hydrologically based model of land surface water and energy fluxes for general circulation models. *Journal of Geophysical Research*, *99*(D7), 14415–14428. https://doi.org/10.1029/94JD00483

Liu, Z., Dreybrodt, W., & Wang, H. (2010). A new direction in effective accounting for the atmospheric CO2 budget: Considering the combined action of carbonate dissolution, the global water cycle and photosynthetic uptake of DIC by aquatic organisms. *Earth-Science Reviews*, *99*(3-4), 162–172. https://doi.org/10.1016/j.earscirev.2010.03.001

Lohmann, D., Raschke, E., Nijssen, B., & Lettenmaier, D. P. (1998). Regional scale hydrology: I. Formulation of the VIC-2L model coupled to a routing model. *Hydrological Sciences Journal*, *43*(1), 131–141. https://doi.org/10.1080/02626669809492107

Maher, K., & Chamberlain, C. P. (2014). Hydrologic regulation of chemical weathering and the geologic carbon cycle. *Science*, *343*(6178), 1502–1504. https://doi.org/10.1126/science.1250770

Martin, G. M., Bellouin, N., Collins, W. J., Culverwell, I. D., Halloran, P. R., Hardiman, S. C., Hinton, T. J., Jones, C. D., McDonald, R. E., McLaren, A. J., O'Connor, F. M., Roberts, M. J., Rodriguez, J. M., Woodward, S., Best, M. J., Brooks, M. E., Brown, A. R., Butchart, N., Dearden, C., … Wiltshire, A. (2011). The HadGEM2 family of Met Office Unified Model climate configurations. *Geoscientific Model Development*, *4*, 723–757. https://doi.org/10.5194/gmd-4-723-2011

McClain, M. E., Boyer, E. W., Dent, C. L., Gergel, S. E., Grimm, N. B., Groffman, P. M., Hart, S. C., Harvey, J. W., Johnston, C. A., Mayorga, E., McDowell, W. H., & Pinay, G. (2003). Biogeochemical Hot Spots and Hot Moments at the Interface of Terrestrial and Aquatic Ecosystems. *Ecosystems*, *6*(4), 301–312. https://doi.org/10.1007/s10021-003-0161-9

Meybeck, M. (1987). Global chemical weathering of surficial rocks estimated from river dissolved loads. *American Journal of Science*, *287*, 401–428. https://doi.org/10.2475/ajs.287.5.401

Moosdorf, N., Hartmann, J., Lauerwald, R., Hagedorn, B., & Kempe, S. (2011). Atmospheric CO2 consumption by chemical weathering in North America. *Geochimica et Cosmochimica Acta*, *75*(24), 7829–7854. https://doi.org/10.1016/j.gca.2011.10.007

Moquet, J.-S., Guyot, J.-L., Crave, A., Viers, J., Filizola, N., Martinez, J.-M., Oliveira, T. C., Sánchez, L. S. H., Lagane, C., Casimiro, W. S. L., Noriega, L., & Pombosa, R. (2016). Amazon River dissolved load: temporal dynamics and annual budget from the Andes to the ocean. *Environmental science and pollution research international*, *23*(12), 11405–11429. https://doi.org/10.1007/s11356-015-5503-6

Mortatti, J., & Probst, J.-L. (2003). Silicate rock weathering and atmospheric/soil CO2 uptake in the Amazon basin estimated from river water geochemistry: seasonal and spatial variations. *Chemical Geology*, *197*(1-4), 177–196. https://doi.org/10.1016/S0009-2541(02)00349-2

Munhoven, G. (2002). Glacial-interglacial changes of continental weathering: estimates of the related CO2 and HCO3 flux variations and their uncertainties. *Global and Planetary Change*, *33*, 155–176. https://doi.org/10.1016/S0921-8181(02)00068-1

Nkounkou, R. R., & Probst, J. L. (1987). Hydrology and geochemistry of the Congo river system. *SCOPE/UNEP-Sonderband*, *64*, 483–508.

Probst, J. L. (1992). *Géochimie et hydrologie de l'érosion continentale. Mécanismes, bilan global actuel et fluctuations au cours des 500 derniers millions d'années.* (Doctoral dissertation). Université Louis-Pasteur. Strasbourg, Institut de Géologie. www.persee.fr/doc/sgeol_0302-2684_1992_mon_94_1

Probst, J. L., Ludwig, W., & Amiotte Suchet, P. (1997). Global modeling of CO2 uptake by continental erosion and of carbon river transport to the oceans. / Modélisation à l'échelle globale des flux de CO2 consommé par l'érosion continentale et des transports fluviaux de carbone vers les océans. *Sciences Géologiques. Bulletin*, *50*(1), 131–156. https://doi.org/10.3406/sgeol.1997.1950

Probst, J. L., Mortatti, J., & Tardy, Y. (1994). Carbon river fluxes and weathering CO2 consumption in the Congo and Amazon river basins. *Applied Geochemistry*, *9*, 1–13. https://doi.org/10.1016/0883-2927(94)90047-7

Richter, D., & Markewitz, D. (1995). How deep is soil? *Bioscience*, *45*(9), 600–609. https://doi.org/10.2307/1312764

Richter, D., & Markewitz, D. (2001). Understanding soil change: Soil sustainability over millennia, centuries, and decades. https://doi.org/10.1046/j.1526-100X.2003.01112.x

Rosentreter, J. A., & Eyre, B. D. (2020). Alkalinity and dissolved inorganic carbon exports from tropical and subtropical river catchments discharging to the Great Barrier Reef, Australia. *Hydrological Processes*, *34*(7), 1530–1544. https://doi.org/10.1002/hyp.13679

Streletskiy, D., Anisimov, O., & Vasiliev, A. (2015). Permafrost Degradation, 303–344. https://doi.org/10.1016/B978-0-12-394849-6.00010-X

Toohey, R. C., Herman-Mercer, N. M., Schuster, P. F., Mutter, E. A., & Koch, J. C. (2016). Multidecadal increases in the Yukon River Basin of chemical fluxes as indicators of changing flowpaths, groundwater, and permafrost. *Geophysical Research Letters*, *43*(23), 12, 120–12, 130. https://doi.org/10.1002/2016GL070817

van Vliet, M. T. H., Franssen, W. H., Yearsley, J. R., Ludwig, F., Haddeland, I., Lettenmaier, D. P., & Kabat, P. (2013). Global river discharge and water temperature

under climate change. *Global Environmental Change*, *23*(2), 450–464. https://doi.org/10.1016/j.gloenvcha.2012.11.002

van Vliet, M. T. H., van Beek, L., Eisner, S., Flörke, M., Wada, Y., & Bierkens, M. (2016). Multi-model assessment of global hydropower and cooling water discharge potential under climate change. *Global Environmental Change*, *40*, 156–170. https://doi.org/10.1016/j.gloenvcha.2016.07.007

van Vliet, M. T. H., Wiberg, D., Leduc, S., & Riahi, K. (2016). Power-generation system vulnerability and adaptation to changes in climate and water resources. *Nature Climate Change*, *6*, 375–380. https://doi.org/10.1038/NCLIMATE2903

van Vliet, M. T. H., Yearsley, J. R., Franssen, W. H., Ludwig, F., Haddeland, I., Lettenmaier, D. P., & Kabat, P. (2012). Coupled daily streamflow and water temperature modelling in large river basins. *Hydrology and Earth System Sciences*, *16*(11), 4303–4321. https://doi.org/10.5194/hess-16-4303-2012

van Vuuren, D. P., Edmonds, J., Kainuma, M., Riahi, K., Thomson, A., Hibbard, K., Hurtt, G. C., Kram, T., Krey, V., Lamarque, J.-F., Masui, T., Meinshausen, M., Nakicenovic, N., Smith, S. J., & Rose, S. K. (2011). The representative concentration pathways: an overview. *Climatic Change*, *109*(1-2), 5–31. https://doi.org/10.1007/s10584-011-0148-z

Watanabe, S., Hajima, T., Sudo, K., Nagashima, T., Takemura, T., Okajima, H., Nozawa, T., Kawase, H., Abe, M., Yokohata, T., Ise, T., Sato, H., Kato, E., Takata, K., Emori, S., & Kawamiya, M. (2011). MIROC-ESM 2010: model description and basic results of CMIP5-20c3m experiments. *Geoscientific Model Development*, *4*(4), 845–872. https://doi.org/10.5194/gmd-4-845-2011

Xie, J., Liu, X., Wang, K., Yang, T., Liang, K., & Liu, C. (2020). Evaluation of typical methods for baseflow separation in the contiguous United States. *Journal of Hydrology*, *583*, 124628. https://doi.org/10.1016/j.jhydrol.2020.124628

Yearsley, J. R. (2009). A semi-Lagrangian water temperature model for advection-dominated river systems. *Water Resources Research*, *45*(12). https://doi.org/10.1029/2008WR007629

Part IV

CONCLUSION

CHAPTER 8

General discussion

The role of chemical weathering on the matter transfer between rocks and water, considering its major ion constituents, is of interest for Earth scientists researching on biogeochemical cycling at past, current and future epochs (Aufdenkampe et al., 2011; Lupker et al., 2013; Parsekian et al., 2015); for oceanographers studying the oceanic cycling of elements (e.g. Sun et al., 2016; Tréguer and de La Rocha, 2013); for ecologists quantifying wetland dynamics (Day et al., 2008); for hydro-chemists evaluating water composition in rivers (Balagizi et al., 2015; Stallard & Edmond, 1987); and stakeholders for resource management and policymaking in catchments (Meybeck, 2003). All these agents have geochemical modelling tools to complement their field and laboratory approaches to study chemical weathering and assess its influence on their study area, but detailed data is needed to implement such tools, becoming a common challenge for modellers. Such a challenge becomes a barrier when the study area is a large spatial

scale, such as in Earth System analysis, due to the lack of input databases at such spatial scale and to the computational resources needed to carry this modelling exercise. Despite of the great effort put in recent years on creating these global databases, there is still work to do in compiling data, especially on describing the Critical Zone in terms of physical variables such as porosity, and chemical variables like mineralogical description (Parsekian et al., 2015). An alternative to physical modelling is the empirical modelling approach which, despite the larger uncertainties on their results, have been proven useful in identifying hot spots and hot moments to focus research or attention (McClain et al., 2003).

In the present work, an empirical model on chemical weathering to estimate major ionic riverine fluxes has been developed, its performance has been tested on different spatial and temporal scales, it has been coupled to a physically-based hydrological model, and applied to identify hot spots and hot moments of mass transfer between rock and water, as well as its implication on the C cycle in climate change scenarios. The objective in this section is to discuss the conceptualization of the model, the insights derived from the modelling approach, the applicability, and the limits of the developed tool. This chapter is divided in four sections:

- Section 8.1 discusses the conceptualization of chemical weathering model.
- Section 8.2 covers the role of hydrology on the modelling approach.
- Section 8.3 focuses on the model's performance at different spatial and temporal scales.
- Section 8.4 emphasis the applicability of the model at the global scale to evaluate the role of chemical weathering on the global carbon cycle.

8.1 Model development: chemical weathering conceptualization

Chemical weathering has been the main geochemical process studied in the present PhD thesis, responsible for the chemical decomposition of bedrock into soil, as well as of the major chemical composition found in rivers at the basin scale (Gibbs, 1970; Parsekian et al., 2015). Particularly, focus has been put into estimating the delivery of major ions — Ca^{2+}, Mg^{2+}, Na^{+}, K^{+}, SO_4^{2-}, Cl^{-}, and alkalinity— to water, as well as into assessing its role on biogeochemical cycles across spatial and temporal scales. The conceptualization of this process and the transport of matter is displayed on Figure 8.1, similar to that published by S. P. Anderson et al. (2007). Water arrives to the system through precipitation, leaves it through evapotranspiration, and percolates depending on hydrology and soil types, part of which reaches the unsaturated and saturated zone, where it reacts with minerals delivering ions to groundwater and, subsequently to the river. Distinction between congruent and incongruent reactions have not been distinguished in the present modelling approach, since the study of these reactions requires a higher degree of complexity on the model structure — following a closer approach as those in mechanistic modelling — where not only primary dissolution is computed, but secondary products are considered as well, as done in physically based models such as PHREEQC (Parkhurst, 1995; Parkhurst & Appelo, 2013). In contrast, a black-box approach has been considered, where water composition is function of the soil and lithological abundance, as well as of the amount of water entering and exiting the critical zone.

Along the model development process, several insights have been confirmed and generated. Firstly, the global-to-local approach followed in the present study has confirmed the long recognised key factors regarding chemical weathering at the global scale: hydrology, lithology, and soil (Amiotte Suchet & Probst, 1995; Gaillardet et al., 1999; Garrels & Mackenzie, 1972; Hartmann et al., 2009; Meybeck, 1986). Despite of considering other variables such as temperature, hydraulic conductivity, or regolith

thickness, their inclusion could not be successfully achieved because, either failure at establishing the hypothesis on how these variables influence the process, either they are secondary key factors in the processes considered, and their influence is heterogeneous between systems. Secondly, the change in the temporal consideration, from a spatially explicit static to a dynamic approach, allowed to confirm the relevance of discharge and its deconvolution on the temporal variability found at the outlet of the basins. The assumption of a stable concentration on the groundwater has been considered after the conclusions of several previous studies (Maher, 2010, 2011; Maher & Chamberlain, 2014), which have highlighted the common transport limited chemical weathering rates of rivers. Such an assumption allowed the establishment of three different periods depending on the hydrological regime, which are further discussed in section 8.2. These two steps in the model development process have allowed the establishment of the conceptual model described on Figure 8.1, for application at global scale studies. At the critical zone scale, the chemical weathering rate may be averaged through differentiation on lithological classes, bearing in mind the soil units responsible for the soil shielding effect (Hartmann, Moosdorf, et al., 2014). Considering these reactions between the solid rock and liquid water phases stable in time, the amount of dissolved matter found in the river water is a function of hydrology.

The spatial and temporal evaluation of the model performance has allowed to confirm that, at the global scale, the water composition is conditioned mainly by physical variables such as lithological classes and soil units, while the ionic fluxes depend on the hydrological evolution. Hot spots are found in sensible lithologies covered by not-shielding soil units (Lechuga-Crespo, Sánchez-Pérez, et al., 2020, Chapter 4). Three main kinds of rocks may be distinguished: evaporites, carbonates, and silicates (Gaillardet et al., 1999), according to their resistance to chemical weathering. Their mineralogical composition implies a large heterogeneity regarding elements conforming their solid structure, elements which are delivered to water as ions. Thus, different lithological compositions yield different salinities and water major composition. The model developed in the present study does not take into account minerals, but groups of minerals instead, in form of lithological classes (Dürr et al., 2005; Hartmann & Moosdorf, 2012), a commonly used simplification which allows for its application to large

spatial scales, thus for the identification of hot spots and hot moments, of interest in biogeochemical cycling studies (McClain et al., 2003). Understanding not only the Total Dissolved Solids (TDS) loadings but the different ionic contribution of each lithological groups poses an opportunity for characterising the chemical composition of natural waters, and for assessing the role of chemical weathering in other biogeochemical cycles, such as the carbon cycle (Amiotte Suchet, 1995).

The conceptual approach followed in this study is a simplification of the complex system found in the critical zone. At the basin scale, it is possible to found differences on the relative contributions, both spatially and temporally, depending on other variables which have not been able to be included at the present development, but which may pose a relevant contribution to the chemical weathering assessment at the local study. Such contribution has been highlighted when downscaling the model at a local case study, where evaporitic springs were present implying a point source contribution controlling major ion chemistry in the river (see Chapter 5, Lechuga-Crespo, Ruiz-Romera, Probst, et al., 2020) which was not well captured by the model. Despite of the simple approach followed in the conceptualization of the processes, the results presented in this PhD thesis are relevant for global scale assessments of biogeochemical cycles, land-to-ocean matter assessments, and chemical weathering studies. This model is also interesting for its application at lower scales where the availability of input data is scarce, increasing the difficulty of establishing a mechanistic approach, and the need for an exploratory assessment is present.

8.2 Model validation: The role of hydrology on geochemical fluxes

Hydrology has been repeatedly noted as a key factor when assessing chemical weathering rates (Amiotte Suchet, 1995; Hartmann et al., 2009; Stallard & Edmond, 1987). In the critical zone, water is the liquid phase that acts as a reagent in the geochemical processes (dissolution, redox, ion exchange, etc.), as well as the vector of transport for

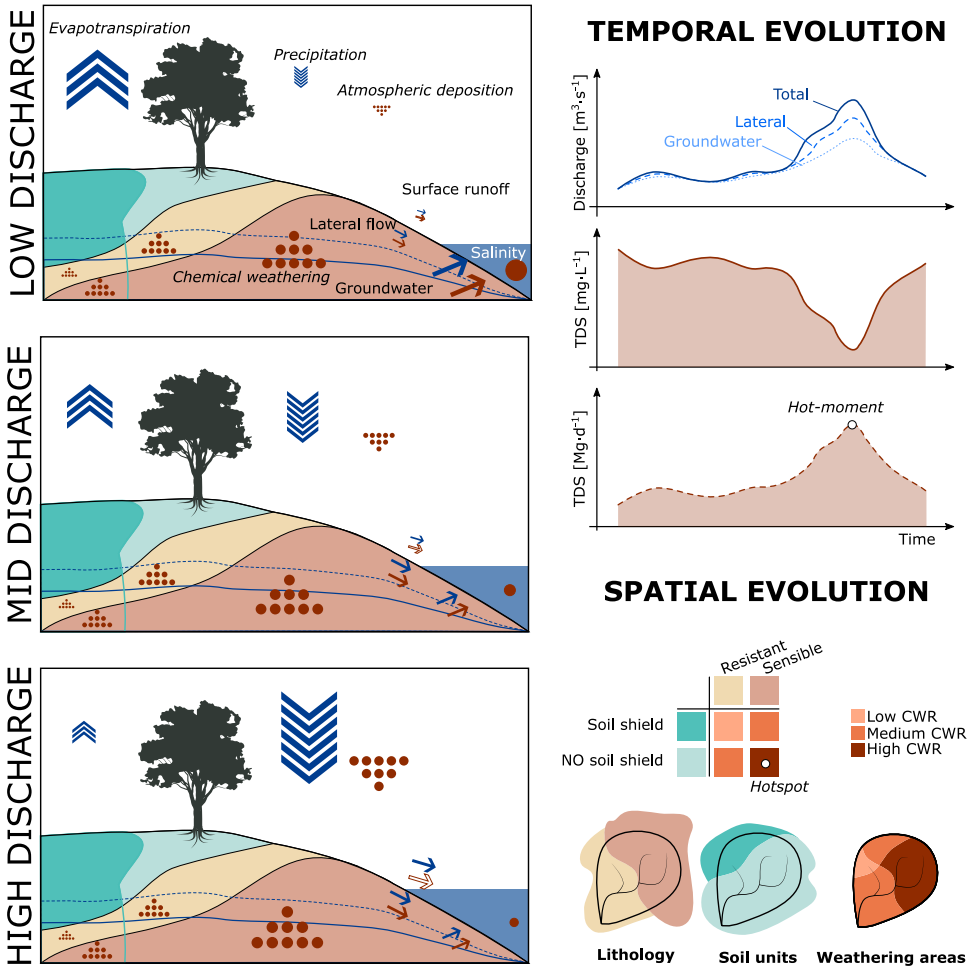

Figure 8.1: Conceptualization of the chemical processes (italics), water fluxes (straight), and river characteristics (white straight) considered in this study in the critical zone level under three periods (low, mid and high discharge). Temporal and spatial evolution are displayed on the right side of the image, highlighting the role of water deconvolution on dilution (TDS concentration) and on saline exports (TDS loads). A hot moment and hot spot is identified on the time series and on the map. Two physical characteristics are used to discretize the weathering units: lithology and soil units.

the solutes retrieved from rocks. In the present study, steady state of the geochemical processes is assumed, hence the temporal evolution of ionic concentration derived from chemical weathering is a function of hydrology. Such assumption has yielded large discrepancies in some local cases (Chapter 4) suggesting that, in these cases, detailed studies are needed to be performed at a basin-to-basin scale in order to understand the role of hydrology. In such systems the water transit time may be lower than the time needed to reach chemical equilibrium among phases, thus there is a kinetically dominated chemical weathering (Calabrese et al., 2017), explaining the poorer performance of the model. However, the strong and significant correlation found at the global scale (Lechuga-Crespo, Sánchez-Pérez, et al., 2020, Chapter 4), considering all ions and median values, suggests that considering larger transit times in comparison to chemical equilibrium times is generally valid at a global and annual scale. Thus, chemical composition is commonly transport dependent, i.e. dominated by water advection (Maher & Chamberlain, 2014) and, in these cases, the model's performance is better, suggesting that temporal downscaling needs an accurate description of hydrology.

Transport limited chemical weathering implies that riverine ionic fluxes are function of hydrology, directly depending on the water percolating into the weathering zone or leaving it as baseflow (Calabrese et al., 2017). In the present study, a simplification of the hydrological cycle has been performed by considering that other components of the hydrological cycle (such as surface runoff) increase the water discharge in the river but do not alter the total ionic load leaving the basin. Considering this approach when downscaling the model from the annual to the daily timescale, both the riverine composition and the dissolved exports assessments need the estimation of the baseflow. There are numerous mathematical ways of deconvoluting the hydrograph (i.e. distinguishing the surface, sub-surface, and groundwater time series) such as physically-based hydrological modelling or digital filters. Hydrological models face the same challenge as geochemical models when applying them at a large scale: the need of detailed input data. In contrast, digital filters are based on observed time series and fewer parameters. In the present study, both approaches have been followed: the Soil and Water Assessment Tool (SWAT, Arnold, Williams, et al., 1995) code as a physically-based model, and the Eckhardt deconvolution as a digital filter (Eckhardt, 2005).

The SWAT code is based on a water balance performed at the daily time scale, using a semi-distributed spatial approach, where space is discretized based on slope, land use, and soil units in the catchment to generate the Hydrological Response Units (HRUs) (Arnold et al., 2012). Here, we have modified the spatial discretization by including a fourth layer —the lithological groups— that allows for a finer spatial classification (QSWATLitho, Chapter 6). Despite of the higher resolution derived from a larger number of spatial units, the water balance calculation for each of these units has not been modified. Instead, the new spatial discretization has allowed the definition of monolithological units (each new defined HRU), where the ionic fluxes derived from chemical weathering of rocks have been computed and routed to the main channel (see Chapter 6).

SWAT separates the water balance into surface runoff, lateral flow, and groundwater flow (Arnold, Williams, et al., 1995) and, since chemical weathering is found in the belowground layers of the critical zone, it is the sum of the groundwater and lateral flow which discharges dissolved solids to the river stream. In contrast, surface runoff is diluted in comparison with the other two fluxes, thus responsible for diluting the concentration in the river stream. Many other hydrological models are available, such as MIKE-SHE, TOPMODEL, VIC (Devi et al., 2015), where the ICWR model could have been coupled to. The choice of using SWAT has been based on the balance between input data needs, computational resources needed, and the widespread use of this model in research (Fu et al., 2019).

The application of the SWATLitho module at the daily time step using the SWAT hydrological deconvolution in a local scale project (the Deba basin) has been proven limited when other geochemical processes (such as the presence of evaporitic saline inputs) condition the water composition, yielding mean BIAS of 60%. However, a much lower discrepancy is obtained when evaporitic springs are not present, such as in the Oñati tributary (mean 13% of BIAS). Considering the large scale at which the model's parameters have been fitted, the local scale results are considered as satisfactory, even though finer results are probably obtained when using a physically based modelling approach, such as that recently presented by Bailey et al. (2019) if the input data were

available.

The application of the Eckhardt digital filter has long been used for hydrograph deconvolution, and its applicability in large scale studies has recently been assessed (Xie et al., 2020) as suitable. This method is based on the groundwater outflow being a linear function of the previous water content, thus there is a linearity between these two signals, and this allows for the distribution between hydrological fluxes. The comparison of the ionic fluxes derived from applying a digital filter deconvolution in a local case study are comparable with those derived from the SWATLitho. This comparability suggests that despite of loosing spatial resolution on the hydrological description, the digital filter is a suitable method to compute the hydrological deconvolution, which allows for the estimation of fluxes when the physical model set up is not possible.

These insights derived from the local case study support the three-periods differentiation based on the hydrological conditions established in the model conceptualization. Regarding ionic fluxes in rivers in the three annual periods considered. The *low discharge* period is characterised by a lower total (riverine) discharge, which is mainly composed of concentrated groundwater flux, representing the highest concentration, but not implying higher loadings. On *mid discharge* period, the relative amount of the groundwater flux in the river is decreased by a higher lateral (sub surface) flow. At *high discharge* period, despite of presenting the moment with highest dilution caused by a largest input of surface runoff, the total load is considered as largest. The relevance of diluted surface runoff increases in mid and high discharge periods where, even though lower concentration values are found, highest exports are derived from largest groundwater contribution (hot moments). This is more clearly seen in the local study considered in the present analysis (Lechuga-Crespo, Ruiz-Romera, Probst, et al., 2020), where the three hydrological periods have shown different patterns regarding water composition, and relevant relative importance regarding dissolved loading in the decreasing branch of flood events (mid-discharge periods), related to a larger input from groundwater concentrated water.

8.3 Downscaling: Modelling chemical weathering at different spatial and temporal scales

The assessment of chemical weathering products and their implication on water composition and ionic fluxes is a complex task regarding the large number of variables, parameters, and functions in terms of chemical equilibrium vs transport processes (S. P. Anderson et al., 2004; Goddéris & Brantley, 2013; Goddéris et al., 2009). Mechanistic models accurately estimate the state and evolution of these processes following physical laws, but the coupling of equilibrium and transport models at large scales is challenging, both due to computational costs (Goddéris & Brantley, 2013) and input data availability. In contrast, parametric laws require less computational costs and, despite of carrying a larger uncertainty, their results yield useful insights. In the present study, an empirical model has been developed at a global scale and tested on regional and local scale, both at annual, seasonal, monthly, and daily time-steps. In addition, the results suggest that the simple regression developed is an efficient tool to compute ionic fluxes, showing that the use of lithological classifications is a suitable alternative when the mineralogical description needed for physically based model set up is not available.

The training data used to fit the model's parameters account for 1751 basins distributed worldwide, with a draining area ranging from 1 to $2.9 \cdot 10^4$ km^2, presenting a better performance (PBIAS$<$20%) at the annual scale for the 10 to 10^4 km^2 basins. Considering that among the basins included in the analysis there is a large heterogeneity, it has been assumed that the model is applicable at any location of the Earth surface, yielding the first spatially explicit distributed map on ionic fluxes derived from chemical weathering of rocks, at a resolution of 0.5x0.5º (around 3000 km^2 in the Equator) (c.f. Chapter 4). Such assumption has been tested in a local (Deba catchment) case study, yielding heterogeneous results when contrasting them with monitoring data. Such difference on the model's performance avoids the hypothesis to be fully tested, a closer and finer look is needed. Initially, the different model's performance is attributed to either the hydrological representation (consisting on one single registry at the outlet) where

the contribution of several parts of the basin is overestimating the total flux, either the spatial resolution of the lithological classes.

Aiming at testing which of these variables has a larger effect when spatially downscaling the model, a local study contrasted the results using several hydrological and lithological input data. The comparison resulted in closer results to reality when using local lithological and hydrological data. Regarding lithology, the use of the Global Lithological Map (GLIM, Hartmann and Moosdorf, 2012) discretize the space in 3 main lithological classes, while the use of a finer map results in 10 different lithologies. In fact, the fluxes derived from the local lithological map are about half of those obtained from the global input data, suggesting that the global scale dataset is scarce when applying the model at the local scale, a finer resolution input data is needed. A similar insight is derived when contrasting the effect of hydrology, where the derived fluxes from the global hydrological input data are close to those obtained from the local hydrological information, as do the specific discharge values (∼10% difference between model set-ups). These insights support the linear impact of hydrology, as concluded in the GEM-CO2 model (Amiotte Suchet & Probst, 1995), and by Hartmann, 2009 –for the case of carbon–, and direct but non-homogeneous effect of lithology on ionic fluxes like in Hartmann, Moosdorf, et al. (2014) model configuration on chemical weathering rates, as opposed to the GEM-CO2 model.

Initially, the ICWR model was calibrated at an annual scale, using the median value of all samples within a sampling location. However, the temporal evolution of ionic fluxes is of interest for characterising the riverine endmember in estuarine dynamics (Tueros et al., 2008) and for biogeochemical scientists focusing in riverine exports to other water bodies (such as lakes, estuaries, or oceans) (Chapra et al., 2012). In this sense, the performance of the model under a dynamic approach (considering temporal evolution) has been tested following a cascade modelling tactic: first, the hydrology in the system is studied distinguishing among surface, lateral, and groundwater flow; second, the ionic flux derived from chemical weathering of rocks is estimated; lastly, the routing is computed. Under the local case study, using the temporal evolution has allowed us to estimate the limits of the model application. When there are not external

forces, e.g. evaporitic saline springs input, the model at the local scale is able to estimate mean ionic fluxes with a PBIAS <13% which, considering the rather simple approach of the model, it's a fair starting point for hydrogeochemical modelling.

Considering the results from the analysis, the global fluxes derived from chemical weathering of rocks amount to $3374 \cdot 10^6$ $Mg \cdot y^{-1}$, being within the range of previous studies (Gaillardet et al., 1999; Meybeck, 1979; J. L. Probst, 1992) even though larger than the most recent assessment (Hartmann, Moosdorf, et al., 2014, further discussed in Chapter 4). Focusing on the regional scales (results derived from the annual aggregation of daily results shown in Chapter 7), there is a very significant correlation between simulation and observations ($\rho = 0.83$, $p<0.01$, $n = 173$), with a general PBIAS of -31%, suggesting a general underestimation of the model. A more detailed analysis of the results shows that cold climate rivers (according to the Köppen Geiger classification presented by Beck et al., 2018) are underestimated, which has been associated to permafrost dnamics not included in the model (Toohey et al., 2016, Chapter 7) while tropical basins like the Niger are commonly overestimated, associated to a high discharge value (van Vliet et al., 2013; van Vliet, van Beek, et al., 2016; van Vliet, Wiberg, et al., 2016). In summary, the use of physically based models vs digital filters for hydrological description has been discussed in the previous section, but the results from applying such approach with the ICWR model suggests that this model's performance is valid as a starting point or when the applicability of mechanistic models is constrained by computational coasts or data input scarcity. The model's parameters seem valid at different spatial scales, but the input data must be adjusted when downscaling the model.

8.4 Model application: The role of chemical weathering on CO_2 sequestration

Chemical weathering of rocks has an impact on the carbon cycle, since the dissolution of carbonate and silicate rocks require carbonic acid, derived from CO_2 dissolution in

water. Being able to assess its influence at the global scale is of interest for climate change forecast studies (IPCC, 2013) and for other scientists in biogeochemical cycling (e.g. Hartmann, 2009). The model developed here is an opportunity to estimate present daily spatial and temporal chemical weathering through its constituents –i.e. major ions–, and the estimation of carbon sequestration may be derived by coupling these results to the MEGA model (Amiotte Suchet & Probst, 1996), which estimates the C exchanged by the dissolution of carbonates, silicates, evaporites, and pyrite. This is one of the applications that the ICWR model poses for modellers focusing on biogeochemical cycling at a global scale.

Acknowledging that large basins are subject of large uncertainties when studied individually, the ICWR model's performance at a global scale regarding ionic fluxes has been validated. The application of a cascade model considering the 300 largest basins, according to the HydroBASINS dataset (Lehner & Grill, 2013) has yielded two insights: first, the C sequestration derived from this cascade model presents a strong and significant correlation to calculated by independent methods values (Gaillardet et al., 1999), and a low PBIAS thus the modelling approach is considered as valid for estimating annual average C sequestration at the global scale; and second, the role of chemical weathering on CO_2 sequestration is spatially and temporally heterogeneous at the global scale (c.f. Chapter 7). Application of these empirical models has highlighted the importance of considering not only spatial, but temporal evolution on studying hot spots and hot moments in biogeochemical cycles. Despite of these large uncertainties regarding their estimates, their application has permitted the establishment of the first global scale product for C sequestration through chemical weathering, which presents a strong and significant correlation to previous literature and introduces new results, such as annual and seasonal hot spots.

Assuming that before the end of the XXI century the rates of chemical weathering at which ion fluxes are released from rocks is maintained, hence considering still valid the conceptual model presented in the first section of this discussion, a first snapshot on the potential evolution of C sequestration in different scenarios is presented (c.f. Chapter 7). Even considering the dissolution rates as constant in time, the influence of hydrological

change (related to changes on land use, vegetation, and climate changes) will have an impact on C sequestration, increasing in the two future scenarios considered, but not equally distributed along the year. Such temporal evolution should be included in Earthcasting analysis.

Bibliography

Amiotte Suchet, P. (1995). *Cycle du carbone, érosion chimique des continents et transferts vers les océans* (Doctoral dissertation). Université Louis-Pasteur. Strasbourg, Institut de Géologie. https://www.persee.fr/doc/sgeol_0302-2684_1995_mon_97_1

Amiotte Suchet, P., & Probst, J. L. (1995). A global model for present-day atmospheric/soil CO2 consumption by chemical erosion of continental rocks (GEM-CO2). *Tellus B*, *47B*(1-2), 273–280. https://doi.org/10.1034/j.1600-0889.47.issue1.23.x

Amiotte Suchet, P., & Probst, J. L. (1996). Origines du carbone inorganique dissous dans les eaux de la Garonne. Variations saisonnières et interannuelles. / Sources of dissolved inorganic carbon in the Garonne river water. Seasonal and inter annual variations. *Sciences Géologiques. Bulletin*, *49*(1), 101–126. https://doi.org/10.3406/sgeol.1996.1938

Anderson, S. P., Blum, J., Brantley, S. L., Chadwick, O., Chorover, J., Derry, L. A., Drever, J. I., Hering, J. G., Kirchner, J. W., Kump, L. R., Richter, D., & White, A. F. (2004). Proposed initiative would study Earth's weathering engine. *EOS*, *85*(28), 265–269. https://doi.org/10.1029/2004EO280001

Anderson, S. P., von Blanckenburg, F., & White, A. (2007). Physical and Chemical Controls on the Critical Zone. *Elements*, *3*(5), 315–319. https://doi.org/10.2113/gselements.3.5.315

Arnold, J. G., Moriasi, D. N., Gassman, P. W., Abbaspour, K. C., White, M. J., Srinivasan, R., Santhi, C., Harmel, R. D., van Griensven, A., Van Liew, M. W., Kannan, N., & Jha, M. K. (2012). SWAT: Model use, calibration, and validation. *Transactions of the ASABE*, *55*(4), 1491–1508. https://doi.org/10.13031/2013.42256

Arnold, J. G., Williams, J. R., & Maidment, D. R. (1995). Continuous-time water and sediment-routing model for large basins. *Journal of Hydraulic engineering*, *121*(2), 171–183. https://doi.org/10.1061/(ASCE)0733-9429(1995)121:2(171)

Aufdenkampe, A. K., Mayorga, E., Raymond, P. A., Melack, J. M., Doney, S. C., Alin, S. R., Aalto, R. E., & Yoo, K. (2011). Riverine coupling of biogeochemical cycles be-

tween land, oceans, and atmosphere. *Frontiers in Ecology and the Environment*, *9*(1), 53–60. https://doi.org/10.1890/100014

Bailey, R. T., Tavakoli-Kivi, S., & Wei, X. (2019). A salinity module for SWAT to simulate salt ion fate and transport at the watershed scale. *Hydrology and Earth System Sciences*, *23*(7), 3155–3174. https://doi.org/10.5194/hess-23-3155-2019

Balagizi, C. M., Darchambeau, F., Bouillon, S., Yalire, M. M., Lambert, T., & Borges, A. V. (2015). River geochemistry, chemical weathering, and atmospheric CO 2 consumption rates in the Virunga Volcanic Province (East Africa). *Geochemistry, Geophysics, Geosystems*, *16*(8), 2637–2660. https://doi.org/10.1002/2015GC005999

Beck, H. E., Zimmermann, N. E., McVicar, T. R., Vergopolan, N., Berg, A., & Wood, E. F. (2018). Present and future Köppen-Geiger climate classification maps at 1-km resolution. *Scientific data*, *5*, 180214. https://doi.org/10.1038/sdata.2018.214

Calabrese, S., Parolari, A. J., & Porporato, A. (2017). Hydrologic Transport of Dissolved Inorganic Carbon and Its Control on Chemical Weathering. *Journal of Geophysical Research: Earth Surface*, *122*(10), 2016–2032. https://doi.org/10.1002/2017JF004346

Chapra, S. C., Dove, A., & Warren, G. J. (2012). Long-term trends of Great Lakes major ion chemistry. *Journal of Great Lakes Research*, *38*(3), 550–560. https://doi.org/10.1016/j.jglr.2012.06.010

Day, J. W., Christian, R. R., Boesch, D. M., Yáñez-Arancibia, A., Morris, J., Twilley, R. R., Naylor, L., Schaffner, L., & Stevenson, C. (2008). Consequences of Climate Change on the Ecogeomorphology of Coastal Wetlands. *Estuaries and Coasts*, *31*(3), 477–491. https://doi.org/10.1007/s12237-008-9047-6

Devi, G. K., Ganasri, B. P., & Dwarakish, G. S. (2015). A Review on Hydrological Models. *Aquatic Procedia*, *4*, 1001–1007. https://doi.org/10.1016/j.aqpro.2015.02.126

Dürr, H. H., Meybeck, M., & Dürr, S. H. (2005). Lithologic composition of the Earth's continental surfaces derived from a new digital map emphasizing riverine material transfer. *Global Biogeochemical Cycles*, *19*(4). https://doi.org/10.1029/2005GB002515

Eckhardt, K. (2005). How to construct recursive digital filters for baseflow separation. *Hydrological Processes*, *19*(2), 507–515. https://doi.org/10.1002/hyp.5675

Fu, B., Merritt, W. S., Croke, B. F., Weber, T. R., & Jakeman, A. J. (2019). A review of catchment-scale water quality and erosion models and a synthesis of future prospects. *Environmental Modelling & Software*, *114*, 75–97. https://doi.org/10.1016/j.envsoft.2018.12.008

Gaillardet, J., Dupré, B., Louvat, P., & Allègre, C. J. (1999). Global silicate weathering and CO2 consumption rates deduced from the chemistry of large rivers. *Chemical Geology*, *159*, 3–30. https://doi.org/10.1016/S0009-2541(99)00031-5

Garrels, R. M., & Mackenzie, F. T. (1972). A quantitative model for the sedimentary rock cycle. *Marine Chemistry*, *1*, 27–41. https://doi.org/10.1016/0304-4203(72)90004-7

Gibbs, R. J. (1970). Mechanisms controlling world water chemistry. *Science*, *170*(3962), 1088–1090. https://www.jstor.org/stable/1730827

Goddéris, Y., & Brantley, S. L. (2013). Earthcasting the future Critical Zone. *Elementa: Science of the Anthropocene*, *1*, 000019. https://doi.org/10.12952/journal.elementa.000019

Goddéris, Y., Roelandt, C., Schott, J., Pierret, M.-C., & Francois, L. M. (2009). Towards an Integrated Model of Weathering, Climate, and Biospheric Processes. *Reviews in Mineralogy and Geochemistry*, *70*(1), 411–434. https://doi.org/10.2138/rmg.2009.70.9

Hartmann, J. (2009). Bicarbonate-fluxes and CO2-consumption by chemical weathering on the Japanese Archipelago — Application of a multi-lithological model framework. *Chemical Geology*, *265*(3-4), 237–271. https://doi.org/10.1016/j.chemgeo.2009.03.024

Hartmann, J., Jansen, N., Dürr, H. H., Kempe, S., & Köhler, P. (2009). Global CO2-consumption by chemical weathering: What is the contribution of highly active weathering regions? *Global and Planetary Change*, *69*(4), 185–194. https://doi.org/10.1016/j.gloplacha.2009.07.007

Hartmann, J., & Moosdorf, N. (2012). The new global lithological map database GLiM: A representation of rock properties at the Earth surface. *Geochemistry, Geophysics, Geosystems*, *13*(12). https://doi.org/10.1029/2012GC004370

Hartmann, J., Moosdorf, N., Lauerwald, R., Hinderer, M., & West, A. J. (2014). Global chemical weathering and associated P-release — The role of lithology, temper-

ature and soil properties. *Chemical Geology*, *363*, 145–163. https://doi.org/10.1016/j.chemgeo.2013.10.025

IPCC. (2013). Climate Change 2013: The Physical Science Basis. Contribution of Working Group I to the Fifth Assessment Report of the Intergovernmental Panel on Climate Change (T. F. Stocker, D. Qin, G.-K. Plattner, M. Tignor, S. K. Allen, J. Boschung, A. Nauels, Y. Xia, V. Bex, & P. M. Midgley, Eds.). https://www.ipcc.ch/report/ar5/wg1/

Lechuga-Crespo, J. L., Ruiz-Romera, E., Probst, J. L., Unda-Calvo, J., Cuervo-Fuentes, Z. C., & Sánchez-Pérez, J. M. (2020). Combining punctual and high frequency data for the spatiotemporal assessment of main geochemical processes and dissolved exports in an urban river catchment. *Science of The Total Environment*, *727*, 138644. https://doi.org/10.1016/j.scitotenv.2020.138644

Lechuga-Crespo, J. L., Sánchez-Pérez, J. M., Sauvage, S., Hartmann, J., Amiotte Suchet, P., Probst, J. L., & Ruiz-Romera, E. (2020). A model to evaluate chemical weathering from riverine transports of dissolved major elements at global scale. *Global and Planetary Change*, *192*. https://doi.org/10.1016/j.gloplacha.2020.103226

Lehner, B., & Grill, G. (2013). Global river hydrography and network routing: baseline data and new approaches to study the world's large river systems. *Hydrological Processes*, *27*(15), 2171–2186. https://doi.org/10.1002/hyp.9740

Lupker, M., France-Lanord, C., Galy, V., Lavé, J., & Kudrass, H. (2013). Increasing chemical weathering in the Himalayan system since the Last Glacial Maximum. *Earth and Planetary Science Letters*, *365*, 243–252. https://doi.org/10.1016/j.epsl.2013.01.038

Maher, K. (2010). The dependence of chemical weathering rates on fluid residence time. *Earth and Planetary Science Letters*, *294*(1-2), 101–110. https://doi.org/10.1016/j.epsl.2010.03.010

Maher, K. (2011). The role of fluid residence time and topographic scales in determining chemical fluxes from landscapes. *Earth and Planetary Science Letters*, *312*(1-2), 48–58. https://doi.org/10.1016/j.epsl.2011.09.040

Maher, K., & Chamberlain, C. P. (2014). Hydrologic regulation of chemical weathering and the geologic carbon cycle. *Science*, *343*(6178), 1502–1504. https://doi.org/10.1126/science.1250770

McClain, M. E., Boyer, E. W., Dent, C. L., Gergel, S. E., Grimm, N. B., Groffman, P. M., Hart, S. C., Harvey, J. W., Johnston, C. A., Mayorga, E., McDowell, W. H., & Pinay, G. (2003). Biogeochemical Hot Spots and Hot Moments at the Interface of Terrestrial and Aquatic Ecosystems. *Ecosystems*, *6*(4), 301–312. https://doi.org/10.1007/s10021-003-0161-9

Meybeck, M. (1979). Concentrations des eaux fluviales en éléments majeurs et apports. *Revue de géologie dynamique et de géographie physique*, *21*(3), 215.

Meybeck, M. (1986). Composition chimique des ruisseaux non pollués de France. *Sciences Géologiques*, *39*(1), 3–77.

Meybeck, M. (2003). Global Occurrence of Major Elements in Rivers. In H. D. Holland & K. K. Turekian (Eds.), *Treatise on Geochemistry* (pp. 207–223). https://doi.org/10.1016/B0-08-043751-6/05164-1

Parkhurst, D. L. (1995). User's guide to PHREEQC - A computer program for speciation, reaction-path, advective-transport, and inverse geochemical calculations.

Parkhurst, D. L., & Appelo, C. A. J. (2013). Description of Input for PHREEQC Version 3—A Computer Program for Speciation, Batch-Reaction, One-Dimensional Transport, and Inverse Geochemical Calculations.

Parsekian, A. D., Singha, K., Minsley, B. J., Holbrook, W. S., & Slater, L. (2015). Multiscale geophysical imaging of the critical zone. *Reviews of Geophysics*, *53*(1), 1–26. https://doi.org/10.1002/2014RG000465

Probst, J. L. (1992). *Géochimie et hydrologie de l'érosion continentale. Mécanismes, bilan global actuel et fluctuations au cours des 500 derniers millions d'années.* (Doctoral dissertation). Université Louis-Pasteur. Strasbourg, Institut de Géologie. www.persee.fr/doc/sgeol_0302-2684_1992_mon_94_1

Stallard, R. F., & Edmond, J. M. (1987). Geochemistry of the Amazon: 3. Weathering chemistry and limits to dissolved inputs. *Journal of Geophysical Research*, *92*(C8), 8293–8302. https://doi.org/10.1029/JC092iC08p08293

Sun, X., Higgins, J., & Turchyn, A. V. (2016). Diffusive cation fluxes in deep-sea sediments and insight into the global geochemical cycles of calcium, magnesium, sodium and potassium. *Marine Geology*, *373*, 64–77. https://doi.org/10.1016/j.margeo.2015.12.011

Toohey, R. C., Herman-Mercer, N. M., Schuster, P. F., Mutter, E. A., & Koch, J. C. (2016). Multidecadal increases in the Yukon River Basin of chemical fluxes as indicators of changing flowpaths, groundwater, and permafrost. *Geophysical Research Letters*, *43*(23), 12, 120–12, 130. https://doi.org/10.1002/2016GL070817

Tréguer, P. J., & de La Rocha, C. L. (2013). The world ocean silica cycle. *Annual review of marine science*, *5*, 477–501. https://doi.org/10.1146/annurev-marine-121211-172346

Tueros, I., Rodríguez, J. G., Borja, A., Solaun, O., Valencia, V., & Millán, E. (2008). Dissolved metal background levels in marine waters, for the assessment of the physico-chemical status, within the European Water Framework Directive. *The Science of the total environment*, *407*(1), 40–52. https://doi.org/10.1016/j.scitotenv.2008.08.026

van Vliet, M. T. H., Franssen, W. H., Yearsley, J. R., Ludwig, F., Haddeland, I., Lettenmaier, D. P., & Kabat, P. (2013). Global river discharge and water temperature under climate change. *Global Environmental Change*, *23*(2), 450–464. https://doi.org/10.1016/j.gloenvcha.2012.11.002

van Vliet, M. T. H., van Beek, L., Eisner, S., Flörke, M., Wada, Y., & Bierkens, M. (2016). Multi-model assessment of global hydropower and cooling water discharge potential under climate change. *Global Environmental Change*, *40*, 156–170. https://doi.org/10.1016/j.gloenvcha.2016.07.007

van Vliet, M. T. H., Wiberg, D., Leduc, S., & Riahi, K. (2016). Power-generation system vulnerability and adaptation to changes in climate and water resources. *Nature Climate Change*, *6*, 375–380. https://doi.org/10.1038/NCLIMATE2903

Xie, J., Liu, X., Wang, K., Yang, T., Liang, K., & Liu, C. (2020). Evaluation of typical methods for baseflow separation in the contiguous United States. *Journal of Hydrology*, *583*, 124628. https://doi.org/10.1016/j.jhydrol.2020.124628

CHAPTER 9

Conclusion and perspectives

9.1 ENGLISH - Conclusions and perspectives

The main objective of this research work has been ***to assess the role of chemical weathering on biogeochemical cycling, paying special attention on the major ion fluxes derived from rocks, by means of modelling at different spatial and temporal scales.*** The main chapters of this PhD thesis have worked towards the partial objectives established to accomplish this main objective, thus helping on answering the research question. In this last chapter, the main results and conclusions are presented, as well as some recommendations for future lines of research.

9.1.1 Conclusions

Earth system analysis is based on the understanding of all processes given within environmental reservoirs, and on the description of their feedbacks through different pathways in the biogeochemical cycles. In this sense, knowledge growth depends on the identification of the drivers controlling these processes, as well as on the awareness of their role within those cycles. Such understanding and description support stakeholders on resource management under the challenges derived of global change. However, the local heterogeneity within the Earth poses a great challenge for studies at the global scale since accounting for the drivers and their roles requires the careful development and application of useful and efficient tools. Within this framework, the present PhD thesis has worked towards the development of a modelling tool in a global-to-local approach, evaluating its performance on different contrasted spatial and temporal scales, and for its application on the frame of the carbon cycle.

The focus on the chemical weathering process has been derived from the long interest on this process and the lack of consensus on the results at large spatial scales regarding dissolved exports to ocean. Chemical weathering is an overlapping process between the biogeochemical and geochemical cycles occurring on the critical zone, and its role on life sustainment has been long recognised. Assessing its influence at the global and local scale is relevant not only for geologists studying chemical weathering, but a broad range of scientists somehow related to water quality, concerned about chemical composition of freshwater environments.

Using riverine exports as a proxy for studying chemical weathering is a long established approach. However, despite of the large amount of data existing regarding chemical composition of worldwide rivers, a global comprehensive field survey to evaluate these fluxes is not practical. Consequently, modelling presents a suitable alternative since the development of computational resources has facilitated the application of these methods to research. The use of riverine exports has permitted the development of a spatially distributed model which permits the estimation of major ion fluxes derived

from chemical weathering: fluxes of inorganic compounds which act as nutrients for plants and conditions water salinity.

One of the main challenges of hydro-geochemical modelling is the data availability, which limits the application of physically-based model at large spatial scales. An alternative solution to these models is those empirically-based which, despite of not addressing physical laws on their structure, they are less data demanding allowing to its deployment on large scale studies, yielding first snapshots to where direct future research. In this sense, the present PhD thesis has opted to follow an empirically based model, developed on large field data, calibrated, and validated at the global scale.

During the development of the model, even though several variables have been considered, three main drivers at the global scale regarding chemical weathering have been successfully included. The first conclusion of this study is that **chemical weathering at the global scale is mainly affected by hydrology, lithology, and soil, but their role on ionic fluxes is not equally distributed**(Chapter 4). In fact, the second conclusion of this PhD thesis is that **the effect that soil exerts on the ion fluxes is not equally distributed among ions, but some soils have a greater shielding effect on some ions, while lower in others** (Chapter 4). Despite of failing to include other variables such as hydraulic conductivity, regolith (soil) thickness, or temperature in the model configuration, this does not mean that these variables do not pose a relevant role on chemical weathering. It only indicates that it has not been able to include them in the modelling approach at the present stage.

Lower spatial set ups are usually easier at the data availability step and the computational resources needed, but sometimes these regional or local studies also lack these resources. Hence, the model developed at a global scale has been evaluated a regional (Chapter 7) and local scales, paying special attention to the Deba basin (Chapter 5), which presents a characteristic geological set up by the presence of evaporitic springs on the southwest part of the catchment which conditions the major ion composition downstream to the outlet. This set up has highlighted other conclusion of this study: **with regards to lower scale application of the model, the presence of relevant geologi-**

cal set ups which play an important role on the freshwater chemical composition pose a limitation for the model's performance (Chapter 6).

From the local study, two contrasting insights support this conclusion: first, local studies where the water chemical composition is conditioned by the presence of singular geological set ups (like the Deba catchment) present a higher deviation on the simulation results, suggesting that the model performance on this situation is poor since it has not been developed to account for such set up. Second, one tributary of the Deba catchment is not influenced by the evaporitic springs, and the performance of the model at this place has highlighted the potential of using the globally fitted model on establishing a first snapshot of the ionic fluxes derived from chemical weathering of rocks at the local scale.

Considering the temporal variability within a year's timescale (down to daily), hydrology was initially hypothesized as the main responsible of ionic fluxes variability. The incorporation of the model into the hydrological Soil and Water Assessment Tool (SWAT) model–by developing the QSWATLitho plugin and the SWATLitho module–has allowed to test this hypothesis, confirming **the role of hydrology on these ionic fluxes, which is dominated by the groundwater and lateral flow** (Chapter 6). The development of the QSWATLitho plugin and SWATLitho module present an opportunity for researchers interested on chemical weathering and the ionic fluxes at local case studies.

Finally, acknowledging that the main driver of ionic fluxes temporal evolution is hydrology, it has been possible to perform a global assessment of the carbon biogeochemical cycle, studying the potential effect that climate change may exert on the carbon sequestration through chemical weathering. It has been shown that global scale hot spots are not equally distributed along the year, but the differentiation between seasons is needed to understand which are the zones with greater dissolved exports to the ocean derived from chemical weathering, as well as with the larger carbon sequestration. According to the results, **the potential influence of climate change on hydrology will cause a general increase on the annual carbon sequestration, which is specially noted between the months of January-March, presenting larger changes for cold**

climates, specially for the RCP 8.5 scenario (Chapter 7).

9.1.2 Perspectives

The results of the present PhD thesis have highlighted the value of empirically based modelling approaches on the description of the Earth system when the application of other methodologies is constrained. In this study, focus has been put on chemical weathering as an integrative process regarding geochemical and biogeochemical processes, but the further recommendations may be applied in other model developing studies.

First, the initial conceptualization of the process has been performed under a global-to-local perspective, trying to elucidate the main drivers at a global scale and identify secondary drivers on local studies. An alternative strategy would be to develop different simplifications of the reality based on extensively studied local cases on enough heterogeneous locations to account for different climatic, lithological, hydrological, physical settings. The development of empirical models in these locations may yield common patterns of the variables not successfully included in the present study. Regarding these conceptualizations, and based on the experience carried during this study, three new hypotheses are stated:

- Temperature was not successfully included in the present analysis, but its implication on chemical weathering has long been confirmed. Recent studies (Gaillardet et al., 2019; Romero-Mujalli, Hartmann, Börker, et al., 2019) has proposed an alternative approach of the temperature effect, based on a "boomerang-shaped" curve regarding carbonate weathering. Thus, the temperature effect on chemical weathering enhances mineral dissolution up to a certain temperature, but higher values decline these rates due to carbonate equilibrium, *the inclusion of the temperature factor on the global scale model development requires the inclusion of a carbonate equilibrium term*–which accounts for this trend–*at a site-by-site level*.
- Vegetation uses inorganic compounds such as K^+ as nutrient for plant growth,

thus the soil shielding effect should be studied including the land coverture as well. *The soil shielding effect on ionic fluxes derived from chemical weathering of rocks is not only conditioned by the soil characteristics, but by the land coverture as well.*

- Chemical weathering is boosted with higher specific surface of the critical zone particles so the water-rock interaction is enhanced, thus chemical weathering description should include the size of the particles or a proxy of this variable. *The finer the particles are in the critical zone, the higher the chemical weathering rates become, thus yielding more relevant ionic fluxes to water streams.* A potential descriptor of this proxy would be the sediment fraction description on the suspended solids found in rivers.

The calibration of the model's parameters has been performed under a subset of sampling locations which, even though covering a broad range of lithologies and soil classes, lack some characteristics (like plutonic intermediate, or evaporites) which did not cover the whole spectrum of variation. The application of the model in such non-covered characteristics could lead to poor performance of the model. A future line of research could be to study which are the variables that condition the calibrated values, which could be used to estimate and adjust the values of these parameters at local case studies.

The identification of hot spots should be used to prioritize biogeochemical cycling research in these areas. Field studies taken in these locations could help to develop understanding of the drivers at different spatial scales. In addition, a temporal assessment could also help in elucidating the effects of biology (such as soil respiration) on the chemical weathering process.

Finally, the insights derived from the model configuration in this global-to-local strategy could be used, together with physically-based models in a local-to-global approach so to bring closer the applicability of these physically based models at large spatial and temporal scales.

9.2 ESPAÑOL - Conclusiones y perspectivas

El objetivo principal de este trabajo de investigación ha sido ***evaluar el papel de la alteración química en los ciclos biogeoquímicos, prestando especial atención a los iones mayoritarios derivados de las rocas, a través de la modelización a diferentes escalas espaciales y temporales.*** Los capítulos principales de esta tesis de doctorado se han enfocado en los objetivos parciales establecidos para cumplir este objetivo general, ayudando a responder a la pregunta de investigación. En este último capítulo, los principales resultados y conclusiones se presentan, así como algunas recomendaciones para futuras líneas de investigación.

9.2.1 Conclusiones

El análisis del sistema Tierra está basado en la comprensión de todos los procesos dados en los reservorios medioambientales, y en la descripción de las retroalimentaciones entre las diferentes vías de los ciclos biogeoquímicos. En este sentido, el aumento del conocimiento depende de la identificación de los elementos que controlan estos procesos, así como el reconocimiento de su papel en estos ciclos. Dicho entendimiento y descripción apoya a los agentes en la gestión de recursos bajo retos derivados del cambio global. Sin embargo, la heterogeneidad global en la Tierra presenta un gran reto para los estudios a escala global, ya que tener en cuenta los factores y su papel requiere el desarrollo y aplicación cuidadoso de herramientas útiles y eficientes. Dentro de este contexto, esta tesis de doctorado ha trabajado para el desarrollo de una herramienta de modelización en un enfoque global-a-local, evaluando su desempeño en diferentes escalas espaciales y temporales, y para su aplicación en el ciclo del carbono.

El foco en el proceso de alteración química ha sido derivado del interés establecido en este proceso y la falta de consenso en los resultados en grandes escalas espaciales respecto a las cargas disueltas exportadas al océano. La alteración química es un proceso común entre los ciclos biogeoquímicos y geoquímicos que ocurre en la zona crítica,

y su papel en el mantenimiento de la vida ha sido largamente reconocido. Evaluar su influencia en la escala global y local es relevante no sólo para los geólogos que estudian la alteración química, sino para un gran abanico de científicos relacionados de alguna manera con la calidad del agua, involucrados en la composición química de los ambientes acuáticos.

El uso de las cargas de los ríos como indicador para estudiar la alteración química es un enfoque largamente establecido. Sin embargo, a pesar del gran número de datos existentes respecto a la composición química de los ríos mundiales, un monitoreo completo de estos flujos no es práctico. Consecuentemente, la modelización se presenta como una alternativa eficiente, ya que el desarrollo de los recursos computacionales ha permitido la aplicación de estos métodos a la investigación. El uso de las cargas de los ríos ha permitido el desarrollo de un modelo espacialmente distribuido para la estimación de los flujos de iones mayoritarios derivados de la alteración de la roca: flujos inorgánicos que actúan como nutrientes para las plantas y condicionan la salinidad del agua.

Uno de los principales retos de la modelización hidro-geoquímica es la disponibilidad de datos, que limita la aplicación de modelos de base física a grandes escalas espaciales. Una solución alternativa a estos modelos son los de base empírica que, a pesar de no integrar leyes físicas en su estructura, requieren menos datos para su aplicación en estudios a grandes escalas, permitiendo unos resultados preliminares hacia los que dirigir la investigación futura. En este sentido, en esta tesis de doctorado se ha optado por seguir un modelo de base empírica, desarrollado en gran número de datos de campo, calibrado y validado a escala global.

Durante el desarrollo del modelo, aunque algunas variables no han sido consideradas, hay tres factores principales a la escala global respecto a la alteración química que han sido incluidos. La primera conclusión de este estudio es que **la alteración química a escala global está principalmente determinada por la hidrología, la litología, y el suelo, pero su efecto en los flujos iónicos no está distribuido uniformemente** (Capítulo 4). De hecho, la segunda conclusión de esta tesis de doctorado es que **el**

efecto que el suelo ejerce sobre los flujos de iones no está distribuido equitativamente entre los iones, pero algunos suelos tienen un mayor efecto de protección, mientras que es más bajo en otros (Capítulo 4). A pesar de fallar en la inclusión de otras variables como la conductividad hidráulica, el espesor del regolito (suelo), o la temperatura en la configuración del modelo, esto no significa que estas variables no jueguen un papel relevante en la relevante en la alteración química. Únicamente indica que no ha sido posible incluirlos en el enfoque de modelización en esta etapa.

Aplicaciones a escalas más pequeñas son normalmente más fáciles respecto a la disponibilidad de datos y los recursos computacionales necesarios, pero algunas veces estos estudios regionales o locales también tienen falta de estos recursos. Por lo tanto, el modelo desarrollado a escala global ha sido evaluado en escalas regionales (Capítulo 7) y locales (Capítulo 6), prestando especial atención a la cuenca del Deba (Capítulo 5), que presenta una estructura geológica característica por la presencia de manantiales evaporiticos en la parte sudoeste de la cuenca que condiciona la composición mayoritaria hasta la desembocadura. Esta estructura ha subrayado otra conclusión de este estudio: respecto a la aplicación del modelo a escalas más pequeñas, la presencia de estructuras geológicas que juegan un papel importante en la composición mayoritaria de los entornos acuáticos significa una limitación para el desempeño del modelo (Capítulo 6).

Del caso de estudio local, se han derivado dos ideas para apoyar esta conclusión: primero, los estudios locales donde la composición química del agua esté condicionada por la presencia de estructuras geológicas singulares (como la cuenca del Deba) presenta una desviación mayor de los resultados de simulación, sugiriendo que el desempeño del modelo en esta situación peor ya que no ha sido desarrollado para tener en cuenta este tipo de estructuras. Segundo, uno de los tributarios de la cuenca del Deba no se encuentra influenciado por los manantiales salinos, y el desempeño del modelo en este lugar ha permitido subrayar el potencial de usar el modelo global para establecer unos resultados preliminares de los flujos iónicos derivados de la alteración de las rocas a la escala local.

Considerando la variabilidad temporal dentro de la escala temporal de un año (hasta la escala diaria), la hidrología se hipotetizó como la principal responsable de la variabilidad de los flujos iónicos. La incorporación del modelo global en el modelo hidrológico Soil and Water Assessment Tool (SWAT) – a través del desarrollo de la extensión de QSWATLitho y del módulo SWATLitho – ha permitido comprobar esta hipótesis, **confirmando el papel de la hidrología en estos flujos iónicos, dominado principalmente por el flujo subterráneo y lateral** (Capítulo 6). El desarrollo de la extensión de QSWATLitho y del módulo SWATLitho presenta una oportunidad para los investigadores que estén interesados en la alteración química y en los flujos iónicos en escalas locales.

Finalmente, reconocimiento que el principal condicionante de la variabilidad de los flujos iónicos es la hidrología, ha sido posible desarrollar una evaluación global del ciclo biogeoquímico del carbono, estudiando el efecto potencial que el cambio climático pueda generar sobre el consumo de carbono a través de la alteración química. Se ha mostrado que los puntos calientes a escala global no están distribuidos igualmente a lo largo del año, pero que la diferenciación entre estaciones es necesaria para entender qué zonas son las que tienen unas mayores exportaciones disueltas al océano derivadas de la alteración química, así como un mayor consumo de carbono. De acuerdo con los resultados, **la influencia potencial del cambio climático en la hidrología causará un aumento generalizado del consumo de carbono, que se notará principalmente entre los meses de Enero-Marzo, presentando unos cambios más importantes en las zonas frías, especialmente para el escenario RCP 8.5** (Capítulo 7).

9.2.2 Perspectivas

Los resultados de esta tesis de doctorado han destacado el valor del enfoque empírico en la modelización para la descripción del sistema Tierra cuando la aplicación de otras metodologías está limitada. En este estudio, el foco ha sido puesto en la alteración química como un proceso integrativo de los procesos geoquímicos y biogeoquímicos,

pero las siguientes recomendaciones pueden aplicarse a otros estudios de desarrollo del modelo.

Primero, la conceptualización inicial del proceso ha sido realizada bajo un enfoque global-a-local, intentando elucidar los principales condicionantes a escala global, así como identificar los condicionantes secundarios a escala local. Una estrategia alternativa sería desarrollar diferentes simplificaciones de la realidad basada en estudios locales ampliamente documentados en localizaciones heterogéneas diferentes, para considerar diferentes características climáticas, litológicas, hidrológicas, y físicas. El desarrollo de modelos empíricos en estas localizaciones puede resultar en unos patrones similares de las variables que no han sido incluidas en este estudio. Respecto a estas conceptualizaciones, y basadas en la experiencia adquirida en este estudio, tres hipótesis nuevas se enuncian:

- La temperatura no se pudo incluir en este análisis, pero su implicación en la alteración química ha sido confirmada largamente. Estudios recientes (Gaillardet y col., 2019; Romero-Mujalli, Hartmann, Börker y col., 2019) ha propuesto un enfoque alternativo al efecto de la temperatura, basado en una curva en "forma de bumerang" respecto a la alteración de los carbonatos. Por lo tanto, el efecto de la temperatura en la alteración química facilita la disolución de los minerales hasta una temperatura determinada, pero valores mayores pueden decrecer estas tasas debido al equilibrio de carbonatos, *la inclusión del efecto de la temperatura en modelización a escala global requiere la inclusión de un término de equilibrio de carbonatos* – que incluya esta tendencia – *a nivel de cada sitio de estudio.*
- La vegetación utiliza compuestos inorgánicos como el K^+ como nutriente para su crecimiento, por lo que el efecto protector del suelo debería estudiarse incluyendo la cobertura vegetal. *El efecto protector del suelo en los flujos iónicos derivados de la alteración química de las rocas no está condicionado únicamente por las características del suelo, sino por la cobertura vegetal igualmente.*
- La alteración química está potenciada por una mayor superficie específica de las partículas de la zona crítica, aumentando la interacción entre el agua y la roca,

por lo tanto la descripción de la alteración química debería incluir el tamaño de las partículas o un indicador de estas variables. Cuanto más finas sean las partículas en la zona crítica, mayor será la tasa de alteración química, aportando un mayor flujo de iones al agua. Un descriptor potencial de este indicador sería la descripción de la fracción sedimento en los sólidos suspendidos de los ríos.

La calibración de los parámetros del modelo ha sido desarrollada bajo una serie de localizaciones que, aunque cubren un gran abanico de litologías y tipos de suelo, carecen de algunas características (como rocas plutónicas, o evaporitas) que no cubren todo el espectro de variación. La aplicación del modelo en estas zonas no cubiertas podría derivar en un desempeño pobre del modelo. Una futura línea de investigación sería estudiar cuáles son las variables que condicionan los valores calibrados, variables que podrían ser utilizadas para estimar y ajustar el valor de estos parámetros en casos de estudio locales.

La identificación de puntos calientes debería utilizarse para priorizar la investigación en ciclos biogeoquímicos en estas áreas. Estudios de campo tomados en estas localizaciones podrían ayudar a desarrollar conocimiento en los factores a diferentes escalas espaciales. Además, una evaluación temporal podría también ayudar a elucidar los efectos de la biología (como la respiración del suelo) en el proceso de alteración química.

Finalmente, las ideas derivadas de la configuración del modelo en esta estrategia global-a-local podrían ser utilizadas, en conjunto con modelos físicos desarrollados en una estrategia local-a-global para acercar la aplicabilidad de estos modelos físicos en escalas espaciales y temporales grandes.

9.3 FRANÇAIS - Conclusions et perspectives

L'objectif principal de ce travail de recherche c'était d'***évaluer le rôle de l'altération chimique sur le cycle biogéochimique, en accordant une attention particulière aux principaux flux ioniques dérivés des roches, par modélisation à différentes échelles spatiales et temporelles***. Les principaux chapitres de cette thèse ont travaillé vers les objectifs partiels établis pour atteindre cet objectif, contribuant ainsi à répondre à la question de recherche. Dans ce dernier chapitre, les principaux résultats et conclusions sont présentés, ainsi que quelques recommandations pour de futurs axes de recherche.

9.3.1 Conclusions

L'analyse du système terrestre repose sur la compréhension de tous les processus donnés dans les réservoirs environnementaux et sur la description de leurs rétroactions à travers différentes voies dans les cycles biogéochimiques. En ce sens, la croissance des connaissances dépend de l'identification des moteurs contrôlant ces processus, ainsi que de la conscience de leur rôle au sein de ces cycles. Une telle compréhension et description soutiennent les parties prenantes dans la gestion des ressources face aux défis dérivés du changement global. Cependant, l'hétérogénéité locale au sein de la Terre pose un grand défi pour les études à l'échelle mondiale, car la prise en compte des moteurs et de leurs rôles nécessite le développement et l'application minutieux d'outils utiles et efficaces. Dans ce cadre, la présente thèse a œuvré au développement d'un outil de modélisation dans une approche globale-locale, évaluant ses performances à différentes échelles spatiales et temporelles contrastées, et à son application sur le cadre du cycle du carbone.

L'accent mis sur le processus d'altération chimique découle du long intérêt suscité par ce processus et de l'absence de consensus sur les résultats à grande échelle spatiale concernant les exportations dissoutes vers l'océan. L'altération chimique est un processus qui se chevauche entre les cycles biogéochimiques et géochimiques qui se

produisent dans la zone critique, et son rôle sur le maintien de la vie est reconnu depuis longtemps. L'évaluation de son influence à l'échelle mondiale et locale est pertinente non seulement pour les géologues qui étudient l'altération chimique, mais pour un large éventail de scientifiques liés à la qualité de l'eau, préoccupés par la composition chimique des environnements d'eau douce.

L'utilisation des exportations fluviales comme indicateur indirect de l'étude de l'altération chimique est une approche établie de longue date. Cependant, en dépit de la grande quantité de données existantes concernant la composition chimique des fleuves du monde, une étude globale sur le terrain pour évaluer ces flux n'est pas practicable. Par conséquent, la modélisation présente une alternative appropriée puisque le développement de ressources informatiques a facilité l'application de ces méthodes à la recherche. L'utilisation des exportations fluviales a permis le développement d'un modèle distribué spatialement, qui permet d'estimer les principaux flux ioniques dérivés de l'altération chimique, les flux de composés inorganiques qui agissent comme nutriments pour les plantes et conditionnent la salinité de l'eau.

L'un des principaux défis de la modélisation hydrogéochimique est la disponibilité des données, ce qui limite l'application du modèle physique à grande échelle spatiale. Une solution alternative à ces modèles sont ceux basés sur l'empirie, qui malgré le fait de ne pas aborder les lois physiques sur leur structure, sont moins exigeants en données permettant leur déploiement sur des études à grande échelle, donnant les premiers instantanés où orienter la recherche future. En ce sens, la présente thèse a choisi de suivre un modèle empirique, développé sur de grandes données de terrain, calibré et validé à l'échelle mondiale.

Au cours de l'élaboration du modèle, même si plusieurs variables ont été prises en compte, trois principaux facteurs à l'échelle mondiale concernant l'altération chimique ont été inclus avec succès. La première conclusion de cette étude est **que l'altération chimique à l'échelle mondiale est principalement affectée par l'hydrologie, la lithologie et le sol, mais l'implication sur les flux ioniques n'est pas également répartie** (Chapitre 4). En fait, la deuxième conclusion de cette thèse est que l'effet que le sol

exerce sur les flux ioniques n'est pas réparti également entre les ions, mais certains sols ont un effet de blindage plus important sur certains ions, tandis qu'ils sont plus faibles dans d'autres (Chapitre 4). Bien qu'ils n'aient pas inclus d'autres variables telles que la conductivité hydraulique, l'épaisseur du régolithe ou du sol ou, encore, la température dans la configuration du modèle, cela ne signifie pas que ces variables ne jouent pas un rôle pertinent sur l'altération chimique. Il indique seulement qu'il n'a pas été en mesure de les inclure dans l'approche de modélisation au stade actuel.

Les configurations spatiales inférieures sont généralement plus faciles à l'étape de la disponibilité des données et des ressources informatiques nécessaires, mais parfois ces études régionales ou locales manquent également de ces ressources. Par conséquent, le modèle développé à l'échelle mondiale a été évalué à l'échelle régionale (Chapitre 7) et locale (Chapitre 6), en accordant une attention particulière au bassin de Deba (Chapitre 5), qui présente une configuration géologique caractéristique par la présence de sources évaporitiques sur la partie sud-ouest du bassin versant qui conditionne les principaux composition ionique en aval de la sortie. Cette configuration a mis en évidence une autre conclusion de cette étude : **en ce qui concerne l'application à plus petite échelle du modèle, la présence de configurations géologiques pertinentes qui jouent un rôle important sur la composition chimique de l'eau douce limite la performance du modèle** (Chapitre 6).

De l'étude locale, deux perspectives contrastées soutiennent cette conclusion : premièrement, les études locales où la composition chimique de l'eau est conditionnée par la présence de configurations géologiques singulières (comme le bassin versant Deba) présentent un écart plus élevé sur les résultats de la simulation, suggérant que le modèle les performances dans ces situations sont médiocres car elles n'ont pas été développées pour prendre en compte ces situations. Deuxièmement, un affluent du bassin versant de Deba n'est pas influencé par les sources évaporitiques, et les performances du modèle à cet endroit ont mis en évidence le potentiel d'utiliser le modèle ajusté à l'échelle mondiale pour établir un premier instantané des flux ioniques dérivés de l'altération chimique des roches à l'échelle locale.

Compte tenu de la variabilité temporelle sur une période d'un an (jusqu'à quotidiennement), l'hydrologie a été initialement supposée comme le principal responsable de la variabilité des flux ioniques. L'incorporation du modèle dans le modèle SWAT (hydrological Soil and Water Assessment Tool) - en développant le plugin QSWATLitho et le module SWATLitho - a permis de tester l'hypothèse, **confirmant que le rôle de l'hydrologie sur ces flux ioniques est dominé par les eaux souterraines et écoulement latéral** (Chapitre 6). Le développement du plugin QSWATLitho et du module SWATLitho offre une opportunité aux chercheurs intéressés par l'altération chimique et les flux ioniques lors d'études de cas locales.

Enfin, reconnaissant que le principal moteur de l'évolution temporelle des flux ioniques est l'hydrologie, il a été possible d'effectuer une évaluation globale du cycle biogéochimique du carbone, en étudiant l'effet potentiel que le changement climatique peut exercer sur la séquestration du carbone par l'altération chimique. Il a été démontré que les points chauds à l'échelle mondiale ne sont pas répartis de manière égale tout au long de l'année, mais la différenciation entre les saisons est nécessaire pour comprendre quelles sont les zones avec les exportations dissoutes les plus importantes vers l'océan dérivées de l'altération chimique, ainsi qu'avec la plus grande séquestration du carbone. Selon nos résultats, **l'influence potentielle du changement climatique sur l'hydrologie entraînera une augmentation générale de la séquestration annuelle du carbone, qui est spécialement notée entre les mois de janvier et mars, présentant des changements plus importants pour les climats arides et froids, spécialement pour le RCP 8.5 scénario** (Chapitre 7).

9.3.2 Perspectives

Les résultats de la présente thèse de doctorat ont mis en évidence la valeur des approches de modélisation empiriques sur la description du système terrestre lorsque l'application d'autres méthodologies est limitée. Dans cette étude, l'accent a été mis sur l'altération chimique en tant que processus d'intégration concernant les processus

géochimiques et biogéochimiques, mais les recommandations supplémentaires peuvent être appliquées dans d'autres études de développement de modèles.

Premièrement, la conceptualisation initiale du processus a été réalisée dans une perspective globale à locale, en essayant d'élucider les principaux moteurs à l'échelle mondiale et d'identifier les moteurs secondaires sur les études locales. Une stratégie alternative consisterait à développer différentes simplifications de la réalité en se basant sur des cas locaux largement étudiés sur des emplacements suffisamment hétérogènes pour tenir compte des différents paramètres climatiques, lithologiques, hydrologiques et physiques. Le développement de modèles empiriques à ces endroits peut produire des schémas communs des variables non incluses avec succès dans la présente étude. Concernant ces conceptualisations, et sur la base de l'expérience réalisée au cours de cette étude, quelques nouvelles hypothèses sont formulées :

- La température n'a pas été incluse avec succès dans la présente analyse, mais son implication sur l'altération chimique est confirmée depuis longtemps. Une étude récente (Gaillardet et al., 2019 ; Romero-Mujalli, Hartmann, Börker et al., 2019) a proposé une approche alternative de l'effet de la température, basée sur une courbe "en forme de boomerang" concernant l'altération carbonatée. Ainsi, l'effet de la température sur l'altération chimique améliore la dissolution des minéraux jusqu'à une certaine température, mais des valeurs plus élevées diminuent ces taux en raison de l'équilibre carbonate, *l'inclusion du facteur de température dans le développement du modèle à l'échelle mondiale nécessite l'inclusion d'un terme d'équilibre carbonate* –qui explique cette tendance–*au niveau site par site*.
- La végétation utilise des composés inorganiques tels que le K^+ comme nutriment pour la croissance des plantes. Par conséquent, l'effet de protection du sol doit être étudié, y compris la couverture du sol également. *L'effet de protection du sol sur les flux ioniques dérivés de l'altération chimique des roches est non seulement conditionné par les caractéristiques du sol, mais aussi par la couverture terrestre.*
- L'altération chimique est augmentée avec une surface spécifique plus élevée des

particules de la zone critique de sorte que l'interaction eau-roche est améliorée, ainsi la description de l'altération chimique devrait inclure la taille des particules ou un proxy de cette variable. *Plus les particules sont fines dans la zone critique, plus les taux d'altération chimique deviennent élevés, ce qui donne des flux ioniques plus pertinents aux cours d'eau*. Un descripteur potentiel de ce substitut serait la description de la fraction sédimentaire des solides en suspension trouvés dans les rivières.

L'étalonnage des paramètres du modèle a été effectué sous un sous-ensemble de sites d'échantillonnage qui, même s'ils couvrent un large éventail de lithologies et de classes de sols, manquent de certaines caractéristiques (comme les intermédiaires plutoniques ou les évaporites) qui ne couvraient pas tout le spectre de variation. L'application du modèle à de telles caractéristiques non couvertes pourrait entraîner de mauvaises performances du modèle. Une future piste de recherche pourrait être d'étudier quelles sont les variables qui conditionnent les valeurs calibrées, qui pourraient être utilisées pour estimer et ajuster les valeurs de ces paramètres dans des études de cas locales.

L'identification des points chauds devrait être utilisée pour prioriser la recherche sur le cycle biogéochimique dans ces domaines. Des études sur le terrain prises à ces endroits pourraient aider à développer la compréhension des moteurs à différentes échelles spatiales. De plus, une évaluation temporelle pourrait également aider à élucider les effets de la biologie (comme la respiration du sol) sur le processus d'altération chimique.

Enfin, les informations dérivées de la configuration du modèle dans cette stratégie globale-locale pourraient être utilisées, ainsi que des modèles physiques dans une approche locale-globale afin de rapprocher l'applicabilité de ces modèles physiques à grande échelle spatiale et échelles temporelles.

Bibliography

Gaillardet, J., Calmels, D., Romero-Mujalli, G., Zakharova, E., & Hartmann, J. (2019). Global climate control on carbonate weathering intensity. *Chemical Geology*, *527*, 118762. https://doi.org/10.1016/j.chemgeo.2018.05.009

Romero-Mujalli, G., Hartmann, J., Börker, J., Gaillardet, J., & Calmels, D. (2019). Ecosystem controlled soil-rock pCO2 and carbonate weathering – Constraints by temperature and soil water content. *Chemical Geology*, *527*, 118634. https://doi.org/10.1016/j.chemgeo.2018.01.030

Part V

APPENDIX

APPENDIX A

Articles and contributions to congresses

A.1 Articles

- **Title**: A model for evaluating continental chemical weathering from riverine transports of dissolved major elements at a global scale
- **Authors**: **Juan Luis Lechuga-Crespo**, José Miguel Sánchez-Pérez, Sabine Sauvage, Jens Hartmann, Philippe Amiotte Suchet, Jean Luc Probst, Estilita Ruiz-Romera
- **Journal**: Global and Planetary Change
- **Year**: 2020
- **Volume**: 192
- **Article number**: 103226
- **DOI**: 10.1016/j.gloplacha.2020.103226

- **Title**: Combining punctual and high frequency data for the spatiotemporal assessment of main geochemical processes and dissolved exports in an urban river catchment
- **Authors**: **Juan Luis Lechuga-Crespo**, Estilita Ruiz-Romera, Jean Luc Probst, Jessica Unda-Calvo, Zaira Carolina Cuervo-Fuentes, José Miguel Sánchez-Pérez
- **Journal**: Science of the Total Environment
- **Year**: 2020
- **Volume**: 727
- **Article number**: 138644
- **DOI**: 10.1016/j.scitotenv.2020.138644

A.2 Contributions to congresses

- **Title**: Modelling potential impacts of Climate Change on hydrology of a small urban catchment on the North of Spain
- **Authors**: **Juan Luis Lechuga-Crespo**, Estilita Ruiz-Romera, Zaira Carolina Cuervo-Fuentes, Sabine Sauvage, José Miguel Sánchez-Pérez
- **Congress**: The 2017 International SWAT Conference and Workshops
- **Contribution**: Poster
- **Date**: June 28th-30th 2017
- **Place**: Poland

- **Title**: Developing a hydrogeochemical model for implementation in SWAT model at the global scale
- **Authors**: **Juan Luis Lechuga-Crespo**, José Miguel Sánchez-Pérez, Sabine Sauvage, Estilita Ruiz-Romera
- **Congress**: The 2018 International SWAT Conference and Workshops
- **Contribution**: Oral presentation
- **Date**: July 31st 2018
- **Place**: Belgium

- **Title**: Major ion fluxes in the Amazon watershed derived from a global model on chemical weathering rates
- **Authors**: **Juan Luis Lechuga-Crespo**, José Miguel Sánchez-Pérez, Estilita Ruiz-Romera, Sabine Sauvage
- **Congress**: 8th Scientific meeting of the National Observation Service HYBAM
- **Contribution**: Oral presentation
- **Date**: September 2nd-6th 2019
- **Place**: France

eman ta zabal zazu

Universidad del País Vasco

Euskal Herriko Unibertsitatea

FACULTY OF SCIENCE AND TECHNOLOGY
UNIVERSITY OF THE BASQUE COUNTRY

GOBIERNO DE ESPAÑA

MINISTERIO DE ECONOMÍA Y COMPETITIVIDAD

cnrs

EcoLab
Laboratoire écologie fonctionnelle et environnement